Ribosomal Asc1p/RACK1 in the phosphorylation signaling network of *Saccharomyces cerevisiae*

Dissertation

for the award of the degree

"Doctor rerum naturalium"

of the Georg-August-Universität Göttingen

within the doctoral program "Molecular Biology of Cells"

of the Georg-August University School of Science (GAUSS)

submitted by

Kerstin Schmitt

from Göttingen

Göttingen 2015

Thesis Committee

Dr. Oliver Valerius
Department of Molecular Microbiology and Genetics
Institute of Microbiology and Genetics, Georg-August-University Göttingen

Prof. Dr. Heike Krebber
Department of Molecular Genetics
Institute of Microbiology and Genetics, Georg-August-University Göttingen

Prof. Dr. Rolf Daniel
Department of Genomic and Applied Microbiology
Institute of Microbiology and Genetics, Georg-August-University Göttingen

Members of the Examination Board

Referee: Dr. Oliver Valerius
Department of Molecular Microbiology and Genetics
Institute of Microbiology and Genetics, Georg-August-University Göttingen

2nd Referee: Prof. Dr. Heike Krebber
Department of Molecular Genetics
Institute of Microbiology and Genetics, Georg-August-University Göttingen

Further members of the Examination Board

Prof. Dr. Gerhard H. Braus
Department of Molecular Microbiology and Genetics
Institute of Microbiology and Genetics, Georg-August-University Göttingen

Prof. Dr. Rolf Daniel
Department of Genomic and Applied Microbiology
Institute of Microbiology and Genetics, Georg-August-University Göttingen

Prof. Dr. Kai Heimel
Department of Molecular Microbiology and Genetics
Institute of Microbiology and Genetics, Georg-August-University Göttingen

Prof. Dr. Stefanie Pöggeler
Department of Genetics of Eukaryotic Microorganisms
Institute of Microbiology and Genetics, Georg-August-University Göttingen

Date of oral examination: 17th February 2016

I hereby declare that the doctoral thesis entitled “Ribosomal Asc1p/RACK1 in the phosphorylation signaling network of *Saccharomyces cerevisiae*” has been written independently and with no other sources and aids than quoted.

Kerstin Schmitt

Parts of this work are published in:

Rachfall, N., Schmitt, K., Bandau, S., Smolinski, N., Ehrenreich, A., Valerius, O., and Braus, G.H. (2013). RACK1/Asc1p, a ribosomal node in cellular signaling. Mol Cell Proteomics *12*, 87-105.

Schmitt, K., Smolinski, N., Neumann, P., Schmaul, S., Hofer-Pretz, V., Braus, G.H., and Valerius, O. (2017). Asc1p/RACK1 Connects Ribosomes to Eukaryotic Phosphosignaling. Mol Cell Biol *37*, e00279-16

This work was supported by the Göttingen Graduate School for Neurosciences and Molecular Biosciences (DFG Grant GSC 226/2) and by the DFG Grant VA352/2-1.

Acknowledgements - Danksagung

Ich möchte mich an erster Stelle bei Dr. Oliver Valerius für die hervorragende und engagierte Betreuung dieser Arbeit bedanken: Vielen Dank für die zahlreichen gemeinsamen Gespräche und Diskussionen, das entgegengebrachte Vertrauen und die Begeisterung für das Projekt.

Prof. Dr. Gerhard H. Braus danke ich für die Möglichkeit meine Arbeit in der Abteilung *Molekulare Mikrobiologie und Genetik* anfertigen zu können und für die damit verbundene Unterstützung sowie das Interesse an meiner Arbeit.

Prof. Dr. Heike Krebber und Prof. Dr. Rolf Daniel danke ich für die hilfreichen Diskussionen im Rahmen der Thesis Committee Meetings und darüber hinaus für die Kooperationen mit ihren Abteilungen. Aus der Arbeitsgruppe *Molekulare Genetik* danke ich Dr. Bettina Neumann für die Einführung in die Methode der Dichtegradientenzentrifugation und für viele wichtige Hinweise und Ratschläge. Dr. Andrea Thürmer, Kathleen Gollnow und Dr. Sascha Dietrich aus der Abteilung *Genomische und Angewandte Mikrobiologie* bin ich sehr dankbar für die gemeinsame Versuchsplanung, die Durchführung der cDNA Synthese und Sequenzierung und für die anschließende gemeinsame Datenanalyse.

Ein großer Dank gilt allen ehemaligen und aktuellen Mitgliedern des Labors, insbesondere Dr. Britta Herzog, Anika Kühn, Dr. Harald Kusch, Katharina Mucek, Verena Hofer-Pretz, Dr. Nicole Rachfall, Sabrina Sander, Samantha Schmaul, und Nadine Smolinski für die großartige Unterstützung und die schöne Zeit auch außerhalb des Labors.

Ein besonders großer und herzlicher Dank gilt Verena Hofer-Pretz für ihre ausgezeichnete und verlässliche Arbeit. Nadine Smolinski, Sabrina Sander, Samantha Schmaul und Katharina Mucek haben durch ihre Praktika und Abschlussarbeiten einen wesentlichen Beitrag zu dieser Arbeit geleistet, für den ich sehr dankbar bin. Nadine Smolinski danke ich für die enge Zusammenarbeit an dem Projekt auch über ihre Masterarbeit hinaus. Besonders möchte ich mich auch bei Anika Kühn bedanken, die vor allem bei methodischen Fragen immer eine ausgezeichnete Ansprechpartnerin war.

Der gesamten Abteilung *Molekulare Mikrobiologie und Genetik* danke ich für die angenehme Arbeitsatmosphäre und hilfreiche Diskussionen. Der *Göttinger Graduiertenschule für Neurowissenschaften, Biophysik und Molekulare Biowissenschaften* danke ich für die umfassende finanzielle Unterstützung dieser Arbeit.

Meiner Familie und insbesondere meinen Eltern danke ich für ihre Unterstützung und das Interesse an meiner Arbeit.

Table of Contents

List of Figures

List of Supplementary Figures

List of Tables

List of Supplementary Tables

Abstract

The WD40 scaffold protein Asc1 of *Saccharomyces cerevisiae* solely consists of a seven-bladed β-propeller. The protein is highly conserved among eukaryotes and known as RACK1 in metazoans and plants. Asc1p/RACK1 localizes to the head of the 40S ribosomal subunit next to the mRNA exit channel and associates with proteins of signal transduction pathways, thus providing a link between cellular signaling and mRNA translation. In this work, phosphorylation of Asc1p was analyzed by mass spectrometry resulting in the identification of at least three previously unknown phosphorylation sites. To analyze the impact of phosphorylation on the functionality of the protein, Asc1p phospho-site mutant strains were generated for these residues as well as for five additional phospho-sites known from high-throughput studies. Phenotypic characterization showed slightly increased sensitivity to translation inhibitors caused by dephospho-mimics at T143 and Y250, whereas all other phospho-site mutations caused no obvious effect. However, phosphorylation of T12, T96, T99, and especially T143 is required to maintain the abundance of the ribosome binding-compromised Asc1DEp variant. According to the reduced level of the dephospho-mimicking DE-variants, the respective mutant strains show *asc1*$^{-}$ phenotypes. Mutation of Y250 did not change Asc1DEp abundance, but also resulted in *asc1*$^{-}$ phenotypes with respect to cycloheximide sensitivity. Asc1p has a strong impact on the cellular phospho-proteome. A SILAC-based LC-MS approach identified almost 300 Asc1p-sensitive phosphorylation sites in more than 200 proteins that are mainly involved in translation and signal transduction but also other processes. Identification of Asc1p-associated proteins, including, for instance, mRNA-binding proteins, further corroborate Asc1p's involvement in some of these processes, such as mRNA translation. With RNASeq analysis of polysome-derived mRNAs the translatomes of wild-type *ASC1* and *asc1*$^{-}$ strains were compared. Among 73 transcripts of differentially translated mRNAs, the *YHR177W* mRNA is very remarkable as the total level of the transcript significantly increases, whereas its polysome association decreases. Yhr177wp belongs to the fungal-specific family of WOPR transcription factors that regulate morphology and development. Altogether, this work verifies the conserved β-propeller Asc1p as an important rack-wheel within cellular adaptation, signaling, and process coordination.

1. Introduction

1.1 The WD40 protein Asc1

Asc1p from *S. cerevisiae* is a highly conserved eukaryotic protein and belongs to the family of WD40 proteins (Chantrel et al., 1998). The WD40 domain belongs to the most abundant domain types in eukaryotes, while there are only few examples known for prokaryotic WD40 proteins (Stirnimann et al., 2010). The WD40 domains provide scaffolds for the formation of protein complexes and harbor no intrinsic catalytic function known so far. In contrast to the Asc1 protein, which solely consists of a single WD40 domain, many members of this protein family contain additional catalytic or functional domains (Stirnimann et al., 2010). They function in various processes, such as signal transduction, RNA synthesis, vesicular trafficking, cytoskeleton assembly, cell division, and apoptosis (Li and Roberts, 2001).

A WD40 domain comprises four to sixteen repeats of 44 to 66 amino acids with low sequence conservation. Each repeat typically contains a glycine-histidine dipeptide in its N-terminal region and ends with a tryptophan-aspartate (WD) motif (Figure 1A, Li and Roberts, 2001). The domain folds into a β-propeller with each blade consisting of a four-stranded anti-parallel β-sheet. The four β-strands of each sheet are referred to as A, B, C, and D starting with A from the center of the propeller (Figure 1B). Each WD40 repeat is part of two blades providing strand D of one β-sheet and strands A, B, and C of the following sheet. The narrower side of the propeller with the loops connecting strands D and A as well as B and C is defined as the top side (Figure 1C, Li and Roberts, 2001). Together with the bottom side and the circumference of the propeller the structure provides a large surface for protein-protein, protein-peptide, and protein-nucleic acid interactions (Stirnimann et al., 2010). The Asc1 protein has the most common β-propeller structure with seven blades, which seems to have the optimal β-propeller-fold (Figure 1C, Murzin, 1992; Coyle et al., 2009). In *S. cerevisiae*, high-throughput interaction studies showed that the WD40 domain has a higher number of interactions than any other domain in yeast-two hybrid assays, which identify binary interactions, as well as in mass spectrometry/tandem affinity purification experiments, which include interactions within protein complexes (Stirnimann et al., 2010). The number of interactions found in the latter experiments tremendously exceeds the number found in the yeast-two hybrid assays implicating the participation of WD40 proteins in formation of large protein complexes (Stirnimann et al., 2010).

WD40 proteins can also interact with each other as it was, for instance, described that the mammalian orthologue of Asc1p, RACK1, interacts with different Gβ isoforms (Chen et al., 2004b) and forms homodimers (Thornton et al., 2004; Liu et al., 2007b). So far, there is no

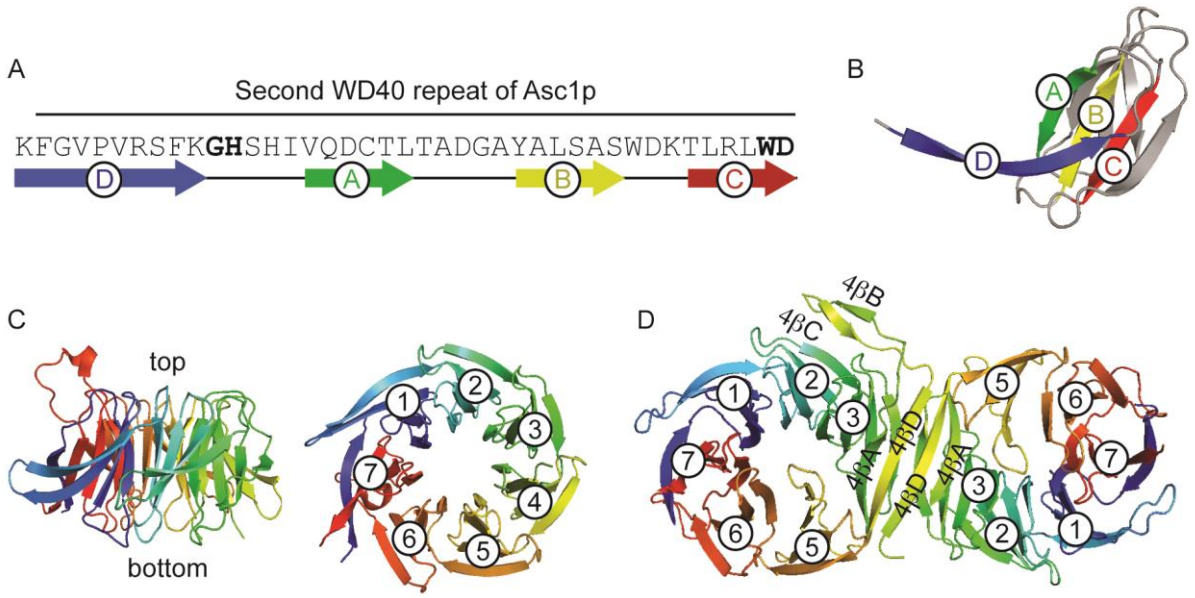

Figure 1. Structural features of the WD40 protein Asc1.
(A) Amino acid sequence of the second WD40 repeat of Asc1p with the characteristic GH and WD motifs printed in bold. The arrows below the sequence labeled D, A, B, and C indicate the amino acids that form β-strands. (B) The structure formed by the second WD40 repeat of Asc1p. β-strands are colored according to the color-code used in A illustrating that each WD40 repeat is in general part of two blades. (C) Side- and bottom-view on the seven-bladed Asc1p colored with a gradient from blue (N-terminus) to red (C-terminus). Blades are labeled from 1 to 7 starting at the N-terminus. (D) Asc1p homodimer. Both Asc1 proteins are depicted with the same coloring as in C. Blades are labeled from 1 to 7. The individual β-strands of blade 4 are labeled from 4βA to 4βD. Strands 4βB and 4βC of Asc1p depicted on the right-hand side were not resolved in the crystal structure and are therefore not present in the depicted structure. All structures were generated with the *PyMOL Molecular Graphics System* software based on the Protein Data Bank (PDB) files 3FRX and 3RFH (Coyle et al., 2009; Yatime et al., 2011). The figure is adapted from Stirnimann et al. (2010).

experimental evidence that *S. cerevisiae* Asc1p forms homodimers *in vivo*, however, a crystal structure of a homodimer derived from recombinantly expressed Asc1p has been resolved (Figure 1D, Yatime et al., 2011). In contrast to other β-propeller dimers, the Asc1p homodimer shows an atypical structural rearrangement. While the overall shape of each Asc1p molecule is preserved in the dimer, the inner strands B and C of both blades number four are expelled from the propeller, and the outer strands A and D form a new blade that is shared by both molecules (Figure 1D, Yatime et al., 2011). In the dimer, the planes of the two Asc1 proteins are oriented in an almost 90° angle to each other. The homodimer does not only provide an extended surface for interactions, it also exposes regions of the protein that are otherwise not accessible in the monomeric form (Yatime et al., 2011). Homodimerization enables Asc1p/RACK1 to scaffold the interaction between two proteins that share the same binding site of the protein as it was shown for the mammalian NMDA receptor and the Fyn kinase that both bind to the first β-propeller blade of RACK1 (Thornton et al., 2004). Homodimerization of mammalian RACK1 also seems to be essential for the interaction

between the transcription factor subunit HIF-1α and the Elongin-C E3 ubiquitin ligase complex that both interact with the sixth WD40 repeat of RACK1 (Liu et al., 2007b). Results from the two studies hint to the same region of RACK1 for dimerization as it is observed for the crystal structure of the Asc1p homodimer.

1.2 The Gβ-like protein Asc1 - an integral component of the ribosome

There is only one WD40 repeat protein known in *S. cerevisiae* that is almost exclusively composed of a single β-propeller like Asc1p, namely the Gβ-protein Ste4 of the pheromone response pathway. Asc1p might act in an analogous way to Ste4p. The Ste4p-comprising heterotrimeric G-protein associates to the transmembrane receptor Ste2p of MATa or Ste3p of MATα cells, respectively. Binding of pheromones (α- or a-factor, respectively) to the receptors triggers their conformational change leading to guanosine diphosphate (GDP) to guanosine triphosphate (GTP) exchange at the Gα-subunit Gpa1p. The reduced affinity of the GTP-bound Gpa1p for the Gβγ-heterodimer (Ste4p and Ste18p) leads to its release from the complex. Gβγ subsequently activates downstream effectors that finally regulate gene expression for the induction of the mating process (pheromone signal transduction in yeast is reviewed in Bardwell, 2005). Asc1p has been described as the Gβ-subunit for the Gα-protein Gpa2 of a nutrient responsive cAMP/PKA signal transduction pathway that regulates pseudohyphal development in diploid and invasive/adhesive growth in haploid cells (Zeller et al., 2007). Like other Gβ-proteins, Asc1p binds to the GDP-bound form of Gpa2p and inhibits the GDP-GTP exchange on the Gα-protein (Zeller et al., 2007). A Gγ-subunit of this pathway has not been identified so far.

The function of Asc1p cannot be exclusively restricted to a putative role as a Gβ. Asc1p belongs to the 5% most abundant proteins in the cell, and this extremely high abundance with approximately 6400 ppm outreaches by far the abundance of Gpa2p with about 60 ppm (PaxDb, Wang et al., 2012; Wang et al., 2015a). The first published study on *S. cerevisiae* Asc1p already described the localization of the protein to the 40S subunit of the ribosome based on its detection in the respective fractions of sucrose-gradients (Chantrel et al., 1998). Subsequent studies corroborated this initial finding, and nowadays the crystal structures of the *Tetrahymena thermophila* 40S subunit and the *S. cerevisiae* 80S ribosome are available providing information on the precise and highly conserved position of Asc1p at the head of the 40S subunit next to the mRNA exit tunnel (Figure 2, Sengupta et al., 2004; Ben-Shem et al., 2011; Rabl et al., 2011). Asc1p contacts the ribosomal proteins Rps3, Rps16, and Rps17 and interacts with the phosphate backbone and nucleotide bases of helix 39 and helix 40 of

the 18S rRNA (Rabl et al., 2011). The binding of Asc1p to ribosomes even under high-salt concentrations (Link et al., 1999; Inada et al., 2002; Rabl et al., 2011) and its frequent presence in cryo-electron microscopy maps of ribosomes implicate that most or even all functional ribosomes in the cell contain Asc1p (Nilsson et al., 2004; Sengupta et al., 2004). Furthermore, the *ASC1* gene shares typical characteristics of ribosomal genes: Like 66% of the *S. cerevisiae* ribosomal genes, the *ASC1* open-reading frame is interrupted by an intron (Chantrel et al., 1998; Link et al., 1999). In contrast, only 3.7% of all *S. cerevisiae* genes contain an intron (Link et al., 1999). The 273 bp large intron is positioned at bp 538 to 810 of the 1233 bp large *ASC1* gene and comprises the *SNR24* gene that codes for the small nucleolar RNA (snoRNA) U24 (Chantrel et al., 1998).

As part of a ribonucleoprotein complex, snoRNA U24 directs the site-specific 2'-O-ribose-methlyation of 25S pre-ribosomal RNA (Kiss-László et al., 1996). Another feature that is shared by *ASC1* and ribosomal genes is the regulation of its mRNA synthesis by the transcription factors Fhl1p and Ifh1p (Kleinschmidt et al., 2006). Despite the characterization of Asc1p as a core component of the 40S ribosomal subunit, a fraction of ribosome-unbound Asc1p seems to exist. It has been shown, for instance, that a ribosome-free form of Asc1p arises in the stationary growth phase of yeast cultures (Baum et al., 2004) indicating that growth conditions and extracellular signals could shift Asc1p to or away from the ribosome.

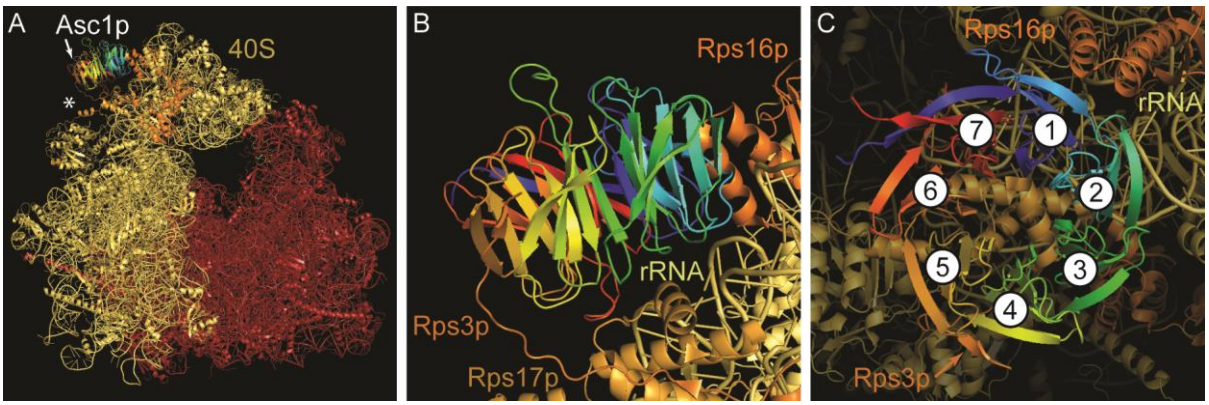

Figure 2. Localization of Asc1p to the ribosome.
(A) Localization of Asc1p to the small 40S subunit of the ribosome next to the mRNA exit tunnel. Asc1p is colored using a gradient from blue (N-terminus) to red (C-terminus). The ribosomal proteins and rRNA of the small 40S subunit are colored in different shades of yellow and orange. The ribosomal proteins and rRNA of the large 60S subunit are colored in red. The mRNA exit tunnel is indicated with an asterisk. (B) Close-up and side-view on Asc1p bound to the ribosome. Asc1p interacts with ribosomal proteins Rps3, Rps16, and Rps17 as well as with rRNA. (C) Close-up and bottom-view of Asc1p bound to the ribosome. According to the definition for β-propeller proteins, Asc1p faces the ribosome with its top side. The β-propeller blades are labeled from 1 to 7. Figures were generated with the *PyMOL Molecular Graphics System* software on the basis of the PDB file 4V88 (Ben-Shem et al., 2011).

This also implicates the presence of Asc1p-deficient ribosomes. A simultaneous interaction of Asc1p with the Gα Gpa2p and the ribosome was disfavored due to sterical hindrance (Coyle et al., 2009), however, Asc1p might dissociate from Gpa2p upon activation of its associated transmembrane receptor Gpr1p and translocate to the ribosome for signal transmission to the regulation of mRNA translation. The viability of yeast *ASC1* deletion strains shows that the protein is not essential for mRNA translation in general. Instead, it might link signal transduction to the translational regulation of specific groups of transcripts (Rachfall et al., 2013).

1.3 Asc1p orthologues within the eukaryotic domain

Asc1p is a highly conserved eukaryotic protein with about 52% amino acid sequence identity to RACK1 of *Homo sapiens* and 46% to RACK1A of *Arabidopsis thaliana*. Comparison of the crystal structures of the orthologous Asc1/RACK1 proteins of *S. cerevisiae, H. sapiens*, *A. thaliana*, and *T. thermophila* shows that this high conservation also manifests on the structural level (Ullah et al., 2008; Coyle et al., 2009; Rabl et al., 2011; Ruiz Carrillo et al., 2012). Besides studies on *S. cerevisiae* Asc1p, there are plenty of publications on its orthologues from different organisms ranging from fungi, plants, and insects, to mammals. Alterations in Asc1p/RACK1 abundance affect fundamental cellular processes. Deletion of the *S. cerevisiae ASC1* gene leads to diverse phenotypes comprising decreased resistance against cell wall stress, absence of haploid adhesive growth and diploid pseudohyphae formation, cold and heat sensitivity, and reduced respiratory activity (Gerbasi et al., 2004; Kleinschmidt et al., 2006; Valerius et al., 2007; Rachfall et al., 2013). In *S. cerevisiae*, Asc1p was first identified in a screen for gene deletions that suppress the growth defect of heme-depleted Δ*hap1* (Δ*cyp1*) cells. Hap1p is a transcription factor required for oxygen and heme-dependent regulation of gene expression. Thus, the protein was termed Absence of growth suppressor of Hap1p/Cyp1p 1 (Asc1p, Chantrel et al., 1998).

1.3.1 Asc1p orthologues in other fungi

Orthologues of Asc1p have been studied in various other ascomycetes besides *S. cerevisiae*. In the fission yeast *Schizosaccharomyces pombe*, the deletion of the *ASC1* orthologous gene *cpc2* increases heat sensitivity and delays cell division at G_2 as well as conjugation and meiosis due to failure of the cells to accumulate in G_1 upon respective stimuli (McLeod et al., 2000). Homozygous Δ*asc1* strains of the opportunistic human pathogen *Candida albicans* are deficient in hyphal development as well as adhesive and invasive growth (Kim et al., 2010;

Liu et al., 2010). The morphological transition of *C. albicans* between yeast, pseudohyphal, and hyphal growth forms is considered as essential for the pathogenicity of the fungus, and in line with this, *ASC1* deleted *C. albicans* strains show strongly reduced pathogenicity in mouse infection models (Kim et al., 2010; Liu et al., 2010). In the filamentous fungi *Aspergillus nidulans* and *Aspergillus fumigatus*, the deletion of the *cpcB* gene results in defects in spore germination, hyphal growth, and asexual conidiospore formation. Moreover, in *A. nidulans* the sexual development of cleistothecia was impaired resulting in the absence of ascospore formation (Kong et al., 2013). Furthermore, *A. fumigatus* shows decreased virulence in an immunosuppressed mouse infection model for invasive aspergillosis (Cai et al., 2015).

In the basidiomycete and opportunistic human pathogen *Cryptococcus neoformans*, absence of the Asc1p orthologue Gib2p results in reduced growth at 37 °C as well as decreased pathogenicity in a mouse infection model (Wang et al., 2014). Absence of the Asc1p orthologue Rak1 also decreases the virulence of the phytopathogenic basidiomycete *Ustilago maydis*. Deletion of *rak1* leads to altered cell morphology, longer doubling times, and increased sensitivity to cell wall stress, and it impairs the mating process, which is a prerequisite for plant infection (Wang et al., 2011).

1.3.2 Plant RACK1 proteins

Plants can possess more than one *RACK1* orthologue within their genome. *A. thaliana* harbors three versions named from *A* to *C* with approximately 87% identity and 94% similarity between RACK1A and each of the other two orthologues on the level of the amino acid sequence (Chen et al., 2006). All three genes are ubiquitously expressed in the plant, but differ in their expression levels with *RACK1A* showing the highest and *RACK1C* the lowest transcript level in various tissues (Chen et al., 2006; Guo and Chen, 2008). A loss-of-function *rack1a* mutant shows various developmental defects in seed germination, leaf production, and flowering as well as deregulation of hormone responses (Chen et al., 2006). In contrast, loss-of-function *rack1b* and *rack1c* single as well as double mutants have no obvious developmental defects (Guo and Chen, 2008). Yet, double mutants lacking RACK1A in combination with one of the other two RACK1s show synergistic effects. Triple mutants missing all three orthologues mostly die off in soil, and those that survive cannot reach maturity. Overexpression of *RACK1B* or *RACK1C* rescues the phenotype of a *rack1a* mutant implicating that the three orthologues are functionally redundant and only differ in the regulation of their expression (Guo and Chen, 2008). The rice species *Oryza sativa* harbors two RACK1 orthologues that are named according to the nomenclature in *A. thaliana*

RACK1A and *RACK1B* (Zhang et al., 2014). Also in rice, the *RACK1A* gene appears to be more prominently expressed than the *RACK1B* gene (Zhang et al., 2014). It is involved in seed germination and regulation of responses to exogenous abscisic acid, a plant hormone, and to H_2O_2, a reactive oxygen species with cell damaging properties that also serves in cellular signal transduction (Zhang et al., 2014).

1.3.3 RACK1 in metazoan organisms

Like in plants, RACK1 is almost ubiquitously expressed in mammals (Chou et al., 1999; Ruan et al., 2012). Metazoan RACK1 is an essential gene, and its depletion leads to lethality in early stages of embryogenesis. Homozygous *RACK1* depletion in mouse results in lethality at gastrulation (Volta et al., 2012). Heterozygous adult mice with only one functional *RACK1* copy in their genome show no differences in RACK1 levels and are viable. However, they show skin pigmentation defects, and eleven days old female pups show a transient growth defect (Volta et al., 2012). At this developmental stage, RACK1 expression differs in the brain and liver. In *Xenopus laevis*, knockdown of *RACK1* results in impaired neuronal tube closure during embryogenesis through defects in convergent extension movements (Wehner et al., 2011). In zebrafish *Danio rerio, rack1* knockdown also impairs convergent extension during gastrulation, as well as oriented cell division and cellular polarization (Li et al., 2011). Depletion of RACK1 through RNA interference in *C. elegans* leads to developmental-timing delay, and its loss-of-function is embryonic lethal (Jannot et al., 2011). In *Drosophila melanogaster*, RACK1 is required throughout embryogenesis, larval development, and pupal stages (Kadrmas et al., 2007). A small percentage of RACK1-deficient flies can reach adulthood, but they exhibit severe phenotypes including sterility (Kadrmas et al., 2007). Silencing of *RACK1* expression specifically in adult flies using a thermosensitive Gal80 system did not affect viability, but reduced the longevity by 20% (Majzoub et al., 2014). Furthermore, the depletion of RACK1 in cell lines of different organisms does not cause lethality indicating that RACK1 is only essential during embryogenesis (Majzoub et al., 2014). A role of RACK1 already in the first stages of embryogenesis has been implicated from the high levels of RACK1 in ovaries as well as from the high abundance of maternally inherited *RACK1* transcripts in zygotes of *D. melanogaster* (Vani et al., 1997; Kadrmas et al., 2007). Analysis of mutant flies devoid of RACK1 in the germ line revealed that the maternally inherited transcripts are indeed essential for the earliest steps of embryogenesis, and their absence cannot be compensated by zygotic RACK1 (Kadrmas et al., 2007).

Beyond its pivotal role in development, RACK1 seems to play a decisive role in cancer proliferation. Aberrant RACK1 expression is associated with different cancer types and was proposed as a biomarker for diagnosis and prognosis of the clinical outcome of certain cancer types (Wang et al., 2009; Cao et al., 2010). The importance of RACK1 in cancer development seems to arise from its role in fundamental cellular processes, such as cell proliferation, cell spreading (Hermanto et al., 2002), angiogenesis (Berns et al., 2000), and apoptosis (Ruan et al., 2012).

1.3.4 *ASC1*/*RACK1* gene expression correlates with ribosomal genes

Expression of plant *RACK1* genes has been reported to be regulated by different hormones. Already the first described plant *RACK1* was identified in a screen for auxin-responsive genes in the tobacco BY-2 cell line (Ishida et al., 1993). In *A. thaliana*, all three *RACK1* genes are down-regulated in their expression levels upon treatment with abscisic acid (Guo et al., 2009), whereas *O. sativa RACK1* mRNA levels increase in response to the same hormone as well as upon treatment with jasmonate and auxin (Nakashima et al., 2008). Guo and colleagues (2011) reported that about 80% of proteins that are co-regulated in their expression with *RACK1* are ribosomal genes. Similarly, increased expression of *ASC1* in *S. cerevisiae* upon growth with ethanol instead of glucose as sole carbon source correlated with increased expression of *RPS26* that encodes a protein of the small ribosomal subunit (Kleinschmidt et al., 2006). Also, the biosynthesis of human *RACK1* appears to correlate with that of other ribosomal genes. The association of human *RACK1* mRNA to polysomes and thus its translation efficiency in response to serum deprivation as well as serum stimulation of human HeLa cells resembles that of the mRNA of the ribosomal protein RPS6 (Loreni et al., 2005). Additionally, the *RACK1* mRNA shows similarity to other ribosomal mRNAs since it starts with an oligopyrimidine sequence and ends with a short 3' untranslated region (3'UTR) of 45 nucleotides (Loreni et al., 2005).

1.3.5 Orthologous genes complement *ASC1*/*RACK1*-deficiency across phyla

As outlined in the previous chapters, misregulation of *ASC1*/*RACK1* expression ranging from deletion to its overexpression in various eukaryotic model organisms interferes with vital cellular events and manifests in diverse and severe phenotypes. It has been repeatedly shown that phenotypes caused by the deletion of *ASC1*/*RACK1* can be complemented by the expression of orthologues from other species underlining its high conservation within the eukaryotic domain. Rat RACK1 expressed in *S. cerevisiae* Δ*asc1* cells can be detected in

ribosomal fractions of sucrose density gradients, and it partially complements the temperature sensitivity phenotype of the Δ*asc1* strain at 37 °C (Gerbasi et al., 2004). Likewise, expression of rat RACK1 in *A. nidulans* strains deficient in the *ASC1*/*RACK1* orthologous *cpcB* gene complements defects in sexual development (Hoffmann et al., 2000). Expression of each of the three *A. thaliana* orthologues in a diploid *S. cerevisiae* Δ*asc1*/Δ*asc1* strain restored the ability of this strain to form pseudohyphae under nitrogen starvation (Guo et al., 2011), and the expression of *U. maydis* Rak1 can complement the adhesive growth defect of a haploid *S. cerevisiae* Δ*asc1* strain (Wang et al., 2011). Expression of human RACK1 in *X. laevis* rescues the defect in neuronal tube closure during embryogenesis upon knockdown of the endogenous *RACK1* mRNA (Wehner et al., 2011).

1.4 Described molecular function of Asc1p/RACK1

Many studies addressed the molecular function of Asc1p/RACK1 that underlies the described phenotypes (chapter 1.3). The following chapter will give an introduction to the current knowledge about the role of the protein in mRNA translation, signal transduction, and protein degradation.

1.4.1 Asc1p/RACK1 as a regulator of mRNA translation

The characterization of Asc1p as an integral component of the small ribosomal subunit suggests a role of the protein in the process of mRNA translation. *S. cerevisiae* Asc1p seems to act as a repressor of translation as shown *in vitro* (Gerbasi et al., 2004) and *in vivo* (Chiabudini et al., 2014). *In vitro* translation assays using cell extracts of *ASC1* wild-type and deletion strains and different templates including capped as well as uncapped luciferase mRNA and wild-type poly(A) mRNA revealed increased translation of mRNAs in extracts from Δ*asc1* cell. Yet, the addition of exogenous and recombinantly-expressed Asc1 protein to the samples of the *in vitro* translation assay did not repress translation activity (Gerbasi et al., 2004). *In vivo*, absence of Asc1p reduces the average ribosome transit time, which is required by a ribosome for elongation and termination of translation, by approximately 30% (Chiabudini et al., 2014). In contrast, overexpression of RACK1 in the human hepatocellular carcinoma derived cell line Huh7 was reported to promote protein biosynthesis in metabolic labeling studies with [^{35}S]-methionine (Ruan et al., 2012). Using firefly and renilla luciferase reporter constructs it could be further shown that RACK1 promotes cap-dependent as well as internal ribosomal entry site (IRES)-mediated translation (Ruan et al., 2012). A role of RACK1 as a promoter of translation was also deduced from experiments measuring the

translation of firefly luciferase reporter constructs within cell extracts from wild-type and *Rack1*-null thoracic muscle cells of *D. melanogaster* (Belozerov et al., 2014). Embryonic fibroblasts of heterozygous mice that carry only one functional copy of *RACK1* showed reduced stimulation of translation through treatment with insulin or phorbol 12-myristate 13-acetate (Volta et al., 2012). Liver cells of 16 days old *RACK1* heterozygous mice show a mild accumulation of 80S ribosomes, and the skin pigmentation phenotype of the adult mutant mice resembles that of *RPL24* mutants (Volta et al., 2012). In conclusion, Asc1p/RACK1 seems to fulfill both a repressive as well as a promoting effect on general mRNA translation rates depending on the cellular context.

1.4.1.1 *S. cerevisiae* Asc1p in co-translational quality control and reading frame maintenance

In *S. cerevisiae*, Asc1p was proposed to function in mRNA quality control systems that act during translation (Kuroha et al., 2010; Matsuda et al., 2014). Different surveillance systems recognize aberrant mRNAs and guide their degradation as well as the clearance of the corresponding peptide products (reviewed in Inada, 2013). Asc1p promotes nascent polypeptide-dependent translation arrest that is caused by translation of stretches of the basic amino acids lysine and arginine encoding sequences within reporter constructs (Kuroha et al., 2010; Brandman et al., 2012; Matsuda et al., 2014). Stretches of lysine in the growing peptide chain can arise, for instance, when the mRNA lacks a stop codon and translation precedes to the poly(A) tail of the mRNA because AAA triplets code for lysine (Lu and Deutsch, 2008). The positively charged amino acids in the growing peptide chain appear to slow down translation through interaction with the negatively charged ribosome tunnel (Lu and Deutsch, 2008). Asc1p further promotes translation arrest at repeats of rare or inefficiently decoded CGA triplets and is required for the co-translational degradation of arrested products via the proteasome and the endonucleolytic cleavage of the corresponding mRNA (Kuroha et al., 2010; Letzring et al., 2013; Matsuda et al., 2014). Furthermore, deletion of *ASC1* causes frameshifting at the inefficiently translated CGA repeats, a phenomenon that is not observed in wild-type cells (Wolf and Grayhack, 2015). The inefficient translation of the arginine encoding CGA triplet is due to wobble decoding and can be suppressed through expression of an anticodon mutated tRNA that perfectly pairs the CGA codon (Letzring et al., 2010). Frameshifting at CGA codons in *ASC1* deleted cells becomes more favored with an increasing distance of the codon from the translational start site (Wolf and Grayhack, 2015). Also, the afore mentioned inhibitory effect of CGA codon repeats on translation depends on a certain

distance from the translation start site and seems to be independent of Asc1p when the CGA repeats lie close to the start codon. Pairs of two adjacent CGA codons are found in 26 genes of *S. cerevisiae* (Wolf and Grayhack, 2015), thus Asc1p might regulate the translation of specific mRNAs. Furthermore, Asc1p was reported to affect the translation in dependence of the 5'UTRs of mRNAs (Rachfall et al., 2013).

1.4.1.2 Asc1p/RACK1-dependent phosphorylation of translation factors

The molecular mechanisms underlying the effects of Asc1p/RACK1 on mRNA translation remain mostly elusive, but some studies provided starting points for a better understanding of its function in protein biosynthesis. Experiments with mammalian cell lines showed that RACK1 localizes activated protein kinase PKCβII to ribosomes leading to phosphorylation of the eukaryotic translation initiation factor 6 (eIF6). This modification induces the release of eIF6 from the 60S ribosomal subunit followed by 80S assembly and translation initiation (Ceci et al., 2003). RACK1-mediated positioning of activated PKCβII is also required for phosphorylation of eIF4E shown in human hepatocellular carcinoma cell lines (Ruan et al., 2012). Blocking the interaction between PKCβII and RACK1 reduces stimulation of translation through activated PKC in human HeLa and Huh7 cell lines (Grosso et al., 2008; Ruan et al., 2012). An interaction of the *A. thaliana* RACK1 proteins with the two orthologous eIF6 proteins A and B was also shown and implicates a possible conservation of this mechanism among different eukaryotic species (Guo et al., 2011). Experiments with human embryonic kidney cell lines HEK293 showed that localization of c-Jun N-terminal kinase (JNK) to ribosomes is also mediated by RACK1 leading to phosphorylation of S205 and S358 of the elongation factor eEF1A2, one of the two mammalian eEF1A isoforms (Gandin et al., 2013a). Phosphorylation of eEF1A2 at these residues enhances its association with newly synthesized and misfolded polypeptides at the ribosome and their degradation by the proteasome (Gandin et al., 2013a).

So far, it has not been shown that *S. cerevisiae* Asc1p recruits kinases to the translational machinery. However, deletion of *ASC1* results in increased phosphorylation of the translation initiation factors eIF2α and eIF4A as well as Ssz1p, a component of the ribosome-associated complex (Valerius et al., 2007). Absence of Asc1p affects phosphorylation of the α-subunit of eIF2 at residue S51 (Valerius et al., 2007). This modification inhibits eIF2B-mediated GDP to GTP exchange at eIF2, a prerequisite for binding of the methionine-carrying initiator tRNA ($^{Met}tRNA_i$) to the initiation factor. Consequently, the amount of the ternary complex consisting of eIF2, GTP, and the $^{Met}tRNA_i$ decreases, when phosphorylation of eIF2α at S51

increases (Dever et al., 1992). Since the ternary complex is essential for translational initiation, overall cellular protein biosynthesis is reduced upon elevated eIF2α phosphorylation. The phosphorylation of eIF2α is thus a key factor in the regulation of mRNA translation, and it is mediated by the sensor kinase Gcn2p in response to nutrient availability (Dever et al., 1992). The kinase activity of Gcn2p is induced through binding of uncharged tRNAs that are tRNAs carrying no amino acid. The abundance of these uncharged tRNAs reflects the availability of amino acids (Wek et al., 1995). In Δ*asc1* cells, phosphorylation of eIF2α at S51 is increased even without amino acid starvation induced by the histidine analogon 3-amino-1,2,4-triazole (3-AT, Valerius et al., 2007). In contrast, absence of Cpc2p in *S. pombe* leads to decreased phosphorylation of eIF2α in response to 3-AT (Tarumoto et al., 2013). In line with this, the autophosphorylation and thus activation of the Gcn2p kinase at residue T818 is reduced in Δ*cpc2* cells under the same conditions (Tarumoto et al., 2013).

1.4.1.3 Asc1p/RACK1-dependent recruitment of proteins to the ribosome

Besides a putative role of Asc1p as a docking site for kinases at the ribosome, it could also localize other proteins to the translational machinery. Asc1p was shown to interact with the c-subunit of eIF3, Nip1p (Kouba et al., 2012). Furthermore, the *C. neoformans* Asc1p orthologue Gib2p interacts with eIF4A (Wang et al., 2014), while *Trypanosoma brucei* RACK1 associates with eEF1A most likely in an indirect way (Regmi et al., 2008; Choudhury et al., 2011).

Asc1p/RACK1 was further shown to associate with mRNA-binding proteins in different organisms. *S. cerevisiae* Asc1p interacts with the mRNA-binding protein Scp160 and is required for its localization to ribosomes (Baum et al., 2004; Coyle et al., 2009). Both proteins can associate with the translation inhibitor Eap1p and the GYF domain containing protein Smy2 to form the so-called SESA network (Scp160p, Eap1p, Smy2p, and Asc1p, Sezen et al., 2009). The complex regulates the translation of the *POM34* mRNA that encodes an integral membrane protein of the nuclear pore complex. Defects in spindle pole body duplication during cytokinesis promote the SESA-mediated inhibition of *POM34* mRNA translation most likely to relieve an inhibitory effect of Pom34p on spindle pole body duplication (Sezen et al., 2009).

The Asc1p orthologue of *S. pombe* Cpc2p was further shown to interact with the mRNA-binding protein Nrd1 (Jeong et al., 2004). Nrd1p represses Ste11p-regulated genes required for sexual differentiation and binds and stabilizes *cdc4* mRNA that encodes a myosin light

chain crucial for cytokinesis (Tsukahara et al., 1998; Satoh et al., 2009). In neuronal mammalian cells, RACK1 binds to the mRNA-binding protein ZBP1 within transport ribonucleoprotein complexes (RNPs, Ceci et al., 2012). These RNA granules contain translationally repressed mRNAs that are transported along dendrites or axons, such as the ZBP1-bound β-actin mRNA. At their destination, RACK1 is required for the recruitment of the activated Src-kinase to the ZBP1/β-actin mRNA complex for phosphorylation of ZBP1 and the subsequent release and translation of the β-actin mRNA (Ceci et al., 2012).

Neuronal RNPs are related to processing bodies (P-bodies) and stress granules that contain untranslated mRNAs and increase in their abundance upon inhibition of translation initiation (Decker and Parker, 2012). P-bodies and stress granules form foci in the cytoplasm that are localized adjacent to each other or partially overlap, and RNPs seem to cycle between these two structures and actively translating polysomes. P-bodies contain proteins involved in mRNA decay and repression of translation (Decker and Parker, 2012). Deletion of *ASC1* in *S. cerevisiae* prevents P-body formation in response to DNA replication stress induced by hydroxyurea, but not in response to osmotic stress/starvation (Tkach et al., 2012). In contrast to P-bodies, stress granules contain different translation initiation factors and components of the small ribosomal subunit including RACK1 as shown for human HeLa cells subjected to certain stress conditions (Arimoto et al., 2008; Decker and Parker, 2012).

1.4.1.4 RACK1's function in IRES-dependent translation initiation and the miRNA pathway

In *D. melanogaster* and in the Huh7.5.1 cell line, silencing of *RACK1* decreases propagation of viruses belonging to the *Dicistroviridae* and *Flaviviridae* families, respectively, due to the requirement of RACK1 for IRES-mediated mRNA translation (Majzoub et al., 2014). Notably, RACK1 is not required for the activity of those IRES containing mRNAs that bind to the 40S subunit and recruit the 60S subunit independently of translation initiation factors. The Hepatitis C virus of the *Flaviviridae* family causes liver disease and hepatocellular carcinoma. Thus, RACK1 might evolve as a target for antiviral therapy (Majzoub et al., 2014). RACK1 has further been described to act in the miRNA pathway of *C. elegans*, *H. sapiens*, and *A. thaliana*, but its function seems to differ between the different organisms (Speth et al., 2013). In metazoans and plants, small non-coding micro RNAs (miRNAs) play an important role in gene silencing on a post-transcriptional level. The miRNA pathway requires processing of primary miRNAs by the Dicer enzyme into 20 to 22 nucleotide long miRNAs. These mature miRNAs assemble together with Argonaute (Ago) and other proteins

into a miRNA-induced silencing complex (miRISC). The complex is directed by the miRNA to target mRNAs via base-pairing to regulate their translation or degradation. Experiments with human hepatoma cell lines showed that RACK1 interacts with Ago2 and with the KH-type splicing regulatory protein that associates with the Dicer complex and is involved in miRNA maturation (Otsuka et al., 2011). RACK1 was proposed to function after miRNA maturation and might be involved in the recruitment of mature miRNA to the RISC (Otsuka et al., 2011). Another study reported that RACK1 interacts with the miRISC in *C. elegans* and human HeLa cells (Jannot et al., 2011). The localization of the miRISC to translating ribosomes is reduced upon depletion of RACK1 resulting in increased expression of specific miRNA targets (Jannot et al., 2011). In *A. thaliana*, however, RACK1 deficiency reduces the level of a large number of primary miRNAs (Speth et al., 2013). RACK1 interacts with the protein SERRATE, a protein involved in miRNA production. RACK1 is further found in complex with the miRISC component AGO1 suggesting more than one role of plant RACK1 in the miRNA pathway (Speth et al., 2013).

1.4.2 Asc1p/RACK1 in signal transduction pathways

Asc1p/RACK1 shows high similarity to the Gβ-subunits of heterotrimeric G-proteins and was described as the Gβ-subunit of the Gα-protein Gpa2. In other organisms, Asc1p/RACK1 has been associated to G-protein-mediated signaling as well, but it also functions in other signal transduction pathways and seems to provide a central hub to link different pathways. The following chapters describe the function of Asc1p/RACK1 in cellular signaling in different organisms ranging from yeast to man.

1.4.2.1 Role of Asc1p and its orthologues in signal transduction pathways in fungi and plants

Immunoprecipitation experiments showed that *S. cerevisiae* Asc1p can be co-purified with the adenylyl cyclase Cyr1p of the cAMP/PKA pathway and with the mitogen-activated protein kinase kinase kinase kinase (MAP4K) Ste20p (Figure 3, Zeller et al., 2007). Asc1p was suggested to inhibit the activity of both enzymes: Cyr1p catalyzes the formation of cAMP from ATP, and absence of Asc1p enhances cAMP levels upon stimulation of starved cells with glucose. Phosphorylation and activation of the Ste20p down-stream MAPK Kss1p is increased in Δ*asc1* cells compared to wild-type cells (Zeller et al., 2007). Additionally, Asc1p was identified in complex with the MAPK Slt2p of the signal transduction pathway that

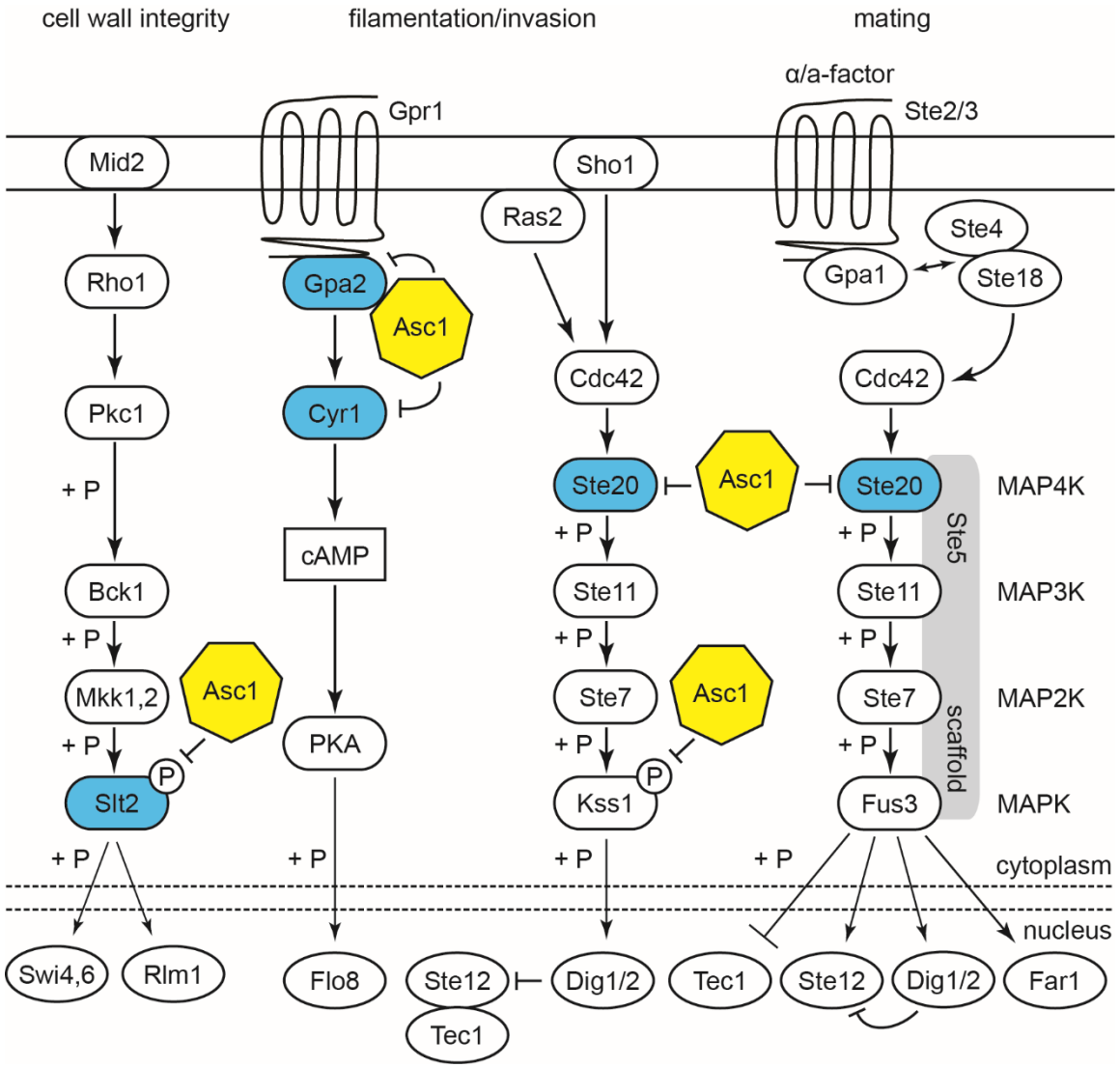

Figure 3. Model on Asc1p's function in the cAMP/PKA pathway and MAPK cascades in *S. cerevisiae*.
The cAMP/PKA pathway and the MAPK cascades regulating cell wall integrity, filamentous and adhesive growth, and mating are depicted. Proteins that were described to associate physically with Asc1p are colored in blue. Asc1p directly interacts with the Gα-protein Gpa2 of the cAMP/PKA pathway and was proposed to function as the Gβ-subunit. The interaction between Asc1p and Gpa2p inhibits the exchange of Gpa2p-bound GDP for GTP, a process that is required for activation of the Gα-protein. Asc1p was further co-purified with the adenylyl cyclase Cyr1p and the MAP4K Ste20p and seems to inhibit the function of these proteins within their respective pathways (Zeller et al., 2007). Asc1p was also identified in complex with the MAPK Slt2p (Breitkreutz et al., 2010). The amount of phosphorylated MAPKs Slt2p and Kss1p is increased in Δ*asc1* cells (Chasse et al., 2006; Zeller et al., 2007). The general overview of the signal transduction pathways is adapted from the KEGG database (http://www.genome.jp/kegg).

regulates cell wall integrity (Breitkreutz et al., 2010). Phosphorylation of Slt2p was increased in Δ*asc1* cells indicating enhanced activity of this pathway (Figure 3, Chasse et al., 2006).

The Asc1p orthologue of the basidiomycete *C. neoformans* Gib2p was also identified to function as a Gβ-subunit through its interaction with the Gα-protein Gpa1 of the cAMP

signaling pathway (Gib2p = Gpa1-interacting β 2, Palmer et al., 2006). In *C. neoformans*, this pathway also regulates the production of virulence factors, such as the antioxidant melanin and the polysaccharide capsule (Alspaugh et al., 1997). In contrast to well characterized Gβ-subunits of heterotrimeric G-proteins, Asc1p/RACK1 lacks the N-terminal coiled-coil domain important for interaction with Gγ-subunits (Zeller et al., 2007; Ullah et al., 2008; Ruiz Carrillo et al., 2012). However, Gib2p of *C. neoformans* has been described to associate with the Gγ-proteins Gpg1 and Gpg2 (Palmer et al., 2006). It further binds to the GTPase Ras1p that in turn interacts with the adenylyl cyclase Cac1p (Wang et al., 2014). Whereas *S. cerevisiae* Asc1p was reported to inhibit the adenylyl cyclase Cyr1p, *C. neoformans* Gib2p positively affects cellular cAMP levels in Gpa1p-deficient cells possibly through reducing the inhibitory effect of Ras1p on Cac1p (Zeller et al., 2007; Wang et al., 2014).

The three RACK1 proteins of *A. thaliana* have not been shown to function as Gβ themselves, but they were reported to interact with the Gβ-protein AGB1 (Cheng et al., 2015). Furthermore, they associate with all three components of the MAPK cascade and seem to provide a scaffold that links the heterotrimeric G-protein to MAPK signaling similar to Ste5p in the pheromone response pathway of *S. cerevisiae*. The plant G-protein/MAPK pathway is activated by pathogen secreted proteases placing RACK1 in the center of the plant innate immune response pathway (Cheng et al., 2015).

1.4.2.2 Metazoan RACK1 - Receptor for activated C kinase 1

Like the plant RACK1 proteins, mammalian RACK1 has also not been reported to function as a Gβ-subunit, but it interacts with the $G\beta_1\gamma_1$ dimer and to a lesser extent with the transducin heterotrimer $G\alpha_t\beta_1\gamma_1$ (Dell et al., 2002). Since RACK1 also interacts with other Gβγ isoforms, it might act as a general Gβγ binding partner (Chen et al., 2005). The association of RACK1 with Gβγ inhibits a specific subset of their signaling functions, whereas Gα-mediated signal transduction seems to be RACK1-independent (Chen et al., 2004a).

Metazoan RACK1 has been described as an interaction partner for a plethora of different signaling molecules comprising proteins localized in the cytoplasm and nucleus as well as the cytosolic domains of membrane-spanning receptors (Li and Xie, 2015). RACK1 has versatile effects on its interaction partners. Similar to yeast Asc1p, RACK1 can influence the enzymatic activity of its associated proteins. Furthermore, it was shown that RACK1 shuttles proteins to their cellular target sites and that it scaffolds protein-protein interactions, thereby also interconnecting different signal transduction pathways and forming a central regulatory node (Gandin et al., 2013b; Li and Xie, 2015).

Already some of the earliest studies on mammalian RACK1 characterized the protein as an interaction partner of activated PKCβII resulting in its name receptor for activated C kinase 1 (Ron et al., 1994; Ron et al., 1995). RACK1 stabilizes the activated conformation of the kinase and shuttles the protein to its cellular target sites (Ron et al., 1994; Ron et al., 1999). The function of RACK1 has also been linked to other PKC isoforms (Liedtke et al., 2002; Robles et al., 2010; Wehner et al., 2011). The function of RACK1 in neuronal tube closure during embryogenesis of *X. laevis*, for example, seems to involve its interaction with PKCδ1 in a membrane localized complex with PTK7, a regulator of planar cell polarity, and Dishevelled, a protein involved in Wnt signaling (Wehner et al., 2011).

1.4.2.3 RACK1 links insulin-like growth factor 1 with integrin signaling

In contrast to its effect on PKC, RACK1 acts as an inhibitor of the Src family of non-receptor protein tyrosine kinases specifically of Src and Fyn (Chang et al., 1998; Yaka et al., 2002; Adams et al., 2011). The release of Src from RACK1 involves the direct interaction of RACK1 with the insulin-like growth factor 1 receptor (IGF-1R), a transmembrane receptor and regulator of cell adhesion, migration, growth, and survival (Kiely et al., 2005). Upon activation of IGF-1R through its ligand IGF-1, RACK1 simultaneously binds the

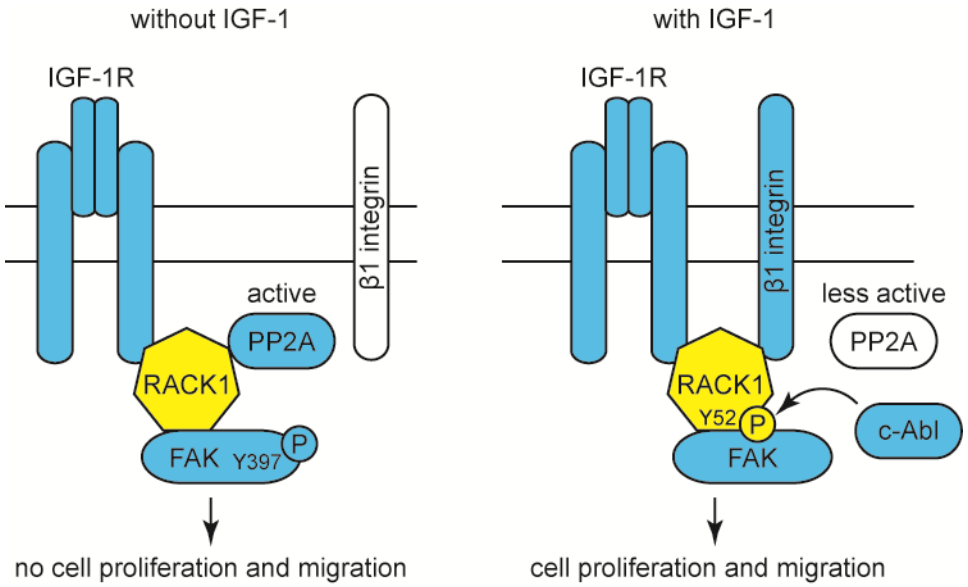

Figure 4. Model on the function of RACK1 in IGF-1R signal transduction.
In the absence of IGF-1, RACK1 recruits PP2A and phosphorylated FAK to the IGF-1R receptor. Upon binding of IGF-1 to its receptor, PP2A is released through binding of β1 integrin to the same binding site on RACK1, and its activity is reduced. Furthermore, RACK1 is phosphorylated by the c-Abl kinase at Y52, a modification that stabilizes the interaction between RACK1 and FAK. This interaction is required for the dephosphorylation of FAK at Y397. These signaling events contribute to the induction of cell proliferation and migration. The model is adapted from Kiely et al. (2006 and 2009). Proteins that interact physically with RACK1 are colored in blue.

transmembrane receptor β1 integrin, another regulator of adhesion, thereby integrating signals coming from the two distinct receptors (Figure 4, Hermanto et al., 2002). Activation of IGF-1R leads to release of Src from RACK1 as well as to dissociation of protein phosphatase PP2A from the complex (Kiely et al., 2005; Kiely et al., 2006). Since PP2A and β1 integrin bind to WD40 repeats 1 to 4 of RACK1 in a mutually exclusive manner, association of the membrane receptor with RACK1 excludes PP2A from the complex, thereby reducing its phosphatase activity (Kiely et al., 2006).

Stimulation of serum starved cells with IGF-1 further stabilizes the interaction of RACK1 with focal adhesion kinase (FAK) through phosphorylation of RACK1 at Y52 by the c-Abl kinase (Figure 4, Kiely et al., 2009). The interaction between RACK1 and FAK is essential for the IGF-1 triggered dephosphorylation of FAK at Y397 that is considered as a prerequisite for the induction of cell migration (Kiely et al., 2009). RACK1 also recruits other proteins to IGF-1R, such as phosphorylated Shc, IRS-1, IRS-2, and Shp2 (Kiely et al., 2005), and serves as an adaptor protein for Kindlin-3 and other signaling proteins at the β1 integrin receptor (Feng et al., 2012).

1.4.2.4 Metazoan RACK1 in cAMP/PKA signaling

While the inhibitory effect of RACK1 on the Src kinase is relieved through IGF-1R signaling, RACK1-dependent inhibition of the non-receptor protein tyrosine kinase Fyn is abrogated through PKA induced dissociation of the two proteins (Figure 5, Yaka et al., 2003). Like yeast Asc1p, mammalian RACK1 is thus linked to cAMP/PKA signaling. In neurons of the hippocampus, RACK1 homodimers localize the Fyn kinase to the *N*-methyl D-aspartate (NMDA) receptor via interaction with the cytoplasmic tail of the receptor subunit NR2B (Yaka et al., 2002; Thornton et al., 2004). As long as RACK1 is part of the complex, phosphorylation of NR2B through Fyn is blocked (Yaka et al., 2002). However, upon activation of the cAMP/PKA pathway, RACK1 is released, and the phosphorylation takes place leading to increased ion channel activity of the NMDA receptor (Yaka et al., 2003). Homodimer formation of RACK1 enables its simultaneous association with NR2B and Fyn since both share the same interaction surface on RACK1 (amino acids 35 to 48, Thornton et al., 2004). This complex seems to be stabilized at membranes through interaction of RACK1 with the Gβ-subunit of a PAC1 receptor-associated heterotrimeric G-protein (Figure 5). Binding of pituitary adenylyl cyclase-activating polypeptide (PACAP) to the PAC1 receptor leads to dissociation of the G-protein that might in turn promote the release of RACK1 from the complex and thus Fyn-mediated phosphorylation of NR2B (Thornton et al., 2004).

Activation of the cAMP pathway further leads to translocation of RACK1 to the nucleus, a process that depends on its direct interaction with the scaffold protein 14-3-3ζ (Figure 5, Neasta et al., 2012). In the nucleus, RACK1 localizes to the promoter region IV of the brain-derived neurotrophic factor (*BDNF*) gene possibly through interaction with histones H3 and H4 (Yaka et al., 2003; He et al., 2010). RACK1 induces the dissociation of the transcription repressor methyl-CpG-binding protein 2 (MeCP2) from the promoter leading to histone H4 acetylation, chromatin remodeling and thus exon-specific transcription of *BDNF* (He et al., 2010).

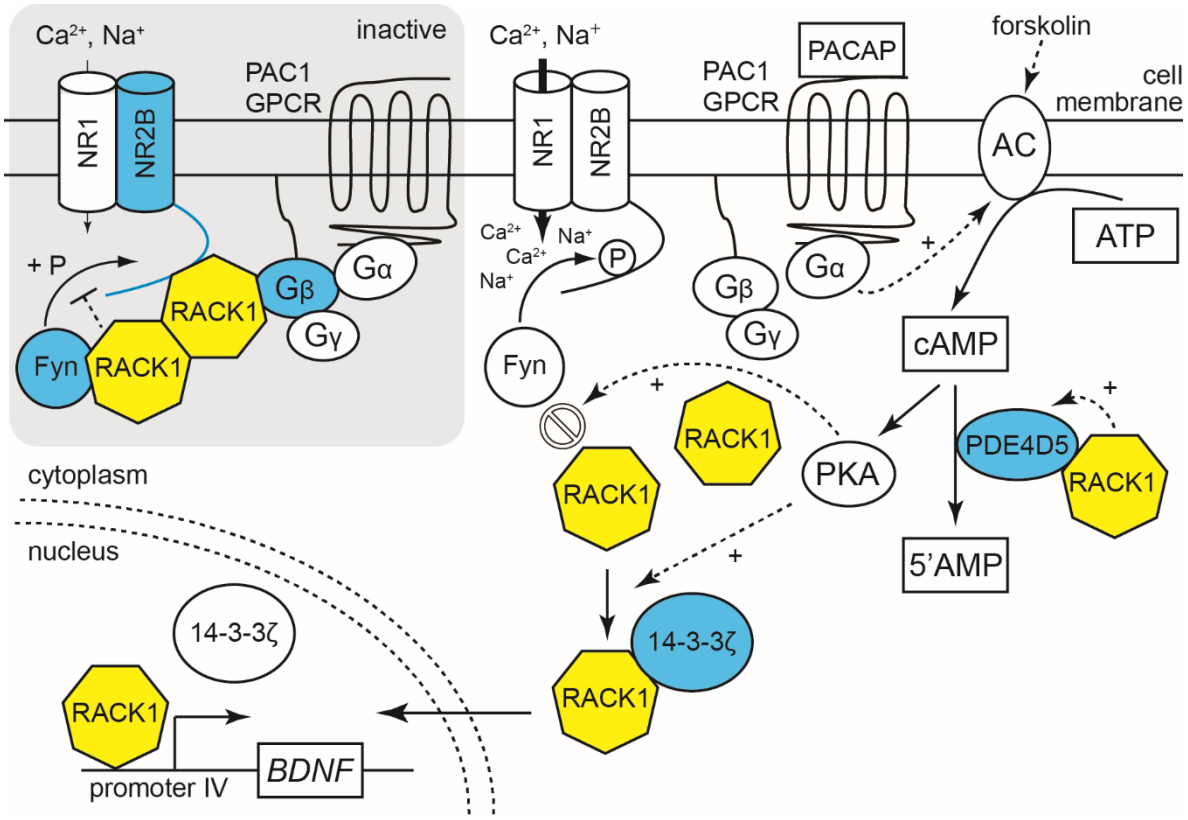

Figure 5. Model on the involvement of RACK1 in G-protein and cAMP/PKA signaling in metazoan.
RACK1 inhibits the phosphorylation of the NMDAR subunit NR2B by the Fyn kinase, thereby causing decreased channel activity. The interaction of RACK1 with Gβ might stabilize the complex at the membrane. Binding of PACAP to the G-protein-coupled receptor (GPCR) PAC1 causes dissociation of the heterotrimeric G-protein into the Gα-subunit and the Gβγ-heterodimer. This might destabilize the complex of NR2B, Fyn, and RACK1 releasing the inhibitory effect of RACK1 on Fyn and enabling phosphorylation of NR2B by the kinase and increasing the channels activity. RACK1's simultaneous interaction with NR2B and Fyn requires its homodimerization. Also, the activation of the adenylyl cyclase (AC) with forskolin and the subsequent activation of the cAMP/PKA pathway promote the release of RACK1 from the complex with NR2B and Fyn and thus the phosphorylation of NR2B. The figure is adapted from Yaka et al. (2003), Thornton et al. (2004), and the KEGG database. Additionally, the interaction between RACK1 and the scaffold protein 14-3-3ζ is depicted, which is promoted by active PKA and leads to translocation of RACK1 into the nucleus where it activates *BDNF* transcription (Neasta et al., 2012). RACK1 seems to promote cAMP hydrolysis through increasing the affinity between PDE4D5 and its substrate (Bird et al., 2010). RACK1-interacting proteins are colored in blue.

RACK1 is further involved in the cAMP pathway through its interaction with the phosphodiesterase (PDE) isoform PDE4D5 (Figure 5, Yarwood et al., 1999). PDEs provide the only mechanism to decrease cellular cAMP levels through catalyzing the hydrolysis of the molecule to 5'AMP. The PDE4 class of cyclic nucleotide PDEs is responsible for the majority of cAMP hydrolysis and is encoded by four genes (A-D) in mammals that provide different isoforms through alternative splicing (Conti et al., 2003). In membrane fractions of HEK293 cells, the interaction between RACK1 and PDE4D5 increases the affinity of the enzyme for its substrate cAMP (Bird et al., 2010).

1.4.2.5 Function of RACK1 in MAPK cascades

Like *S. cerevisiae* Asc1p, RACK1 was not only identified to be involved in the cAMP/PKA pathway, but also to interact with components of MAPK cascades (Figure 6). The MAPK p38b binds RACK1 in cells of *D. melanogaster* thoracic muscles and of the S2 cell line, and *in vitro* experiments showed that the MAPK can phosphorylate RACK1 (Belozerov et al., 2014). Genetic studies revealed that p38b and RACK1 act in a common pathway for the regulation of protein aggregate formation, life-span, and locomotor functions. In aging and stressed cells, activation of p38b seems to shift RACK1 to a ribosome-unbound pool that might repress translation (Belozerov et al., 2014).

In another study on the differentiation of bone marrow-derived macrophages (BMMs) into bone-resorbing osteoclasts, RACK1 was shown to act upstream in the p38 pathway as well (Lin et al., 2015). Mammalian RACK1 is required for p38 activation in response to the cytokine receptor activator of nuclear factor κB (NF-κB) ligand (RANKL) to induce osteoclast formation (Lin et al., 2015). The RANKL receptor RANK associates at its cytoplasmic domain with the E3 ubiquitin ligase tumor necrosis factor receptor-associated factor 6 (TRAF6, Galibert et al., 1998). Upon ligand binding to RANK, TRAF6 recruits the MAP3K transforming growth factor-β activated kinase 1 (TAK1) via an adaptor protein to the complex leading to its activation (Mizukami et al., 2002). Experiments with HEK293T cells revealed that RACK1 mediates the interaction between the TRAF6-TAK1 complex and the p38-targeting MAP2K MKK6 that results in increased downstream phosphorylation of p38 (Figure 6, Lin et al., 2015). Treatment of bone marrow-derived macrophages with RANKL increases RACK1 levels depending on a putative binding site for the transcription factor and target of RANK-signaling NF-κB within the promoter of the RACK1 gene (*GNB2L1*). Overexpression of RACK1 induces p38 phosphorylation and enhances RANKL-

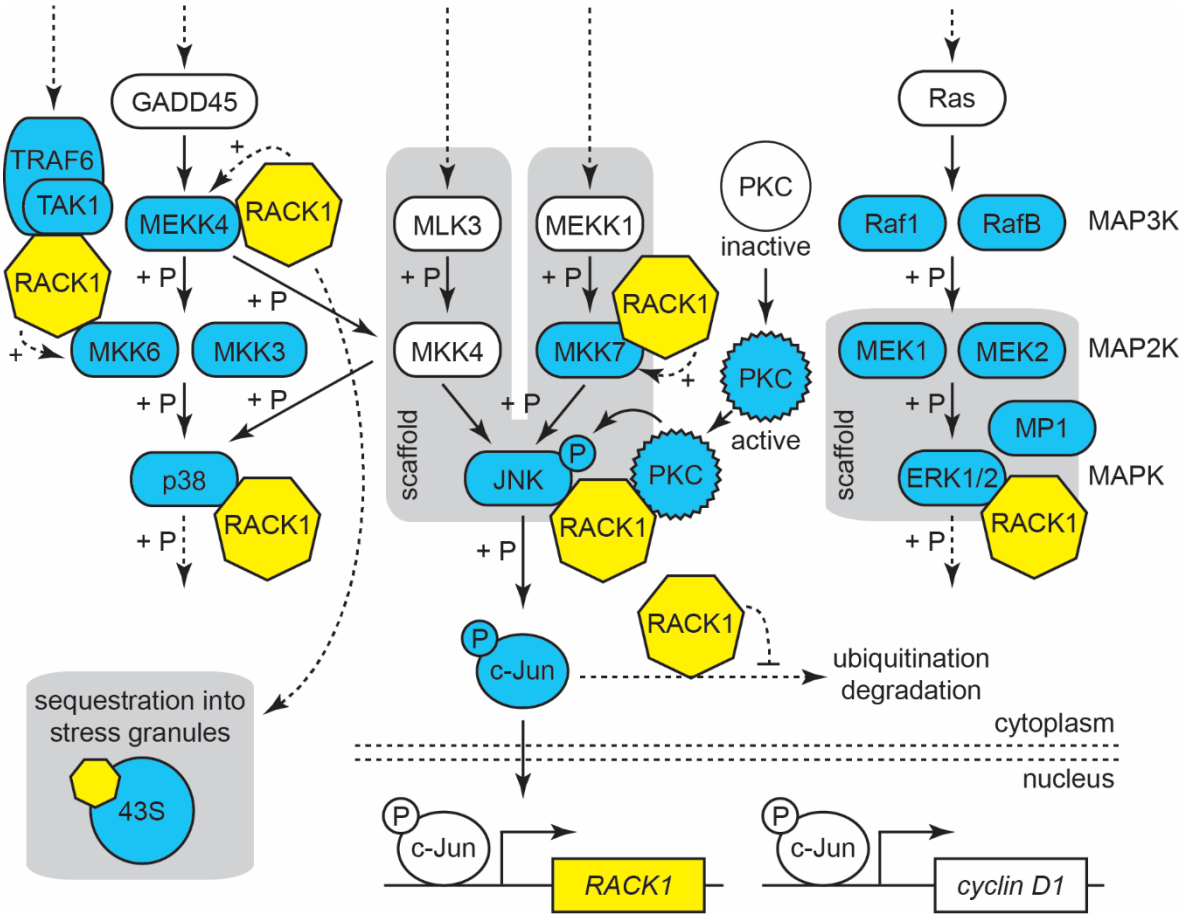

Figure 6. Model on the involvement of RACK1 in MAPK cascades in metazoans.
The model illustrates the interaction of RACK1 with components of different MAPK cascades and related processes. Proteins that have been reported to interact directly or are in a multisubunit complex with RACK1 are colored in blue. Dashed lines indicate up-stream or downstream signal transduction or regulatory processes that are not illustrated in more detail. References for interactions are as follows: MEKK4 (Arimoto et al., 2008), MKK7 (Guo et al., 2013), TRAF6 and TAK1 (Lin et al., 2015), MKK6 (Lin et al., 2015; Wang et al., 2015b), MKK3 (Wang et al., 2015b), JNK and activated PKC (López-Bergami et al., 2005), components of ERK1/2 pathway (Vomastek et al., 2007). The components of the ERK pathway were shown to interact with RACK1 in a complex. The illustrated interaction between ERK and RACK1 is representative for the whole pathway and might occur indirectly (Vomastek et al., 2007). RACK1 also promotes activity of MKK3 that is not illustrated in the figure due to space limitations. The inhibitory effect of RACK1 on the degradation of N-terminally phosphorylated c-Jun was reported by Zhang et al. (2012) and is described in detail in the following chapter 1.4.3. Localization of RACK1 to stress granules was shown by Arimoto et al. (2008). The overview of MAPK pathways is adapted from the KEGG database, and the model for RACK1's involvement in these pathways is partially adapted from Gandin et al. (2013b).

stimulated osteoclast formation. Accordingly, reduction of RACK1 levels reduces phosphorylation of p38 as well as RANKL-stimulated osteoclastogenesis (Lin et al., 2015). Furthermore, ectopic expression of RACK1 in mouse L929 fibroblastoma cells suppresses tumor necrosis factor α (TNFα)-induced cell death most likely due to increased activation of p38 (Wang et al., 2015b). An interaction between RACK1 and the upstream kinases MKK3 and MKK6 of p38 was shown in L929 and human 293T cells. Upon TNFα stimulation,

enhanced binding of RACK1 activates the kinases leading to increased phosphorylation of p38 (Wang et al., 2015b).

Using the *Cercopithecus aethiops* origin-defective SV-40 (COS7) cell line derived from African green monkey kidney cells as well as HEK293 cells, RACK1 was further shown to interact with the MAP3K MEKK4/MTK1 that phosphorylates the upstream MAP2Ks MKK3 and MKK6 of p38 (Figure 6, Arimoto et al., 2008). In the absence of stress, RACK1 seems to tether at least two MEKK4 proteins together in an inactive state, thereby facilitating their activation as soon as the cells become exposed to certain stress conditions (Arimoto et al., 2008). MEKK4 additionally phosphorylates the MAP2K MKK4 that targets p38 as well but also the MAPK JNK.

The JNK signal transduction pathway is further affected by RACK1 through its direct interaction with the MAPK (López-Bergami et al., 2005). In HEK293T cells, PKC becomes activated upon treatment with UV irradiation or phorbol esters and is localized to JNK by RACK1 (Figure 6). PKC phosphorylates the MAPK at S129 and thereby augments the activation of JNK through its upstream MAP2Ks MKK4 and MKK7 (López-Bergami et al., 2005). Thus, RACK1 functions as a node to link PKC with MAPK signal transduction.

RACK1 was further described to directly interact with the upstream MAP2K MKK7 of JNK in human hepatocellular carcinoma (HCC) and HEK293T cells (Guo et al., 2013). The interaction between RACK1 and MKK7 promotes the interaction of MKK7 with its upstream MAP3Ks increasing its activity and leading to elevated JNK phosphorylation (Figure 6). Expression of RACK1 is elevated in clinical HCC tissue and could promote tumor growth through its interaction with MKK7 (Guo et al., 2013).

In the mouse fibroblast cell line NIH 3T3, RACK1 was shown to associate with central components of the MAPK/extracellular signal-regulated kinase (ERK) pathway: The MAP3Ks RafB and Raf1, the MAP2Ks MEK1 and MEK2, the MAPKs ERK1/2, and the scaffolding protein MP1 (Figure 6, Vomastek et al., 2007). The ERK pathway responses to extracellular substances, such as growth factors and hormones, and regulates cell proliferation and differentiation (Rubinfeld and Seger, 2005). RACK1 seems to link the pathway to integrin- and FAK-activation and is required for the localization of ERK to focal adhesions, where it promotes cell motility through the disassembly of these structures (Vomastek et al., 2007).

The afore mentioned experiments performed by Arimoto and colleagues (2008) revealed interaction between RACK1 and the MAP3K MEKK4, but neither confirmed the interaction of RACK1 with the MAP2Ks MKK3, MKK6, and MKK7, nor with the MAPKs JNK, ERK,

and p38. The occasionally inconsistent observations for RACK1's interaction with components of MAPK cascades could be either due to a context-specific interaction of RACK1 with other proteins that varies between different model organisms or cell lines or it might be caused by differences in the experimental design. Interaction between RACK1 and p38b, for instance, was shown for *D. melanogaster* and was specific for a kinase-dead mutant of the MAPK (Belozerov et al., 2014).

1.4.2.6 RACK1 as a central hub linking signal transduction with translation

Most studies on RACK1's function in signal transduction pathways do not take the ribosome-association of the protein into consideration. Yet, as described before (see also chapter 1.4.1.2), RACK1 was identified as an anchoring protein for the kinases PKCβII and JNK at the translational machinery (Ceci et al., 2003; Ruan et al., 2012; Gandin et al., 2013a). Furthermore, activation of the MAP3K MEKK4 is regulated through sequestration of RACK1 into stress granules as part of stalled pre-initiation complexes (Figure 6, Arimoto et al., 2008). Certain stress conditions, such as hypoxia, induce granule formation and consequently reduce the amount of cytoplasmic RACK1 that is available for interaction with MEKK4 leading to decreased basal activity of the kinase and inhibition of its activation (Arimoto et al., 2008). Thus, besides mediating crosstalk between different signal transduction pathways, RACK1 also links these pathways to the translational machinery.

1.4.3 RACK1-dependent protein-degradation of its interaction partners

Mammalian RACK1 regulates the degradation of certain interaction partners, such as the hypoxia-inducible factor 1 (HIF-1, Liu et al., 2007a). The transcription factor HIF-1 is a heterodimer consisting of an α- and β-subunit (Wang and Semenza, 1995). Under low oxygen conditions, HIF-1 induces the transcription of genes that encode proteins required for increased oxygen delivery and adaptation of the energy metabolism (Semenza et al., 1994; Iyer et al., 1998). Hypoxia can be caused by environmental conditions, such as increased altitude or by defects in blood supply to tissues. Furthermore, hypoxia plays an essential role during embryogenesis (Iyer et al., 1998), and it also occurs frequently within cancer tissues where it causes HIF-1-dependent changes in cell-proliferation, angiogenesis, and cellular metabolism (reviewed in Semenza, 2013).

An important mechanism for the regulation of HIF-1 is the degradation of its α-subunit in response to oxygen concentrations. Under normoxia, prolyl-hydroxylases modify HIF-1α and thereby generate a binding site for the von Hippel-Lindau protein/Elongin-B/C E3 ubiquitin

ligase that ubiquitinates the transcription factor subunit and thus triggers its proteasomal degradation. This pathway depends on cellular oxygen-levels and the metabolic status of the cell because the prolyl-hydroxylases use oxygen as well as α-ketoglutarate as substrates for the modification of HIF-1α (Ivan et al., 2001; Jaakkola et al., 2001; Semenza, 2013).

The stability of HIF-1α is also regulated by an oxygen-independent pathway that involves RACK1 (Figure 7, Liu et al., 2007a). The β-propeller protein competes with the heat shock protein HSP90 and the septin-family member SEPT9_v1 for binding to the transcription factor subunit. Whereas binding of HSP90 and SEPT9_v1 stabilizes HIF-1α, RACK1 can recruit the Elongin-B/C E3 ubiquitin ligase to HIF-1α via direct interaction with Elongin-C and thereby promotes ubiquitination and degradation of the transcription factor subunit (Liu et al., 2007a; Amir et al., 2009). The formation of this complex most likely relies on the homodimerization of RACK1 because both HIF-1α as well as the E3 ubiquitin ligase interact with the sixth WD40 repeat of the β-propeller protein and thus only the RACK1 dimer can bind both proteins simultaneously (Liu et al., 2007b). Homodimerization of RACK1 involves the fourth WD40 repeat of each monomer and seems to require phosphorylation of its amino

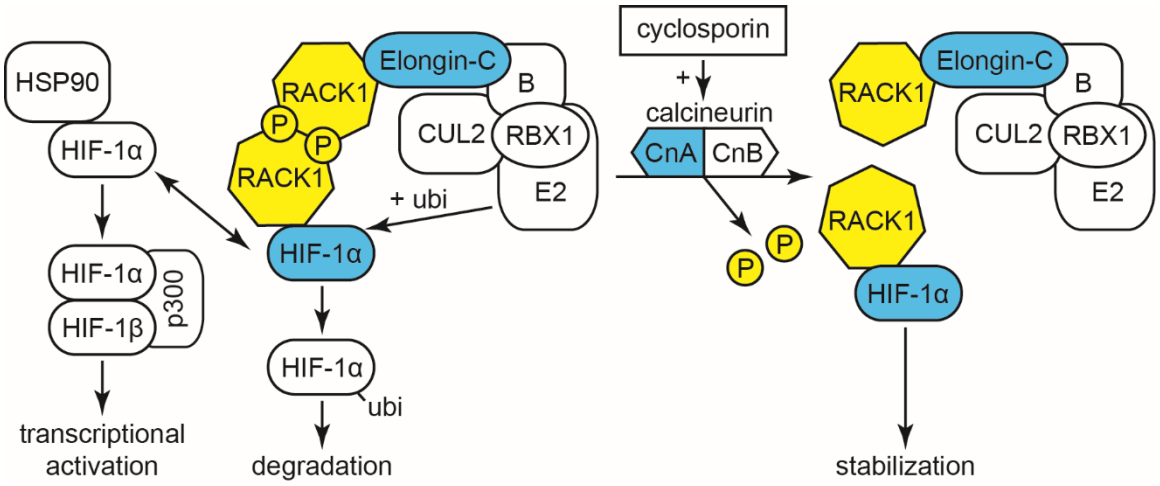

Figure 7. Model on RACK1-dependent and oxygen-independent regulation of HIF-1α stability. RACK1 competes with HSP90 (or SEPT9_v1, not depicted here) for binding to the transcription factor subunit HIF-1α. HSP90-bound HIF-1α is stabilized and can interact with the HIF-1β-subunit and coactivators, such as p300, to induce transcription of target genes. RACK1-bound HIF-1α, however, is recruited to Elongin-C that is part of an E3 ubiquitin ligase complex further consisting of Elongin-B (B), Cullin-2 (CUL2), ring box protein 1 (RBX1), and an E2 ubiquitin-conjugating enzyme (E2). HIF-1α is ubiquitinated and degraded by the 26S proteasome. Localization to the ligase complex is achieved through interaction of RACK1 with Elongin-C. Since both Elongin-C and HIF-1α interact with the sixth WD40 repeat of RACK1, dimerization of the β-propeller protein is required. Dimerization involves the fourth WD40 repeat of each RACK1 monomer and seems to require phosphorylation at S146. RACK1 can interact with the catalytic subunit CnA of the phosphatase calcineurin (CnB is the regulatory subunit). Calcineurin can become activated by cyclosporine and subsequently dephosphorylates RACK1 leading to dissociation of the dimer and thus stabilization of HIF-1α. The figure is modified from Liu et al. (2007a and b). RACK1-interacting proteins are highlighted in blue.

acid residue S146 within the fourth WD40 repeat. RACK1 dimer formation is impaired by activation of the calcium induced protein phosphatase 2B (PP2B) that is also known as calcineurin. The interaction of RACK1 with the catalytic subunit of calcineurin seems to result in dephosphorylation of RACK1 at S146 leading to dissociation of the RACK1 homodimer into its subunits and thus stabilization of HIF-1α (Figure 7, Liu et al., 2007b).

RACK1 further induces the degradation of the pro-apoptotic factor BimEL (Zhang et al., 2008). In the presence of the apoptosis inducing agent paclitaxel, RACK1 mediates the interaction of BimEL with an E3 ligase complex resulting in ubiquitination and proteasome-dependent degradation of BimEL. Through this mechanism, RACK1 could protect cancer cells from apoptosis leading to tumor growth and drug resistance (Zhang et al., 2008).

RACK1 also affects the stability of the transcription factor c-Jun by regulating its interaction with Fbw7, the subunit for substrate recognition of an E3 ubiquitin ligase complex (Zhang et al., 2012a). The N-terminus of the oncoprotein c-Jun can be phosphorylated by the JNKs leading to increased transcriptional activity, DNA-binding, and stability of the protein (Papavassiliou et al., 1995; Musti et al., 1997; Weiss et al., 2003). RACK1 mediates interaction between N-terminally non-phosphorylated c-Jun and Fbw7 leading to ubiquitination and subsequent degradation of the transcription factor (Figure 6, Zhang et al., 2012a). N-terminally phosphorylated c-Jun, however, is excluded from this complex and thus stabilized. This further strengthens the role of the β-propeller protein in tumorigenesis (Zhang et al., 2012a).

In summary, RACK1 regulates degradation of HIF-1α, BimEL, and c-Jun through mediating their interaction with the respective ubiquitin E3 ligase complex. Furthermore, RACK1 induces ubiquitination and subsequent degradation of the pro-apoptotic protein Fem1b and the ΔNp63 transcription factor (Fomenkov et al., 2004; Subauste et al., 2009). Thus, RACK1 is an important regulator in post-translational regulation of protein expression for specific target proteins.

1.5 Regulation of Asc1p/RACK1 through post-translational modifications

Asc1p and its orthologues from higher eukaryotes interact with a plethora of different proteins. The Saccharomyces *Genome Database* (SGD, http://www.yeastgenome.org) currently lists 85 proteins as physical interaction partners of Asc1p. Some of these interactions might occur indirectly via the formation of multi-protein complexes, but others were shown to involve direct protein-protein interaction, such as the binding of the eIF3c-subunit Nip1p to Asc1p (Kouba et al., 2012). The Nip1p interaction site lies within WD

repeats 1 to 3 of Asc1p (Kouba et al., 2012). Based on the crystal structure of the yeast 80S ribosome, the sites within Asc1p that interact with the ribosomal proteins Rps3, Rps16, and Rps17, (which are not included in the SGD list of interaction partners), can be precisely mapped (Figure 2, Ben-Shem et al., 2011). The interaction surface of the Asc1p homodimer is formed by blades 3 and 4 of each Asc1p monomer according to the crystal structure of the recombinantly expressed protein (Yatime et al., 2011). For all other direct physical interaction partners of Asc1p, the binding site has not been confined so far.

In contrast, the binding sites of many metazoan RACK1 interaction partners have been mapped to more specific regions within the β-propeller protein. Figure 8 illustrates that many RACK1 interaction partners share identical or overlapping binding sites. Many of these interactions might not interfere with each other because they are, for example, organism-, tissue-, or cell line-specific. However, considering all the additional interaction partners that are not included in Figure 8, the RACK1 interaction network demands multiple regulatory mechanisms, such as the post-translational modification of RACK1 itself. The previous chapters of this work already provided examples for a regulation of mammalian RACK1 through phosphorylation: The interaction of RACK1 with the focal adhesion kinase becomes stabilized through phosphorylation at Y52 by the c-Abl kinase (Kiely et al., 2009). Phosphorylation of mammalian RACK1 at Y246 by the Src kinase increases the interaction of RACK1 and Src and leads to inhibition of the kinase activity (Chang et al., 2001; Chang et al., 2002). Phosphorylation of RACK1 at Y246 further regulates its interaction with the mRNA-binding protein ZBP1 within transport RNPs in neurons, thereby modulating the translation of β-actin mRNA (Ceci et al., 2012). Moreover, RACK1 interacts with the MAPK p38b of *D. melanogaster* and was shown to be phosphorylated by this kinase at serine and/or threonine residues *in vitro* (Belozerov et al., 2014). In mammals, RACK1 is phosphorylated by the AMP-activated protein kinase at T50 during the onset of autophagy. This modification enhances the binding of RACK1 to components of the Atg14L-Beclin 1-Vps34-Vps15 complex and consequently promotes the formation of the autophagy initiation complex (Zhao et al., 2015).

Although the β-propeller structure is described as a rigid scaffold for protein-protein interactions, the Asc1/RACK1 proteins of *S. cerevisiae*, *H. sapiens*, and *A. thaliana* were shown to harbor flexible regions (Tarnowski et al., 2014). Thus, phosphorylation of Asc1p/RACK1 might contribute to define the shape of the β-propeller. RACK1 was reported to form homodimers in dependence on its phosphorylation at S146 (Liu et al., 2007b), and according to the crystal structure of the *S. cerevisiae* homodimer this interaction requires

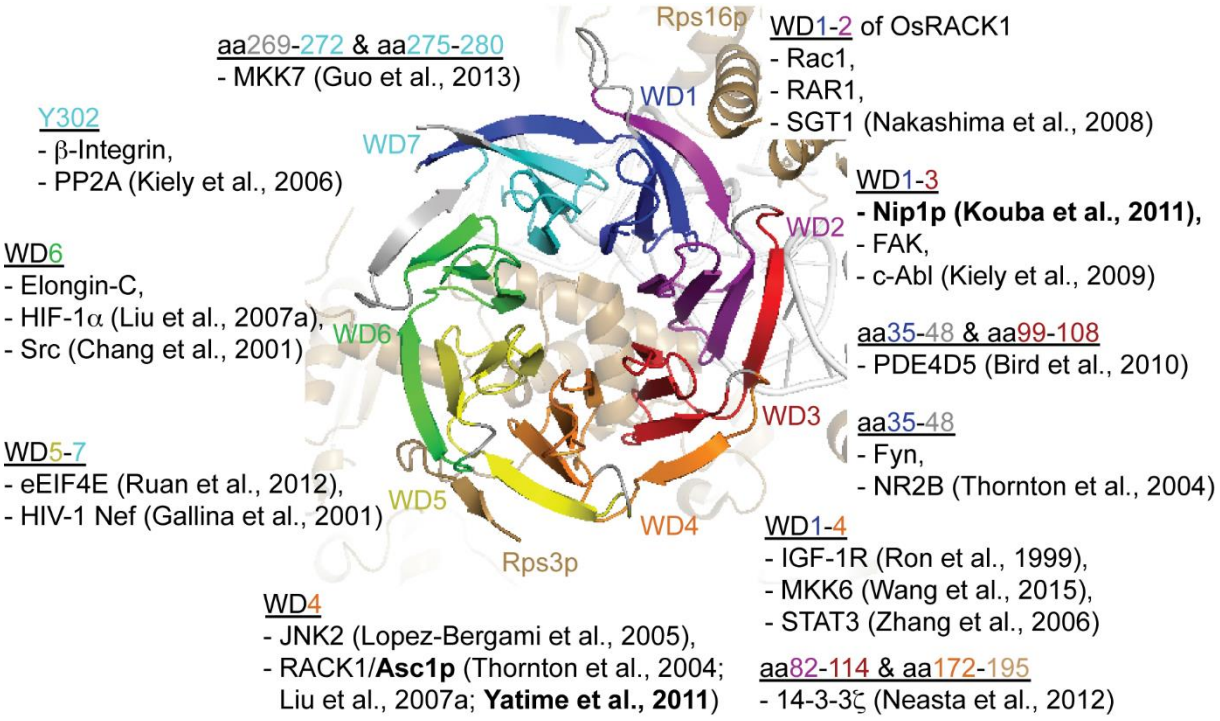

Figure 8. RACK1 interaction map.
The crystal structure of human RACK1 is shown bound to the 40S subunit of the ribosome. The WD40 repeats are differentially colored, and the remaining parts of RACK1 depicted in gray. The surrounding text indicates the localization of RACK1 binding sites for the named interactions partners. Besides interaction partners of metazoan RACK1, also *O. sativa* (Os) RACK1 and *S. cerevisiae* Asc1p binding partners (printed in bold) are included. The depiction of human RACK1 at the ribosome was modeled using the *PyMOL Molecular Graphics System* software on the basis of the PDB files with the IDs 4AOW (Ruiz Carrillo et al., 2012) and 4V88 (Ben-Shem et al., 2011) through merging the structure of human RACK1 on the position of *S. cerevisiae* Asc1p at the ribosome.

drastic rearrangement of the fourth blade of each monomer that might be indeed regulated through phosphorylation in this region (Figure 1D, Yatime et al., 2011). Phosphorylation of RACK1 might further regulate the turn-over of the protein as it was shown for *A. thaliana* RACK1A, which seems to be destabilized through phosphorylation by the with no lysine kinase 8 (WNK8, Urano et al., 2015).

So far, there exists no knowledge about a regulation of *S. cerevisiae* Asc1p through post-translational modifications, although high-throughput studies identified several amino acid residues as targets for modifications. These modifications comprise phosphorylation (Chi et al., 2007; Smolka et al., 2007; Gnad et al., 2009; Holt et al., 2009), acetylation (Henriksen et al., 2012), succinylation (Weinert et al., 2013), and ubiquitination (Swaney et al., 2013). The high degree of conservation of Asc1p on the level of the amino acid sequence might also apply to some of its post-translational modifications. Thus, the analysis of post-translational modifications of *S. cerevisiae* Asc1p might reveal conserved features for the regulation of this protein.

1.6 Aim of this study

The exposed position of the Asc1p β-propeller at the head of the 40S ribosomal subunit and its association with components of signal transduction pathways suggest a function of Asc1p as an interface between the translation machinery and signal transduction. To understand the function of Asc1p in cellular signaling in *S. cerevisiae*, the Asc1p-dependent phospho-proteome was analyzed. Since mammalian RACK1 has been reported to recruit kinases to the ribosome for the phosphorylation of translation initiation factors, a special interest was on proteins that contain Asc1p-sensitive phosphorylation sites and are associated to translational or co-translational processes. Due to its known association with components of phosphorylation cascades, Asc1p itself might be a target of regulatory phosphorylation. Here, phosphorylation sites of Asc1p should be identified, and their impact on Asc1p's function should be characterized through their targeted mutation to phosphorylation- or dephosphorylation-mimicking residues. Phenotypic characterization of the resulting mutant strains should reveal their importance for the functional integrity of Asc1p. Phosphorylation of Asc1p might support signal transduction to the translational machinery to adjust it to cellular needs. This might result in translational regulation of specific transcripts. Here, mRNAs were sought for that show Asc1p-dependent translation efficiency. Altogether, the results aim to contribute to characterize the function of the ribosomal protein Asc1 in signal transduction.

2. Materials and Methods

For centrifugation of samples in 1.5 ml or 2 ml reaction tubes, the Hereaus Instruments *Biofuge Pico* or *Hereaus Fresco 17* centrifuge (Thermo Scientific, Waltham, Massachusetts, USA) was used, and for centrifugation of samples in 15 ml or 50 ml tubes the eppendorf *Centrifuge 5804 R* (Eppendorf Wesseling-Berzdorf, Germany), the Sigma *Laboratory Centrifuge 4K15C* (Sigma Laborzentrifugen, Osterode am Harz, Germany) or the Hettich *Rotanta/RP* centrifuge (Hettich Lab Technology, Tuttlingen, Germany) was used. For picture editing, *Adobe Photoshop Elements 5.0/CS4/CS6* and *Adobe Illustrator CS4/CS6* (Adobe Systems, San Jose, California, USA) were applied, and for text and data processing *Microsoft Word* and *Excel 2007/2010* (Microsoft, Redmond, Washington, USA) were used.

2.1 *S. cerevisiae* strains

The *S. cerevisiae* strains used in this study are of the Σ1278b background (except for the BY4741-derived strain Y02724) and are listed in Table 1. For the generation of the *asc1SNR24* (*asc1*$^{-}$) strain that expresses the snoRNA U24, but not Asc1p, a *loxP::URA3::loxP* cassette was integrated in exon 1 of *ASC1* resulting in strain RH3514. The marker was rescued through transient transformation with plasmid-borne Cre-recombinase (pSH63). This resulted in strain RH3510 with a *loxP* site in the *ASC1* ORF that abrogates the translation of the mRNA (Rachfall et al., 2013). An *ASC1* deletion strain (RH3500) was generated through replacement of the *ASC1* gene by a *loxP::URA3::loxP* cassette amplified from plasmid pUG72 according to Gueldener et al. (2002). This strain was used for subsequent construction of strains with the *ASC1* cDNA (RH3502) or with *ASC1* alleles carrying different codon-exchanges within the open-reading frame at the *ASC1* locus (RH3529-RH3551, RH3574-RH3598, RH3611-RH3616, RH3623-RH3631, RH3635-RH3644). The transformation cassettes contained the *ASC1* cDNA or the mutated *asc1*-alleles carrying flanking regions identical to those of the *ASC1* gene for homologues recombination. Transformants were selected for their resistance against 5-fluoroorotic acid (0.5 mg/ml; #R0812, Thermo Fisher Scientific, Waltham, Massachusetts, USA) due to the loss of the *URA3* marker gene. Successful transformations were verified by polymerase chain reaction (PCR, chapter 2.5.1), Southern blot (chapter 2.7), and sequencing of the *ASC1* locus (chapter 2.5.5). Arginine or arginine and lysine auxotrophic strains RH3487-RH3494 and RH3570-RH3573 derived from strains RH2817 (*ASC1*), RH3263 (Δ*asc1*), and RH3549 (*asc1*DE), respectively. The *ARG4* and *LYS1* genes were also replaced with the recyclable *loxP::URA3::loxP* marker according to Gueldener et al. (2002). As already described, strains

were transiently transformed with plasmid-borne Cre-recombinase (pSH63) for marker rescue. An arginine and lysine auxotrophic *asc1*$^{-}$ strain was generated from the *ASC1* Δ*arg4::loxP* Δ*lys1::loxP* strain RH3493 as already described: Integration of a *loxP::URA3::loxP* cassette in exon 1 of *ASC1* resulted in strain RH3519. The subsequent rescue of the *URA3*-marker led to strain RH3520 with a *loxP* site in exon 1 of *ASC1*. For metabolic labeling with isotopically-labeled arginine and lysine, Δ*arg4::loxP* Δ*lys1::loxP* strains RH3493 (*ASC1*), RH3520 (*asc1*$^{-}$), RH3573 (*asc1*DE), and RH3494 (Δ*asc1*) were used. Strains RH3431 (*ASC1*), RH3504 (*asc1*$^{-}$), and RH3599 (*asc1*DE) expressing C-terminally 3xmyc-tagged Flo8p were constructed by transformation of RH2817, RH3510, and RH3549 according to Janke et al. (2004). *HBN1* and *YHB1* deletion strains were generated as described for the *ARG4* and *LYS1* deletion strains using the *loxP::kanMX::loxP* cassette that was amplified from plasmid pUG6 according to Gueldener et al. (2002).

Table 1. *S. cerevisiae* strains used in this study.
For Asc1p phospho-site mutations that caused Asc1p-dependent phenotypes at least two independent clones with individual strain designations were generated and tested. The only exception is the *asc1*^{T12A}DE strain.

Strains	Genotype	Reference
RH2817	*MATα, ura3-52, trp1::hisG*	Valerius et al., 2007
RH3263	*MATα, ura3-52, trp1::hisG, leu2::hisG,* Δ*asc1::LEU2*	Valerius et al., 2007
Y02724	BY4741, Mat a, *his3Δ1,* Δ*leu2,* Δ*met15,* Δ*ura3, YLR113w(HOG1)::kanMX4*	Euroscarf collection
RH3461	*MATα, ura3-52, trp1::hisG,* Δ*yhb1::kanMX*	Rachfall et al., 2013
RH3462	*MATα, ura3-52, trp1::hisG, leu2::hisG,* Δ*asc1::LEU2,* Δ*yhb1::kanMX*	Rachfall et al., 2013
RH3463	*MATα, ura3-52, trp1::hisG,* Δ*hbn1::kanMX*	Rachfall et al., 2013
RH3464	*MATα, ura3-52, trp1::hisG, leu2::hisG,* Δ*asc1::LEU2,* Δ*hbn1::kanMX*	Rachfall et al., 2013
RH3497	*MATα, ura3-52, trp1::hisG,* Δ*hbn1::loxP,* Δ*yhb1::kanMX*	Rachfall et al., 2013
RH3498	*MATα, ura3-52, trp1::hisG, leu2::hisG,* Δ*asc1::LEU2,* Δ*hbn1::loxP,* Δ*yhb1::kanMX*	Rachfall et al., 2013
RH3514	*MATα, ura3-52, trp1::hisG, asc1-URA3 SNR24*	Nadine Smolinski (Master thesis, MT)
RH3510	*MATα, ura3-52, trp1::hisG, asc1-loxP SNR24*	Rachfall et al., 2013
RH3500	*MATα, ura3-52, trp1::hisG,* Δ*asc1::URA3*	Sabrina Sander (MT)
RH3502	*MATα, ura3-52, trp1::hisG, ASC1* Δ*snr24*	Sabrina Sander (MT)
RH3549, RH3550	*MATα, ura3-52, trp1::hisG, asc1*DE	This work

Table 1. continued 1.

Strains	Genotype	Reference
RH3431	*MATα, ura3-52, trp1::hisG, FLO8*-myc^{3}-*TRP1*	Rachfall et al., 2013
RH3504	*MATα, ura3-52, trp1::hisG, asc1-loxP SNR24, FLO8*-myc^{3}-*TRP1*	Rachfall et al., 2013
RH3599	*MATα, ura3-52, trp1::hisG, asc1*DE, *FLO8*-myc^{3}-*TRP1*	This work
RH3623, RH3624, RH3625	*MATα, ura3-52, trp1::hisG, asc1*^{T12A}	This work
RH3626	*MATα, ura3-52, trp1::hisG, asc1*^{T12A}DE	This work
RH3627, RH3628, RH3629	*MATα, ura3-52, trp1::hisG, asc1*^{T12E}	This work
RH3630, RH3631	*MATα, ura3-52, trp1::hisG, asc1*^{T12E}DE	This work
RH3529	*MATα, ura3-52, trp1::hisG, asc1*^{T96A}	This work
RH3539, RH3540, RH3541	*MATα, ura3-52, trp1::hisG, asc1*^{T96A}DE	This work
RH3530	*MATα, ura3-52, trp1::hisG, asc1*^{T96E}	This work
RH3542, RH3543	*MATα, ura3-52, trp1::hisG, asc1*^{T96E}DE	This work
RH3531	*MATα, ura3-52, trp1::hisG, asc1*^{T99A}	This work
RH3611, RH3612, RH3613	*MATα, ura3-52, trp1::hisG, asc1*^{T99A}DE	This work
RH3532	*MATα, ura3-52, trp1::hisG, asc1*^{T99E}	This work
RH3614, RH3615, RH3616	*MATα, ura3-52, trp1::hisG, asc1*^{T99E}DE	This work
RH3533, RH3534, RH3535	*MATα, ura3-52, trp1::hisG, asc1*$^{T96A\ T99A}$	This work
RH3544, RH3545, RH3546	*MATα, ura3-52, trp1::hisG, asc1*$^{T96A\ T99A}$DE	This work
RH3537, RH3538	*MATα, ura3-52, trp1::hisG, asc1*$^{T96E\ T99E}$	This work
RH3547, RH3548	*MATα, ura3-52, trp1::hisG, asc1*$^{T96E\ T99E}$DE	This work
RH3551	*MATα, ura3-52, trp1::hisG, asc1*^{S120A}	This work
RH3575, RH3576, RH3577	*MATα, ura3-52, trp1::hisG, asc1*^{S120A}DE	This work
RH3574	*MATα, ura3-52, trp1::hisG, asc1*^{S120E}	This work
RH3578, RH3579, RH3580	*MATα, ura3-52, trp1::hisG, asc1*^{T143A}	This work
RH3584, RH3585, RH3586	*MATα, ura3-52, trp1::hisG, asc1*^{T143A}DE	This work
RH3581, RH3582, RH3583	*MATα, ura3-52, trp1::hisG, asc1*^{T143E}	This work
RH3587, RH3588, RH3589	*MATα, ura3-52, trp1::hisG, asc1*^{T143E}DE	This work
RH3590	*MATα, ura3-52, trp1::hisG, asc1*^{S166A}	This work
RH3638	*MATα, ura3-52, trp1::hisG, asc1*^{S166A}DE	This work
RH3591, RH3592	*MATα, ura3-52, trp1::hisG, asc1*^{S166E}	This work
RH3593, RH3594, RH3595	*MATα, ura3-52, trp1::hisG, asc1*^{T168A}	This work
RH3639, RH3640	*MATα, ura3-52, trp1::hisG, asc1*^{T168A}DE	This work
RH3596, RH3597	*MATα, ura3-52, trp1::hisG, asc1*^{T168E}	This work
RH3598	*MATα, ura3-52, trp1::hisG, asc1*$^{S166A\ T168A}$	This work
RH3536	*MATα, ura3-52, trp1::hisG, asc1*$^{S166A\ T168A}$DE	This work

Table 1. continued 2.

Strains	Genotype	Reference
RH3637	*MATα, ura3-52, trp1::hisG, asc1*$^{S166E\ T168E}$	This work
RH3635, RH3641, RH3642	*MATα, ura3-52, trp1::hisG, asc1*^{Y250F}	This work
RH3636, RH3643, RH3644	*MATα, ura3-52, trp1::hisG, asc1*^{Y250F}DE	This work
RH3487	*MATα, ura3-52, trp1::hisG,* Δ*arg4::URA3*	This work
RH3488	*MATα, ura3-52, trp1::hisG, leu2::hisG,* Δ*asc1::LEU2,* Δ*arg4::URA3*	This work
RH3489	*MATα, ura3-52, trp1::hisG,* Δ*arg4::loxP*	This work
RH3490	*MATα, ura3-52, trp1::hisG, leu2::hisG,* Δ*asc1::LEU2,* Δ*arg4::loxP*	This work
RH3491	*MATα, ura3-52, trp1::hisG,* Δ*arg4::loxP,* Δ*lys1::URA3*	This work
RH3492	*MATα, ura3-52, trp1::hisG, leu2::hisG,* Δ*asc1::LEU2,* Δ*arg4::loxP,* Δ*lys1::URA3*	This work
RH3493	*MATα, ura3-52, trp1::hisG,* Δ*arg4::loxP,* Δ*lys1::loxP*	This work
RH3494	*MATα, ura3-52, trp1::hisG, leu2::hisG,* Δ*asc1::LEU2,* Δ*arg4::loxP,* Δ*lys1::loxP*	This work
RH3519	*MATα, ura3-52, trp1::hisG, asc1-URA3 SNR24,* Δ*arg4::loxP,* Δ*lys1::loxP*	This work
RH3520	*MATα, ura3-52, trp1::hisG, asc1-loxP SNR24* Δ*arg4::loxP,* Δ*lys1::loxP,*	This work
RH3570	*MATα, ura3-52, trp1::hisG, asc1*DE, Δ*arg4::URA3*	This work
RH3571	*MATα, ura3-52, trp1::hisG, asc1*DE, Δ*arg4::loxP*	This work
RH3572	*MATα, ura3-52, trp1::hisG, asc1*DE, Δ*arg4::loxP,* Δ*lys1::URA3*	This work
RH3573	*MATα, ura3-52, trp1::hisG, asc1*DE, Δ*arg4::loxP,* Δ*lys1::loxP*	This work

2.2 Bacterial strain and plasmids

The *Escherichia coli* strain DH5α was used for preparation and amplification of plasmids (F', Φ80Δ*lacZ*Δ*M15,* Δ(*lacZYA-argF*)*, U169, deo*R, *rec*A1, *end*A1, *hsd*R17, (r_K^-, m_K^+), *sup*E44, λ-, *thi*-1, *gyr*A96, *rel*A1, Woodcock et al., 1989). Plasmids used in this study are listed in Table 2. Plasmid pME4132 was obtained through insertion of the *ASC1* gene into the pASK-IBA7plus plasmid (#2-1406-000, IBA, Göttingen, Germany) according to the provided instructions. To generate plasmid pME4135, *Strep-ASC1* was amplified from plasmid pME4132 introducing *Nhe*I and *Hind*III restriction sites for cloning into plasmid pME2835 (Nadine Smolinski, personal communication). Plasmid pME4041 was generated through

Table 2. Plasmids used in this study.

Plasmid	Description	Reference
pUG6	*Amp^R, pUCori, loxP::kanMX::loxP*	Gueldener et al., 2002
pUG72	*Amp^R, pUCori, loxP::URA3::loxP*	Gueldener et al., 2002
pSH63	*Amp^R, pUCori, GAL1Prom, cre, TRP1, CEN/ARS*	Gueldener et al., 2002
pME2791	pRS416*GAL1* with *GAL1Prom, CYC1Term, URA3, CEN/ARS*	Mumberg et al., 1994
pME2787	pRS426*MET25* with *MET25Prom CYC1Term, URA3*, 2µm	Mumberg et al., 1994
pME2624	*MET25Prom, CYC1Term, URA3*, 2 µm, *ASC1*	our collection
pME2834	*MET25Prom, CYC1Term, URA3*, 2 µm, *ASC1-Strep*	our collection
pME2835	*MET25Prom, CYC1Term, URA3*, 2 µm, *Strep-ASC1*	our collection
pME4041	*MET25Prom, CYC1Term, URA3*, 2 µm, *ASC1*-cDNA-*Strep*	N. Smolinski (MT)
pASK-IBA7plus	*AmpR, f1 origin, Strep*-tag, Xa cleavage site	IBA
pME4132	*AmpR, f1 origin, Strep-Xa-ASC1*	N. Smolinski
pME4135	*MET25Prom, CYC1Term, URA3*, 2 µm, *Strep-Xa-ASC1*	N. Smolinski
pME4364	pME2791 with *ASC1* and its native promoter (+500bp)	This work
pME4384	pME2791 with *asc1*R38DK40E (*asc1*DE) and the native *ASC1* promoter	This work
pME4124	pME2834 with *asc1*DE	This work
pME4365	pME4364 with *asc1*^{T12A}	This work
pME4366	pME4364 with *asc1*^{T12A}DE	This work
pME4367	pME4364 with *asc1*^{T12E}	This work
pME4368	pME4364 with *asc1*^{T12E}DE	This work
pME4025	pME2834 with *asc1*^{T96A}	N. Smolinski (MT)
pME4370	pME2834 with *asc1*^{T96A}DE	This work
pME4026	pME2834 with *asc1*^{T96E}	N. Smolinski (MT)
pME4371	pME2834 with *asc1*^{T96E}DE	This work
pME4027	pME2834 with *asc1*^{T99A}	N. Smolinski (MT)
pME4372	pME2834 with *asc1*^{T99A}DE	This work
pME4028	pME2834 with *asc1*^{T99E}	N. Smolinski (MT)
pME4373	pME2834 with *asc1*^{T99E}DE	This work
pME4029	pME2834 with *asc1*$^{T96A\ T99A}$	N. Smolinski (MT)
pME4125	pME2834 with *asc1*$^{T96A\ T99A}$DE	This work
pME4030	pME2834 with *asc1*$^{T96E\ T99E}$	N. Smolinski (MT)
pME4374	pME2834 with *asc1*$^{T96E\ T99E}$DE	This work
pME4120	pME2834 with *asc1*^{S120A}	This work

Table 2. continued.

Plasmid	Description	Reference
pME4375	pME4364 with *asc1*^{S120A}DE	This work
pME4121	pME2834 with *asc1*^{S120E}	This work
pME4122	pME2834 with *asc1*^{T143A}	This work
pME4376	pME2834 with *asc1*^{T143A}DE	This work
pME4123	pME2834 with *asc1*^{T143E}	This work
pME4377	pME2834 with *asc1*^{T143E}DE	This work
pME4031	pME2834 with *asc1*^{S166A}	N. Smolinski (MT)
pME4126	pME2834 with *asc1*^{S166A}DE	This work
pME4032	pME2834 with *asc1*^{S166E}	N. Smolinski (MT)
pME4033	pME2834 with *asc1*^{T168A}	N. Smolinski (MT)
pME4127	pME2834 with *asc1*^{T168A}DE	This work
pME4034	pME2834 with *asc1*^{T168E}	N. Smolinski (MT)
pME4035	pME2834 with *asc1*$^{S166A\ T168A}$	N. Smolinski (MT)
pME4128	pME2834 with *asc1*$^{S166A\ T168A}$DE	This work
pME4036	pME2834 with *asc1*$^{S166E\ T168E}$	N. Smolinski (MT)
pME4378	pME2834 with *asc1*^{Y250F}	This work
pME4379	pME2834 with *asc1*^{Y250F}DE	This work

amplification of the *ASC1* cDNA from a cDNA sample generated from total RNA of the Σ1278b strain background with primers introducing *Bam*HI and *Hind*III restriction sites for cloning into pME2834. The *QuantiTect Reverse Transcription Kit* (#205314, Qiagen, Hilden Germany) was used to generate cDNA from RNA according to the manufacturer's instructions. Plasmid pME4364 is derived from pME2791 and carries *ASC1* under control of its native promoter (+500 bp upstream of *ASC1* according to Kleinschmidt et al., 2006). *ASC1* was amplified together with its promoter from genomic *S. cerevisiae* DNA using oligonucleotides that introduced *Sac*I and *Hind*III restriction sites for subsequent cloning. Plasmids carrying *asc1* with codon exchanges were constructed via a two-step PCR strategy: In the first reaction, the codon exchange(s) was (or were) introduced within an oligonucleotide bearing the mutated codon(s) in its center using an *ASC1* wild-type carrying plasmid (pME2834 or pME4364) as template. Codons for serine and threonine were exchanged for GCT (alanine) as well as for GAA (glutamate). The tyrosine 250 codon was substituted for TTT (phenylalanine), and R38 and K40 encoding triplets were exchanged for GAT (aspartate) and GAA (glutamate), respectively. In the second PCR, the complete *asc1* allele was amplified flanked by the respective restriction sites for cloning into the parent

vector (*Bam*HI and *Hind*III restriction sites for cloning into pME2834 and *Sac*I and *Hind*III restriction sites for cloning into pME2791). For construction of plasmids pME4025-pME4036, pME4120-pME4128, pME4370-pME4374, and pME4376-pME4379, plasmid pME2834 served as the parent vector. Plasmid pME4364 served as parent vector for plasmids pME4365-pME4368, pME4375, and pME4384. For plasmids comprising the R38D K40E codon exchanges in combination with a phosphorylation site mutation, either plasmid pME4124 or pME4384 was used as template for PCR. Alternatively, plasmids that already comprised a phosphorylation site mutation were used as template for PCR, and the R38D K40E mutation was introduced by using oligonucleotides bearing the respective codon exchanges. The plasmids served as templates for amplification of transformation cassettes to integrate the mutated *asc1* alleles into the yeast genome at the original *ASC1* locus.

2.3 Cultivation of microorganisms

2.3.1 Cultivation of *S. cerevisiae*

Yeast strains were cultivated in liquid yeast nitrogen base medium (1.5 g/l YNB without amino acids and ammonium sulfate, 5 g/l ammonium sulfate, 2% glucose) containing the respective supplements or in yeast extract peptone dextrose (YEPD) medium (2% peptone, 1% yeast extract, 2% glucose). Solid media contained 2% agar. Minimal with vitamins (MV) plates contained 1.45 g/l YNB, 5.52 g/l ammonium sulfate, 10% succinic acid, 8.5 g/l KOH, and their pH was adjusted to 7.2. If required, 20 mg/l L-arginine, 20 mg/l L-histidine, 30 mg/l L-isoleucine, 30 mg/l L-lysine HCl, 20 mg/l L-methionine, 20 mg/l uracil, 20 mg/l L-tryptophan, 30 mg/l L-leucine, 150 mg/l L-valine. Yeast cells were grown at 30 °C. Liquid cultures were grown on a shaker (100 to 120 rpm), and growth of the cells was monitored by measuring the optical density (OD) at 600 nm. The inoculation volumes (V_i in ml) for main cultures were calculated with the formula:

$$V_i = (V_m \cdot OD_m \cdot e^{-\mu \cdot \Delta t})/OD_p$$

(V_m = volume of main-culture in ml, OD_m = desired optical density of the main-culture after Δt, OD_p = OD of pre-culture, μ = growth rate (0.29/h for YNB), Δt = growth time in h).

For SILAC-based phospho-proteome and proteome analyses cultures were grown in liquid YNB medium supplemented with 100 mg/l differentially labeled L-arginine as well as L-lysine. Stable isotopically labeled amino acids were purchased from Silantes (München, Germany): $^{13}C_6$-L-arginine HCl (#201203902), $^{13}C_6{}^{15}N_4$-L-arginine HCl (#201603902), 4,4,5,5-D_4-L-lysine HCl (#211103912), and $^{13}C_6{}^{15}N_2$-L-lysine HCl (#211603902). Further experiment-specific growth conditions are described in the respective paragraphs.

2.3.2 Cultivation of *E. coli*

E. coli cells were cultivated in liquid lysogeny broth (LB) medium (1% bacto-trypton, 0.5% yeast extract, 1% NaCl) on a shaker at 37 °C. The medium was supplemented with 100 µg/ml ampicillin for selective conditions. Solid media contained 2% agar.

2.4 Isolation of DNA from microorganisms

2.4.1 Plasmid DNA purification from *E. coli*

For isolation of plasmid DNA, *E. coli* cells of a 5 ml LB overnight culture were harvested by centrifugation, and plasmids were isolated using the *QIAprep Spin Miniprep Kit* (#27106, Qiagen) according to the manufacturer's instructions. Plasmid DNA was eluted with 50 µl H_2O. For PCR, samples were diluted 1:50.

2.4.2 Isolation of DNA from *S. cerevisiae* cells

Cells were grown overnight in 10 ml YEPD medium to saturation and harvested by centrifugation for isolation of DNA according to Hoffman and Winston (1987). The pellet was washed in 0.5 ml H_2O and transferred to a 1.5 ml reaction tube. After spinning down the cells, the supernatant was discarded, and the cells were disrupted in the presence of 0.2 ml lysis buffer (2% Triton X-100, 1% SDS, 100 mM NaCl, 10 mM Tris pH 8.0, 1 mM EDTA), 0.2 ml phenol/chloroform/isoamylalcohol (25:24:1, #A156.2, Carl Roth, Karlsruhe, Germany), and an equal volume of glass beads. Cells were disrupted through vigorous shaking for 3 to 4 min. 0.2 ml H_2O were added, and the samples were centrifuged for 5 min at 13,000 rpm. The upper aqueous layer was transferred into a new tube, and 0.2 ml phenol/ chloroform/isoamylalcohol were added. The samples were mixed and centrifuged again at 13,000 rpm for 5 min. The upper phase was transferred into a new tube, and DNA was precipitated by adding 1 ml ethanol followed by incubation at -20 °C for several minutes or overnight. Samples were centrifuged for 5 min at 13,000 rpm followed by removal of the supernatant. Pellets were dissolved in 0.4 ml H_2O, and 3 µl RNase A (10 mg/ml) was added. After 5 to 10 min incubation at 37 °C, 10 µl 4 M ammonium acetate and 1 ml ethanol were added, and samples were stored again at -20 °C to precipitate the DNA. After centrifugation at 13,000 rpm for 5 min, the supernatant was discarded, pellets were dried and then dissolved in 40 to 50 µl H_2O. For PCR, samples were diluted 1:50.

2.5 Cloning techniques

2.5.1 Polymerase chain reaction

DNA was amplified with the polymerase chain reaction (PCR; Saiki et al., 1985). Depending on the subsequent application of the amplified PCR product, different thermostable polymerases were used. For amplification of DNA for site-specific homologous recombination and plasmid construction, *Phusion* High-Fidelity DNA polymerase (#F-530L, Thermo Scientific), *Pfu* DNA polymerase (#EP0572, Thermo Scientific), or *KOD* DNA polymerase (#71085-3, Merck, Darmstadt, Germany) were used. For analytic PCRs, *Taq* DNA polymerase (#EP0404, Thermo Scientific) was applied. 10 mM dNTP stocks (prepared from dATP #0141, dCTP #R0151, dGTP #R0161, dTTP #0171, Thermo Scientific) were used accept for the *KOD* polymerase that was provided together with a 2 mM dNTP stock (molarities apply to each dNTP). All polymerases were used according to the manufacturer's instructions. Primers for PCR were ordered from Eurofins MWG Operon (Ebersberg, Germany).

2.5.2 Restriction digestion of DNA

DNA was digested with type II restriction endonucleases for plasmid construction or prior to Southern blot analysis. Restriction enzymes and their respective buffers (Thermo Scientific or New England Biolabs, Frankfurt am Main, Germany) were used according to the manufacturer's instructions in a sample volume of 20 µl. Samples were incubated for at least 1.5 h at 30 °C or 37 °C depending on the applied enzyme.

2.5.3 Agarose gel electrophoresis

DNA samples were mixed with 0.1 volumes of 10x loading dye (10% Ficoll 400, 200 mM EDTA, pH 8.0, 0.2% bromphenol blue sodium salt, 0.2% xylene cyanol) and applied on horizontal 1% agarose gels containing 0.5 µg/ml ethidium bromide. Agarose gels were prepared in TAE buffer (40 mM Tris base, 20 mM acetic acid, 1 mM EDTA) that was also used as running buffer for separation of the DNA fragments through electrophoresis at 90 V (Voytas, 2001). For visualization of DNA, the *Gel iX20 Imager* (Intas Science Imaging Instruments, Göttingen, Germany) was used. If applicable, DNA bands were excised from agarose gels under UV light, and DNA was extracted using the *QIAquick Gel Extraction Kit* (#28706, Qiagen) according to the manufacturer's instructions.

2.5.4 Ligation of DNA fragments

For ligation of linear DNA fragments, 1 µl T4 DNA ligase (#EL0016, Thermo Scientific), 3 µl of the supplied 10x ligation buffer (Thermo Scientific), 50 to 100 ng digested plasmid DNA, and a 2- to 5-fold excess of insert DNA (or H_2O for controls) were mixed and filled up to 30 µl with H_2O. The sample was incubated for at least 10 min at room temperature and subsequently used for transformation of *E. coli* cells.

2.5.5 DNA sequencing

100 ng of DNA and 5 pmol of the appropriate primer in a volume of 5 µl were submitted to the *Göttingen Genomics Laboratory* (G2L, Göttingen, Germany) for sequencing. Alternatively, sequencing of DNA was carried out by the *SEQLAB Sequencing Laboratories Göttingen GmbH* (Göttingen, Germany): 18 ng per 100 bp of template DNA was used for linear DNA fragments and 720 to 1200 ng for sequencing of plasmids in a final volume of 12 µl. 3 µl of the primer (10 pmol/µl) were added.

2.6 Transformation procedures

2.6.1 Transformation of *E. coli*

Preparation of competent *E. coli* cells was performed according to Inoue et al. (1990). For the preparation of competent *E. coli* cells, 250 ml super optimal broth (SOB) medium (2% tryptone, 0.5% yeast extract, 10 mM NaCl, 2.5 mM KCl, 10 mM $MgCl_2$, 10 mM $MgSO_4$) were inoculated with DH5α cells and incubated at 20 °C at 200 rpm for at least 24 h until an OD_{600} of 0.6 was reached. Cells were placed on ice for 10 min and harvested by centrifugation at 2,500 x g for 10 min at 4 °C. The pellet was resuspended in 80 ml transformation buffer (TB, 10 mM HEPES, 15 mM $CaCl_2$, 250 mM KCl, pH 6.7, 55 mM $MnCl_2$). Cells were stored on ice for 10 min and centrifuged at 2,500 x g for 10 min at 4 °C. The pellet was gently resuspended in 20 ml TB buffer. 1.4 ml DMSO was added with swirling, and cells were incubated for 10 min on ice. Aliquots were prepared, frozen in liquid nitrogen, and stored at -80 °C. For the transformation of *E. coli*, competent cells were thawed on ice. Samples from the DNA ligation were each mixed with 200 µl of these cells. After incubation on ice for 30 min, samples were placed at 42 °C for 90 sec and then placed back on ice for 3 min. Each sample was mixed with 800 µl LB medium and incubated at 37 °C for 1 h on a shaker. After centrifugation at 5,000 rpm for 2 min, the supernatant was discarded. Cells were resuspended in the remaining liquid and spread on solid selective media. Plates were incubated overnight at 37 °C.

2.6.2 Transformation of *S. cerevisiae*

Transformations were performed using the lithium acetate method (Ito et al., 1983). 600 to 800 µl of a 10 ml YEPD pre-culture were transferred to 10 ml fresh YEPD medium and incubated for additional 5 to 6 h. Cells were harvested by centrifugation at 2,000 rpm for 3 min. The cell pellet was resuspended in 10 ml lithium acetate/TE buffer (100 mM lithium acetate, 10 mM Tris-HCl, 1 mM EDTA, pH 8.0). For genomic transformations using linear DNA fragments, cells were incubated for 15 to 20 min on a shaker. For transformation of plasmid DNA, cells were only briefly incubated. Samples were centrifuged again at 2,000 rpm for 3 min. The supernatant was discarded, and cells were resuspended in the remaining liquid. The volume was filled up to 400 µl, and the sample was divided into two 200 µl aliquots. To one of the samples the linear DNA of the transformation cassette or the plasmid DNA was added, while the second one served as negative control. 20 µl of pre-warmed (65 °C) carrier DNA (salmon sperm DNA, 10 mg/ml in TE buffer, pH 8.0) were added to both samples. For the transformation of the same strain with more than one linear DNA fragment or plasmid, all volumes were adjusted accordingly. Samples were mixed with 800 µl 50% PEG 4000 (prepared in lithium acetate/TE buffer) and incubated at 30 °C for 30 min followed by a heat shock at 42 °C for 25 min. Samples were centrifuged at 7,000 rpm for 30 sec, and the supernatant was removed. Cells were resuspended in 1 ml YEPD medium and incubated for 1 h (transformation of plasmid DNA) or 3 h (chromosomal integration) at 30 °C on a shaker. Cells were harvested by centrifugation at 4,000 rpm for 10 to 20 sec. Most of the supernatant was discarded. Cells were resuspended in the remaining liquid, spread onto solid selective media, and incubated for at least 3 d until colonies formed.

2.7 Southern blot analysis

Integration of DNA fragments at the correct locus in the genome of *S. cerevisiae* was confirmed by Southern analysis according to Southern (1975). Chromosomal DNA was digested overnight with the respective restriction enzymes (Thermo Scientific). Samples were heated at 65 °C for 10 min, mixed with loading dye, and applied onto 1% agarose gels. DNA fragments were separated according to their size at 70 V for 10 min followed by 90 V for 90 min. Gels were then washed with the first washing buffer (0.25 M HCl) for 10 min, with the second (0.5 M NaOH, 1.5 M NaCl) for 25 min, and with the third (1.5 M NaCl, 0.5 M Tris, pH 7.5) for 30 min. Afterwards, the DNA was transferred onto a nylon membrane (Hybond-N Membrane, #RPN203N, GE Healthcare, München, Germany) by capillary blotting for at least 3 h. The membrane was then dried at 75 °C for 7 min, and the DNA was

cross-linked to the membrane through 3 min exposure of each side of the membrane to UV light. The membrane was incubated at 55 °C for 30 min in prewarmed hybridization buffer (0.5 M NaCl, 4% Blocking Reagent, #NIP552, GE Healthcare), and the labeled probe was added for hybridization overnight. Probes were labeled using the *AlkPhos Direct Labeling Reagents* (#RPN3680, GE Healthcare) according to the manufacturer's instructions. The membranes were washed twice with the first washing buffer (2 M urea, 0.1% SDS, 50 mM sodium phosphate pH 7.0, 150 mM NaCl, 1 mM $MgCl_2$, 0.2% Blocking Reagent) at 55 °C for 10 min and twice with the second washing buffer (50 mM Tris base, 100 mM NaCl, 2 mM $MgCl_2$, pH 10) at room temperature for 5 min. For the chemiluminescence reaction, the membrane was incubated with 1 ml of the CDP-Star Detection Reagent (#RPN3682, GE Healthcare). For detection of chemiluminescence, membranes were exposed to the *Amersham Hyperfilm™-ECL™* (GE Healthcare) followed by development of the film.

2.8 Protein analyses

2.8.1 Preparation of whole-cell protein extracts from *S. cerevisiae*

This paragraph describes preparation of protein extracts for Western blot analyses as well as proteome analyses. In case that the protocol differs for other applications, the changes are specified in the respective paragraphs. In general, *S. cerevisiae* cultures were grown in 50 ml YNB medium to midlog phase (OD_{600} = 0.8, 40 ml cultures for proteome analysis) and harvested by centrifugation at 3,000 rpm for 4 min at 4 °C. Cells were washed with ice-cold breaking buffer (100 mM Tris-HCl pH 7.5, 200 mM NaCl, 20% glycerol, 5 mM EDTA) and lysed in 500 µl breaking buffer supplemented with 0.5% β-mercaptoethanol, 1 *cOmplete*™ protease inhibitor tablet (#11836145001, Roche Diagnostics, Mannheim, Germany) per 50 ml, 1 *PhosSTOP*™ phosphatase inhibitor cocktail tablet (#04906837001, Roche Diagnostics) per 10 ml, 1 mM NaF, 8 mM β-glycerol phosphate, and 0.5 mM sodium vanadate through vigorous shaking (frequency 30 sec^{-1}, 4 min) with an equal volume of glass beads (Ø 0.25 to 0.50 mm) using the mixer mill *Retsch MM400* (Retsch, Haan, Germany). The samples were incubated in the presence of 4% SDS at 65 °C for 10 min. Samples were subjected to centrifugation at 13,000 rpm for 15 min at room temperature, and the supernatant was collected as protein extract. Protein concentrations were determined using the BCA reagent (#23224 and #23228, Thermo Fisher Scientific) according to the manufacturer's instructions.

2.8.2 Purification of Strep-tagged Asc1p

For identification of Asc1p phospho-sites, strain RH3263 (Δ*asc1*) was transformed with plasmid pME2834 (*ASC1-Strep*) or pME4135 (*Strep-Xa-ASC1*) and cultivated in 1 to 10 l liquid YNB medium to an OD_{600} of 0.8. Harvested cells were washed with ice-cold breaking buffer (10 mM HEPES pH 7.9, 10 mM KCl, 1.5 mM $MgCl_2$) and lysed in breaking buffer (approximately 5 times the volume of the cell pellet) supplemented with 0.5 mM PMSF, 0.5 mM DTT, and protease and phosphatases inhibitors (as described before) through vigorous shaking with glass beads. Samples were centrifuged at 13,000 rpm for 15 min at 4 °C, and the supernatant was applied on *Strep-Tactin® sepharose®* columns for affinity purification of Strep-tagged Asc1p (*Strep-tag® Starter Kit*, #2-1101-000, IBA). The purification was performed at 4 °C following the instructions of the manufacturer's protocol. Eluate fractions were subjected to SDS-polyacrylamide gel electrophoresis (SDS-PAGE, chapter 2.8.3).

For identification of Asc1p and Asc1DEp interaction partners, strain RH3494 (Δ*asc1* Δ*arg4* Δ*lys1*) was transformed with plasmids pME2834 (*ASC1-Strep*), pME4124 (*asc1DE-Strep*), and pME2624 (*ASC1*), respectively. The resulting three different strains were cultivated in 150 ml YNB medium supplemented with differentially labeled amino acids to an OD_{600} of 0.8. Cell pellets were washed with the wash buffer (100 mM Tris-HCl, pH 8.0, 150 mM NaCl, 1 mM EDTA) of the *Strep-tag® Starter Kit*, harvested by centrifugation and resuspended in 500 µl of the same buffer supplemented with 0.5 mM PMSF, 0.5 mM DTT, and protease and phosphatase inhibitors (as described before). Cells were lysed through vigorous shaking with glass beads. Samples were centrifuged for 8 min at 13,000 rpm at 4 °C. The supernatant was transferred into a new tube, and centrifugation was repeated. The three supernatants were mixed and directly applied onto a *Strep-Tactin® Spin Column* (#2-1850-010, IBA). 20 µl of the pooled protein extracts were retained for SDS-PAGE. The columns were used for protein purification according to the manufacturer's instructions. Proteins were eluted from the column with 50 µl elution buffer (100 mM Tris-HCl, pH 8.0, 150 mM NaCl, 1 mM EDTA, 2 mM D-biotin). 5 µl of the total protein extract sample and one half of the eluate fraction were subjected to SDS-PAGE.

2.8.3 SDS-polyacrylamide gel electrophoresis

Protein samples were mixed in a 2:1 ratio with 3x loading dye (0.25 M Tris-HCl pH 6.8, 30% glycerol, 15% β-mercaptoethanol, 7% SDS, 0.3% bromphenol blue) and heated at 65 °C for 10 min before they were subjected to SDS-polyacrylamide gel electrophoresis (SDS-

PAGE) according to Laemmli (1970). Samples were applied onto 12% SDS-polyacrylamide gels that were placed in electrophoresis buffer (25 mM Tris base, 250 mM glycine, 0.1% SDS). SDS-gels consisted of a lower running gel (375 mM Tris pH 8.8, 12% acrylamide/bisacrylamide 37.5:1 (Rotiphorese® Gel 30, #3029.1, Carl Roth), 2 mM EDTA, 0.1% SDS) and an upper stacking gel (125 mM Tris pH 6.8, 5% acrylamide/bisacrylamide 37.5:1, 2 mM EDTA, 0.1% SDS). Proteins were separated electrophoretically for 10 min at 100 V and subsequently at 150-200 V until the separation of proteins was sufficient. This was most often the case when the bromphenol blue left the gel. The *PageRuler™ Prestained Protein Ladder* (#26616, Thermo Fisher Scientific) was used to estimate the sizes of proteins.

2.8.4 Western blot analysis

Western blot experiments were performed according to Burnette (1981). Proteins were transferred from SDS-gels onto nitrocellulose membranes (*Amersham™ Protran® Western blotting membrane*, #GE10600002, Sigma-Aldrich, München, Germany) by electrophoretic blotting in a *Mini-Trans-Blot-Electrophoretic-Cell* (Bio-Rad Laboratories, München, Germany) filled with transfer buffer (25 mM Tris base, 190 mM glycine, 0.02% SDS, 20% methanol) for 1.5 h at 100 V. After blotting, the membranes were stained with Ponceau red (0.2% Ponceau S, 3% trichloroacetic acid) for 5 min, washed with water and photographed using the *FUSION-SL-4* (Peqlab, Erlangen, Germany). Ponceau red staining was removed through washing with phosphate buffered saline (PBS, 8 mM Na_2HPO_4, 2 mM NaH_2PO_4, 150 mM NaCl) and subsequent incubation with the blocking buffer (PBS with 5% milk powder) for at least 1 h at room temperature or overnight at 4 °C. Membranes were incubated for 2 h at room temperature or overnight at 4 °C with the primary antibody diluted in the blocking buffer. The membranes were incubated with monoclonal mouse anti-c-myc (dilution: 1:2,000, #2276, Cell Signaling Technology, Danvers, Massachusetts, USA), polyclonal goat anti-Rap1p (1:500, #yN-18, Santa Cruz Biotechnology, Heidelberg, Germany), polyclonal rabbit anti-Tec1p (1:1,000, Hans-Ulrich Mösch, Philipps-Universität, Marburg, Germany), polyclonal anti-Asc1p (1:1,000, Andrew Link, Vanderbilt University Medical Center, Nashville, USA), or polyclonal phospho-p38 MAPK (Thr180/Tyr182) (1:500, #9211, Cell Signaling Technology) antibodies. The anit-Rap1p, anti-Tec1p, and anti-Asc1p antibodies were diluted in PBS with 5% milk powder. Tris buffered saline (TBS, 150 mM Tris, 150 mM NaCl, pH 7.2-7.4) with 5% milk powder and 0.1% Tween 20 was used for dilution of the anti-c-myc antibody. TBS with 5% bovine serum albumin (BSA) and 0.1% Tween 20 was used for blocking and preparation of the antibody dilution when the

phosphorylation-specific antibody phospho-p38 MAPK (Thr180/Tyr182) was applied. Membranes were washed three times with PBS or TBS, respectively, followed by incubation with the peroxidase-coupled goat anti-mouse (1:5,000, #115-035-003, Dianova, Hamburg, Germany), donkey anti-goat (1:2,000, #sc-2020, Santa Cruz Biotechnology), or goat anti-rabbit (1:2,000, #G21234, MoBiTec, Göttingen, Germany) secondary antibodies. The goat anti-rabbit antibody was diluted in TBS with 5% BSA when it was used in combination with the phospho-p38 MAPK (Thr180/Tyr182) antibody. The membranes were washed as described before. For the peroxidase reaction, 100 µl 2.5 mM luminol, 44 µl 40 µM paracumaric acid, and 6.15 µl 30% H_2O_2 were added to 20 ml 100 mM Tris pH 8.5 and applied onto the membrane followed by 1 min incubation on a shaker. Chemiluminescence was detected using the *FUSION-SL-4*. Signals were quantified relative to the Ponceau red staining as loading control according to Rivero-Gutiérrez et al. (2014) using the *Bio1D software Version 15.01* (Vilber Lourmat, Eberhardzell, Germany).

2.8.5 Colloidal Coomassie staining of proteins

Protein staining within SDS-gels was done using colloidal Coomassie G250 and was performed according to Kang et al. (2002). All steps of the procedure were performed with constant shaking of the SDS-gel in the respective solutions and at room temperature. After SDS-PAGE, the gel was incubated in fixing solution (40% ethanol, 10% acetic acid) for at least 1 h. The gel was washed twice for at least 10 min with H_2O followed by staining with the Coomassie G250 solution (0.1% Coomassie Brilliant Blue G250, 5% aluminium sulfate-(14-18)-hydrate, 10% methanol, 2% orthophosphoric acid) overnight. To prepare the staining solution, aluminium sulfate was first dissolved in H_2O followed by the addition of methanol. Coomassie Brilliant Blue G250 was added and dissolved. Finally, phosphoric acid was added, and the solution was filled up with H_2O to the final volume. After staining, the gel was washed with H_2O. Prior to in-gel trypsin digestion of proteins (chapter 2.8.6) the Coomassie staining was reduced through incubation of the gel or the gel pieces in fixing solution overnight. To remove the fixing solution, gels were washed with H_2O at least twice for 10 min.

2.8.6 In-gel protein digestion with trypsin

The in-gel digestion of proteins with trypsin was performed according to Shevchenko et al. (1996). Gel lanes were cut into pieces of approximately 1.5 to 2 mm^2. The pieces were transferred into reaction tubes, covered with acetonitrile and shaken for 10 min. Acetonitrile

was removed, and the gel pieces were dried in the *Savant SPDIIIV SpeedVac Concentrator* (Thermo Scientific). 150 ml 10 mM DTT solution (in 100 mM NH_4HCO_3) were added to each sample followed by incubation at 56 °C for 1 h. The DTT solution was removed, and 150 µl 55 mM iodoacetamide (prepared in 100 mM NH_4HCO_3) were added. After 45 min incubation at room temperature and in the dark, the solution was removed, and 150 µl 100 mM NH_4HCO_3 were added. On a shaker, samples were incubated for 10 min. The liquid was exchanged for 150 µl acetonitrile, and the samples were incubated again for 10 min. The washing steps with 100 mM NH_4HCO_3 and with acetonitrile were repeated once. Gel pieces were dried in the *SpeedVac* and subsequently covered with trypsin (#37283.01, SERVA Electrophoresis, Heidelberg, Germany) digestion buffer, which was prepared according to the manufacturer's instructions. After 45 min incubation on ice, remaining trypsin digestion buffer was removed. The gel pieces were covered with 25 mM NH_4HCO_3, and samples were incubated at 37 °C overnight. The supernatant was collected in a new reaction tube. Gel pieces were covered with 20 mM NH_4HCO_3 and shaken for at least 10 min. The supernatant was collected again in the same tube, and the gel pieces were covered with 50% acetonitrile/5% formic acid. After shaking of the samples for at least 20 min, the supernatant was collected. The last step was repeated twice. Prior to the collection of supernatants samples were always centrifuged for 1 min at 13,000 rpm. The peptide-containing samples were dried in the *SpeedVac*. Peptides were reconstituted in 20 µl liquid chromatography-mass spectrometry (LC-MS) sample buffer (2% acetonitrile, 0.1% formic acid) and directly subjected to LC-MS analysis (chapter 2.8.9) or purified using C18 stop and go extraction (stage) tips according to Rappsilber et al. (2003 and 2007). Two C18 disks were punched out from a *Solid Phase Extraction Disk* (#2215, 3M, Neuss, Germany) and placed in a 100 to 200 µl pipette tip. This stage tip was in turn placed into a reaction tube using an adaptor. The C18 material was equilibrated with 100 µl methanol/0.1% formic acid, followed by 100 µl 70% acetonitrile/0.1% formic acid, and twice 100 µl 0.1% formic acid. For each step, the samples were centrifuged for 2 min at maximum speed. After loading of the peptide solution on the C18 material, the samples were centrifuged for 5 min at 4,000 rpm. Two times 100 µl 0.1% formic acid were applied followed by 2 min centrifugation at 10,000 rpm for washing of the samples. Peptides were eluted from the C18 material with 60 µl 70% acetonitrile/0.1% formic acid. Samples were centrifuged for 5 min at 4,000 rpm. The eluted peptides were dried in the *SpeedVac*, reconstituted in 20 µl LC-MS sample buffer, and subjected to LC-MS analysis.

2.8.7 In-solution digestion of proteins with LysC and trypsin

Proteins were digested in-solution when high amounts of peptides were required for phospho-peptide enrichment. Protein samples were prepared as described in chapter 2.8.1 with the exceptions that cell extracts were subjected to sonication for subsequent filter-aided sample preparation (FASP, Wiśniewski et al., 2009). Protein concentrations were determined as described before (chapter 2.8.1). For the in-solution digest, 1 mg protein of each sample was subjected to chloroform-methanol extraction to reduce the amount of SDS in the samples (Wessel and Flügge, 1984). For the chloroform-methanol extraction, 100 µl aliquots of the protein extract were prepared. If necessary, volumes were adjusted accordingly. Successively, each sample was mixed with 400 µl methanol, followed by 100 µl chloroform and 300 µl H_2O. After each step, the samples were mixed through vigorous shaking for 1 min. After centrifugation at 13,000 rpm for 5 min at 4 °C, the upper phase was discarded, and 300 µl methanol were added. After vigorous shaking for 1 min, the samples were centrifuged at 13,000 rpm for 10 min at 4 °C, and afterwards the supernatant was discarded. The pellets were dried and then dissolved in 200 µl buffer UA each (8 M urea prepared in 100 mM Tris-HCl pH 8.5). Proteins were in-solution digested with LysC (#125-05061, Wako Chemicals, Neuss, Germany) and trypsin (#37283.01, SERVA Electrophoresis) according to the FASP protocol (Wiśniewski et al., 2009) using centrifugal filter units (#MRCF0R030, Merck). The protein concentration was determined using the BCA reagent as described before and adjusted to 1.25 µg/µl with UA. For one phospho-proteome analysis, four filter units were each loaded with 200 µl of the protein solution. All steps were performed at room temperature, and all centrifugation steps were carried out at 13,000 rpm for 15 min except when stated otherwise. If necessary, the flow-through was removed between the centrifugation steps. The filter units were centrifuged, refilled twice with 200 µl UA and centrifuged again. 200 µl UA with 3 µl 1 M DTT were added followed by gentle mixing. After 30 min incubation, the filter units were centrifuged, refilled with 200 µl UA followed by another round of centrifugation. 100 µl 50 mM iodoacetamide prepared in 8 M UA were added, and the samples were gently mixed. After incubation for 20 min at room temperature, the filter units were centrifuged for 10 min. 100 µl buffer UB (8 M urea prepared in 100 mM Tris-HCl pH 8.0) were added followed by centrifugation. The step was repeated twice. Protein samples were mixed with 40 µl UB containing LysC in an enzyme to protein ratio of 1:50. Filter units were sealed with parafilm and incubated overnight. The filter units were transferred into a new collection tube. Samples were mixed with 120 µl 25 mM NH_4HCO_3 containing trypsin in an enzyme to protein ratio of 1:100. Samples were incubated for 4 h and then centrifuged for 15 min. 50 µl

0.5 M NaCl were added to the membrane of the filter unit, and the samples were centrifuged for 20 min. Peptide samples were acidified and desalted with C18 cartridges (#98060401985, 3M) according to Wiśniewski et al. (2009). Each cartridge was placed into a 15 ml tube, 1 ml methanol was applied onto the cartridge followed by centrifugation at 1,500 x g for 1 min. The step was repeated with 0.5 ml 70% acetonitrile/0.1% TFA and with 0.5 ml 0.1% TFA. The peptide sample was loaded onto the cartridge followed by centrifugation at 150 to 500 x g until the complete liquid was in the flow-through. The step was repeated with 0.5 ml 0.1% TFA for washing. The cartridge was transferred into a new tube, and the previous centrifugation step was repeated with 0.5 ml 70% acetonitrile for elution of the peptides. Samples were dried in the *SpeedVac*. A fraction of the sample was dried separately and reconstituted in LC-MS sample buffer (2% acetonitrile, 0.1% formic acid) for measurement of the peptide concentrations using the BCA assay as described before and with the *MassPREP*^{TM} E. coli *Digest Standard* (#186003196, Waters, Eschborn, Germany) as reference.

2.8.8 Phospho-peptide enrichment

To enrich phospho-peptides from complex peptide mixtures, a protocol modified from Mazanek et al. (2007) was used. Peptide samples were reconstituted in 50 µl loading solvent (70% acetonitrile, 420 mM 1-octanesulfonic acid (#O0133, Sigma-Aldrich), 50 mg/ml dihydroxybenzoic acid (#39319, Sigma-Aldrich), 0.1% heptafluorobutyric acid (#77249, Sigma-Aldrich), 3% TFA) and applied onto equilibrated TiO_2 columns (TT2TIO, Glygen Corporation, Columbia, Maryland, USA) in an estimated ratio of 400 µg peptides per 1 mg of TiO_2 for optimized recovery of phospho-peptides from TiO_2 according to Kanshin et al. (2013). Equilibration of the columns was done by applying 40 µl of the first wash solution (70% acetonitrile) followed by 40 µl loading solvent. A syringe was used to gently press the liquid through the stationary phase. After loading of the peptide samples, columns were washed twice with 40 µl loading solvent, once with the second washing solution (70% acetonitrile, 125 mM asparagine, 125 mM glutamine, 3% TFA), and twice with 40 µl of the third washing solution (70% acetonitrile, 3% TFA). The second washing solution comprised asparagine and glutamine to displace N/Q-rich peptides on the TiO_2 (Kanshin et al., 2013). Peptides were eluted from the column by applying two times 40 µl elution buffer (50 mM ammonium dihydrogen phosphate adjusted to pH 10.5 with ammonium hydroxide). Samples were acidified with 20 µl TFA, dried, reconstituted in LC-MS sample buffer (2% acetonitrile,

0.1% formic acid), and again desalted using C18 cartridges. For LC-MS analyses, all samples were dissolved in 20 µl sample buffer.

2.8.9 Liquid chromatography-mass spectrometry analysis

Liquid chromatography (LC) coupled to an *Orbitrap Velos Pro™ Hybrid Ion Trap-Orbitrap* mass spectrometer (MS) was employed for protein and phospho-peptide identification and for relative quantification by SILAC-ratios. Peptides of 1 to 6 µl sample solution were trapped and washed on an *Acclaim® PepMap 100* pre-column (#164564, 100 µm x 2 cm, C18, 3 µm, 100 Å, Thermo Fisher Scientific) at a flow rate of 25 µl/min for 6 min in 100% solvent A (2% acetonitrile, 0.07% TFA). Analytical peptide separation by reverse phase chromatography was performed on an *Acclaim® PepMap RSLC* column (#164540, 75 µm x 25 cm or 50 cm, C18, 3 µm, 100 Å, Thermo Fisher Scientific) typically running a gradient from 98% solvent A (0.1% formic acid) and 2% solvent B (80% acetonitrile, 0.1% formic acid) to 42% solvent B within 95 min and to 65% solvent B within the next 26 min at a flow rate of 300 nl/min (solvents and acids from Fisher Chemicals). Chromatographically eluting peptides were on-line ionized by nanoelectrospray (nESI) using the *Nanospray Flex Ion Source* (Thermo Fisher Scientific) at 2.4 kV and continuously transferred into the mass spectrometer. Full scans within the mass range of 300 to 1850 m/z were taken within the Orbitrap-FT analyzer at a resolution of 30,000 or 60,000 (SILAC experiments) with parallel data-dependent top ten MS2 collision-induced dissociation (CID) fragmentation with the *LTQ Velos Pro* linear ion trap. Phospho-peptide samples were analyzed with CID fragmentation applying the multistage activation (MSA) method as well as with higher energy collisional dissociation (HCD) fragmentation in a separate run. When HCD fragmentation was used, data-dependent top five MS2 fragmentation was performed, and fragment ions were analyzed in the Orbitrap. For analysis of Asc1p phospho-peptides, also targeted data acquisition with parent mass lists was applied. LC-MS method programming and data acquisition was done with the software *XCalibur 2.2* (Thermo Fisher Scientific). For identification of Asc1p-derived phospho-peptides, MS/MS2 data were searched against an *S. cerevisiae*-specific protein databases (SGD, 6110 entries including common contaminants, S288C_ORF_database release version 2011, Stanford University) using the *Proteome Discoverer Software version 1.4*, and phospho-site localization was evaluated using *phosphoRS* (Olsen et al., 2006; Olsen and Mann, 2004). The digestion mode was trypsin, and a maximum of two missed cleavage sites was considered. Carbamidomethyl at cysteines was set as fixed modification. Oxidation at methionines and phosphorylation at serines, threonines, and tyrosines were considered as

variable modifications. Mass tolerances of precursors and fragment ions were 10 ppm and 0.6 Da, respectively. False discovery rates were calculated by the *Proteome Discoverer* using the reverse-decoy mode, and the filter for valid peptide sequence matches was set to 0.01. For quantitative proteome analyses, MS/MS2 data were analyzed with the *MaxQuant* 1.5.1.0 software with the program's default parameters using an *S. cerevisiae*-specific protein database derived from *UniProt* (http://www.uniprot.org, Proteome ID UP000002311, 6721 entries, download 2014, Cox and Mann, 2008). The digestion mode was trypsin/P, and a maximum of two missed cleavage sites was considered. Carbamidomethyl at cysteines was set as fixed modification, and acetylation at the N-terminus, oxidation at methionines, phosphorylation at serines, threonines, and tyrosines (only for raw data from MSA and HCD LC-MS runs) were considered as variable modifications. Arg6 and Lys4 were defined as medium peptide labels and Arg10 and Lys8 as heavy peptide labels. Mass tolerances of precursors and fragment ions were 4.5 ppm and 0.5 Da, respectively. *Match between runs*, *requantification*, and *FTMS recalibration* were enabled. For protein quantification, the minimum ratio count was two, and unique plus razor peptides were considered. False discovery rates were calculated by *MaxQuant* using the revert-decoy mode, and the filter for valid peptide sequence matches was set to 0.01. *MaxQuant* output data were further processed using the *Perseus* software 1.5.0.15 (Cox and Mann, 2008).

2.9 RNA analyses

2.9.1 Northern blot analysis

Total RNA was isolated from yeast according to Cross and Tinkelenberg (1991). 40 µg RNA was mixed with 30 µl sample buffer (66.7% formamide, 9.25% glycerol, 0.18% bromphenol blue, 1.8% ethidium bromide), heated at 65 °C for 15 min, and kept on ice for 10 min. RNA was separated on a 1.4% agarose gel containing 3% formaldehyde and 1% 3-(N-morpholino)propanesulfonic acid (MOPS, 23 mM MOPS, 5 mM sodium acetate, 1 mM EDTA, pH 7) in running buffer (6.7 % formaldehyde and 1% MOPS) at 70 V. Transfer of RNA onto a nylon membrane was performed by capillary blotting overnight. Cross-linking of the RNA to the membrane, generation and labeling of the probe, and signal detection were carried out as described for the Southern blot (chapter 2.7).

2.9.2 Sucrose density gradients

Sucrose-density gradient fractionation experiments were performed as described by Mašek et al. (2011). *S. cerevisiae* cultures were grown overnight to midlog phase in 100 ml liquid YNB medium. The culture was supplemented with cycloheximide at a final concentration of 100 µg/ml and incubated for 15 min on ice. Cells were harvested by centrifugation, resuspended in washing buffer (20 mM HEPES-KOH pH7.5, 10 mM KCl, 2.5 mM $MgCl_2$, 1 mM EGTA) and transferred into a 2 ml reaction tube. After another round of centrifugation, the cells were resuspended in lysis buffer (20 mM HEPES-KOH pH 7.5, 10 mM KCl, 2.5 mM $MgCl_2$, 1 mM EGTA, 1 mM DTT, 100 µg/ml cycloheximide, 1.5 µl *RiboLock* RNase Inhibitor (40 U/µl, #EO0381, Thermo Fisher Scientific), 1 *cOmplete*™ EDTA-free protease inhibitor tablet (#05056489001, Roche Diagnostics) per 50 ml, 1 *PhosSTOP*™ phosphatase inhibitor cocktail tablet (#04906837001, Roche Diagnostics) per 10 ml). The volume of lysis buffer and the amount of glass beads that were added equaled the volume of the cell pellet. Cells were disrupted using the *Fast-Prep-24* (MP Biomedicals, Illkirch, France) two times for 20 sec at 5.0 m/sec. Samples were centrifuged for 5 min at 13,000 rpm at 4 °C. The supernatant was transferred into a new reaction tube, and centrifugation was repeated for 7 min. The supernatant was again transferred into a new reaction tube, and the OD_{260} of a 1:100 dilution was measured with the *NanoDrop 2000* (Thermo Scientific). A volume of cell extracts equaling an OD_{260} of 20 was loaded onto a 7 to 47% sucrose gradient. The gradient was generated with the *Gradient Master 108* (BioComp Instruments, Fredericton, Canada) using 7% and 47% sucrose solutions prepared in the washing buffer. After centrifugation at 40,000 rpm for 2 h and 50 min at 4 °C in a TH-641 rotor and a *Sorvall WX80* ultracentrifuge, (Thermo Scientific) the gradient was fractionated using a fraction collector (*Foxy Jr. Fraction Collector*, Optical Unit Type 11, Absorbance detector UA-6, Teledyne Isco, Lincoln, Nebraska, USA) by pumping a 60 % sucrose solution into the bottom of the tube. During fractionation, the absorbance at 254 nm was measured to monitor the distribution of RNA in the gradient and thus to obtain the polysome profile.

2.9.3 Isolation of RNA from sucrose gradient fractions and mRNA enrichment

Fractions from the sucrose-density gradient centrifugation were collected starting from the first polysome peak. 2 volumes of *TRIzol*® *Reagent* (#15596-026, Thermo Fisher Scientific) were added to the samples followed by vigorous shaking. 0.2 volumes of 3 M sodium acetate and 0.4 volumes of chloroform were added followed by 3 min shaking. Samples were then centrifuged at 4,200 rpm for 30 min at 4 °C. The upper aqueous phase was transferred into a

new reaction tube, and 50 µg glycogen (#77534, Affymetrix, Cleveland, Ohio, USA) were added per 1 ml of the sucrose gradient. Isopropanol was added in a 1:1 ratio. Samples were mixed and incubated overnight at 4 °C. They were transferred into SS-34 tubes and centrifuged for 30 min at 13,000 rpm in a *Sorvall® RC 5B Plus* centrifuge (Thermo Scientific). The supernatants were removed, and the pellets were washed with 25 ml ice-cold 75% ethanol. The previous centrifugation step was repeated, and ethanol was removed. Pellets were dried and then resuspended in 250 µl H_2O. The *Oligotex Direct mRNA Kit* (#70022, Qiagen) was used for enrichment of mRNAs according to the provided *Batch Procedure Protocol*. Samples were eluted using two times 25 µl *Oligotex* Elution Buffer. To remove DNA from the samples, digestion with DNase I (#EN0521, Thermo Scientific) was performed. For digestion of 7.5 µl sample from the previous elution step, 1 µl DNase I, 1 µl 10x reaction buffer with $MgCl_2$ (#B43, Thermo Scientific), and 0.5 µl *RiboLock* RNase Inhibitor (40 U/µl, #EO0381, Thermo Fisher Scientific) were added, and the samples were incubated at 37 °C for 45 min. Samples were then purified using the *RNeasy MinElute Cleanup Kit* (#74204, Qiagen) according to the manufacturer's instructions.

2.9.4 cDNA synthesis and RNASeq analysis

The experimental steps and data analysis described in this chapter were performed together with the Department of *Genomic and Applied Microbiology* of the *Institute of Microbiology and Genetics, Georg-August University Göttingen*. Samples enriched for mRNA (see chapter 2.9.3) were subjected to cDNA synthesis using the *NEBNext® Ultra™ RNA Library Prep Kit for Illumina®* (#E7530S, New England Biolabs). After second strand cDNA synthesis, sample clean-up with the *QIAquick PCR purification kit* (#28106; Qiagen) was performed. For the removal of adapter dimers and adapter monomers after library preparation, the *Agencourt® AMPure® XP Beads* (#A63881, Beckman Coulter, Krefeld, Germany) were applied. For the purification of cDNA, the *GeneRead Size Selection Kit* (#180514, Qiagen) was used. All kits and reagents were used according to the manufacturer's instructions. Sequencing was performed on an Illumina Genome Analyzer IIx (Illumina, San Diego, USA). The sequence reads were mapped on the genome of *S. cerevisiae* (SGD) using *Bowtie2* (Langmead and Salzberg, 2012) with standard parameters. The output Sequence Alignment/Map files were used to obtain readcount data for the *S. cerevisiae* genes to be used in a differential expression analysis applying the *baySeq* algorithm (Hardcastle and Kelly, 2010). Transcripts with a likelihood ≥ 90% and a false discovery rate ≤ 0.05 were considered as differentially abundant in the analyzed translatomes.

2.10 Phenotypic tests

Yeast cells were grown to midlog phase and diluted to an OD_{600} of 0.1. Three consecutive ten-fold dilutions were prepared, and 10 µl or 20 µl of each dilution were dropped on YEP plus 2% glucose/glycerol and on YNB medium, respectively. Media tested were YEP with 2% glycerol, YEPD with Congo red (125 µg/ml) or NaCl (75 mM), and YNB with canavanine (600 ng/ml) or cycloheximide (0.15 µg/ml). YEPD and YNB plates were used for growth controls. To assess the respiratory activity of the strains, a 2,3,5-triphenyltetrazolium chloride (TTC, #93140, Sigma-Aldrich) assay (Ogur et al., 1957) was performed: 100 µl of the highest dilution were streaked on YNB plates (Ø 9.2 cm) containing 0.4% glucose, and the plates were incubated for 3 d at 30 °C. Colonies were then overlaid with liquid 1.2% top agar containing 0.5% TTC and incubated for 20 to 30 min at 30 °C. To observe glucose-dependent colony morphology, 100 µl of the highest dilution of the cell suspensions were streaked on YEP plates containing either 2% glucose or 0.4% glucose to obtain single colonies after 3 d growth at 30 °C. To test the resistance of yeast strains against DETA-NONOate (#82120, Cayman Chemical, Ann Arbor, Michigan, USA), an agar diffusion/halo assay was performed. Cells were grown to an OD_{600} of 0.6 in YNB medium, and 100 µl of the culture were transferred to 10 ml 0.5% liquid agar (40 °C) that was poured onto MV plates after mixing. Two filter papers soaked with 2 µl and 4 µl of 1 M DETA-NONOate, respectively, were immediately placed onto the agar surface. The ability of the yeast strains to grow adhesively was tested by growth on YNB plates containing 10 mM 3-amino-1,2,4-triazole (3-AT, #A8056, Sigma-Aldrich) at 30 °C for 3 d followed by washing of the plates under a constant stream of water. Plates were photographed using the *Gel iX Imager*. Colonies from the TTC and glucose-dependent colony morphology assays were documented using the stereomicroscope *Olympus SZX12* (Olympus Corporation, Hamburg, Germany) and the *cellSens Dimension software 1.4* (Olympus Corporation).

3. Results

3.1 Asc1p-dependent phenotypes

Deletion of the *RACK1* gene in metazoans leads to lethality during embryogenesis, whereas *S. cerevisiae ASC1* deletion strains are viable. Yeast Δ*asc1* strains exhibit multiple phenotypes related, for instance, to cell wall integrity, respiration, and translation. These strains are also deficient in the *SNR24* gene that is located within the intron of the *ASC1* gene and codes for the snoRNA U24 (Figure 9A, Chantrel et al., 1998). Thus, the absence of the snoRNA U24 in a Δ*asc1* strain might account for, or at least contribute to, the observed phenotypes.

The two major classes of snoRNAs are named according to conserved sequence motifs box C/D and H/ACA snoRNAs (Balakin et al., 1996; Ganot et al., 1997). The snoRNAs of the two families form ribonucleoprotein (RNP) complexes with distinct sets of proteins (reviewed in Watkins and Bohnsack, 2012). Members of the C/D snoRNP family catalyze 2'-O-ribose-methylation of pre-rRNA, whereas members of the H/ACA snoRNP family are responsible for pseudouridinylation of pre-rRNA (Kiss-László et al., 1996; Ni et al., 1997). Substrate specificity of the snoRNPs is provided by sequences in the snoRNA that are complementary to the modified rRNA target (Watkins and Bohnsack, 2012). The snoRNA U24 belongs to the C/D box family and is required for three site-specific 2'-O-ribose-methylations of 25S pre-rRNA (Kiss-László et al., 1996). Although the *SNR24* gene is highly conserved among eukaryotes, its position within an intron of *ASC1*/*RACK1* is less well conserved. The human snoRNA U24 encoding gene, for instance, lies within the second intron of the *RPL7A* gene (Qu et al., 1995). The function of snoRNP U24 catalyzed 2'-O-methylation of 25S rRNA is not clear. The absence of snoRNA U24, but not the lack of Asc1p, leads to a halfmer phenotype in sucrose density gradients of *S. cerevisiae* cell extracts (Kouba et al., 2012). Halfmers are polysomes or monosomes bound to an additional 43S preinitiation complex, and they are detected as additional peaks in polysome profiles (Helser et al., 1981). The formation of halfmers might be due to reduced amounts of mature 60S ribosomal subunits in the cell as a consequence of loss of the snoRNA U24 (Rotenberg et al., 1988; Kouba et al., 2012).

To test whether also other phenotypes observed for the Δ*asc1* strain are eventually caused by the deletion of the *SNR24* gene, two different strains were generated: 1) a strain expressing the snoRNA U24, but not Asc1p, and 2) a strain only deleted for the *SNR24*-containing intron. For construction of the first strain, a *loxP::URA3::loxP* cassette was inserted into exon 1 of the *ASC1* gene (Figure 9B). After the verification of transformants, the Cre-recombinase was

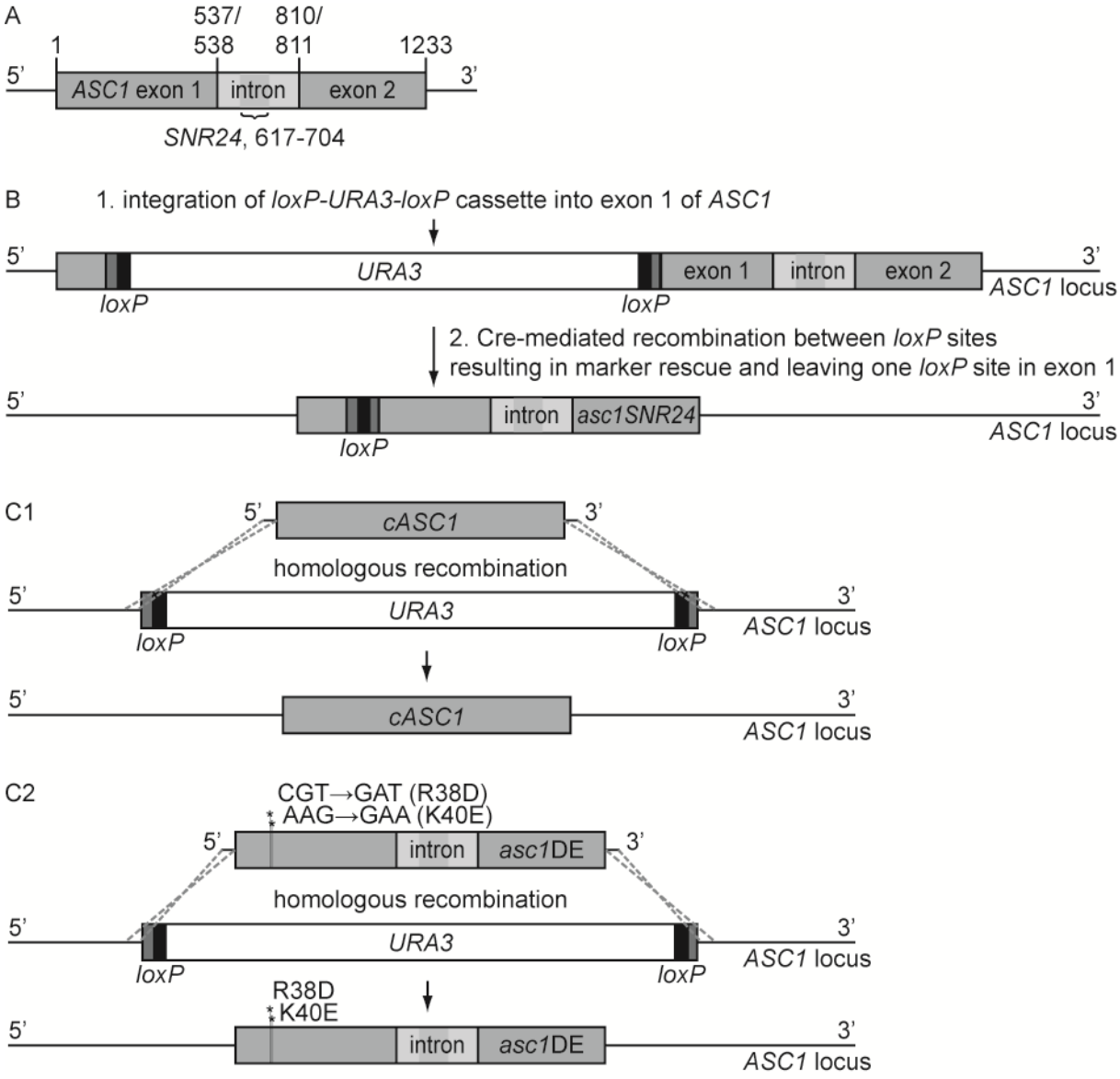

Figure 9. Construction of *S. cerevisiae ASC1* and *SNR24* mutant strains.
(A) The genomic *ASC1* locus. The *ASC1* gene is interrupted by an intron that contains the snoRNA U24 encoding *SNR24* gene. (B) Construction of a yeast strain still expressing the snoRNA U24, but no Asc1p. In the first step, the *loxP-URA3-loxP* cassette was introduced into exon 1 of the *ASC1* gene between base pairs 164 and 165. After verification of the transformant, the marker was rescued through expression of plasmid-borne Cre-recombinase that mediates homologous recombination between the two *loxP* sites (indicated with black rectangles) flanking the *URA3* gene. One *loxP* site of 34 bp remains in exon 1 of the *asc1* ORF. The *loxP* site is flanked by two short regions (indicated with dark gray rectangles) that are derived from the amplification of the *loxP-URA3-loxP* cassette by PCR. In total, the sequence remaining in exon 1 has a size of 109 bp. The resulting strain is termed *asc1SNR24* or *asc1*$^{-}$. (C) Introduction of mutated alleles of *ASC1* into the yeast genome at the native locus. For transformations, a Δ*asc1::URA3* yeast strain was used, and the *loxP-URA3-loxP* cassette was replaced by different mutant alleles of the *ASC1* gene that were amplified from plasmids with 45 bp overhangs homologous to the up- and down-stream regions of the *ASC1* gene. C1 shows the generation of a strain expressing the *ASC1* cDNA (*cASC1*) without the intron, and C2 illustrates the construction of a yeast strain expressing mutated *asc1* with defined codon exchanges at specific positions within its ORF, such as R38D K40E.

transiently expressed to induce homologous recombination between the two *loxP* sites flanking the *URA3* marker, finally yielding in a single *loxP* site in exon 1 of *ASC1*. The presence of this *loxP* site in the *asc1* mRNA should result in the abrogation of Asc1p synthesis during translation due to a stop codon within the *loxP* site (see Supplementary Figure 1). However, it should not interfere with the splicing of the mutated *ASC1* pre-mRNA to generate functional snoRNA U24. The strain was designated *asc1SNR24* and abbreviated as *asc1*$^-$ in the following chapters.

For the generation of the second strain, *ASC1* was amplified from a cDNA sample and cloned into a vector. The *ASC1* cDNA was then amplified from this plasmid with oligonucleotides that introduced 5' and 3' flanking regions for genomic integration through homologous recombination at the native *ASC1* locus. The replacement cassette was transformed into a Δ*asc1::URA3* strain with *ASC1* replaced by *loxP::URA3::loxP* (Figure 9C1). This enabled the selection of transformants on 5-fluoroorotic acid-containing media. The obtained verified strain was designated as *cASC1*. Both the *asc1*$^-$ and the *cASC1* strains were verified by PCR, Southern blot, and sequencing of the mutated locus. Furthermore, Northern blot experiments were performed to verify the expression of snoRNA U24 in the *asc1*$^-$ strain. Western blot experiments were performed to confirm the expression of Asc1p in the *cASC1* strain and the absence of the protein in the *asc1*$^-$ strain (not all data shown, in part depicted in Figure 19). Both strains were analyzed for phenotypes that are known to rely on Asc1p and will be introduced in the following paragraphs. Total deletion of the *ASC1* locus actually represents an *ASC1 SNR24* double deletion, but is referred to as Δ*asc1* in this study.

Deletion of *ASC1* reduces the resistance of *S. cerevisiae* cells against translation inhibitors, such as cycloheximide, which interferes with the translocation step during elongation (Parsons et al., 2004). Also, the natural resistance against the non-proteinogenic amino acid canavanine is compromised in a Δ*asc1* strain. The Δ*asc1* strain is further impaired in its cell wall integrity that manifests in its increased sensitivity to Congo red, calcofluor white, or the glucanase zymolyase (Valerius et al., 2007; Rachfall et al., 2013). Deletion of *ASC1* results in the loss of adhesive growth of haploid yeast cells and pseudohyphae formation of diploid cells due to reduced expression of the cell surface glycoprotein Flo11 (Valerius et al., 2007). The Δ*asc1* strain shows reduced growth on non-fermentable carbon sources, such as ethanol or glycerol, indicating impairment of respiration. This is further confirmed by strongly reduced red staining of Δ*asc1* cells through triphenyltetrazolium chloride (TTC), a compound that gets reduced by electrons of the respiratory chain leading to the formation of a red dye (Ogur et al., 1957). In the presence of high amounts of glucose (2%), *S. cerevisiae* cells cover their energy

supply mainly through fermentation. Therefore, the TTC assay is performed with colonies grown on medium containing low concentrations of glucose (0.4%).

Impairment in respiration and low oxygen concentrations (hypoxia) can lead to the formation of reactive oxygen and nitrogen species (Figure 10A, Castello et al., 2006). These reactive compounds can lead to harmful modification of proteins and other cellular components. Asc1p-deficient cells show highly increased levels of the proteins Hbn1 and Yhb1, which are both assumed to function in the detoxification of such reactive compounds (Rachfall et al., 2013). Hbn1p (homologous to bacterial nitroreductases 1) is similar to bacterial nitroreductases, and cells deficient in this protein show decreased antioxidant activity, for example, mediated by the superoxide dismutase (Figure 10A, de Oliveira et al., 2010). Yhb1p (yeast flavohemoglobin 1) functions in the detoxification of nitric oxide (NO, Liu et al., 2000). NO inhibits the cytochrome c oxidase of the respiratory chain, and it reacts with superoxide to peroxynitrite, which causes protein tyrosine nitration (Brown, 2001; Radi, 2004). The increased sensitivity of the single deletion strains Δ*hbn1*, Δ*yhb1*, and Δ*asc1* to the NO donor DETA-NONOate in a halo assay shows that all three proteins are required for resistance against nitrosative stress (Figure 10B). Double deletion strains of all three possible combinations of Δ*asc1*, Δ*hbn1*, and Δ*yhb1* are more sensitive to nitrosative stress than the single deletion strains. A triple deletion mutant Δ*asc1* Δ*hbn1* Δ*yhb1* was generated that is hypersensitive to DETA-NONOate. Strains with an *ASC1* deletion showed slightly impaired growth on the minimal medium used for the halo assay that might contribute to some minor extent to the reduced resistance against DETA-NONOate (Figure 10C). The data indicate that Δ*asc1* cells are prone to oxidative/nitrosative stress, such as externally applied NO. Loss of additional factors involved in the detoxification of reactive species, such as Hbn1p and Yhb1p, increases the sensitivity of Δ*asc1* cells to DETA-NONOate (Rachfall et al., 2013).

The *asc1*$^{-}$ strain and the *cASC1* strain were analyzed with respect to a representative selection of the described phenotypes (Figures 10 and 11). The *asc1*$^{-}$ strain behaved identical to the Δ*asc1* strain and the *cASC1* strain identical to the wild-type *ASC1* strain. Thus, the phenotypes of a Δ*asc1* strain observed here are caused by the absence of the Asc1 protein and not by the lack of the snoRNA U24. To exclude any impact of a loss of snoRNA U24 on observations made for Asc1p-deficient strains, the *asc1*$^{-}$ strain was used instead of the Δ*asc1* strain for subsequent experiments in this study.

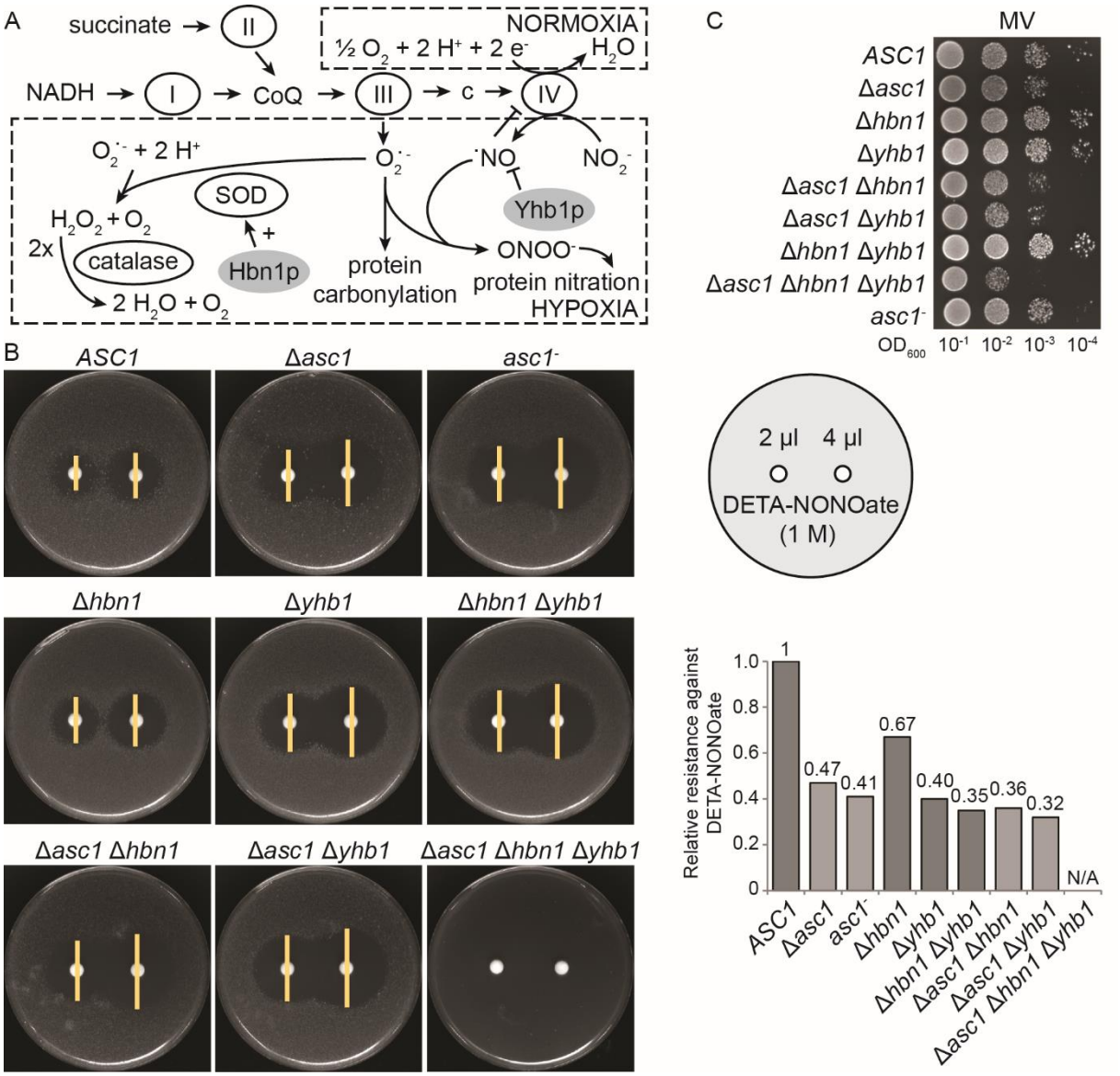

Figure 10. Nitrosative stress in Asc1p-deficient strains.
(A) The generation of reactive oxygen and nitrogen species within the respiratory chain upon hypoxia. Under normoxia, the cytochrome c oxidase complex (IV) of the respiratory chain transfers electrons onto oxygen leading to the formation of water molecules. Upon hypoxia, electrons are also transferred to nitrite (NO_2^-) yielding in nitric oxide ($^{\cdot}NO$). Furthermore, accumulating electrons on the cytochrome bc1 complex (III) are released by superoxide ($O_2^{\cdot -}$) formation. $^{\cdot}NO$ and $O_2^{\cdot -}$ react to form peroxynitrite ($ONOO^-$), which can modify proteins through tyrosine nitration. $O_2^{\cdot -}$ can be detoxified through the enzymes superoxide dismutase (SOD) and catalase. Yhb1p can consume $^{\cdot}NO$, and Hbn1p seems to be involved in activation of SOD (Liu et al., 2000; de Oliveira et al., 2010). (NADH = nicotinamide adenine dinucleotide, CoQ = coenzyme Q, c = cytochrome c; I = NADH coenzyme Q reductase, II = succinate dehydrogenase; modified from Castello et al., 2006). (B) Agar diffusion/halo assay to determine the sensitivity to the nitric oxide donor DETA-NONOate. Yeast cells were diluted in liquid top agar that was poured on MV plates (pH 7.2), and filter papers containing 2 µl or 4 µl of 1 M DETA-NONOate were applied. Plates were incubated for 2 days at 30 °C, and the size of growth inhibition zones was determined. The graph shows the resistance of the deletion strains against DETA-NONOate relative to the wild-type determined by the reciprocal values of the halo diameters. (C) Drop dilution assay. Serial ten-fold dilutions of the cell suspensions used for the halo assay were dropped onto MV-plates to evaluate total growth of the strains on this medium. (N/A = not applicable; modified from Rachfall et al., 2013).

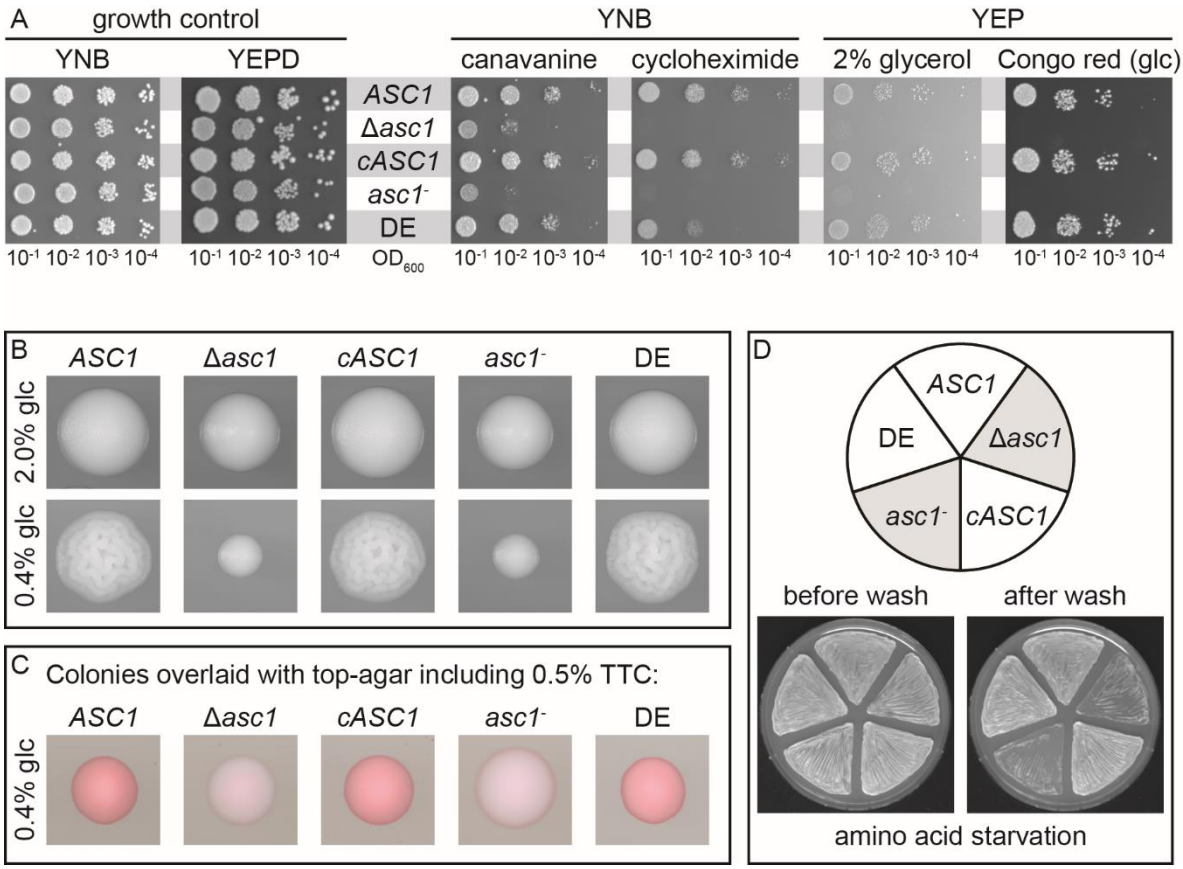

Figure 11. Phenotypic characterization of the *asc1*SNR24, *cASC1*, and *asc1*DE strains.
(A) Drop-dilution assays. Cell suspensions were spotted onto different growth media. YNB media containing 600 ng/ml canavanine or 0.15 µg/ml cycloheximide were used to test strains for their sensitivity to inhibitors of protein biosynthesis. To evaluate the growth of strains on non-fermentable carbon sources, cells were grown on YEP medium containing 2% glycerol as sole carbon-source. Sensitivity to cell wall stress was analyzed through growth on 125 µg/ml Congo red containing YEPD plates (glc = glucose). YNB and YEPD plates served as growth controls. (B) Colony morphology under low glucose. Cells were spread on YEP plates containing 2% glucose (high glucose) or 0.4% glucose (low glucose) to form single colonies with distinct morphologies after 3 d growth at 30 °C. (C) TTC assay to evaluate respiratory activity. Cells were spread on YNB plates containing low amounts of glucose (0.4%). After 3 d incubation at 30 °C, colonies were overlaid with top-agar containing 0.5% TTC that is reduced by electrons of the active respiratory chain to a red dye. (D) Test for adhesive growth. Haploid cells were patched onto 10 mM 3-AT containing YNB plates and incubated for 3 d at 30 °C. Afterwards, plates were washed under a constant stream of water to remove non-adherent cells from the agar surface. Non-adherent strains are highlighted in gray.

In addition to the *asc1*$^{-}$ and the *cASC1* strain, the *asc1*R38D K40E (*asc1*DE) strain was included in the phenotypic characterizations. This strain expresses an Asc1p variant that is supposed to bind less efficiently to the ribosome due to the exchange of two highly conserved, positively charged residues R38 and K40 to negatively charged aspartate (D) and glutamate (E, Coyle et al., 2009). R38 of Asc1p seems to contact D27 of Rps17p, and K40 appears to form a salt-bridge with a phosphate residue of the sugar-phosphate backbone of the rRNA (Adams et al., 2011). An *S. cerevisiae asc1*DE strain has originally been constructed and

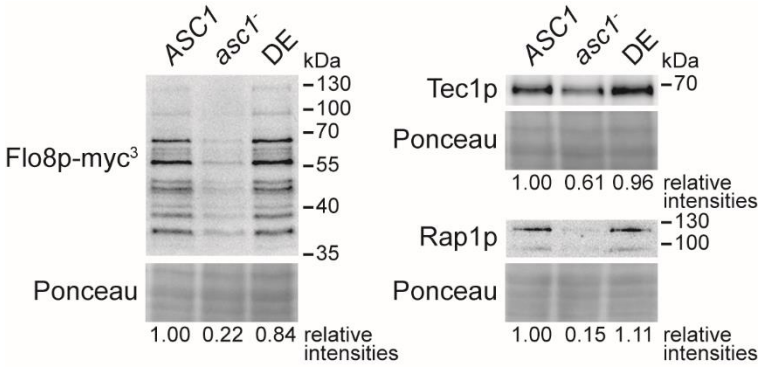

Figure 12. Asc1p-dependent transcription factor levels.
Immunodetection of Flo8p-myc^3, Tec1p, and Rap1p within cell extracts from *ASC1* wild-type, *asc1*$^-$, and *asc1*DE cultures. A c-myc antibody was used to detect myc^3-tagged Flo8p. Tec1p and Rap1p were detected using protein-specific antibodies. Ponceau red staining of proteins served as loading control, and a part of the lower half of the stained Western blot membrane is depicted. Fold changes relative to wild-type signal intensities are given below each lane.

phenotypically characterized by Coyle and colleagues (2009). They observed a shift of the majority of Asc1DEp from the ribosomal to the ribosome-free fraction during sucrose gradient ultracentrifugation. Nevertheless, the *asc1*DE strain was shown to behave phenotypically mainly like the *ASC1* wild-type strain, apart from the staining of cells with calcofluor white that revealed elevated levels of chitin in the cell wall similar to an *ASC1* deletion strain (Coyle et al., 2009). Here, an *asc1*DE mutant strain was generated as well in the used *S. cerevisiae* Σ-strain background (Figure 9C2) and tested for additional phenotypes. Similar to what was observed by Coyle and colleagues, the *asc1*DE strain behaved mostly like the *ASC1* wild-type strain. However, it showed a slightly reduced resistance against cycloheximide (Figure 11). Loss of Asc1p causes decreased abundance of the transcription factors Flo8p, Tec1p, and Rap1p. The *asc1*$^-$ strain confirms that this effect depends on the lack of Asc1p and not on the absence of the snoRNA U24. The abundance of these transcription factors, however, remained unaffected in the *asc1*DE strain (Figure 12). Altogether, these observations indicate that compromised binding of Asc1p to the ribosome due to the DE exchange only slightly reduces the functionality of the protein.

3.2 Phosphorylation of Asc1p

Asc1p/RACK1 is known to interact with protein kinases both in yeast and higher eukaryotes. The phosphorylation of Asc1p itself likely regulates its protein-interactions, stability, and subcellular localization (Chang et al., 2002; Zeller et al., 2007). Phospho-sites within Asc1p have been identified in high throughput studies (Smolka et al., 2007; Holt et al., 2009). Here, phosphorylation of Asc1p was studied with a targeted approach based on the purification of

the protein from yeast cultures and identification of phospho-peptides using LC-MS. Subsequently, *S. cerevisiae* mutant strains were generated with amino acid exchanges at the newly identified and the previously known phospho-sites of Asc1p and subjected to phenotypic characterizations to reveal the impact of phosphorylation on the functionality of Asc1p.

3.2.1 The surface of Asc1p is target for multiple phosphorylations

Strep-tagged Asc1p was purified from exponentially growing *S. cerevisiae* cell cultures, and tryptic peptides of the protein were analyzed with LC-MS for in-depth characterization of its phosphorylation. The raw data search against an *S. cerevisiae*-specific protein database using the *Proteome Discoverer 1.4* software and the *SequestHT* and *Mascot* search algorithms resulted in the identification of seven singly phosphorylated peptides, two of them with an overlapping sequence due to a trypsin missed cleavage site at K161 (Figure 13). Since all phospho-peptides identified contained more than one serine, threonine, and/or tyrosine residue, the *phosphoRS* algorithm was used to calculate phospho-site probabilities (Olsen and

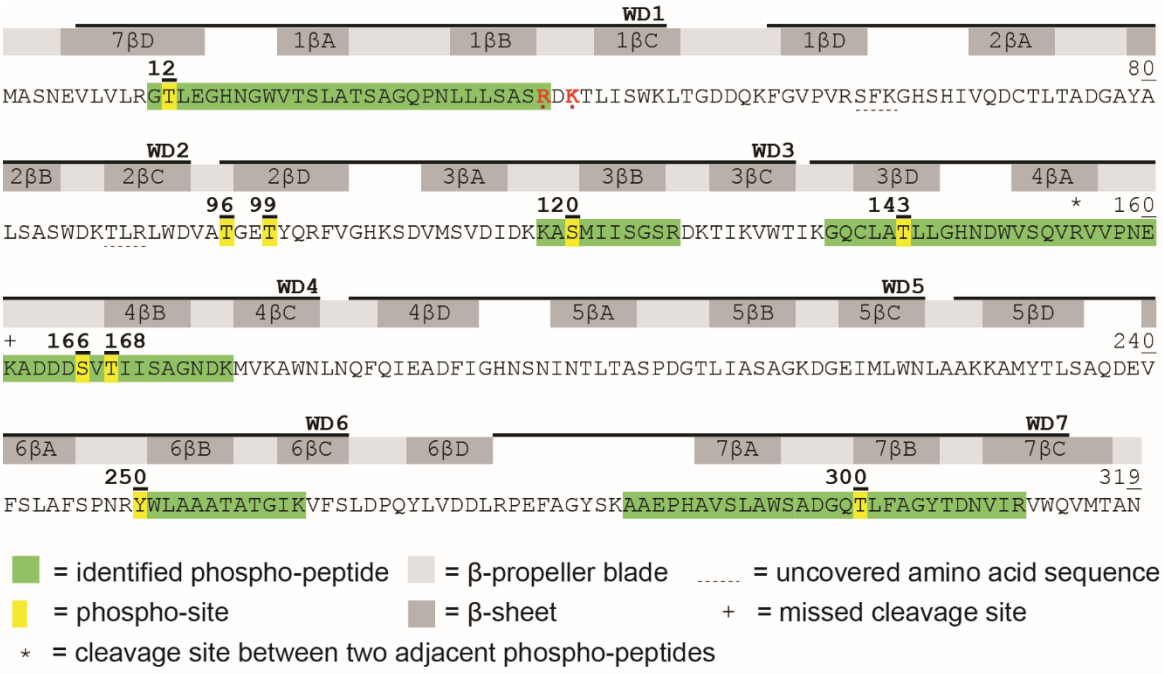

Figure 13. LC-MS-based identification of Asc1p phospho-sites.
Asc1p amino acid sequence is depicted with identified phosphorylated peptides and sites. The amino acid sequence coverage of Asc1p considering all identified high confident peptides was 97.81% (false discovery rate ≤ 0.01). Phospho-sites S166 and T168 were identified within a phospho-peptide ranging from residue A162 to K176 and within a second peptide from residue V156 to K176 bearing a missed cleavage site at the C-terminus of K161 that is indicated with a plus (+). Residues R38 and K40, which lead to compromised ribosome-association of Asc1p when mutated to D and E, respectively, are written in red and marked with dots (Sengupta et al., 2004; Coyle et al., 2009). WD40 repeats are indicated according to SGD (SMART domain SM0032). See Supplementary Table 1 for details on the identification of phospho-peptides and Supplementary Figure 2 for fragmentation spectra.

Mann, 2004; Olsen et al., 2006). Six amino acid residues of Asc1p, T12, S120, T143, S166, T168, and Y250, were identified with a site probability of 100% to be unambiguous phospho-sites. These data confirmed the already known phospho-sites S120, S166, and T168 (Smolka et al., 2007; Holt et al., 2009) and led to the identification of three previously unknown sites, T12, T143, and Y250. Furthermore, a phospho-peptide was identified with 99.9% as the highest localization probability for residue T300. For more details on peptide identification and phospho-site localization, see Supplementary Table 1 and Supplementary Figure 2. This study focused on T12, S120, T143, S166, T168, and Y250 as well as on T96 and T99 (Chi et al., 2007) that were not detected in the experiments presented here. The position of these eight phospho-sites within the protein bound to the 40S subunit of the ribosome is illustrated in Figure 14. T12, T99, and T143 are localized in the βD-strands of blades 7, 2, and 3 thus being localized at the circumference of the protein. T96, S120, S166, and Y250 are localized at sides of Asc1p that do not directly face the ribosome. T96 lies next to T99 in close proximity to the ribosomal protein Rps16. S166 is positioned within the loop between βA- and βB-strands of blade 4 adjacent to T168, which is the N-terminal amino acid of strand 4βB. None of the phospho-sites is localized at the side of Asc1p known to directly contact other ribosomal proteins indicating that kinases can access the protein in its ribosome-bound state.

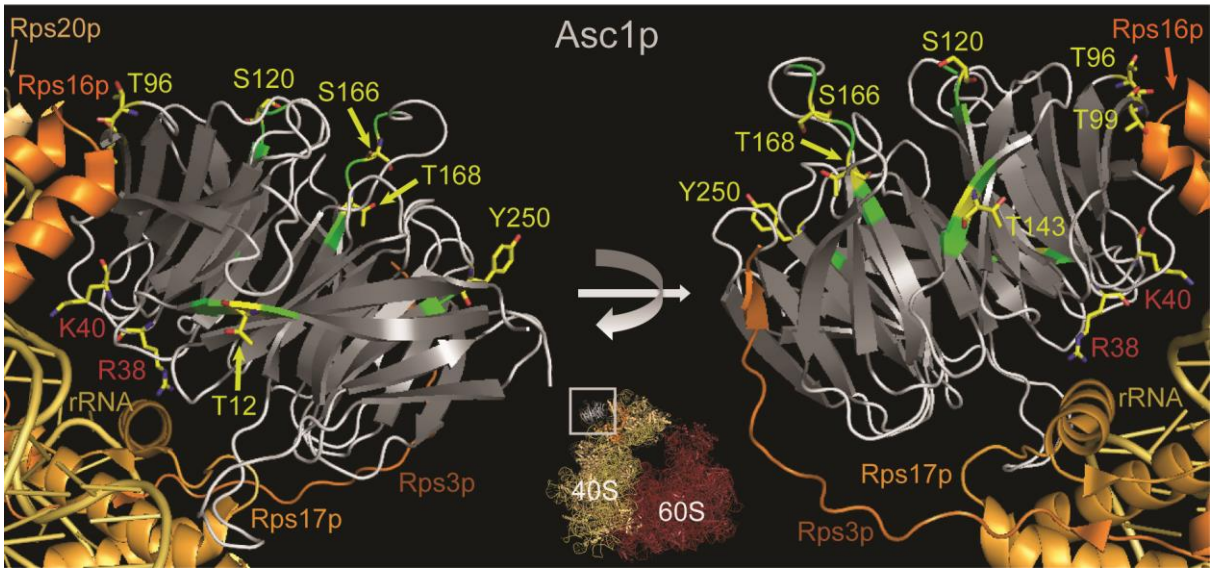

Figure 14. Cartoon view of Asc1p bound to the 40S subunit of the ribosome.
The Asc1p β-propeller is depicted in white (loops) and gray (β-strands). Positions of phospho-sites that were further analyzed in this study are highlighted in yellow, and the amino acids are depicted as sticks with carbon atoms in yellow, nitrogen atoms in blue, and oxygen atoms in red. For better recognizability, neighboring amino acids within the LC-MS-identified peptides are colored in green. Additionally, residues R38 and K40 are highlighted. For the ribosomal protein Rps3, the C-terminal last 14 amino acids were structurally not resolved and are therefore missing. Figures of structures were generated with *PyMOL Molecular Graphics System* software on the basis of the PDB file 4V88 (Ben-Shem et al., 2011).

3.2.2 Construction of yeast strains expressing Asc1p isoforms with amino acid exchanges at phospho-sites

To analyze the impact of phosphorylation on Asc1p, *S. cerevisiae* Asc1p phospho-site mutant strains were generated. These strains express Asc1p having either glutamate or alanine at one of the phospho-sites to mimic their constitutively phosphorylated or dephosphorylated state, respectively. Y250 was mutated to phenylalanine instead of alanine due to the higher similarity between these two amino acids. For phospho-sites lying close to each other within the amino acid sequence (T96 and T99 as well as S166 and T168), strains with both sites mutated simultaneously were generated in addition.

Furthermore, strains carrying each phospho-site substitution in combination with the two amino acid exchanges R38D K40E were constructed. These two amino acid exchanges are considered to compromise the ribosome binding of Asc1p (see chapter 3.1). The DE mutation causes only a marginal loss of Asc1p's functionality, but it might cause synthetic effects in combination with the phospho-site mutations. All constructed strains are listed in Table 1. Growth phenotypes studied with these strains are summarized in Table 3 and are illustrated and described in the following chapter.

3.2.3 Asc1p phospho-sites T143 and Y250 confer resistance against translation inhibitors and together with T12, T96, and T99 are essential to maintain overall functionality of the Asc1DEp variant

The phospho-site mutant strains constructed were analyzed with respect to the Asc1p-dependent phenotypes introduced in chapter 3.1 and the *ASC1* wild-type, *asc1*$^{-}$, and *asc1*DE strains were used as references. Figures 15-17 give an overview of the main observations. The dephosphorylation mimicking mutations T143A and Y250F increased the sensitivity to cycloheximide similar to the DE mutation, and the Y250F mutation also caused sensitivity to canavanine (Figure 15). In the absence of an additional DE mutation, all other phospho-site mutant strains showed wild-type behavior (Figures 15-17 and data not shown). DE-compromised localization of Asc1p at the ribosome, however, enhances the effects caused by amino acid exchanges at T143 and Y250. The *asc1*^{T143A}DE and *asc1*^{Y250F}DE strains showed synthetic hypersensitivity to cycloheximide in comparison to the strains bearing only the dephosphorylation mimic or the DE mutation (Figure 15). They were even phenotypically similar to the *asc1*$^{-}$ strain. Irrespective of the DE mutation, phenylalanine at position 250 affected the sensitivity to cycloheximide and canavanine. The *asc1*^{T143A}DE strain behaved similar to the *asc1*$^{-}$ strain in all tests showing, for example, strongly reduced red pigmentation

Table 3. Overview of Asc1p phospho-site mutant strains and their phenotypes.
As references the phenotypes of the *ASC1* wild-type strain were defined as +, and the phenotypes of the Asc1p-deficient *asc1*$^{-}$ strain as - - -. The phenotypes of the Asc1p phospho-site mutant strains were classified accordingly. Dark gray background color highlights strains and their phenotypes that differed significantly from the *ASC1* wild-type strain.

	cana-vanine	cyclo-heximide	glycerol	TTC assay	Congo red	wrinkled colonies	adhesive growth
reference strains							
ASC1	+	+	+	+	+	+	+
asc1^{-}	- - -	- - -	- - -	- - -	- - -	- - -	- - -
*asc1*DE	+	-	+	+	+	+	+
phospho-site mutant strains							
T12A	+	+	+	+	+	+	+
T12A DE	+	-	+	+	+	+	-
T12E	+	+	+	+	+	+	+
T12E DE	+	-	+	+	+	+	+
T96A	+	+	+	+	+	+	+
T96A DE	-	- -	- -	-	-	- -	- - -
T96E	+	+	+	+	+	+	+
T96E DE	-	- -	- -	-	-	- -	- - -
T99A	+	+	+	+	+	+	+
T99A DE	+	-	+	+	+	-	-
T99E	+	+	+	+	+	+	+
T99E DE	+	-	+	+	+	+	+
T96A T99A	+	+	+	+	+	+	+
T96A T99A DE	- -	- - (-)	- - -	- -	- -	- -	- - -
T96E T99E	+	+	+	+	+	+	+
T96E T99E DE	-	+	+	+	-	-	- - -
S120A	+	+	+	+	+	+	+
S120A DE	+	-	+	+	+	+	+
S120E	+	+	+	+	+	+	+
T143A	+	-	+	+	+	+	+
T143A DE	- - (-)	- - -	- - -	- - -	- -	- - -	- - -
T143E	+	+	+	+	+	+	+
T143E DE	-	- - -	+	- -	+	-	- -
S166A	+	+	+	+	+	+	+
S166A DE	+	-	+	+	+	+	+
S166E	+	+	+	+	+	+	+
T168A	+	+	+	+	+	+	+
T168A DE	+	-	+	+	+	+	+
T168E	+	+	+	+	+	+	+
S166A T168A	+	+	+	+	+	+	+
T166A T168A DE	+	-	+	+	+	+	+
S166E T168E	+	+	+	+	+	+	+
Y250F	- -	-	+	+	+	+	+
Y250F DE	- -	- -	+	+	+	+	+

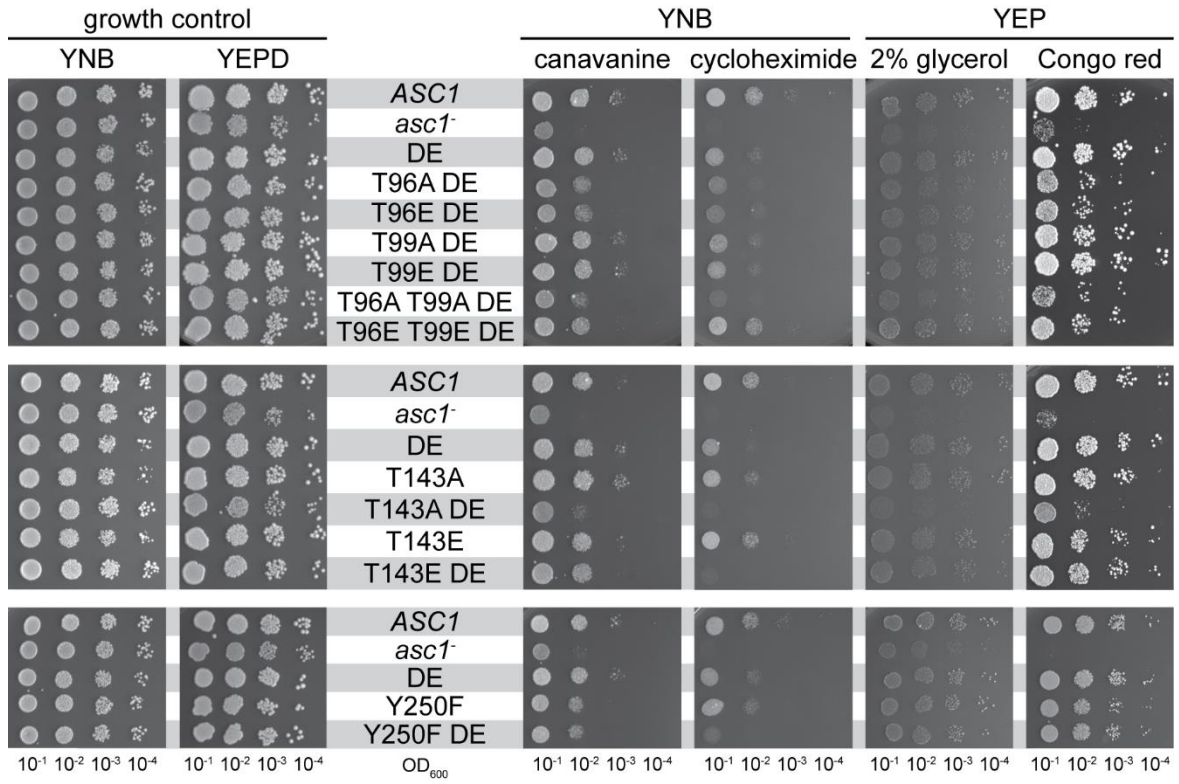

Figure 15. Drop dilution assays to analyze the impact of phospho-site mutations on Asc1p-dependent phenotypes.
Cell suspensions were spotted on YNB plates with or without 0.15 µg/ml cycloheximide or 600 ng/ml canavanine, respectively, to assess sensitivity to translation/protein biosynthesis inhibitors. To evaluate cell wall integrity, cells were dropped on YEPD plates with or without 125 µg/ml Congo red, and to test fermentative activity, cells were spotted onto YEP medium with 2% glycerol instead of glucose.

in the presence of TTC (Figure 16B2). Only its sensitivity to Congo red was less pronounced than for the *asc1*$^{-}$ strain. The *asc1*^{T143E}DE strain with a phosphorylation mimic at position 143 showed similar but in most cases milder phenotypes than the *asc1*^{T143A}DE strain.

Combination with the DE mutation also caused strong effects of the amino acid substitutions at T12, T96, and T99. The *asc1*^{T12A}DE strain showed impaired adhesive growth (Figure 17). The *asc1*^{T96A}DE and the *asc1*^{T96E}DE strain were non-adhesive and showed no wrinkled colony morphology on 0.4%. Other phenotypes were only mildly affected (Figures 15-17). The substitution of T99 by alanine, but not by glutamate, combined with the DE mutation affected the same two phenotypes though less severely. The *asc1*$^{T96A\ T99A}$DE strain with both neighboring amino acids replaced by alanine behaved like the *asc1*^{T96A}DE strain except for its slightly increased sensitivity to cycloheximide (Figure 15). Interestingly, the sensitivity of the *asc1*^{T96E}DE strain to cycloheximide and its reduced growth on the non-fermentable carbon source glycerol were suppressed by an additional T99E exchange (*asc1*$^{T96E\ T99E}$DE strain). In all other assays, the additional T99E mutation only partially suppressed the phenotype caused

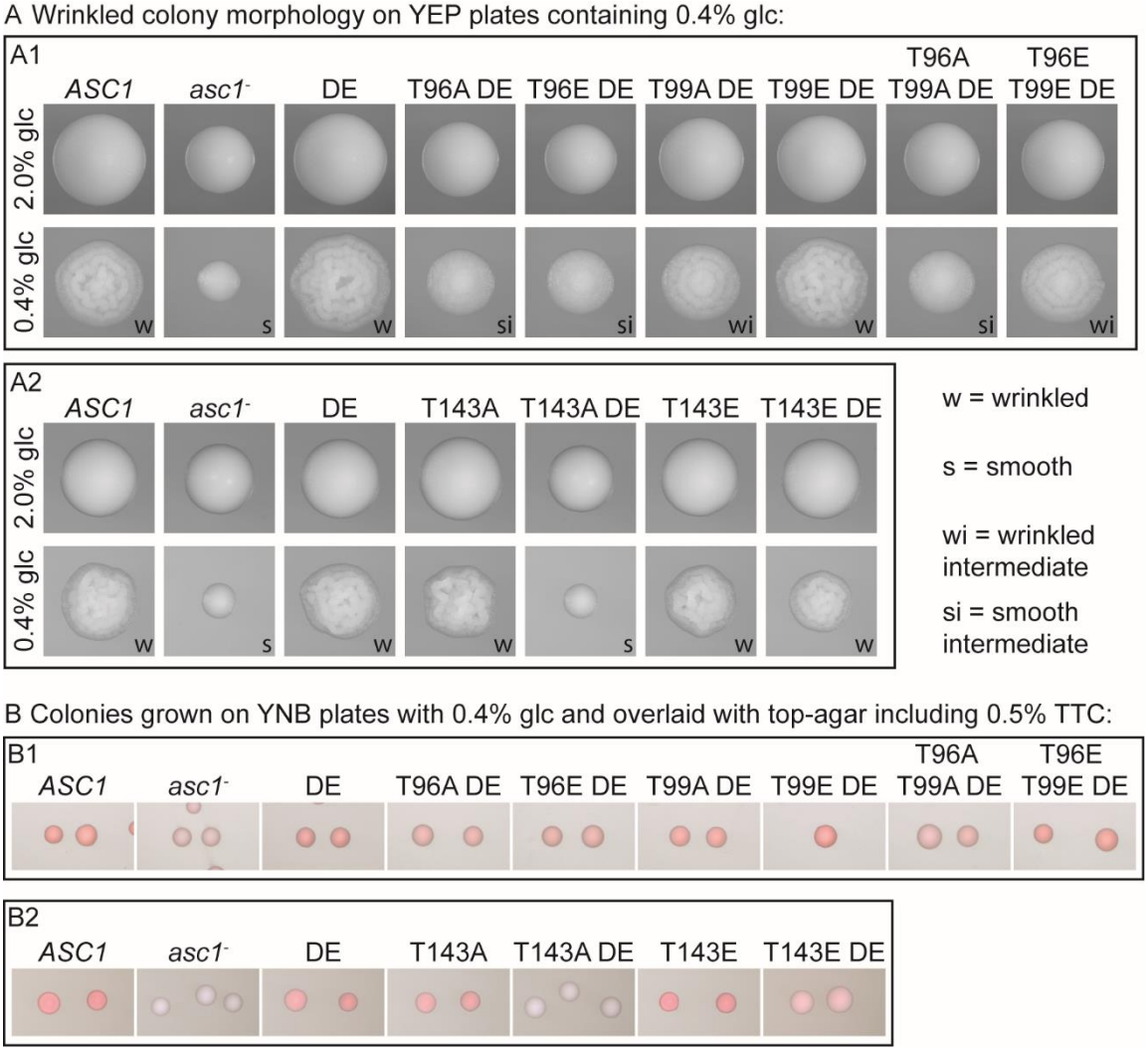

Figure 16. Impact of Asc1p phospho-site mutations on colony morphology and respiratory activity.
(A) Colony morphology under glucose limitation. Cells were grown on YEP 2% glucose plates (no limitation) and YEP 0.4% glucose plates (glucose limitation). (B) TTC assay to evaluate respiratory activity. Cells were grown on 0.4% glucose containing YNB plates. Colonies were overlaid with 1.2% top agar containing 0.5% TTC and incubated for 20 to 30 min at 30 °C. (glc = glucose)

by the T96E DE mutation. Combination of the DE mutation with dephosphorylation mimics at S120, S166, and T168 did not affect any of the tested phenotypes (data not shown, substitution to glutamate was not tested). Thus, DE-induced alterations in Asc1p-binding to the ribosome caused phenotypes when combined with specific phospho-site mutations. A high-copy plasmid bearing the wild-type *ASC1* gene complemented all mutations and by that revealed a recessive nature of the described *asc1* mutations (Figure 18).

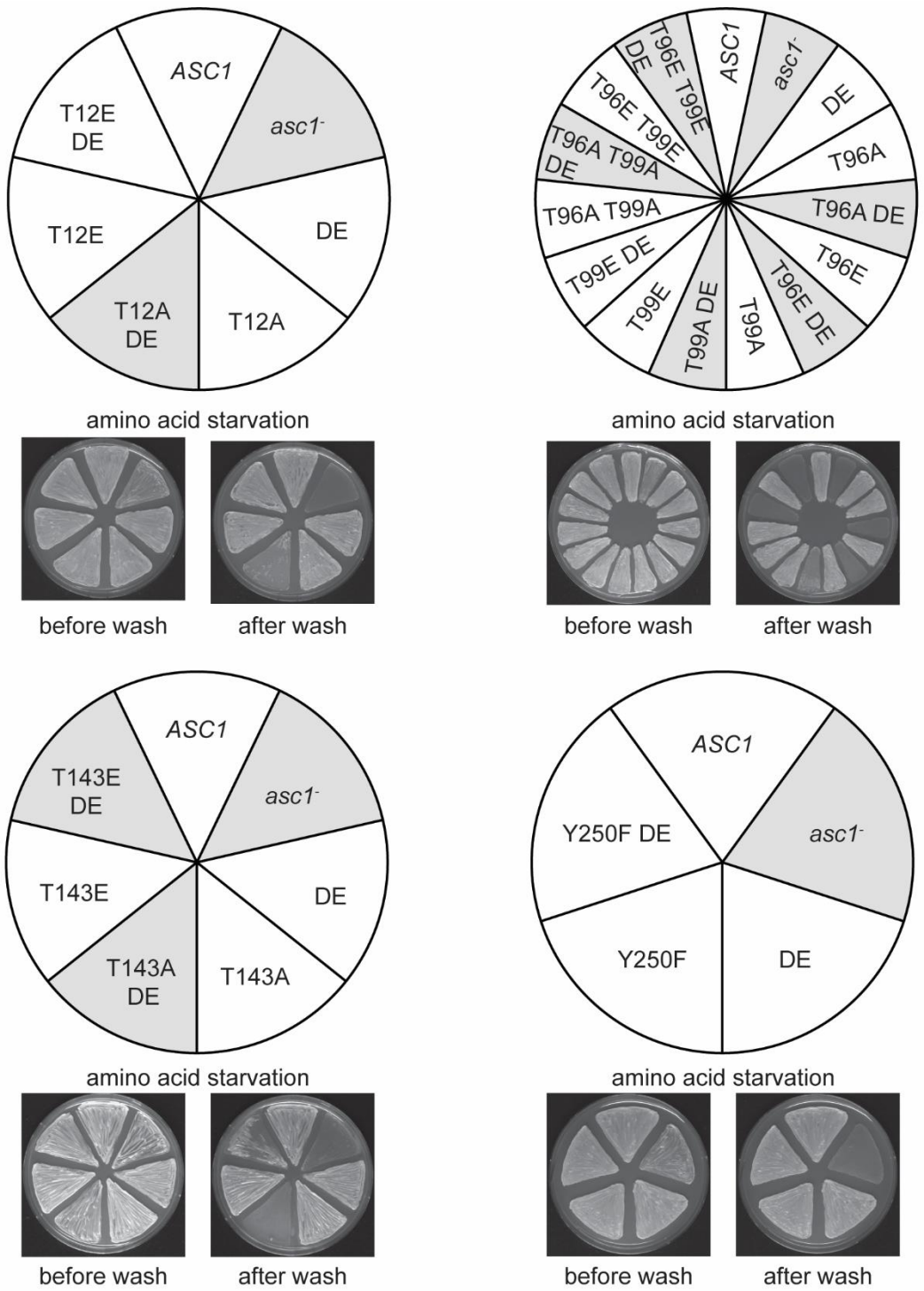

Figure 17. Test for haploid adhesive growth of phospho-site mutant strains.
Cells were patched on 10 mM 3-AT containing YNB plates and incubated for 3 d. Plates are depicted before and after washing with a constant stream of water.

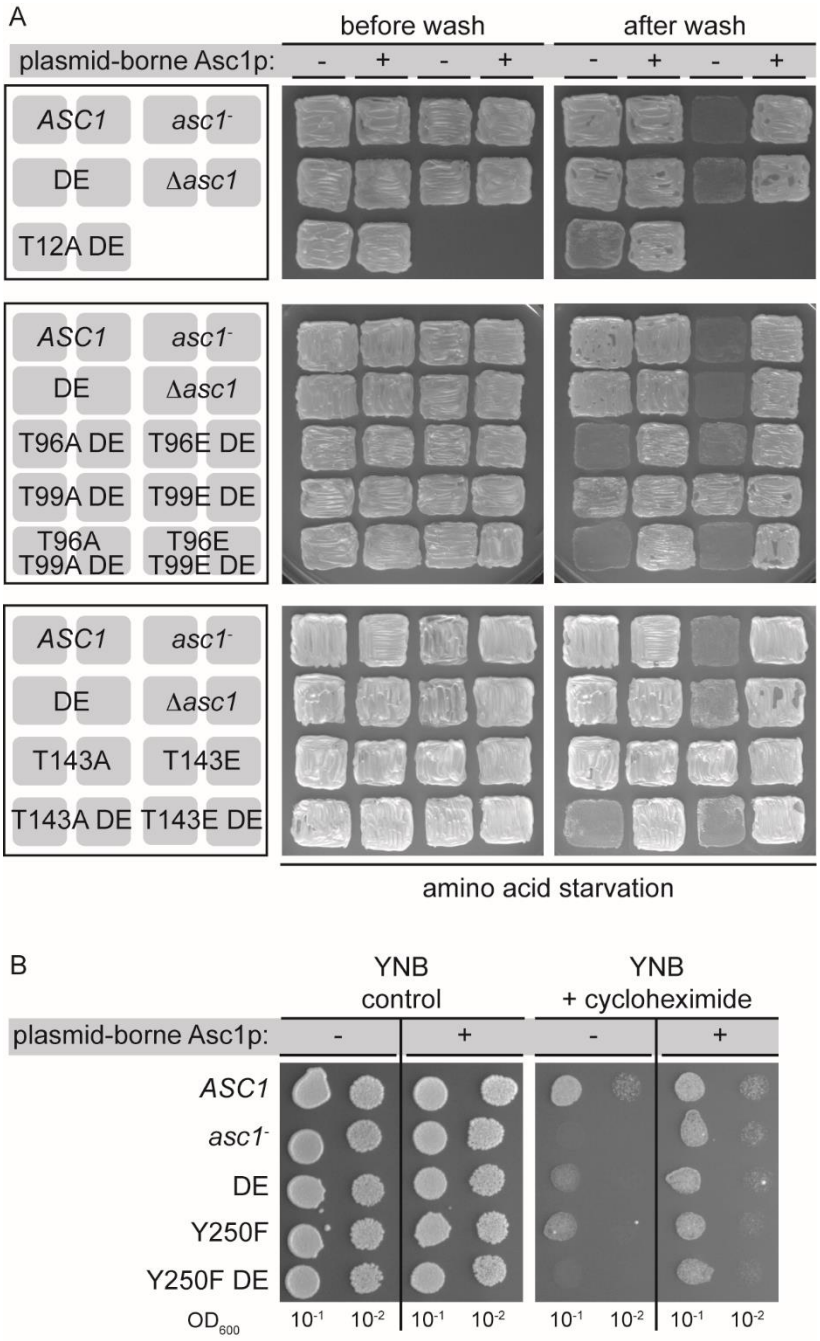

Figure 18. Complementation of *ASC1* phospho-site mutant phenotypes by expression of plasmid-borne wild-type *ASC1*.

Phospho-site mutants were transformed with a high-copy number plasmid carrying the wild-type *ASC1* gene under the control of the *MET25*-promoter (*ASC1*; pME2624) or with the empty vector (EV; pME2787) as control. The *ASC1* wild-type, *asc1*$^{-}$, Δ*asc1*, and *asc1*DE strains were transformed with the same plasmids as further controls. (A) Haploid adhesive growth at amino acid starvation caused by 10 mM 3-AT. Plasmid-transformed phospho-site mutants *asc1*^{T12A}DE, *asc1*^{T96A}DE, *asc1*^{T96E}DE, *asc1*^{T99A}DE, *asc1*$^{T96A\ T99A}$DE, *asc1*$^{T96E\ T99E}$DE, *asc1*^{T143A}DE, and *asc1*^{T143E}DE as well as control strains were patched on the 3-AT containing YNB plates and subjected to wash tests after 3 d of growth. The *asc1*^{T99E}DE, *asc1*^{T143A}, and *asc1*^{T143E} strains, which are not impaired in adhesive growth, served as additional controls. Plates are shown before and after the washing step. (B) Drop dilution assay to evaluate cycloheximide sensitivity. Cell suspensions of plasmid-transformed phospho-site mutant strains *asc1*^{Y250F} and *asc1*^{Y250F}DE as well as control strains were applied onto YNB plates containing 0.15 µg/ml cycloheximide.

3.2.4 Phosphorylation of T12, T96, T99, and especially T143 is required for cellular abundance of Asc1DEp

The cellular abundance of the Asc1DE protein was found to be rather increased compared to that of Asc1p in the wild-type strain (Figure 19). The abundance of Asc1DEp requires the integrity of the phospho-sites T12, T96, T99, and especially T143, but not Y250. Yet, none of the phospho-site exchanges alone affected the abundance of Asc1p in the absence of the DE mutation (Figure 19 and data not shown). Replacing residue T143 by alanine caused the severest reduction in Asc1DEp abundance even far below the Asc1p levels in wild-type cells. This correlates with the phenotypes of this strain that are reminiscent of those of the *asc1*$^{-}$ strain. The exchange of T143 by a phosphorylation-mimicking glutamate residue reduced the Asc1DEp levels, yet, to a lesser extent.

The combination of DE with T96 replaced either by alanine or by glutamate caused a severe reduction of Asc1p abundance below wild-type levels as well. This effect was enhanced for the T96 alanine substitution through the simultaneous exchange of its neighboring amino acid T99 to alanine in strain *asc1*$^{T96A\ T99A}$DE. In contrast, the *asc1*$^{T96E\ T99E}$DE strain exhibited

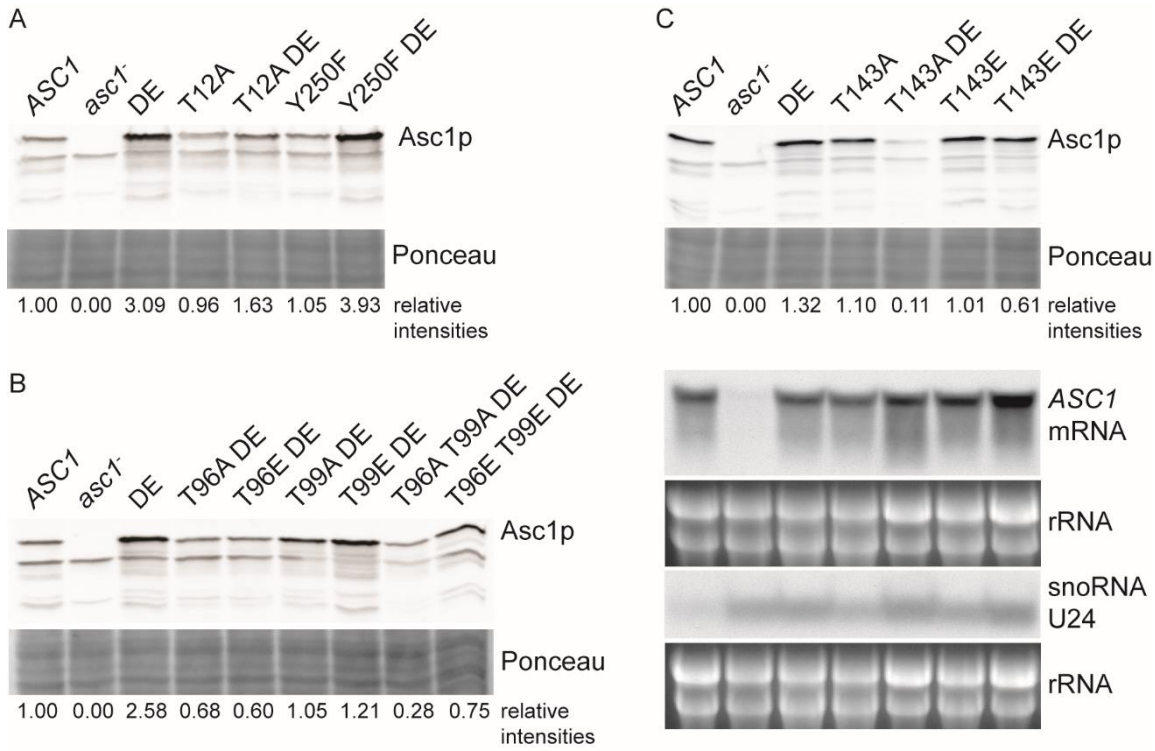

Figure 19. Asc1 protein abundance in phospho-site mutant strains.
(A-C top) Immunodetection of Asc1p within cell extracts derived from *ASC1* wild-type, *asc1*DE, and phospho-site mutant strains and the *asc1*$^{-}$ strain as negative control. Ponceau red staining of proteins served as loading control, and a part of the lower half of the stained Western blot membrane is depicted. Fold changes relative to wild-type signal intensities are given below each lane. (C bottom) Northern blot analyses for detection of *ASC1* mRNA and *SNR24* snoRNA U24 levels in T143 phospho-site mutant strains. rRNA served as loading control.

higher levels of Asc1p, an observation that is also in line with the phenotypes of this strain. Remarkably, the T96E T99E exchanges rescued the sensitivity of the *asc1*DE strain to cycloheximide independently of Asc1p levels in the *asc1*$^{T96E\ T99E}$DE strain that are reduced in comparison to the *asc1*DE strain.

The *asc1*^{Y250F}DE strain displayed Asc1p levels similar to the *asc1*DE strain. Thus, the increased sensitivity of both the *asc1*^{Y250F} and the *asc1*^{Y250F}DE strain to cycloheximide and canavanine cannot be explained by the cellular abundance of Asc1p in these strains. To exclude that the changes in Asc1p expression were caused at the *ASC1* mRNA level, Northern blot experiments were performed with a probe against exon 1 of *ASC1*. The *asc1*^{T143A}DE strain with the strongest reduction of Asc1p abundance revealed unchanged levels of *ASC1* mRNA suggesting that the reduced Asc1p-levels were caused post-transcriptionally either through mRNA translation or protein stability (Figure 19C).

3.3 The Asc1p-dependent phospho-proteome

The evidence for Asc1p-phosphorylation and the knowledge about Asc1p being an important player in cellular signal transduction prompted us to investigate Asc1p-dependent protein-phosphorylation beyond its own phosphorylation. Previous studies reported that the absence of Asc1p leads to increased phosphorylation of the MAPKs Kss1p and Slt2p, which control filamentous growth, mating, and cell wall integrity (Chasse et al., 2006; Zeller et al., 2007). Here, the phosphorylation of the MAPK of the high osmolarity response pathway, Hog1p, was analyzed using an antibody for the protein phosphorylated at residues T174 and/or Y176 by its upstream MAP2K, Pbs2p. A significant decrease in Hog1p phosphorylation was detected in the *asc1*$^{-}$ strain, but not in the *asc1*DE strain (Figure 20A). This might explain the sensitivity of the *asc1*$^{-}$ strain to osmotic stress (Figure 20B, Melamed et al., 2010).

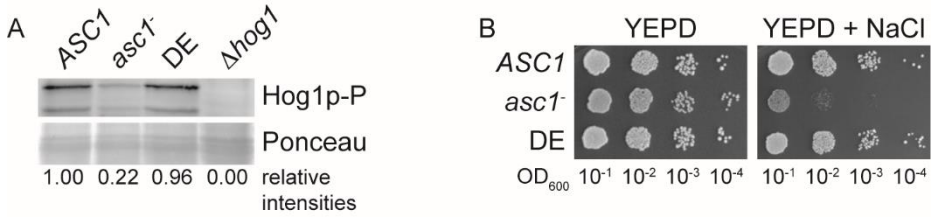

Figure 20. Asc1p-dependency of the high osmolarity response pathway.
(A) Immunodetection of Hog1p phosphorylated at T174 and/or Y176 within cell extracts obtained from *ASC1* wild-type, *asc1*$^{-}$, and *asc1*DE cells using a phospho-p38 MAP kinase-specific antibody. As loading control, proteins were stained with Ponceau red, and a part of the stained Western blot membrane approximately at the level of the Hog1p-P signals is depicted. Fold changes relative to wild-type signal intensities are given below each lane. (B) Drop dilution assay on YEPD plates containing 75 mM NaCl to evaluate osmotic stress sensitivity.

3.3.1 Asc1p affects the phosphorylation of more than 200 proteins at almost 300 different sites

To get an unbiased and comprehensive view on Asc1p-dependent phosphorylation of other proteins besides MAPKs, a LC-MS-based quantitative phospho-proteome analyses was performed using *stable isotope labeling with amino acids in cell culture* (SILAC). The proteomes of the following strains were quantitatively compared to that of the wild-type *ASC1* strain: 1.) The *asc1*$^{-}$ strain, to study the impact of the absence of Asc1p, 2.) the *asc1*DE strain, to observe the consequences of a displaced Asc1p at the ribosome, 3.) the *asc1*^{T143A}, *asc1*^{T143E}, and *asc1*^{T143E}DE strains, to investigate the impact of the phospho-site T143 in the presence and absence of the DE mutation. Prior to the quantitative phospho-proteome analysis that requires the enrichment of phospho-peptides from overall peptide-samples, the total proteomes were quantitatively compared to analyze the overall changes in protein abundance. The total proteome data were used to correlate changes in phosphorylation to changes in protein abundance enabling correction of the phospho-peptide SILAC-ratios with the corresponding protein ratios. For efficient incorporation of the isotopically labeled arginine and lysine, Δ*arg4* Δ*lys1* strains were generated for the *ASC1* wild-type, the *asc1*$^{-}$, and the *asc1*DE background. Strains with the phospho-site T143 mutated were arginine and lysine prototroph and therefore cultivated in the presence of the naturally occurring light amino acids (Arg^0, Lys^0). To distinguish between changes caused by the Asc1p mutations or differences in arginine and lysine metabolism (prototroph *ARG4 LYS1* strains versus auxotroph Δ*arg4* Δ*lys1* strains), an *auxotrophy-control ASC1*^{Aux} was included in the experiments that is an *ASC1* wild-type strain prototrophic for arginine and lysine (*ARG4 LYS1*). The triple SILAC approach using *light* (Arg^0, Lys^0), *medium* (Arg^6, Lys^4), and *heavy* (Arg^{10}, Lys^8) variants of the labels enables the quantitative comparison of these proteomes in one experiment.

The workflow for the peptide sample preparation of the Asc1p-dependent proteome and phospho-proteome analyses is depicted in Figure 21. All experiments included the *ASC1* Δ*arg4* Δ*lys1* strain as constant reference for SILAC-ratio reporting. In the following text, the term SILAC-ratio refers to ratios with the respective *ASC1* Δ*arg4* Δ*lys1* value in the denominator. A detailed description of the LC-MS data evaluation using the *MaxQuant*/*Perseus* software is provided in the *Materials and Methods* section and in Supplementary Tables 2 (proteome) and 3 (phospho-proteome). Briefly, a one-sample *t*-test (p-value < 0.01) was applied for the protein SILAC-ratios of the *asc1*$^{-}$ and *asc1*DE strains to identify proteins that are significantly regulated. A two-sample *t*-test (p-value < 0.01) was used to assess the difference between the protein SILAC-ratios of the *asc1*^{T143} mutant strains

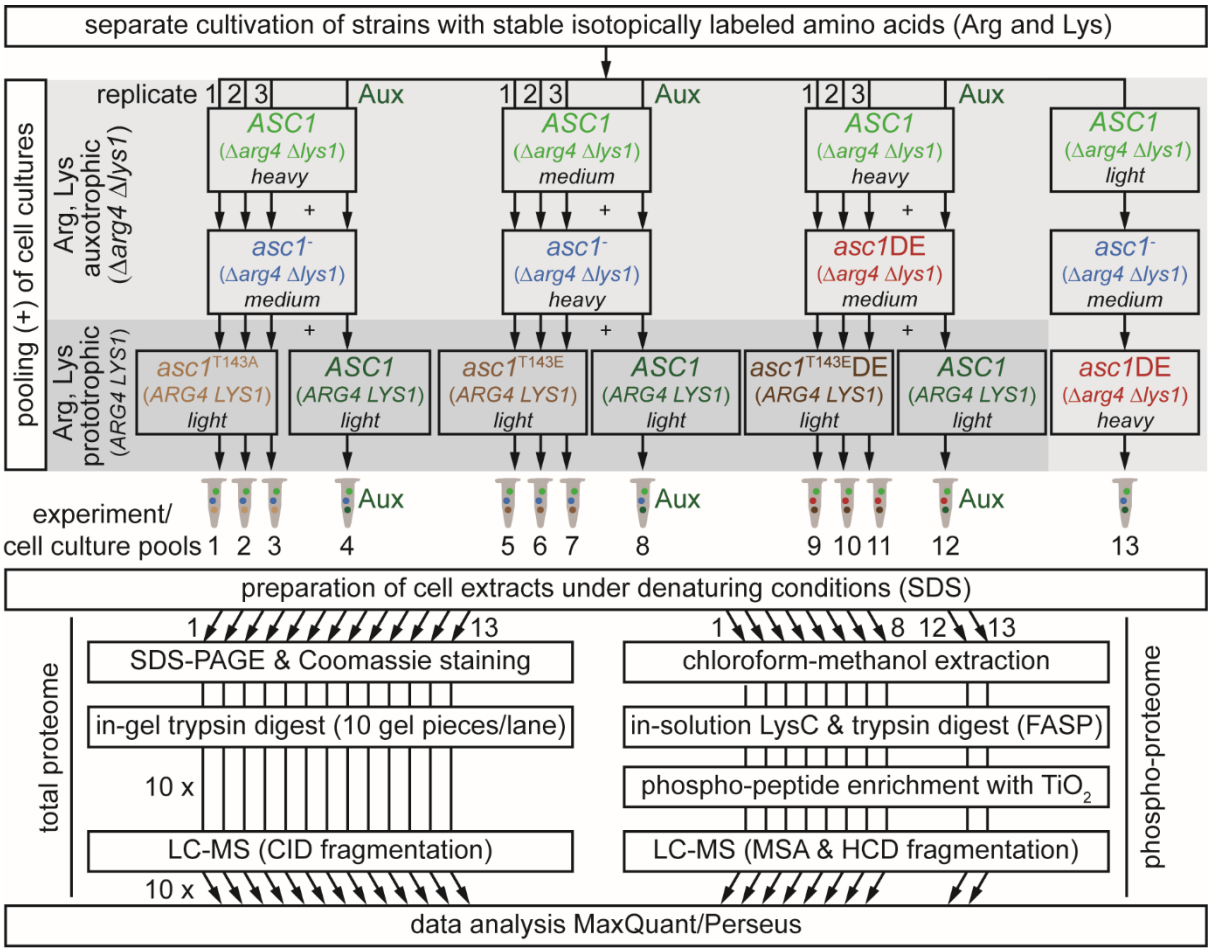

Figure 21. Analysis of the Asc1p-dependent phospho-proteome.
Peptide sample preparation for SILAC and LC-MS-based Asc1p-dependent phospho-proteome and proteome analyses. *S. cerevisiae* strains were cultivated in the presence of *light*, *medium*, or *heavy* labeled arginine and lysine. Arrows indicate which strains were pooled and indicate the number of replicates. The *auxotrophy control* (Aux) comprised cells of the *ASC1 ARG4 LYS1* strain. In total, 13 independent cell pools were obtained and subjected to the subsequent preparation of cell extracts. The protein extracts were split in two and processed separately for the proteome and phospho-proteome analyses. For the proteome analysis, cell extract containing 100 µg protein was separated by SDS-PAGE, followed by staining with Colloidal Coomassie and in-gel trypsin digestion. For the phospho-proteome analysis, only protein extracts of experiments 1-8 and 12-13 were further processes. 1 mg protein of each sample was subjected to chloroform-methanol extraction to remove SDS from the samples followed by in-solution digestion (filter-aided sample preparation, FASP, Wiśniewski et al., 2009) with LysC and trypsin. Phospho-peptides were enriched using TiO_2 affinity chromatography. The peptide samples were analyzed individually by LC-MS using appropriate fragmentation techniques (CID, MSA-CID, or HCD). All raw data files were searched in one set against an *S. cerevisiae*-specific protein database with the *MaxQuant* software. The downstream data evaluation was performed with *Perseus* as described in Supplementary Tables 2 and 3.

and the corresponding values of the auxotrophy controls. In the *asc1*$^{-}$ strain, 604 proteins were significantly affected in their abundance with an averaged $\log_2$ SILAC-ratio < -0.26 or > 0.26 (Supplementary Table 4). Using this threshold for regulation twelve proteins for the *asc1*DE, one and four for the *asc1*^{T143A} and *asc1*^{T143E} strains, respectively, and 111 for the *asc1*^{T143E}DE

strain were identified as regulated (Supplementary Tables 5-8). The rather marginal changes in the *asc1*DE, *asc1*^{T143A}, and *asc1*^{T143E} proteomes reflect the observation that these strains behaved phenotypically mainly like the wild-type strain in our tests. Accordingly, 88 of the 111 proteins affected in their abundance by the T143E DE mutation were identified as regulated in the *asc1*$^{-}$ strain as well, and in line with this, the *asc1*^{T143E}DE strain mostly showed similar or equal phenotypes as the Asc1p-deficient strain.

Based on these observations, the phospho-proteome analysis focused on the *asc1*$^{-}$ strain. The respective peptide samples were subjected to the enrichment of phospho-peptides and LC-MS analysis. In total, 1947 distinct phospho-sites (localization probability ≥ 0.5) were identified. 1245 of these sites were detected and quantified in at least two independent samples for the comparison between the *asc1*$^{-}$ and *ASC1* wild-type strain and considered for further analysis. A two-sample *t*-test (p-value < 0.01) was applied comparing the SILAC-ratios of the phospho-sites with those of the corresponding proteins. The significantly regulated phospho-sites were further filtered for their degree of regulation considering only sites with a normalized median $\log_2$ SILAC-ratio < -0.26 or > 0.26 (Supplementary Table 9). Table 4 lists phospho-sites with an even stronger regulation of median $\log_2$ SILAC-ratios ≤ -0.58 or ≥ 0.58. Phospho-sites with zero to two quantification values for the corresponding protein were also considered applying a one-sample *t*-test on their SILAC-ratios. In total, 289 phospho-sites in 208 proteins showed Asc1p-dependent changes in their degree of phosphorylation. 139 of these sites were found to be up-regulated and 151 down-regulated including one site (S222 of Vid27p) that was identified as up-regulated for the singly phosphorylated peptide and down-regulated for the doubly phosphorylated peptide (T220 and S222). Six other sites were also identified twice within singly and doubly phosphorylated peptides, but showed the same direction of regulation. 62 proteins were identified with more than one Asc1p-dependently regulated phospho-site, and eight of these proteins contained sites that were increased and others that were decreased in their degree of phosphorylation.

Table 4. Asc1p-dependently regulated phospho-sites.

All proteins containing phospho-sites with a proteome-corrected median $\log_2$ *asc1*$^{-}$*/ASC1* SILAC-ratio ≤ -0.58 or ≥ 0.58 are listed together with their regulated sites and the corresponding localization probabilities (site & prob). The colors reflect the values of the median SILAC-ratios for the phospho-site (phos), the corresponding protein (prot), and the proteome-correction ($\log_2$ ratio phospho-site minus $\log_2$ ratio protein, named *phospho regulation*). Gray indicates that the protein was not quantified in the total proteome analysis. In this case, the *phospho regulation* is identical with the quantification value for the phospho-site. 1 indicates that only one quantification value was obtained. Phospho-sites that are printed in italics are previously unknown sites according to *PhosphoGRID* (http://www.phosphogrid.org, Stark et al., 2006) and SGD including data from Swaney et al. (2013). See Supplementary Table 9 for details and additional phospho-sites with a proteome-corrected $\log_2$ *asc1*$^{-}$*/ASC1* SILAC-ratio < -0.26 or > 0.26.

Table 4.

protein	site & prob	asc1⁻/ASC1 phos	asc1⁻/ASC1 prot	phospho regulation
Edc1	S82 0.99			2.15
Tpi1	S215 1.00			1.47
Csr1	S2 1.00			1.45
Pre8	*S15* 1.00			1.16
Rpn7	*S196* 1.00			1.11
Isc1	*T361* 1.00			0.95
Rpl12a/b	S38 1.00			0.93
Rcn1	S117 1.00			0.91
Rcn1	S113 1.00			0.91
Ste20	T572 0.61			0.90
Pin4	S194 1.00			0.87
Nte1	S634 0.99			0.83
Ste20	S169 1.00			0.82
Ty2a*	*S424* 0.99			0.81
Imh1	*T304* 0.65			0.81
Acm1	S48 1.00			0.80
Aim3	S843 0.93			0.79
Imh1	S308 0.98			0.72
Smi1	S389 0.92			0.72
Nnk1	Y739 1.00			0.70
Iml2	S7 1.00			0.70
Pgm3	*T156* 0.66			0.69
Kri1	Y482 0.63			0.68
Rlp7	T120 1.00			0.67
Rpn1	S19 1.00			0.67
Tif1	S2 1.00			0.67
Acc1	*S9* 0.87			0.66
Fyv8	S441 0.99			0.65
Dig2	T83 0.76			0.64
Rpo21	T1471 0.93			0.64
Pgm3	S158 0.97			0.64
Imh1	S827 0.52			0.64
Ste20	S502 1.00			0.63
Rrp36	S14 1.00			0.63
Myo3	S357 1.00			0.62
Pda1	S313 1.00			0.62
Dig2	T82 0.94			0.62
Pdr16	S349 0.69			0.61
Pdr16	S346 0.97			0.61
Stb1	T99 1.00			0.60
Stb1	S72 1.00			0.58
Ppq1	S208 0.89			0.58
Ysc84	S301 1.00			0.58

protein	site & prob	asc1⁻/ASC1 phos	asc1⁻/ASC1 prot	phospho regulation
additional 96 sites 0.58 > x > 0.26				
additional 74 sites -0.26 > x > -0.58				
Acc1	S1157 1.00			-0.59
Hom3	S332 0.94			-0.59
Tsa1	T174 1.00			-0.60
Yap1	S14 1.00			-0.60
Bni1	S1889 0.99			-0.62
Sod1	S39 1.00			-0.62
Ura2	T1859 0.77			-0.62
Cue4	S48 1.00		1	-0.64
Sch9	S726 1.00			-0.64
Yjl070c	S43 1.00		1	-0.65
Pup2	S56 0.89			-0.65
Prr1	S132 1.00			-0.65
Rps19a/b	S117 1.00			-0.65
Ssd1	S231 0.96			-0.65
Trm2	*S98* 0.95			-0.66
Rad16	S25 1.00			-0.66
Sec21	T638 1.00			-0.67
Yjl070c	S41 0.99		1	-0.67
Trm2	S92 0.95			-0.68
Rsc2	S682 1.00			-0.68
Abp1	S167 0.94			-0.70
Ent3	*S2* 1.00			-0.70
Ycr023c	S313 1.00			-0.72
Rad16	*S78* 0.99			-0.73
Vps1	S599 1.00			-0.73
Rps7b	S31 0.87			-0.74
Trm2	T96 0.87			-0.74
Trm2	S93 0.97			-0.74
Par32	S39 1.00			-0.75
Gpd2	S70 0.97			-0.77
Orm2	S9 1.00			-0.77
Pup2	T55 0.96			-0.78
Cdc60	T142 1.00			-0.78
Rps7b	*S30* 0.90			-0.78
Rad9	S494 0.81			-0.79
Sui3	T116 1.00			-0.80
Sum1	S736 0.71			-0.80
Sui3	S118 0.69			-0.80
Gat1	S262 0.98			-0.82
Yhr020w	*T38* 0.50			-0.82
Yhr020w	*S36* 0.50			-0.82

protein	site & prob	asc1⁻/ASC1 phos	asc1⁻/ASC1 prot	phospho regulation
Zeo1	T49 1.00			-0.83
Zeo1	S40 1.00			-0.83
Gcs1	S157 0.81			-0.85
Ura2	S1857 0.98			-0.86
Ty1b**	*S1004* 0.67			-0.86
Kin2	S549 1.00		1	-0.87
Vid27	T220 1.00			-0.94
Vid27	S222 1.00			-0.94
Def1	T258 0.90			-0.95
Meh1	S146 0.99			-0.95
Vtc3	S198 1.00			-0.99
Tdh1/2/3	S201 1.00			-1.01
Gvp36	*S2* 1.00			-1.03
Rho5	S223 1.00			-1.03
Abp1	S169 1.00			-1.03
Mnr2	T177 0.99			-1.05
Hsp42	S223 0.99			-1.06
Def1	S260 1.00			-1.08
Nrg2	S100 0.77			-1.08
Kns1	T562 1.00			-1.10
Mnr2	S152 1.00			-1.14
Tif4632	T196 1.00			-1.18
Bre5	S282 1.00			-1.20
Grx2	S94 0.94			-1.30
Ctr9	S1017 1.00			-1.31
Puf3	S86 1.00			-1.34
Ugp1	Y13 0.55			-1.42
Grx2	S91 1.00			-1.42
Cdc28	Y19 0.98			-1.46
Abp1	T181 1.00			-1.53
Abp1	S183 1.00			-1.53
Nrg2	*T99* 0.95			-1.64
Mep2	*S460* 0.73			-1.67
Mep2	T459 0.63			-1.70
Tpo1	S72 1.00			-1.71
Egd1	T151 1.00			-3.36

*Ty2a-Dr3;Ty2a-C;Ty2a-Or1; Ty2a-Lr2;Ty2a-Gr2;Ty2a-F

**Ty1b-Lr4;Ty1b-Pr1;Ty1b-Gr2; Ty1b-Pr2;Ty1b-Er1;Ty1b-MI2; Ty1b-Ol; Ty1b-Jr1;Ty1b-A;Ty1b-Ml1;Ty1b-Pl;Ty1b-Lr2, S445/S1004/S1005

Due to the triple-SILAC approach the analyzed samples also contained information about the *asc1*^{T143A} and *asc1*^{T143E} phospho-proteomes that were further evaluated (see Supplementary Tables 10-11). As expected from the results for the total proteomes, only a few changes were observed in the phospho-proteomes of the T143 mutant strains with nine regulated phospho-proteins. Four of them were already found as regulated in the *asc1*$^{-}$ strain (Ent3p, Sec31p, Rps1a/bp, and Tif1p). Phosphorylation of S2 of Tif1p was down-regulated in the *asc1*^{T143E} strain, whereas the modification was increased in *asc1*$^{-}$ cells, and Sec31p phosphorylation was altered at a different site (S980 instead of S999) in the *asc1*^{T143A} strain. In total, 213 proteins were identified as Asc1p-dependently regulated in their phosphorylation that were further evaluated according to their related biological processes.

3.3.2 Asc1p spreads signals to fundamental processes of eukaryotic gene expression

To evaluate which processes are affected by the Asc1p-dependent phosphorylation network, the 213 Asc1p-dependently regulated phospho-proteins were assigned to biological processes (gene ontology term) making use of the *Database for Annotation, Visualization and Integrated Discovery* (DAVID) *v6.7* (Huang da et al., 2009a, b). From this initial computational analysis seven different groups were established, and all but 18 proteins were assigned to these functional categories in a non-exclusive manner (Figure 22A, Supplementary Table 12). One of the largest groups consists of proteins related to mRNA *translation*. Some of them are directly involved in this process, such as ribosomal proteins (e.g., Rpl12a/bp), translation factors, and mRNA-binding proteins (e.g., Puf3p). Eight translation initiation factors were identified to be regulated comprising the RNA-helicase eIF4A, which was found with increased phosphorylation in the absence of Asc1p in an earlier study of our group (Valerius et al., 2007). Besides initiation factors, this category also comprises the elongation factor Yef3p and the termination factor Sup35p. Egd1p, a component of the nascent polypeptide-associated complex, and Ssz1p, a part of the ribosome-associated complex, were further shown to be affected in their phosphorylation status. The observed increase in phosphorylation of Ssz1p at residue S480 confirms again an earlier finding of our group (Valerius et al., 2007). Proteins indirectly involved in translation, such as tRNA-modifying enzymes, ribosome biogenesis factors, and tRNA-synthethases, were assigned to the group of *translation* as well.

The Asc1p-dependent phosphorylation network is connected to further processes that contribute to cellular protein homeostasis including *transcription* and *protein turnover*. Absence of Asc1p alters, e.g., phosphorylation of the transcription factor Fhl1p, a key

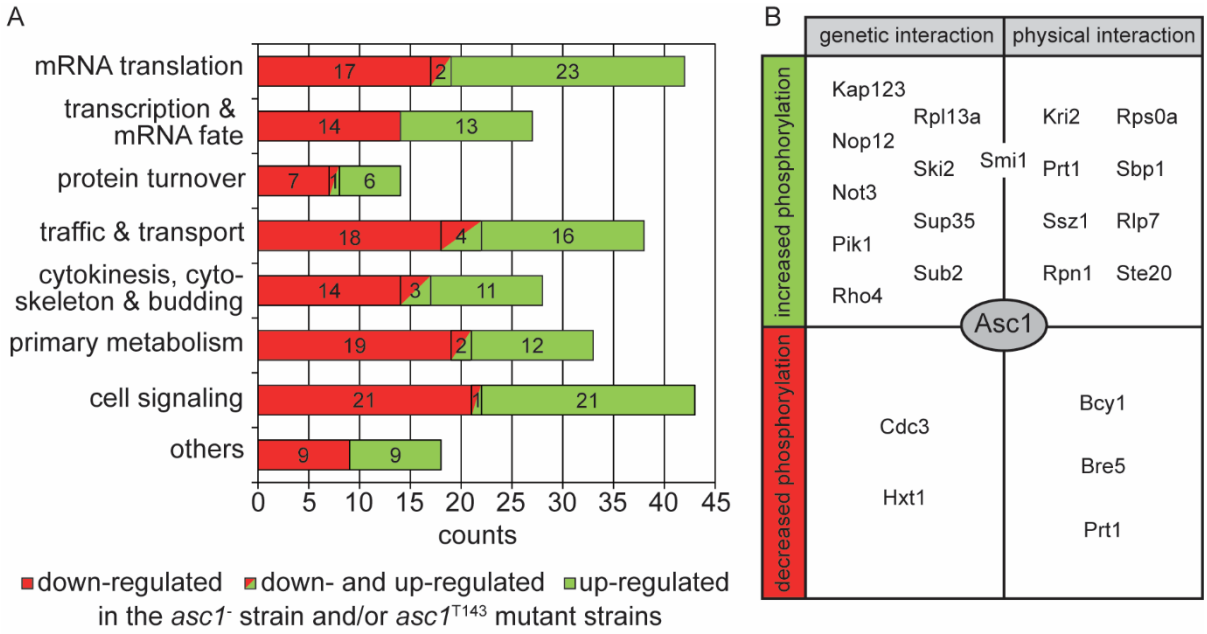

Figure 22. Cellular processes and known Asc1p-interaction partners that are targeted by Asc1p-dependent phosphorylation.
(A) Assignment of the Asc1p-dependently regulated phospho-proteins to cellular processes. The graph depicts the number of proteins assigned to the different groups (see Supplementary Table 12 for the identity of proteins in each group). The 213 proteins were grouped in a non-exclusive manner meaning that 30 proteins are present in two groups. (B) Known Asc1p-interacting proteins Asc1p-dependently regulated on the level of phosphorylation.

regulator of ribosomal protein encoding genes including *ASC1* itself (Kleinschmidt et al., 2006). The category *transcription* was additionally expanded for proteins affecting *mRNA fate*, such as the decapping protein Edc1. The group *protein turnover* includes three components of the regulatory particle of the 26S proteasome (Rpn1p, Rpn7p, and Rpn13p) and two components of its catalytic core (Pre8p and Pup2p), as well as Bre5p, a deubiquitination cofactor of Ubp3p, which regulate bulk protein degradation during ribophagy and mitophagy (Müller et al., 2015). The group *traffic and transport* comprises central structural components of vesicle coats (e.g., Sec21p) and regulators of vesicle-mediated transport (e.g., Gcs1p). Also, transmembrane transporters, such as the polyamine transporter Tpo1p and the ammonium transporter Mep2p, were assigned to this category. Asc1p affects the phosphorylation of several proteins that are related to *cytokinesis*, *cytoskeleton* organization, and *budding*, for instance, proteins involved in actin patch assembly at sites of polarized growth (Sla2p and Ent1p), polarisome components (Spa2p and Bni1p), actin nucleation promoting factors (Myo3/5p and Abp1p), regulators of actin filament elongation (Aim3p and Abp1p), and profilin (Pfy1p). Another group comprises enzymes of the *primary metabolism* that are, e.g., involved in amino acid biosynthesis (e.g., Hom3p), glycolysis and gluconeogenesis (e.g., Tpi1p and Tdh1/2/3p), and pyrimidine biosynthesis (Ura2p).

Finally, the largest group contains proteins implicated in *cell signaling*. This group stands in close relation to all other groups since it comprises 14 protein kinases, such as Cdc28p, Sch9p, and Ste20p, and regulatory subunits of the protein phosphatase Glc7p (Glc8p and Ypi1p) that could be directly responsible for the observed Asc1p-dependent changes in the phospho-proteome. In summary, the proteome data reveal an unprecedented strong impact of a single WD40 repeat protein on the phosphorylation of proteins involved in the regulation and realization of fundamental processes in a eukaryotic cell. Figure 22B shows proteins that were identified here with Asc1p-sensitive phospho-sites and were found in previous studies to genetically or physically interact with Asc1p. The physical interaction partners are potential candidates for an Asc1p-mediated kinase/phosphatase-target interaction.

3.4 Identification of Asc1p-interacting proteins

The results presented in the previous chapter showed a severe impact of Asc1p on the *S. cerevisiae* phospho-proteome. As a scaffold protein, Asc1p is supposed to provide proximity of proteins, and it might localize kinases or phosphatases to their substrates. Mammalian RACK1 was shown to contribute to the recruitment of kinases to the ribosome for the subsequent phosphorylation of translation initiation factors (Ceci et al., 2003; Ruan et al., 2012). Considering a similar function for Asc1p in yeast, the protein was purified from protein extracts to identify co-purifying proteins. C-terminally Strep-tagged Asc1p was affinity captured via *Strep-Tactin*® columns followed by LC-MS-based identification of proteins. Also, Asc1DEp-Strep with the two amino acid exchanges R38D and K40E was enriched via *Strep-Tactin*®. This variant is supposed to be compromised in its association to the ribosome and might lead to the identification of interactions that are specific for the mutated protein (Sengupta et al., 2004; Coyle et al., 2009).

In general, the analysis of eluate fractions derived from affinity purification or pull-down experiments with LC-MS results in the identification of hundreds of proteins as unspecific background due to the high sensitivity of modern mass spectrometers, such as the *LTQ Orbitrap Velos Pro* used in this study. Thus, interaction partners of a bait protein might also be identified with high confidence from negative controls although with lower abundance. In this study, a strain expressing untagged Asc1p was used for the negative control. Reliable quantification methods are essential to compare the abundance of each identified protein between the sample enriched for the bait protein and the negative control. Here, a SILAC-based approach was applied for relative peptide and thus protein quantification as described before (chapter 3.3.1). SILAC-labeling allows the pooling of differentially labeled cell

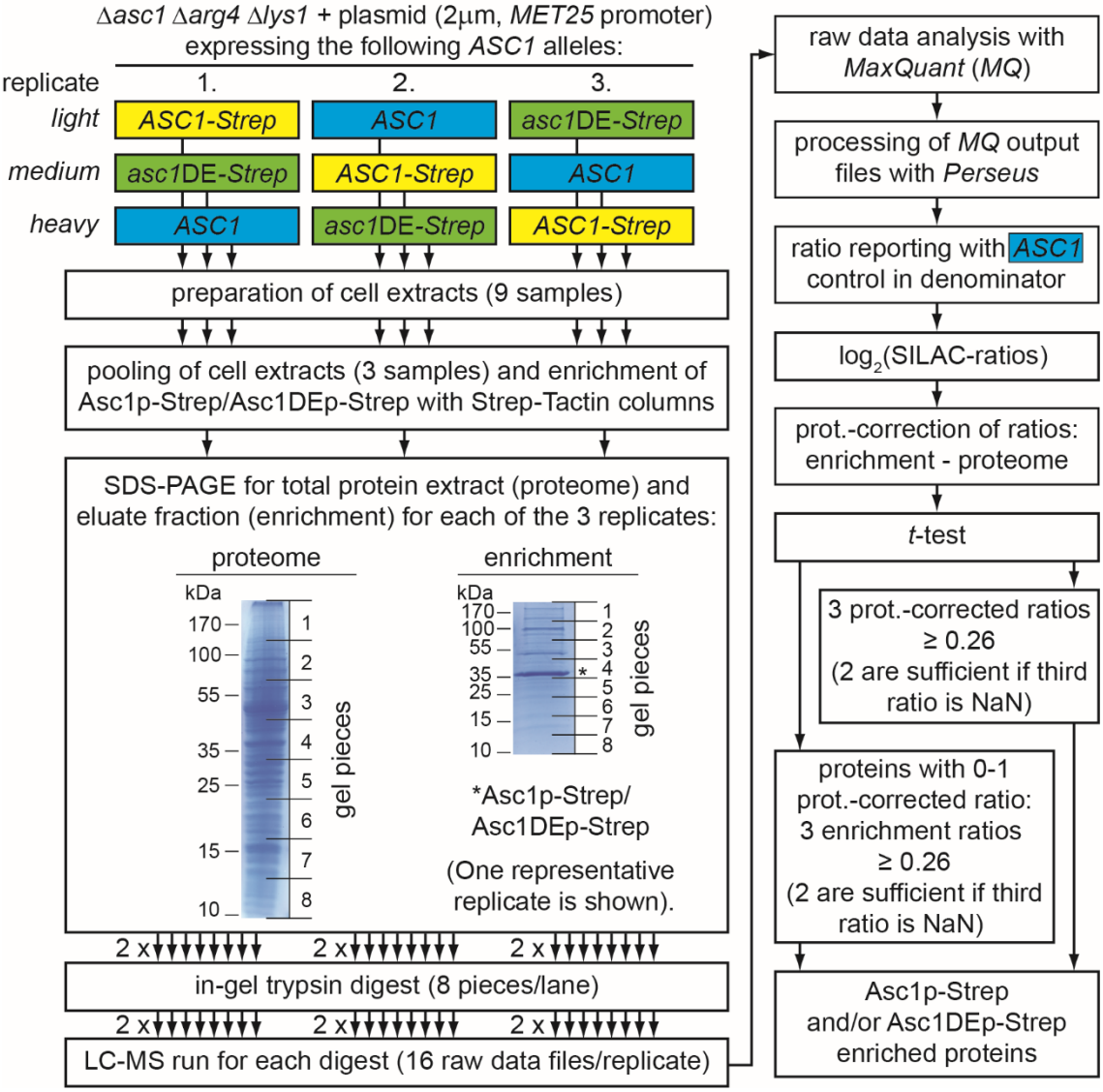

Figure 23. Workflow for the identification of putative interaction partners of Asc1p-Strep and Asc1DEp-Strep.

On the left-hand side of the figure the experimental workflow is illustrated. The experiment was performed with three biological replicates. In each replicate, the cells of three different independently cultured strains were analyzed expressing either Asc1p-Strep, Asc1DEp-Strep, or the untagged Asc1p. For each experiment, the *light*, *medium*, and *heavy* amino acid labels were swapped between the different strains. The steps of cultivation and preparation of cell extracts were performed individually for each sample to prevent the interchange of proteins bound to Asc1p-Strep or Asc1DEp-Strep. The three cell extracts of one replicate were mixed immediately before capturing of Asc1p-Strep and Asc1DEp-Strep with *Strep-Tactin*® spin columns. The eluate fractions and aliquots of the pooled protein extracts were subjected to SDS-PAGE. A representative SDS-gel after staining of proteins with Colloidal Coomassie is depicted. Each lane was cut into eight gel pieces as indicated in the figure with black lines, and proteins were in-gel digested with trypsin followed by LC-MS analysis of the peptides. In total, 16 LC-MS runs were performed for each biological replicate: 8 for the proteome plus 8 for the enrichment. Raw-data files were searched against an *S. cerevisiae*-specific database using the *MaxQuant* software. On the right-hand side of the figure, an overview of the most important steps of the downstream data evaluation with the *Perseus* software is provided. The pathway splits up into two branches: one for the analysis of proteins identified in the eluate fraction with two or three proteome (prot.)-corrected SILAC-ratios available and a second for the analysis of proteins with no or one proteome-corrected SILAC-ratio. NaN is the abbreviation for *not a number* and states that the protein was not identified or not quantified in one of the replicates.

Table 5. Logarithmized SILAC-ratios of proteins co-captured with Asc1p-Strep.
The listed proteins were identified to be enriched together with Strep-tagged Asc1p based on their relative quantification using SILAC. The top part lists proteins with 2-3 proteome-corrected SILAC-ratios and the bottom part those with 0-1 proteome-corrected SILAC-ratios. The colors reflect the SILAC-ratios according to the scale below the table. (Abbreviations/symbols: ** = *t*-test p-value < 0.05, * = *t*-test p-value < 0.1, Ø = mean of respective SILAC-ratios, SD = standard deviation, DE = mean Asc1DEp-Strep/control SILAC-ratios). The last column of the upper part of the table gives the mean and SD of the proteome-corrected Asc1DEp-Strep/control ratios. The last column of the bottom part gives the mean and SD of the enrichment Asc1DEp-Strep/control ratios.

2-3 proteome-corrected SILAC-ratios ≥ 0.26												
	proteome-corrected ratios				enrichment ratios				proteome ratios				DE
protein	Ø (SD)	1	2	3	Ø (SD)	1	2	3	Ø (SD)	1	2	3	Ø (SD)
Asc1**	**7.41** (1.00)	7.66	8.27	6.31	5.21 (0.90)	5.31	6.06	4.27	-2.20 (0.16)	-2.35	-2.20	-2.04	7.15 (0.76)
Def1*	**1.38** (0.96)	1.81	2.05	0.28	1.54 (0.96)	1.91	2.26	0.45	0.16 (0.05)	0.10	0.20	0.17	1.25 (0.85)
Dsk2	**0.95** (0.84)	0.50	1.92	0.43	1.13 (0.84)	1.50	1.73	0.17	0.18 (0.71)	1.00	-0.19	-0.26	1.24 (0.64)
Kel1**	**0.95** (0.52)	0.77	1.53	0.54	0.85 (0.55)	0.70	1.45	0.39	-0.10 (0.05)	-0.07	-0.08	-0.15	0.83 (0.60)
Sis1**	**0.76** (0.33)	1.02	0.86	0.39	0.66 (0.26)	0.91	0.66	0.39	-0.10 (0.10)	-0.10	-0.20	0.00	0.73 (0.79)
She2**	**0.66** (0.21)	-	0.80	0.51	0.57 (0.28	-	0.77	0.38	-0.04 (0.09)	0.05	-0.03	-0.13	0.16 (0.05)
Spt5*	**0.57** (0.33)	0.80	-	0.34	0.57 (0.33)	0.53	0.91	0.25	-0.17 (0.13)	-0.26	-	-0.08	0.43 (0.10)
Prx1**	**0.56** (0.01)	-	0.56	0.57	0.16 (0.08)	-	0.11	0.21	-0.44 (0.07)	-0.50	-0.45	-0.36	0.05 (0.08)
Ssd1	**0.54** (0.32)	0.40	0.91	0.31	0.67 (0.42)	0.62	1.12	0.28	0.14 (0.14)	0.23	0.21	-0.03	0.47 (0.50)
Mcm6**	**0.42** (0.14)	0.56	0.42	0.28	0.37 (0.16)	0.54	0.33	0.23	-0.05 (0.04)	-0.01	-0.09	-0.06	0.45 (0.28)
only 0-1 proteome-corrected SILAC-ratio, 2-3 enrichment ratios ≥ 0.26													
Mnl2*	-	-	-	5.09	**5.50** (0.83)	-	6.33	4.67	-	-	-	-0.42	4.92 (0.92)
Nop1*3	-	-	-	0.50	**0.63** (0.27)	0.54	1.00	0.35	-	-	-	-0.14	0.47 (0.50)
Cue5**	-	-	-	0.36	**0.60** (0.10)	0.68	0.46	0.67	-	-	-	0.32	0.65 (0.10)
Rav1*	-	-	-	-	**0.58** (0.23)	0.60	0.30	0.85	-	-	-	-	0.44 (0.28)
Mcm4*	-	-	-	0.28	**0.51** (0.18)	0.61	0.67	0.27	-	-	-	-0.01	0.16 (0.08)
Gsy1	-	-	-	-	**0.50** (0.19)	0.68	-	0.31	-	-	-	-	0.25 (0.27)

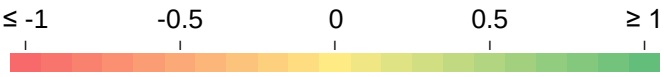

Table 6. Logarithmized SILAC-ratios of proteins co-captured with Asc1DEp-Strep.
The listed proteins were found to be enriched together with Strep-tagged Asc1DEp based on their relative quantification using SILAC. The layout of the table and abbreviations/symbols are as described for Table 5. (wt = wild-type, mean Asc1p-Strep/control SILAC-ratios equivalent to DE in Table 5).

2-3 proteome-corrected SILAC-ratios ≥ 0.26													
	proteome-corrected ratios				enrichment ratios				proteome ratios				wt
protein	Ø (SD)	1	2	3	Ø (SD)	1	2	3	Ø (SD)	1	2	3	Ø (SD)
Asc1**	**7.15** (0.76)	6.87	8.01	6.58	4.42 (0.76)	4.22	5.26	3.78	-2.73 (0.08)	-2.65	-2.75	-2.80	7.41 (1.00)
Def1	**1.25** (0.85)	1.24	2.11	0.41	1.61 (1.02)	1.25	2.76	0.82	0.36 (0.32)	0.01	0.65	0.41	1.38 (0.96)
Dsk2**	**1.24** (0.64)	0.97	1.97	0.79	1.21 (0.59)	1.31	1.75	0.58	-0.03 (0.32)	0.34	-0.23	-0.21	0.95 (0.84)
Rvs161	**1.04** (1.32)	0.28	2.57	0.28	0.93 (1.25)	0.18	2.38	0.25	-0.11 (0.08)	-0.10	-0.20	-0.04	0.15 (0.19)
Kel1*	**0.83** (0.60)	0.56	1.52	0.41	1.04 (0.63)	0.71	1.77	0.66	0.21 (0.06)	0.15	0.24	0.25	0.95 (0.52)
Ssa1**	**0.63** (0.02)	0.64	0.61	0.65	0.70 (0.07)	0.76	0.63	0.72	0.07 (0.05)	0.12	0.02	0.08	0.14 (0.08)
Ssa2**	**0.63** (0.06)	0.63	0.68	0.57	0.61 (0.02)	0.63	0.59	0.60	-0.02 (0.06)	0.00	-0.09	0.03	0.17 (0.09)
Ape3**	**0.49** (0.28)	-	0.29	0.68	0.53 (0.04)	-	0.50	0.56	0.05 (0.17)	0.06	0.21	-0.13	-0.03 (0.35)
Sup35**	**0.47** (0.10)	0.38	0.58	0.45	0.54 (0.21)	0.32	0.73	0.59	0.07 (0.12)	-0.06	0.14	0.14	0.22 (0.23)
Mvp1**	**0.45** (0.17)	0.33	0.57	-	0.22 (0.14)	0.19	0.37	0.10	-0.16 (0.04)	-0.13	-0.19	-	0.29 (0.28)
Spt5*	**0.43** (0.10)	0.36	-	0.50	0.40 (0.27)	0.17	0.70	0.33	-0.18 (0.02)	-0.19	-	-0.17	0.57 (0.33)
Svl3	**0.41** (0.13)	0.32	-	0.51	0.49 (0.58)	0.00	1.13	0.35	-0.24 (0.11)	-0.32	-	-0.16	0.61 (0.78)
only 0-1 proteome-corrected SILAC-ratio, 2-3 enrichment ratios ≥ 0.26													
Mnl2*	-	-	-	4.49	**4.92** (0.92)	-	5.57	4.27	-	-	-	-0.23	5.50 (1.17)
Fra1	-	-	-	0.41	**0.52** (0.28)	0.72	-	0.32	-	-	-	-0.09	-0.08 (0.08)
Rxt2	-	-	-	-	**0.51** (0.37)	0.34	0.94	0.26	-	-	-	-	0.48 (0.23)
Pba1**	-	-	-	-	**0.49** (0.04)	0.46	-	0.52	-	-	0.16	-	0.35 (0.09)
Bur2	-	-	-	-	**0.49** (0.23)	-	0.65	0.32	-	-	-	-	0.47 (0.39)
Pam1*	-	-	-	-	**0.42** (0.21)	0.31	0.67	0.29	-	-	-	-	0.42 (0.38)
Bud14**	-	-	-	-	**0.37** (0.14)	0.27	0.54	0.31	-	-	-	-	0.40 (0.17)

cultures directly after their cultivation, thereby treating them in the following steps as one sample and preventing any experimental bias due to individual sample processing. However, *light* and *heavy* labeled forms of proteins bound to the bait protein might interchange during the enrichment procedure if their interaction is highly dynamic (Wang and Huang, 2008). One possibility to address this problem is to pool samples at a later stage. Here, the cell lysis of independent cultures was done separately, and samples were pooled immediately prior to the affinity purification of Strep-tagged Asc1p (Figure 23). *Strep-Tactin*® spin columns were used that enable fast downstream processing of the samples after their pooling. Using a triple SILAC approach, three different strains expressing either Asc1p-Strep, Asc1DEp-Strep, or the untagged protein as a negative control were processed in a single affinity purification experiment. The proteins were expressed from high copy plasmids (2 µm) under control of the *MET25*-promoter in the Δ*asc1* Δ*arg4* Δ*lys1* strain. In total, three biological replicates were analyzed. The eluate fraction and a sample from the total protein extract (after pooling but prior to affinity purification) were subjected to SDS-PAGE followed by in-gel trypsin digestion. Peptide samples were analyzed with LC-MS, and the obtained raw data files were analyzed against an *S. cerevisiae*-specific protein database using the *MaxQuant* software with the *Andromeda* search engine for the identification and quantification of peptides and their corresponding proteins. SILAC-ratios were reported with the values for the Asc1p control in the denominator so that high ratio values indicate the Asc1p-dependent co-enrichment of a protein. To avoid misinterpretation due to expression effects, the total protein extracts were analyzed as well to get quantitative proteome data as an input-control. SILAC-ratios for proteins of the enriched fractions were corrected for SILAC-ratios of proteins from the proteome (as it was described in chapter 3.3.1 for the correction of phospho-peptide ratios with protein ratios). Reduced sample complexity derived from the enrichment led to identifications (and quantifications) of proteins that were not covered from the very complex samples obtained from total protein extracts. Thus, the described proteome-correction of SILAC-ratios was not applicable to all proteins.

The *MaxQuant* data were downstream analyzed using the *Perseus* software as briefly illustrated in Figure 23. For a detailed overview of all processing steps, see Supplemental Table 13. The normalized SILAC-ratios from the *MaxQuant* protein groups output file were used in *Perseus*. The normalization step of *MaxQuant* centers the normal distribution of SILAC-ratios on a ratio of 1:1 for the bulk of proteins, thereby correcting experimental biases. This mathematical correction is performed under the assumption that most proteins do not differ in their abundance between the samples.

Values were logarithmized (log_2) so that a ratio value of 0 indicates no enrichment, and a ratio value considerably greater than 0 hints to a specific enrichment of a protein through its association with Asc1p-Strep or Asc1DEp-Strep. Two-sample *t*-tests (p-value < 0.1 and p-value < 0.05) were applied to obtain statistical validation for the enrichment of candidates. For each protein, the SILAC-ratios from the enriched fractions (x) were proteome-corrected with the respective SILAC-ratios from the proteome (y) by subtraction (x-y). All proteome-corrected SILAC-ratios of the three replicates had to be ≥ 0.26 (approximately 20% enrichment) to identify a protein as a putative Asc1p-Strep interaction partner. In case that only two ratios were determined, both had to be ≥ 0.26. These thresholds resulted in the identification of nine proteins for Asc1p-Strep and eleven proteins for Asc1DEp-Strep plus the bait proteins Asc1-Strep and Asc1DE-Strep.

For proteins with no or only one proteome-corrected SILAC-ratio, the same filter (two values ≥ 0.26 and no value < 0.26) was applied on the non-proteome-corrected SILAC-ratios from the eluate fraction. If a proteome-corrected SILAC-ratio was available, this should not be less than 0.26. With these thresholds six and seven proteins were additionally considered as enriched together with Asc1p-Strep and Asc1DEp-Strep, respectively. Additionally, a one-sample *t*-test instead of a two-sample *t*-test was applied on these proteins for statistical validation of candidates.

All candidates and their quantification values are listed in Tables 5 and 6, and the resulting Asc1p-interaction map is depicted in Figure 24. Five proteins were found as putative interaction partners for Asc1p-Strep as well as for Asc1DEp-Strep namely Def1p, Dsk2p, Kel1p, Mnl2p, and Spt5p. The remaining 23 proteins were identified for the enrichment of only one of the two Asc1p variants. The interaction map also indicates interactions between proteins that were already reported in literature (according to interactions listed in SGD). Bud14p is the only protein that has been reported as a physical interaction partner of Asc1p before. Bud14p is one of the regulatory subunits of the phosphatase Glc7p and might therefore be directly responsible for Asc1p-mediated dephosphorylation processes (Knaus et al., 2005). As a regulatory subunit of the Bur1p protein kinase, the Asc1DEp-Strep-associated cyclin Bur2p is involved in regulation of phosphorylation as well (Yao et al., 2000). Additionally, three proteins with Asc1p-sensitive phosphorylation sites namely Def1p, Sup35p, and Ssd1p were found.

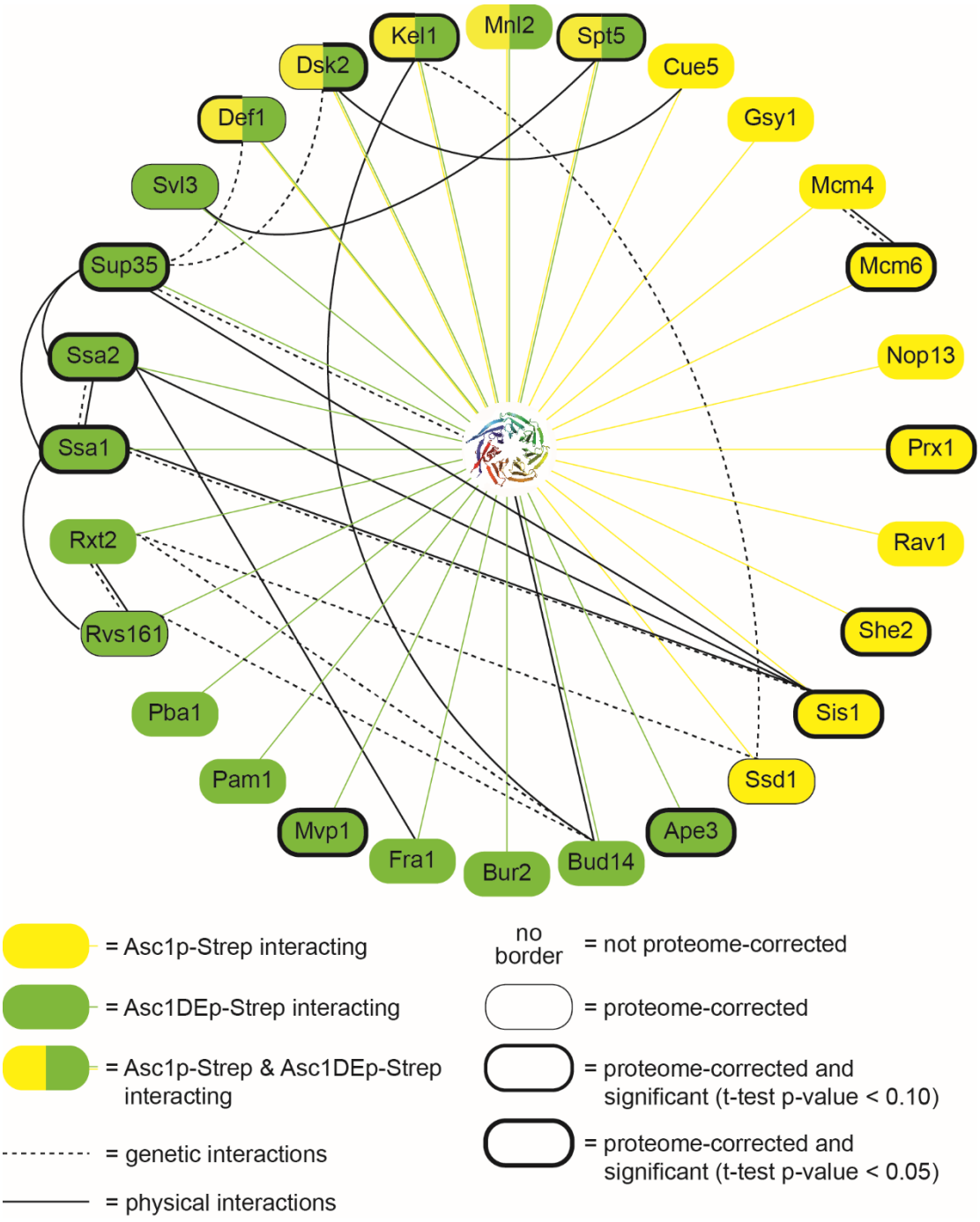

Figure 24. Interaction map of Asc1p-Strep and Asc1DEp-Strep.
All proteins identified as putative interaction partners of Asc1p-Strep (colored in yellow) or Asc1DEp-Strep (colored in green). Proteins highlighted in both colors were found to interact with both Asc1p variants. The Asc1p structure is placed in the center, and the colored lines illustrate the interactions identified in this work. (The structure figure of Asc1p was generated with the *PyMOL Molecular Graphics System* software on the basis of the PDB file 3FRX). Black lines and dashed black lines connect proteins that have already been reported as physical or genetic interaction partners, respectively, in other studies according to SGD. For proteins without a black border, no or only one proteome-corrected SILAC-ratio could be obtained. A black border indicates that at least two proteome-corrected SILAC-ratios could be obtained for the respective protein. Thick black borders indicate that the two-sample *t*-test was positive (p-value < 0.1 or p-value < 0.05).

3.5 The Asc1p-dependent translatome

Based on its exposed position at the head of the 40S ribosomal subunit next to the mRNA exit tunnel, Asc1p is considered to be directly involved in regulation of translation (Sengupta et al., 2004). It has been shown to interact with translation factors and mRNA-binding proteins and might affect translation in general or for specific transcripts (Baum et al., 2004; Kouba et al., 2012). Here, the translatomes - meaning the entity of actively translated mRNAs - of *ASC1* wild-type and the *asc1*$^{-}$ cells were quantitatively compared to identify transcripts that are targets of an Asc1p-dependent translational regulation.

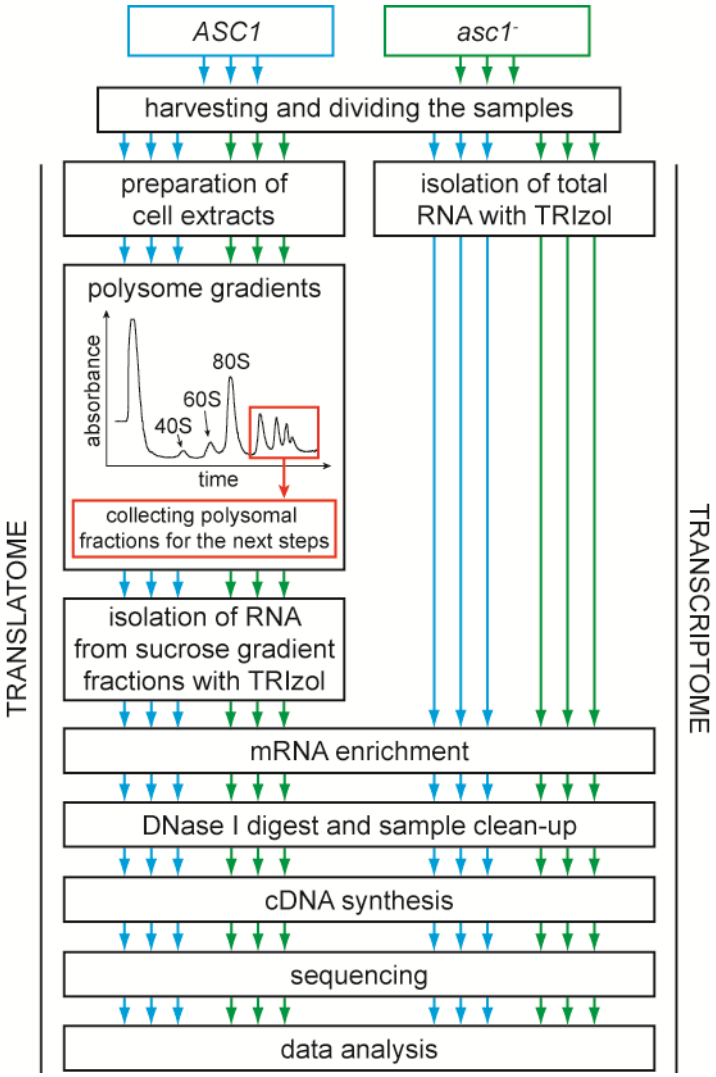

Figure 25. Workflow for the Asc1p-dependent translatome and transcriptome analysis.
The *ASC1* wild-type and *asc1*$^{-}$ strains were cultivated in three replicates. After harvesting of the cells, each sample was divided and one half processed for the translatome and the other half for the transcriptome analysis. For the translatome analysis, cell extracts were prepared and subjected to sucrose-density ultracentrifugation. Polysomal fractions were collected, and RNA was isolated. For the transcriptome analysis, total RNA was directly isolated from the cells. RNA samples from both experimental lines were subjected to mRNA enrichment and DNase I digest. cDNA was synthesized from the RNA, and samples were subjected to sequencing followed by data analysis.

Table 7. Asc1p-dependent changes in the translatome.
An expanded view of this table with the normalized readcounts for all three replicates for each strain can be found in Supplementary Table 14. For each transcript and strain, the mean of the normalized readcounts was calculated. Logarithmized (log_2) *asc1⁻/ASC1* ratios of these mean values are provided in this table and colored according to the color scale. (FDR = false discovery rate).

gene	*asc1⁻/ASC1*	likeli-hood	FDR
COS8	2.68	0.9965	1.7E-03
ZPS1	2.35	0.9973	1.3E-03
PRM5	1.84	0.9981	7.7E-04
HBN1	1.69	0.9995	1.4E-04
GSY1	1.65	0.9994	2.2E-04
HSP42	1.61	0.9916	3.5E-03
HSP26	1.48	0.9160	3.2E-02
YCL021W-A	1.45	0.9909	4.0E-03
GAL3	1.38	0.9595	1.3E-02
YLL053C	1.36	0.9834	5.5E-03
ZRT1	1.35	0.9397	1.8E-02
YKL070W	1.34	0.9268	2.8E-02
FET4	1.32	0.9935	2.6E-03
VTI1	1.27	0.9608	1.2E-02
AHA1	1.26	0.9973	1.1E-03
AQY2	1.22	0.9322	2.4E-02
FKS3	1.22	0.9886	4.5E-03
STI1	1.17	0.9983	6.0E-04
AGA1	1.16	0.9495	1.5E-02
GAL80	1.15	0.9826	5.9E-03
GSY2	1.12	0.9986	4.2E-04
NDJ1	1.07	0.9298	2.5E-02
URA10	1.05	0.9182	3.1E-02
HXK1	1.05	0.9409	1.7E-02
GRX3	1.02	0.9943	2.2E-03
SMA2	1.01	0.9343	2.2E-02
DCS1	1.01	0.9921	3.3E-03
YGR161W-C	1.00	0.9970	1.5E-03
YHB1	0.95	0.9749	8.0E-03
UBC1	0.91	0.9280	2.6E-02
LST8	0.91	0.9278	2.7E-02
ALG13	0.90	0.9891	4.2E-03
HSP78	0.86	0.9564	1.4E-02
APE1	0.84	0.9644	1.2E-02
YMR315W	0.84	0.9340	2.3E-02
FMP41	0.82	0.9207	2.8E-02
GLO2	0.80	0.9352	2.2E-02

gene	*asc1⁻/ASC1*	likeli-hood	FDR
GLK1	0.78	0.9392	1.9E-02
TWF1	0.77	0.9140	3.2E-02
MXR1	0.76	0.9046	3.4E-02
SFG1	0.76	0.9011	3.5E-02
ARC18	0.76	0.9075	3.3E-02
YKL151C	0.76	0.9710	8.6E-03
EXG2	0.71	0.9366	2.0E-02
YDR327W	0.70	0.9187	3.0E-02
DFR1	-0.66	0.9357	2.1E-02
HTB1	-0.68	0.9396	1.8E-02
FAA2	-0.75	0.9290	2.5E-02
HO	-0.75	0.9699	1.0E-02
TDA1	-0.91	0.9708	9.1E-03
YHR177W	-0.93	0.9188	2.9E-02
URA4	-1.02	0.9922	3.1E-03
AAC3	-1.02	0.9702	9.7E-03
SNO1	-1.04	0.9755	7.5E-03
ARN1	-1.06	0.9594	1.4E-02
ALD6	-1.06	0.9682	1.1E-02
YJL213W	-1.16	0.9800	7.0E-03
BAP3	-1.23	0.9802	6.7E-03
YIL165C	-1.25	0.9970	1.4E-03
AQR1	-1.29	0.9823	6.2E-03
ECM13	-1.36	0.9960	2.0E-03
SNZ1	-1.47	0.9933	2.8E-03
RIB4	-1.49	0.9976	9.5E-04
TPO1	-1.64	0.9961	1.8E-03
YGR035C	-1.64	0.9909	3.7E-03
YMR141W-A	-1.67	0.9491	1.6E-02
FMP48	-1.71	0.9877	4.8E-03
TPO4	-1.74	0.9650	1.1E-02
TIS11	-1.86	0.9857	5.1E-03
URA3	-1.87	0.9936	2.4E-03
URA1	-2.14	1.0000	2.5E-05
EEB1	-2.56	1.0000	8.6E-06
MDH2	-2.64	1.0000	2.0E-05

The experiments were performed with three biological replicates for each strain (Figure 25). Total cell extracts derived from exponentially growing yeast cells were subjected to sucrose density ultracentrifugation to separate polysomes from ribosomal subunits, monosomes, and mRNP particles. The polysome fractions with highly translated mRNAs were collected, and RNA was isolated. The samples were enriched for mRNAs to reduce the rRNA amount in the samples. DNA in the samples had to be removed by enzymatic DNase I digestion. The RNA was transcribed into cDNA and subjected to sequencing. The readcounts for each mRNA were used for a differential expression analysis with the *baySeq* algorithm (Hardcastle and Kelly, 2010).

Transcripts differentially abundant in the translatomes of the *ASC1* wild-type strain and the *asc1*$^{-}$ strain that had ≥ 90% likelihood for regulation were further considered. For the 73 transcripts that passed this threshold, the normalized readcounts of all six samples are given in the Supplementary Table 14. The mean value of the normalized readcounts was calculated for the three replicates of each strain, and the *asc1*$^{-}$*/ASC1* ratio of these values was determined (Table 7 and Supplementary Table 14). 45 polysomal transcripts were found to be increased and 28 decreased in their abundance in the *asc1*$^{-}$ strain in comparison to the *ASC1* wild-type strain.

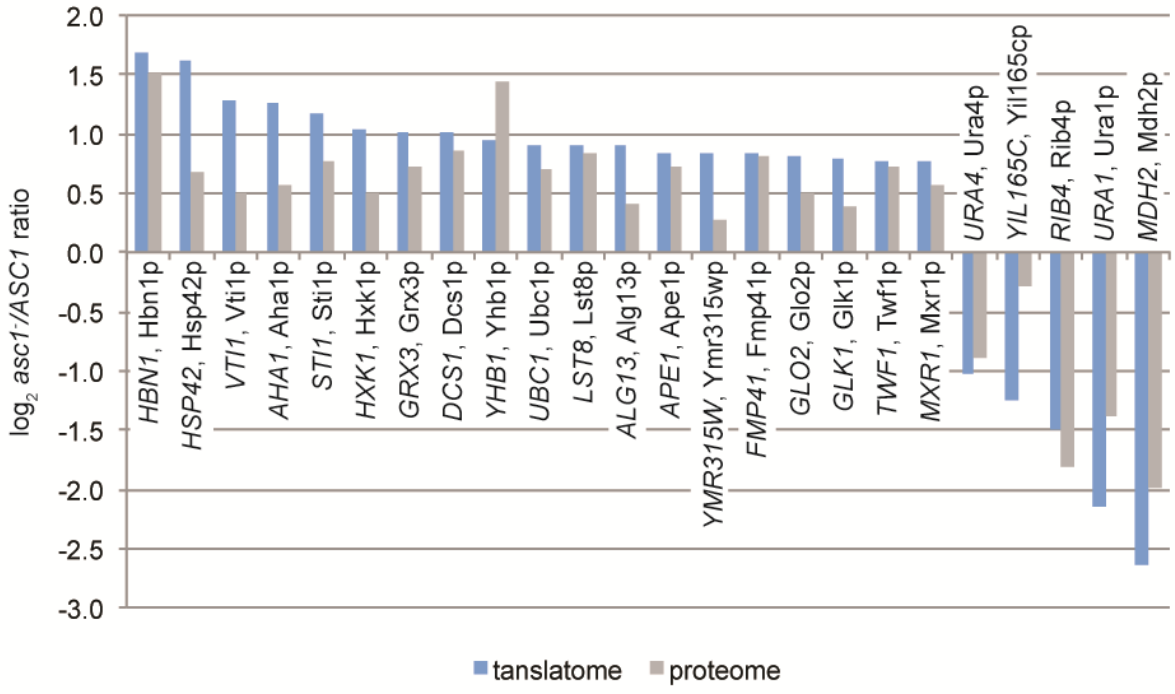

Figure 26. Asc1p-dependent translatome versus proteome.
The graph provides the $\log_2$ *asc1*$^{-}$*/ASC1* ratios for mRNAs and proteins that were found to be Asc1p-dependently affected in their abundance in the translatome as well as in the total proteome.

For 24 of the polysomal transcripts, a relative quantification value for the corresponding protein can be found in the list of Asc1p-dependently regulated proteins (Figure 26 and Supplementary Table 4). For all 24 candidates, the direction of regulation was identical in the translatome and proteome hinting to a correlation between the translation efficiency for an mRNA and the expression level of the respective mature protein. Alteration of the abundance of a transcript in the translatome could reflect the general changes in the abundance of the transcript. Therefore, the translatome data were compared with a former microarray-based quantitative transcriptome analysis for the Δ*asc1* strain (Rachfall et al., 2013). 13 transcripts were found to be altered in their abundance in the translatome as well as in the transcriptome (Figure 27). 12 of these transcripts showed the same direction of regulation in the translatome and the transcriptome. Thus, Asc1p-dependently increased or decreased abundance of these transcripts might lead to differences in their translation rates. Yet, one mRNA, the transcript of the *YHR177W* gene, was increased in its total abundance, but showed severely decreased association with translating ribosomes upon Asc1p-deficiency. *YHR177W* is a paralog of the gene encoding Muc1p expressed independent of *TEC1* 1 (Mit1p). Their gene products belong to the WOPR family of transcriptional regulators that is named for its members Wor1p, Pac1p, and Ryp1 and contain a WOPR box for DNA-binding (Lohse et al., 2010). The WOPR box is highly conserved within the fungal kingdom and found in regulators of morphology and pathogenesis (Lohse et al., 2010). For example, Mit1p is required for pseudohypal growth in *S. cerevisiae*, and Wor1p regulates the transition of yeast cells from white to opaque cell morphology in *C. albicans* (Huang et al., 2006; Cain et al., 2012).

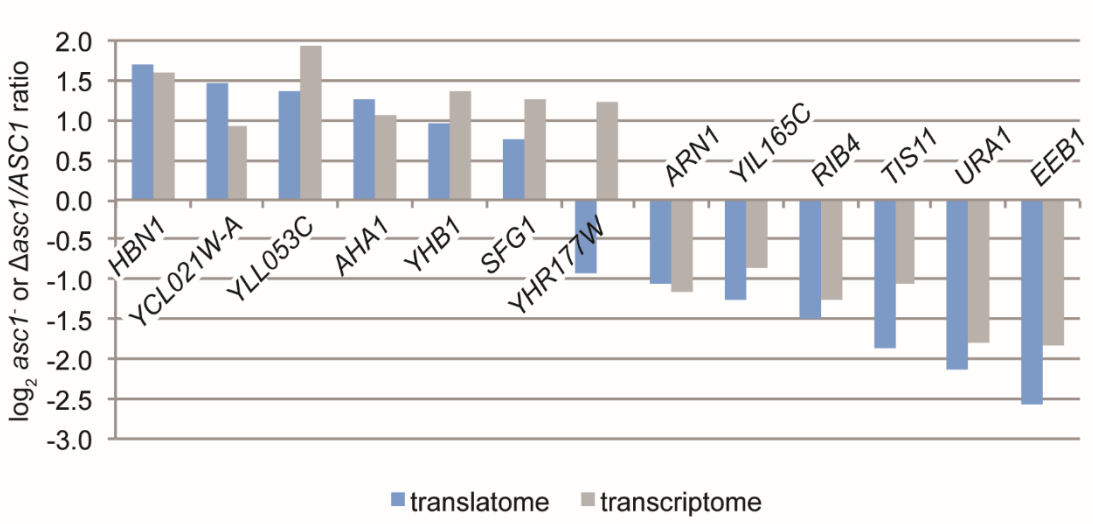

Figure 27. Asc1p-dependent translatome and transcriptome.
The columns provide the $\log_2$ *asc1*$^-$/*ASC1* ratios for mRNAs found to be Asc1p-dependently affected in their levels in the translatome as well as in the transcriptome. Transcriptome data derived from a microarray analysis comparing the *ASC1* wild-type strain with the Δ*asc1* strain (Rachfall et al., 2013).

The comparison with the microarray data implicates that RNASeq-based transcriptome data for the *asc1*$^{-}$ strain are required to differentiate between mRNAs that change in their abundance in the translatome due to an Asc1p-dependent regulation in their expression level or an Asc1p-dependent alteration of their translation efficiency. Experiments for a quantitative transcriptome analysis of the *asc1*$^{-}$ strain with RNASeq are in progress (Figure 25).

4. Discussion

4.1 Does the R38D K40E amino acid exchange within Asc1p cause a ribosome binding defect *in vivo*?

The Asc1 protein of *S. cerevisiae* is not essential for viability of yeast cells under laboratory conditions, but is required to adapt cells to a variety of different stress conditions. As a constituent of the ribosome, it is likely that Asc1p's molecular function is tightly linked to the process of mRNA translation. The crystal structures of the *T. thermophila* 40S subunit and the *S. cerevisiae* 80S ribosome confirm Asc1p's integral position within the ribosome (Ben-Shem et al., 2011; Rabl et al., 2011). In cells of the stationary growth phase of a yeast culture, Asc1p seems to bind ribosomes less tightly (Baum et al., 2004). This gives rise to the question whether Asc1p also acts apart from the ribosome as it has been suggested for other ribosomal proteins (reviewed in Warner and McIntosh, 2009). Asc1p was described to function as the G-protein β-subunit of the Gα Gpa2p, which is localized to membranes via its interaction with the nutrient sensor Gpr1p. A simultaneous interaction of Asc1p with Gpa2p and the ribosome was considered to be unlikely due to sterical hindrance (Zeller et al., 2007; Coyle et al., 2009). In metazoans, several known interactions of RACK1 also seem to occur in its ribosome-free state since the respective interaction surface was mapped to the ribosome-facing side of the β-propeller. Yet, homodimerization of Asc1p/RACK1 would enable a simultaneous interaction with the ribosome and a second interaction partner that binds to the same regions on the second β-propeller surface. Still, ribosome binding of RACK1 seems incompatible with the simultaneous interaction with the Fyn kinase and NR2B. The interaction with these two proteins in complex was proposed to rely on homodimer formation since the binding sites of both proteins involve amino acids 35 to 48 of RACK1 (Thornton et al., 2004). Many studies with metazoan systems do not even consider ribosome-localization of RACK1 for their experiments or the discussion of their results. In conclusion, a ribosome-independent impact of the β-propeller protein on cellular adaptation seems possible.

A ribosome binding mutated variant of Asc1p has been proposed and expected to contribute to the differentiation between ribosome-dependent and ribosome-independent functions of Asc1p. The mutated Asc1 protein contains an exchange of the two highly conserved residues R38 and K40 to aspartate (D) and glutamate (E), respectively, which weakens the binding to the ribosome (Sengupta et al., 2004; Coyle et al., 2009). In comparison to wild-type Asc1p, Asc1DEp is shifted from the ribosomal to the ribosome-free fraction during sucrose-gradient ultracentrifugation (Coyle et al., 2009). However, *S. cerevisiae asc1*DE strains behave phenotypically mainly like the wild-type *ASC1* strain (this study; Coyle et al., 2009). The

rather marginal phenotypic effects are confirmed here and reflected by our findings on the molecular level: While in Asc1p-deficient cells the protein levels of the transcription factors Flo8p, Tec1p, and Rap1p are significantly reduced and more than 600 additional proteins are altered in their abundance, the transcription factors are not affected by the DE exchange, and there are almost no changes observed within the total proteome. Yet, Kuroha and colleagues (2010) were able to show that a promoting effect of Asc1p on nascent polypeptide-dependent translation arrest is lost in the *asc1*DE mutant strain.

It is surprising that a reduction in ribosome-association of almost 90% (Coyle et al., 2009) should have only a minor impact on the functionality of Asc1p in *S. cerevisiae*. This would suggest either that Asc1p acts to a great extent independently from the ribosome or that a small percentage of Asc1p bound to ribosomes is sufficient for the protein to function. However, it has to be considered that the reduced ribosome-association of Asc1DEp in sucrose gradient ultracentrifugation might not reflect the *in vivo* situation: Although the DE mutation obviously compromises the interaction of Asc1p with the ribosome, its dissociation from the 40S subunit might only occur during cell lysis or subsequent ultracentrifugation.

It also has to be taken into consideration that the DE mutation impairs the interaction of Asc1p with other components besides the ribosome. For example, the interaction of mammalian RACK1 with the Fyn kinase as well as with the NR2B-subunit of the NMDA receptor involves amino acids 35 to 48 of RACK1 (Thornton et al., 2004), and R36 and K38 of mammalian RACK1 correspond to R38 and K40 of Asc1p. In *S. pombe*, exchange of these residues (R36 and K38) to alanine in combination with simultaneous R125A and K127A substitutions reduced the association of Cpc2p with Ran1p, a protein kinase regulating the transition between mitosis and meiosis (McLeod et al., 2000). This study was published four years before the R38D K40E exchange was first shown to affect ribosome binding of Asc1p (Sengupta et al., 2004). These two residue pairs were chosen for mutagenesis because they are both part of a short motif that is found in the sequence of other direct interaction partners of Ran1p and might be responsible for substrate specificity (McLeod et al., 2000).

Here, Asc1p-Strep as well as Asc1DEp-Strep were purified to identify potential interaction partners of the wild-type protein and the variant. The experimental set-up did not result in the enrichment of ribosomal proteins with the Strep-tagged wild-type Asc1p. Thus, no difference in ribosome-association was observed between Strep-tagged Asc1p and Asc1DEp. Yet, proteins were identified that were specifically enriched with one of the two Asc1p variants. For example, the mRNA-binding protein She2 was exclusively enriched with Asc1p-Strep, whereas the heat shock proteins Ssa1 and Ssa2 and the translation termination factor Sup35p

were only co-purified with Asc1DEp-Strep (see below for the discussion of these candidates and their relation to Asc1p). The direct or indirect interaction of these proteins with Asc1p might involve residues R38 and K40 as it was described for the Cpc2p-Ran1p interaction.

DE variants have also been studied in other organisms to analyze the effect of a reduced ribosome binding on the function of Cpc2p/RACK1. In *S. pombe*, a *cpc2*DE strain shows neither increased sensitivity to 3-AT nor decreased phosphorylation of eIF2α as it was observed for the Δ*cpc2* strain (Tarumoto et al., 2013). Yet, another study reported that expression of plasmid-borne wild-type Cpc2p, but not Cpc2DEp, rescues the reduced protein abundance of the MAPK phosphatases Pyp1p and Pyp2p and of the stress-responsive transcription factor Atf1p in a Δ*cpc2* strain (Nuñez et al., 2009). Furthermore, expression of Cpc2DEp results in the same defect in G_2/M transition as caused by a *CPC2* deletion evident through increased cell size at cell division (Nuñez et al., 2009; Nuñez et al., 2010).

The following paragraph provides four examples for observations made with the RACK1-DE variant in metazoan systems. Arimoto and colleagues (2008) observed translocation of RACK1 to stress granules upon certain stress conditions presumably as part of the small ribosomal subunit. RACK1-DE did not show this cellular translocation implicating a reduction in ribosome-association of this RACK1 variant *in vivo* (Arimoto et al., 2008). In *D. melanogaster* S2 cell lines, a stable knock-down of RACK1 decreases propagation of viruses of the *Dicistroviridae* family due to the requirement of RACK1 for IRES-mediated translation of the viral mRNA. Transfection of this cell line with a vector carrying the RACK1-DE variant cannot rescue this phenotype in contrast to transfection with the same vector carrying the wild-type RACK1 gene (Majzoub et al., 2014). The RACK1-DE mutant was further used to ascribe an enhancing effect of RACK1 on chemoresistance and growth of human hepatocellular carcinoma to the ribosome-bound state of the protein (Ruan et al., 2012). The authors of this study showed, for example, that the transfection of Huh7 cells with wild-type RACK1, but not with RACK1-DE, mediates resistance against doxorubicin-induced apoptosis. Whereas overexpression of RACK1 promotes *de novo* protein biosynthesis in metabolic labeling studies in Huh7 cells, overexpression of RACK1-DE slightly inhibits this process. This observation might be caused by the reduced binding of the RACK1 interaction partner PKCβII to the ribosome in the presence of RACK1-DE and consequently decreased phosphorylation of the PKCβII-targets eIF4E and eIF6 (Ruan et al., 2012). Gandin and colleagues (2013a) used the RACK1-DE variant to show that RACK1 recruits activated JNK to ribosomes. At the ribosome, JNK phosphorylates eEF1A2 that subsequently binds to

newly synthesized polypeptides and induces their proteasomal degradation (Gandin et al., 2013a).

These results from the metazoan systems support the assumption that the DE exchange also causes *in vivo* reduction of ribosome-association of Asc1p/RACK1. Yet, it has to be considered that there might be substantial differences in the nature of Asc1p/RACK1's association with the ribosome between various organisms. The *Leishmania major* orthologue of Asc1p/RACK1, for example, harbors a glycin residue instead of the highly conserved lysine residue at position 36 and is nevertheless found tightly associated to ribosomes in sucrose-density centrifugation experiments (Choudhury et al., 2011). Furthermore, Coyle and colleagues (2009) also analyzed the importance of other lysine and arginine residues besides R38 and K40 at the ribosome-facing side of Asc1p for ribosome binding. The exchange of two less conserved residues (K62 and K87) to alanine affects the ribosome-association of Asc1p as well, yet to a significantly lesser extent than the R38D K40E mutation (Coyle et al., 2009; Adams et al., 2011).

Besides differences in characteristics of the interaction between Asc1p/RACK1 and the ribosome, there might be additional organism-specific factors, such as post-translational modification of Asc1p/RACK1, that influence its localization to the ribosome or at least its precise positioning at this site *in vivo*. Although the DE mutation had only marginal effects on Asc1p-dependent phenotypes, this work revealed tremendous synthetic effects when the DE mutation was combined with amino acid substitutions at Asc1p phospho-sites.

4.2 The DE exchange and phospho-site mutations synergistically compromise Asc1p's functionality and integrity

In this study, at least three previously unknown phosphorylation sites of Asc1p were identified: T12, T143, and Y250. These three residues and five additional phospho-sites of Asc1p (T96, T99, S120, S166, T168), which were known from previous high-throughput studies, were characterized in detail through the generation of respective *asc1* mutant strains (Chi et al., 2007; Smolka et al., 2007; Holt et al., 2009). The resulting strains synthesize Asc1p variants with replacements of the phospho-sites by either alanine/phenylalanine (dephosphorylation mimic) or by glutamate (phosphorylation mimic). The systematic phenotypic analysis of these strains revealed an increased sensitivity to translation inhibitors for the *asc1*^{T143A} and *asc1*^{Y250F} strains. All other phospho-site mutant strains showed wild-type behavior for the tested phenotypes. Yet, the combination of phospho-site mutations at T143 and Y250 as well as T12, T96, and T99 with the DE mutation caused strong synthetic

phenotypes revealing the importance of these phospho-sites in combination with the conserved residues R38 and K40. Phosphorylation of Asc1p/RACK1 has also been reported in other organisms, such as *S. pombe*, *H. sapiens*, and *A. thaliana* (Chang et al., 2001; Liu et al., 2007b; Wilson-Grady et al., 2008; Kiely et al., 2009; Urano et al., 2015). The amino acids T12, T143, and Y250 of Asc1p are highly conserved in these organisms. (Figure 28, RACK1A is shown representatively for the three RACK1 proteins of *A. thaliana*). *S. pombe*

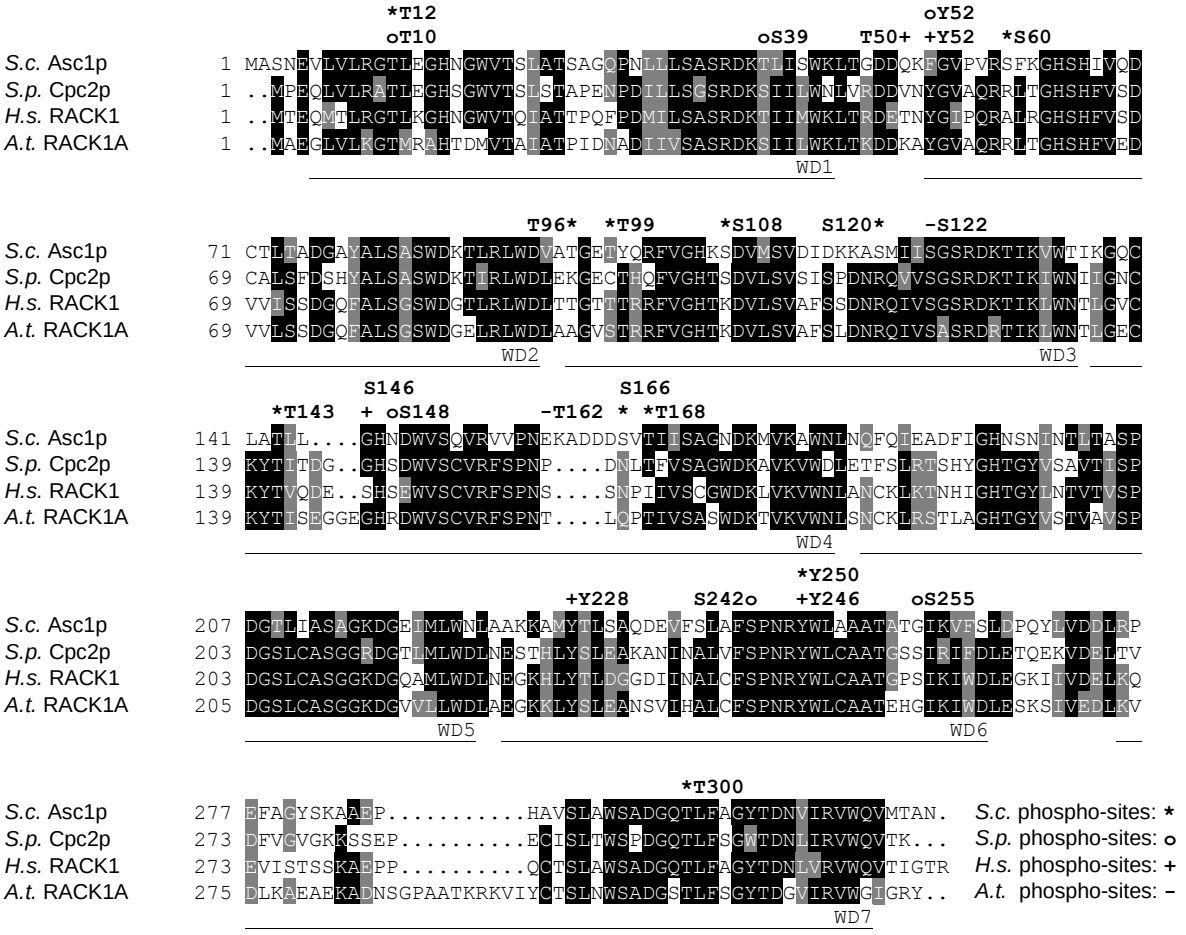

Figure 28. Phospho-site locations within Asc1p and its orthologues.
Amino acid sequence alignment of Asc1p with its orthologues and their phospho-sites. Amino acid residues that are conserved in at least three of the depicted sequences are shaded in black, those that are similar in at least three sequences are shaded in gray. Phospho-sites are indicated above the sequences according to the legend in the figure. For *S. cerevisiae* (*S.c.*) Asc1p, phospho-sites T12 (this study), S60 (Gnad et al., 2009), T96 and T99 (Chi et al., 2007), S108 and S120 (Holt et al., 2009), T143 (this study), S166 and T168 (Smolka et al., 2007), Y250 and T300 (this study) are indicated with an asterisk (*). For *S. pombe* (*S.p.*) Cpc2p, phospho-sites T10, S39, Y52, S148, S242, and S255 (Wilson-Grady et al., 2008) are labeled with a circle (o). Phospho-sites S122 and T162 of *A. thaliana* (*A.t.*) RACK1A (T161 of RACK1B and RACK1C, Urano et al., 2015) are indicated with a minus (-) and phospho-sites T50 (Zhao et al., 2015), Y52 (Kiely et al., 2009), S146 (Liu et al., 2007b), Y228 (Chang et al., 2001), and Y246 (Chang et al., 2001; Chang et al., 2002) of *H. sapiens* (*H.s.*) RACK1 are indicated with a plus (+). The seven WD40 repeats are labeled below the sequences. Sequences were retrieved from the *UniProt* database, aligned with the *Clustal Omega* program (http://www.uniprot.org/align) and shaded with the *BoxShade* tool (http://www.ch.embnet.org/software/BOX_form.html).

Cpc2p and human RACK1 have been reported to be phosphorylated at residues T10 and Y246, respectively, corresponding to positions T12 and Y250 of yeast Asc1p (Chang et al., 2001; Chang et al., 2002; Wilson-Grady et al., 2008). Phosphorylation of *S. pombe* Cpc2p was observed in a high-throughput study and has so far not been studied in detail. Here, impaired adhesive growth of the *asc1*^{T12A}DE strain was observed. Phosphorylation of human RACK1 at Y246 is catalyzed by the non-receptor protein tyrosine kinase Src. The modification enhances the interaction between RACK1 and Src leading to an inhibition of the kinase activity (Chang et al., 2001; Chang et al., 2002). Phosphorylation of RACK1 at Y246 also regulates its interaction with the mRNA-binding protein ZBP1, another target for the Src at the ribosome (Ceci et al., 2012). In our analyses, the *asc1*^{Y250F} strain specifically showed sensitivity to inhibitors of mRNA translation suggesting a role of this phosphorylation site in (co-)translational processes. The mutation of mammalian RACK1 at Y246 does not reduce the association of the β-propeller protein to ribosomes (Ceci et al., 2012) suggesting that the observed phenotypes for the *asc1*^{Y250F} strain are not caused by enhanced release of the protein from the site of translation. However, impairment of Asc1p's correct localization to the ribosome through the DE mutation enhanced the effect of Y250F on the sensitivity of yeast cells to cycloheximide. To the best of our knowledge, this is the first study that showed the phosphorylation of Y250/Y246 of Asc1p/RACK1 *in vivo*. The high conservation of this amino acid residue and its surrounding sequence together with the experimental evidence for phosphorylation of Y246 in mammals suggest that the phosphorylation of this residue is highly conserved among eukaryotes and provides a common mechanism to regulate the protein.

According to the data compiled in the *PhosphoGRID* database only approximately 3% of all known phosphorylation sites in *S. cerevisiae* are tyrosine residues, whereas about 25% and 75% are threonine and serine residues, respectively (Stark et al., 2006). No *S. cerevisiae* homologues are known for the Src kinase or other members of the family of non-receptor protein tyrosine kinases. Furthermore, no true tyrosine kinases were described for yeast, yet, dual-specificity kinases that phosphorylate serine/threonine as well as tyrosine residues and function, for example, in MAPK cascades (Hunter and Plowman, 1997).

So far, amino acid T143 of Asc1p has not been described as a phospho-site in other organisms. However, the comparison of the amino acid sequences and the crystal structures of Asc1p and its orthologues reveals that the phospho-sites S122 of *A. thaliana* RACK1A, S146 of human RACK1, and S148 of *S. pombe* Cpc2p are located in the same region of the protein (Figure 29, Liu et al., 2007b; Wilson-Grady et al., 2008; Urano et al., 2015). Putative

phosphorylation of human RACK1 at S146 was proposed to be a prerequisite for dimer formation *in vivo* and consequently for a RACK1-mediated degradation of the α-subunit of the transcription factor HIF-1 (Figure 7, Liu et al., 2007b). So far, there is no evidence for the *in vivo* homodimerization of Asc1p, but a crystal structure of an Asc1p homodimer could be resolved using a protein sample derived from recombinant expression in *E. coli* (Yatime et al., 2011). Hence, phosphorylation of Asc1p does not seem to be essential for homodimer formation. However, the yeast phosphorylation site T143 not only lies in close proximity of human S146 (see superposition view of the crystal structures in Figure 29), but also in the center of strand 3βD that is directly positioned at the dimer interface (Yatime et al., 2011). Since S146 is not conserved in *S. cerevisiae* Asc1p, phosphorylation of T143 of Asc1p could instead regulate a putative homodimer formation of the β-propeller protein.

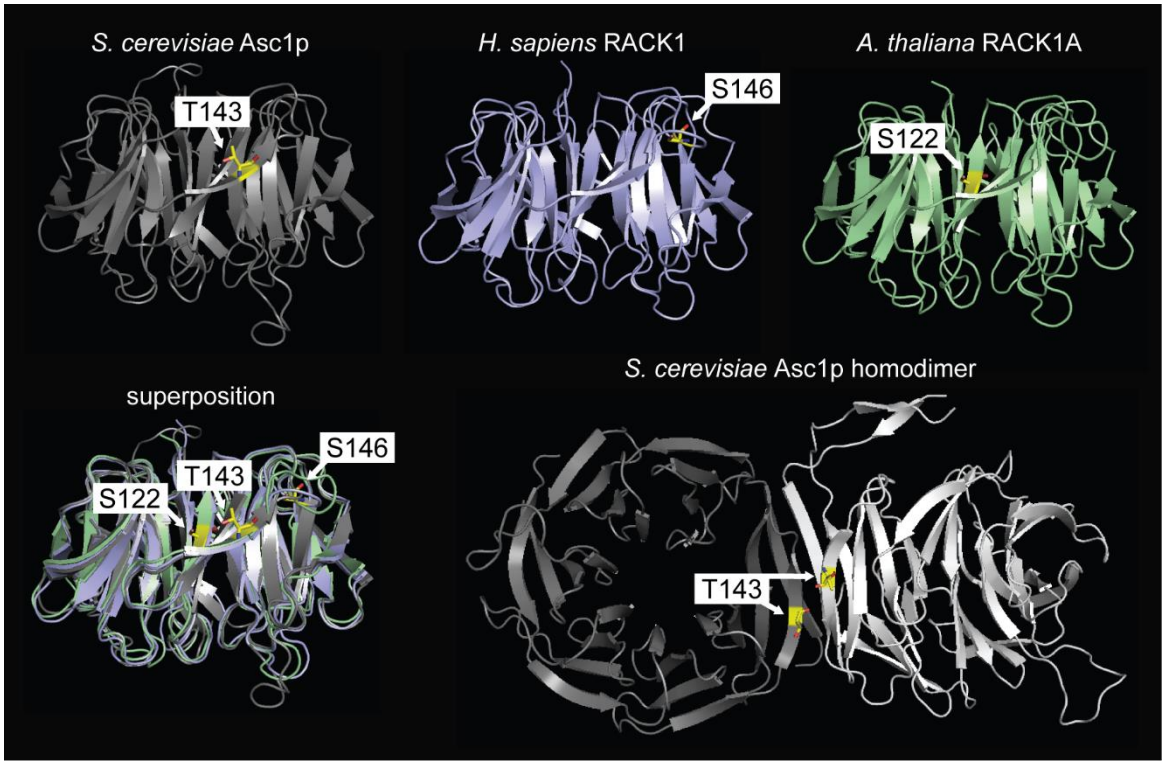

Figure 29. Phosphorylation in the blade 3 region of Asc1p/RACK1.
Structures of *S. cerevisiae* Asc1p (gray), *H. sapiens* RACK1 (blue), and *A. thaliana* RACK1A (green) are shown with their respective phosphorylation sites T143, S146, and S122 highlighted. Phosphosites are depicted as sticks with carbon atoms in yellow, nitrogen atoms in blue, and oxygen atoms in red. Additionally, a superposition view of all three structures is depicted. The Asc1p homodimer is displayed with the two interacting Asc1p molecules in gray and white and with the T143 residues from both proteins highlighted. Structure figures were generated with the *PyMOL Molecular Graphics System* software on the basis of the PDB files 3FRX (Asc1p, Coyle et al., 2009), 4AOW (hRACK1, Ruiz Carrillo et al., 2012), 3DM0 (AtRACK1, Ullah et al., 2008), and 3RFG (Asc1p dimer, Yatime et al., 2011).

The substitution of T143 for alanine in combination with the DE mutation resulted in a drastic reduction of Asc1 protein levels and significantly changed the phenotypes of the mutant strain. Phosphorylation of Asc1p might regulate the protein's stability as it was proposed for phosphorylation of S122 of *A. thaliana* RACK1A by WNK8 (Urano et al., 2015). Since S122 of *A. thaliana* RACK1A lies in close proximity to T143 of *S. cerevisiae* Asc1p (see the superposition view of the structure in Figure 29), the phosphorylation state of this region may determine the stability of the protein. Not only the amino acid exchange of T143 but also that of T12 and T96 resulted in significant reduction of Asc1 protein levels when combined with the DE mutation. In contrast, the DE mutation itself resulted in increased levels of Asc1p. Furthermore, the additional mutation of T99 to alanine, but not to glutamate, enhanced the effect of the T96A DE mutation on protein levels and certain phenotypes. It is important to note, that neither one of the phospho-site mutations at T12, T96, T99, and T143 alone changed protein levels of Asc1p. Apparently, these residues are all located near the Asc1p-ribosome binding interface in contrast to S120, S166, T168, and Y250 (Figure 14). Compromised association of Asc1p to the ribosome or even changes in its precise positioning might expose these residues and make them accessible for other proteins. The phosphorylation of T12, T96, T99, or T143 might regulate the integrity of Asc1p as a ribosomal protein and might thereby amplify the ribosome-repulsing effect of the DE mutation. The loss of ribosome-association of Asc1p or its increase in undesired interactions with other proteins could eventually lead to increased degradation rates for the protein.

4.3 Absence of Asc1p significantly changes the phospho-proteome of *S. cerevisiae*

Asc1p and its mammalian orthologue RACK1 have emerged as key factors in signal transduction pathways that adjust the phospho-proteome to cellular needs. Here, reduced abundance of the phosphorylated and active form of the MAPK Hog1p of the high osmolarity response pathway was observed in the *asc1*$^{-}$ strain. A reduced phosphorylation of the metazoan orthologue of Hog1p, p38, upon depletion of RACK1 has been reported as well (Lin et al., 2015; Wang et al., 2015b). Accordingly, overexpression of RACK1 was shown to induce p38 phosphorylation. RACK1 seems to mediate the activation of the MAPK through the interaction with upstream MAP2Ks of p38 (Figure 6, Lin et al., 2015; Wang et al., 2015b). In *S. cerevisiae*, an interaction between Asc1p and the p38-activating MAP2K homologue, Pbs2p, has not been described so far. However, Asc1p associates with the MAP4K Ste20p that acts not only upstream of Hog1p but also of the MAPKs Kss1p and Fus3p, and increased activation of Kss1p through phosphorylation has been detected as well in Asc1p-deficient

cells (Figure 3, Zeller et al., 2007). In *D. melanogaster*, a direct interaction between p38b and RACK1 was observed, and RACK1 even seems to be a target of p38b-mediated phosphorylation (Belozerov et al., 2014).

Besides the impact of Asc1p on the phosphorylation status of MAPKs (Chasse et al., 2006; Zeller et al., 2007), the translation factors eIF2α and eIF4A and a component of the ribosome-associated complex, Ssz1p, were also reported to harbor Asc1p-sensitive phosphorylation sites (Valerius et al., 2007). Here, SILAC quantification through high-resolution mass-spectrometry was used to get a comprehensive overview of Asc1p-sensitive phosphorylation sites of proteins in *S. cerevisiae*. The increased phosphorylation of eIF4A and of Ssz1p was confirmed. Previously, the position of the affected phosphorylation site could be determined only for Ssz1p (Valerius et al., 2007). Here, increased phosphorylation of S2 within eIF4A was observed. Besides eIF4A and Ssz1p, more than 200 proteins were identified to be Asc1p-dependently altered in their phosphorylation status at almost 300 different sites. This finding characterizes Asc1p as a key regulator within the cellular phosphorylation network.

4.4 Versatile Asc1p-dependent changes in the phospho-proteome: How does Asc1p act?

How does Asc1p affect the phosphorylation status of so many proteins? The scaffold protein might position kinases and/or phosphatases in the proximity to their targets for their subsequent modification as it was shown for mammalian RACK1 that positions the activated PKCβII at the ribosome for the phosphorylation of eIF6 and eIF4E (Ceci et al., 2003; Ruan et al., 2012). Here, ribosome-associated proteins with Asc1p-sensitive phosphorylation sites were identified that could depend on a similar regulatory mechanism, among them, for instance, ten translation initiation factors with three subunits of eIF3, namely Rpg1p, Prt1p, and Tif35p. The b-subunit of eIF3, Prt1p is one of 15 proteins with Asc1p-sensitive phosphorylation sites that have been described as physical interaction partners of Asc1p according to the SGD (Figure 22B) and the Asc1p-Strep co-purification experiments presented here. Asc1p was also reported to interact with the c-subunit of eIF3 confirming a physical proximity of Asc1p to eIF3 at ribosomes (Kouba et al., 2012).

The list of proposed physical Asc1p interaction partners comprises the MAP4K Ste20p, which acts upstream of the MAPKs Kss1p, Fus3p, and Hog1p (Zeller et al., 2007). Ste20p contains three phospho-sites that are up-regulated in *asc1*$^{-}$ cells and are possibly involved in the regulation of Ste20p's general kinase activity or target/pathway specificity. Asc1p was suggested to inhibit the kinase activity of Ste20p (Zeller et al., 2007). Thus, Asc1p could not only position kinases at their cellular target sites, but also affect their activity.

In line with an Asc1p-dependent regulation of Ste20p, increased phosphorylation of Myo3p at the Ste20p target site S357 was detected in the absence of Asc1p. Phosphorylation of Myo3p at S357 through Ste20p was shown *in vitro* and seems to be required for the protein's function (Wu et al., 1997). Furthermore, increased phosphorylation of residues T82 and T83 of the MAPK-target Dig2p was observed. Together with Dig1p, it represses the activity of the transcription factor Ste12p through direct interaction (Figure 3). Upon phosphorylation by MAPKs Kss1p and/or Fus3p, Dig2p, and Dig1p are released from the complex leading to the activation of Ste12p (Tedford et al., 1997). However, it has not been addressed whether the phosphorylation status of T82 and T83 is involved in the MAPK-dependent regulation of Dig2p.

Besides Ste20p, 42 additional proteins involved in signal transduction processes were identified with Asc1p-sensitive phosphorylation sites including also other protein kinases like Cdc28p and Sch9p. In the Asc1p-deficient strain, reduced phosphorylation of residues Y19 of Cdc28p and S726 of Sch9p was detected. These sites are known to be involved in the regulation of the catalytic activities of the kinases (Booher et al., 1993; Urban et al., 2007). The cyclin-dependent kinase Cdc28p coordinates cell cycle progression through phosphorylation of various targets. Phosphorylation of Cdc28p at Y19 by the Swe1p kinase provides one of the mechanisms to regulate the catalytic activity of Cdc28p. Phosphorylation of the kinase at this residue is highly conserved and leads to its inhibition and subsequent entry into mitosis (reviewed in Enserink and Kolodner, 2010). In *S. pombe*, the absence of the Asc1p orthologue Cpc2p leads to a defect in G_2/M transition, possibly caused by an increased abundance of the Swe1p-homologous kinase Wee1p and decreased levels of the Wee1p-inhibitor Cdr2p. In line with this, phosphorylation of the Cdc28p-homologue Cdc2p at Y15 (equivalent to Y19 in *S. cerevisiae*) showed delayed kinetics during the cell cycle (Nuñez et al., 2010). In this study, increased protein levels of Cdc28p were also observed that have not been detected for Cdc2p in *S. pombe*. Mammalian RACK1 was described to affect cell cycle progression at the stage of G_1/S transition through its inhibitory effect on Src kinase activity (Mamidipudi et al., 2004). Collectively, these data suggest that Asc1p and its orthologues influence cell cycle progression.

The Sch9p kinase is phosphorylated by the TOR complex 1 (TORC1) at six residues in its C-terminal domain including S726, which was identified here to be Asc1p-dependently regulated (Urban et al., 2007). TORC1 is one of two complexes that contain the Target of rapamycin Tor1/2 kinase as catalytic subunit and that regulate cellular growth in response to nutrient signals (Loewith et al., 2002). Sch9p is required for the TORC1-mediated regulation

of ribosome-biosynthesis, translation initiation, and entry into stationary phase. Phosphorylation of the C-terminal domain of Sch9p is required for the protein's activity and is abolished upon rapamycin treatment and carbon or nitrogen starvation (Urban et al., 2007). In this study, phosphorylation of S726 was found to be decreased in *asc1*$^{-}$ cells.

Considering Asc1p-dependent regulation of specific kinases, such as Ste20p, Cdc28p, and Sch9p, the *motif-x* software tool was applied to find overrepresented kinase motifs surrounding the regulated phospho-sites (localization probability ≥ 0.75, Schwartz and Gygi, 2005; Chou and Schwartz, 2011). 38% of the serine and 43% of the threonine residues were directly followed by a proline residue (Figure 30). Such SP or TP motifs are preferred target sites for MAPKs and cyclin-dependent kinases (Mok et al., 2011). However, these motifs were also high abundant - albeit less frequent - among all phospho-sites identified here by LC-MS irrespective of their SILAC-ratios (31% SP and 30% TP). Furthermore, 13% of all regulated serines were followed by a glutamate at the third C-terminal position, yet, 15% of all identified phospho-sites harbored this SxxE motif excluding a specific enrichment of this motif. As expected from the many kinases affected by Asc1p, rather a phosphorylation network than a specific motif and its respective kinase are subject to Asc1p-dependent regulation.

The following paragraphs will focus on the impact of Asc1p on the regulation of specific cellular processes. Several candidates of the Asc1p-sensitive phospho-proteome and their associated biological processes will be discussed considering known or putative relations to Asc1p and further taking into account the results obtained from the Asc1p-Strep co-purification experiments.

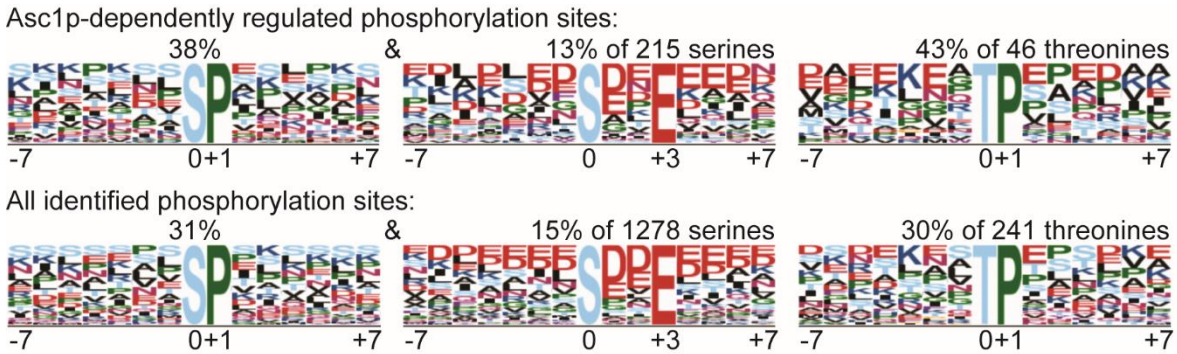

Figure 30. Overrepresented motifs for Asc1p-sensitive phosphorylated serine and threonine residues.

Abundances of motifs for Asc1p-dependently regulated phospho-sites were compared with the occurrence of the same motifs for all phospho-sites identified in this study. Motifs were searched for sites with a localization probability ≥ 0.75 using the *motif-x* software (Schwartz and Gygi, 2005; Chou and Schwartz, 2011). Additional motifs identified for the complete phospho-proteome are not depicted.

4.5 Asc1p affects localized mRNA translation and cytoskeleton organization

Among the 213 proteins identified here with Asc1p-sensitive phospho-sites, 42 are involved in processes related to mRNA translation comprising, for example, eIF3 subunits, eIF4A, and Ssz1p. Another protein of this group is the mRNA-binding protein Puf3 with S86 as one of the strongest down-regulated phosphorylation sites in the *asc1*$^{-}$ strain. Puf3p associates with mRNAs that encode mitochondrial proteins and promotes their localized translation at mitochondria (Saint-Georges et al., 2008). Yet, Puf3p was also reported to support the degradation of its bound transcripts (Olivas and Parker, 2000). These opposing roles of Puf3p in mRNA translation and degradation were suggested to be regulated by its phosphorylation (Lee and Tu, 2015). Upon glucose deprivation, Puf3p gets phosphorylated at several residues within its N-terminal region - including the Asc1p-sensitive phospho-site S86 - and promotes the translation of bound transcripts instead of their degradation (Lee and Tu, 2015). In line with the reduced phosphorylation of Puf3p at S86 in *asc1*$^{-}$ cells, our quantitative proteome data revealed that Asc1p-deficiency causes decreased abundance of many mitochondrial proteins, such as ribosomal proteins and subunits of the transporter complexes of the outer and inner mitochondrial membrane (Supplementary Table 15). This regulation of mitochondrial proteins is consistent with the reduced respiratory activity of *asc1*$^{-}$ cells and their compromised growth on non-fermentable carbon sources (Rachfall et al., 2013).

Reduced phosphorylation was also observed for residue S231 of the mRNA-binding protein Ssd1 in Asc1p-deficient cells. Additionally, Ssd1p was co-purified together with Asc1p-Strep. Ssd1p suppresses the translation of its associated mRNAs until it gets phosphorylated by the kinase Cbk1p at eight residues (Jansen et al., 2009). Many Ssd1p-bound transcripts code for cell wall remodeling proteins. Cbk1p seems to activate the translation of Ssd1p-bound transcripts at sites of cell growth and cell wall remodeling, and disturbance of this regulation leads to defects in cell wall organization. The Asc1p-sensitive residue S231 of Ssd1p has not yet been reported to be involved in the Cbk1p-mediated inhibition of Ssd1p, but lies in close proximity to S228, one of the known target sites of Cbk1p (Jansen et al., 2009). Both the interaction of Ssd1p with Asc1p-Strep and the identification of an Asc1p-sensitive phospho-site within the mRNA-binding protein hint to a functional relationship between the two proteins. This interaction might contribute to the observed defects of Asc1p-deficient cells in cell wall integrity (Valerius et al., 2007; Rachfall et al., 2013).

Asc1p might further be involved in the regulation of specific transcripts through physical association with the mRNA-binding proteins She2 and Scp160 (this study; Baum et al., 2004). Here, She2p was co-purified with Asc1p-Strep. She2p is required for the localization of *ASH1*

mRNA to the bud during cell division (Jansen et al., 1996). In the daughter cell, the transcription repressor Ash1p prevents mating type switching (Sil and Herskowitz, 1996). To mediate the asymmetric localization of the *ASH1* mRNA, She2p first has to translocate to the nucleus where it is co-transcriptionally recruited to RNA polymerase II by the universally conserved transcription factor heterodimer Spt4p-Spt5p and subsequently binds the nascent *ASH1* mRNA (Shen et al., 2010). In the cytoplasm, a transport mRNP is formed through the interaction between She2p and the Myo4p-adaptor protein She3 (Böhl et al., 2000). The mRNP moves along the actin cytoskeleton to the bud tip, and translation is suppressed through the presence of Puf6p and Khd1p in the mRNP (Irie et al., 2002; Gu et al., 2004). When the destination of the *ASH1* mRNA is reached, phosphorylation of Puf6p and Khd1p triggers the translation of *ASH1* mRNA (Paquin et al., 2007; Deng et al., 2008). Besides the *ASH1* mRNA, She2p is required for the localization of more than 30 transcripts (reviewed in Heym and Niessing, 2012). Most of these mRNAs contain *cis*-elements, known as zip-code elements that were shown to be required for the recognition through She2p (Heym and Niessing, 2012). She2p shows similarities to the mammalian mRNA-binding protein ZBP1 (Zipcode-binding protein 1). Remarkably, ZBP1 interacts with RACK1 in transport mRNPs in neuronal cells to regulate the localized translation of β-actin mRNA (Ceci et al., 2012; Heym and Niessing, 2012). Thus, Asc1p and RACK1 are both involved in mRNA transport.

The involvement of Asc1p in She2p directed mRNA localization is further supported by the co-purification of the already mentioned She2p-interacting transcription factor Spt5p with Asc1p-Strep and Asc1DEp-Strep. The Spt4p-Spt5p heterodimer is involved in the elongation process of RNA polymerase II transcription, but has also been found to function in RNA polymerase I-mediated transcription, mRNA capping, and splicing (Hartzog et al., 1998; Wen and Shatkin, 1999; Lindstrom et al., 2003; Schneider et al., 2006). Additionally, the cyclin of the Bur1p kinase, Bur2p (Yao et al., 2000), was co-purified with Asc1DEp-Strep. The Bur1p-Bur2p complex phosphorylates Spt5p in its C-terminal region, which is required for transcription elongation and histone modification (Liu et al., 2009; Zhou et al., 2009).

Asc1p further interacts with the mRNA-binding protein Scp160 (Baum et al., 2004). Binding of Scp160p to ribosomes requires Asc1p, and as part of a multiprotein complex called SESA network, both proteins regulate the translation of the *POM34* mRNA (Baum et al., 2004; Sezen et al., 2009). Like She2p, Scp160p is involved in mRNA transport through targeting of pheromone-induced mRNAs to the shmoo tip during mating (Gelin-Licht et al., 2012). Scp160p was described as an effector protein of Gpa1p, the Gα-protein of the pheromone-response pathway (Guo et al., 2003). Through the interaction with Scp160p, Asc1p might link

the pheromone response pathway to nutrient sensing based on its proposed function as the Gβ-protein for Gpa2p. A role of Asc1p in the pheromone signal transduction pathway has been previously proposed based on the already mentioned interaction of Asc1p with the MAP4K Ste20p and increased activation of the downstream MAPK Kss1p (Zeller et al., 2007). Furthermore, Asc1p-deficient MATa cells exhibit increased sensitivity to the α-factor pheromone (Chasse et al., 2006). Altogether, Asc1p seems to be involved in translational regulation through interaction with mRNA-binding proteins. This regulation might not only involve Asc1p-dependent recruitment of mRNA-binding proteins to the ribosome as it was shown for Scp160p but also Asc1p-dependent mRNA transport for localized translation as it was shown for its mammalian orthologue (Baum et al., 2004; Ceci et al., 2012). Furthermore, Asc1p affects the phosphorylation status of mRNA-binding proteins and consequently most likely the fate of their bound transcripts.

Cellular localization of mRNAs most often involves the actin cytoskeleton and motor proteins. Casolari and colleagues (2012) studied the association of mRNAs with cytoskeletal motor proteins. The type I myosin Myo3p was identified to associate with mRNAs that encode key regulators of actin branching and endocytosis. The motor protein seems to be required for the transport of its associated transcripts to actin patches and/or for their anchoring at these sites (Casolari et al., 2012). In *asc1*$^{-}$ cells, Myo3p is strongly increased in its phosphorylation at S357. As already discussed, Myo3p is most likely phosphorylated at S357 by the MAP4K Ste20p, whose activity seems to be suppressed by Asc1p (Wu et al., 1997; Zeller et al., 2007).

Besides Myo3p, 27 other proteins with Asc1p-sensitive phospho-sites are related to cytoskeleton-associated processes, and 37 proteins are associated with transport and trafficking. One of the proteins involved in cytoskeleton-associated processes is the formin Bni1p/She5p, which was identified in the initial screen for genes required for the asymmetric localization of *ASH1* mRNA (Jansen et al., 1996). Phosphorylation of Bni1p was down-regulated upon Asc1p-deficiency at S1889. Yet, is has to be noted that no quantitative proteome value was obtained for the protein. The formins Bni1p and Bnr1p nucleate unbranched actin cables and cytokinetic rings, whereas the formation of actin patches at sites of endocytosis requires the Arp2/3 complex (reviewed in Goode et al., 2015). The Arp2/3 complex associates with nucleation-promoting factors, such as the already mentioned Myo3/5p and the acting binding protein Abp1 (Evangelista et al., 2000; Goode et al., 2001). Abp1p harbors four sites that are reduced in phosphorylation in *asc1*$^{-}$ cells, whereas the total protein level of Abp1p is increased by more than 70%. Abp1p acts together with Aim3p to

regulate actin filament barbed end elongation in the Arp2/3-nucleated networks (Michelot et al., 2013). Phosphorylation of Aim3p at S843 is enhanced in Asc1p-deficient cells, however, a corresponding quantitative proteome value is missing.

The proteins Bud14 and Kel1 were found to interact with Strep-tagged Asc1p variants in this study. A complex of Bud14p with the Kelch proteins Kel1 and Kel2 regulates the displacement of formin Bnr1p from the growing ends of actin filaments and is consequently required for the normal actin cable architecture (Gould et al., 2014). An interaction between Asc1p and Bud14p was suggested from a high throughput study (Gavin et al., 2002). As an additional component of this complex, Asc1p could be directly involved in the coordination of actin cytoskeleton organization. Bud14p was further described as one of the regulatory subunits of the protein phosphatase Glc7p and is required for the localization of Glc7p at sites of polarized growth (Knaus et al., 2005). The localization of Bud14p to these sites in turn relies on the interaction with the Kelch proteins (Knaus et al., 2005; Gould et al., 2014). The Bud14p-Glc7p complex contributes to the regulation of microtubuli interactions at sites of polarized growth (Knaus et al., 2005). Furthermore, it seems to control post-translational modification of the stress-responsive transcription factor Msn2p in dependence of the Ccr4p-Not complex (Lenssen et al., 2005). Two other regulatory subunits of Glc7p (Glc8p and Ypi1p) were found to be affected in their phosphorylation status in the *asc1*$^{-}$ cells providing further evidence for a link between Asc1p and Glc7p function. Thus, several changes in the Asc1p-dependent phospho-proteome might be caused by altered Glc7p activity. In conclusion, Asc1p might affect cytoskeleton-related processes through mediating the phosphorylation status of key-components of actin-organization.

4.6 Asc1p's impact on protein folding and degradation

Phosphorylations of core components of the 26S proteasome are sensitive to Asc1p. Furthermore, the abundance of almost all subunits of the 20S core particle and two components of the 19S regulatory particle were increased upon Asc1p-deficiency (Figure 31 and Supplementary Table 16). The proteasome and eIF3 were described to form a supercomplex with the ribosome, elongation factors, tRNA synthetases, and chaperones called the translasome that reveals a close connection of protein synthesis and degradation (Sha et al., 2009). Different co-translational quality control pathways exist that recognize aberrant translation processes and involve the proteasome for degradation of the nascent polypeptide chain (reviewed in Inada, 2013). Asc1p is required for nascent polypeptide-dependent translation arrest that is, for example, caused by polybasic sequences in the growing peptide

chain. This results in the degradation of the translated mRNA and the nascent polypeptide chain (Kuroha et al., 2010; Brandman et al., 2012; Matsuda et al., 2014).

The correct folding of nascent polypeptides is essential to protect newly synthesized proteins from immediate degradation. In eukaryotic cells, the nascent polypeptide-associated complex (NAC) can bind to emerging polypeptides to prevent inappropriate interactions and misfolding (Wang et al., 1995). Moreover, the NAC functions in the co-translational delivery of proteins to mitochondria as well as in the translocation of nascent polypeptide chains to the endoplasmic reticulum mediated by the signal recognition particle (George et al., 2002; Zhang et al., 2012b). The NAC is a highly conserved heterodimer formed by the proteins Egd1 and Egd2 in *S. cerevisiae*. Here, phosphorylation of Egd1p at T151 was identified as the strongest down-regulated phospho-site in the *asc1*$^{-}$ strain.

A role of Asc1p in co-translational protein folding is deduced from the observation that mammalian RACK1 recruits activated JNK to the ribosome in order to phosphorylate eEF1A and with that to induce association of the translation factor with the newly synthesized peptide chain (Gandin et al., 2013a). The translation elongation factor is involved in the recruitment of aminoacyl-tRNAs to the ribosomes, but it can also mediate the co-translational degradation of nascent polypeptide chains by the proteasome (Hotokezaka et al., 2002; Chuang et al., 2005). In *T. brucei*, RACK1 was shown to associate with eEF1A (Regmi et al., 2008). Moreover, the mRNA-binding protein and interaction partner of Asc1p, Scp160p, was found

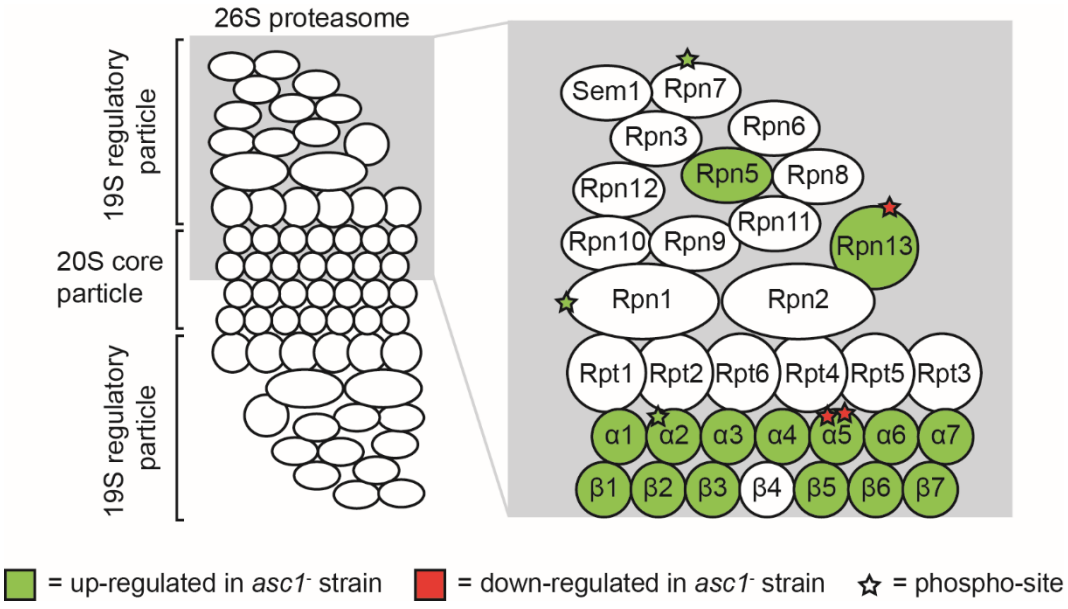

Figure 31. Asc1p-dependent alterations of the 26S proteasome.
Asc1p-sensitive phospho-sites within components of the 26S proteasome are indicated with asterisks. Proteins regulated in their abundance in the Asc1p-deficient cells are colored. Colors indicate whether the phospho-sites or the proteins were up- or down-regulated in the *asc1*$^{-}$ strain. The schematic depiction of the 26S proteasome was adapted from the KEGG database.

to associate with eEF1A at ribosomes implicating a physical proximity of eEF1A to Asc1p also in yeast (Baum et al., 2004).

The heat shock protein 70 (Hsp70) chaperones Ssb1p and Ssb2p (Stress-seventy subfamily B) together with the ribosome-associated complex consisting of the Hsp70 Ssz1p and the Hsp40 Zuo1p also assist in the folding of nascent polypeptide chains (Gautschi et al., 2002). Ssz1p contains an Asc1p-sensitive phosphorylation site (this study; Valerius et al., 2007). The family of Hsp70 chaperones further comprises four Ssa (Stress-seventy subfamily A) proteins. Here, Asc1DEp-Strep, but not Asc1p-Strep, was shown to co-purify with Ssa1p and Ssa2p. Ssa1p associates with the Hsp40 Sis1p predominantly on translating ribosomes and both proteins are required for intact mRNA translation (Horton et al., 2001). Although Ssa1p and Ssa2p clearly did not interact with Asc1p-Strep, Sis1p was found enriched with the Strep-tagged wild-type Asc1 protein. Ssa1/2p and Sis1p are involved in prion propagation (reviewed in Liebman and Chernoff, 2012). The [*PSI*$^+$] prion is formed through a refolding of the translation termination factor Sup35p, and deletion of *ASC1* results in induction of [*PSI*$^+$] (Manogaran et al., 2011). Like Ssa1/2p, Sup35p was found to interact with Asc1DEp-Strep, but most likely not with Asc1p-Strep. Sup35p has been proposed to function in a process named premature translation termination that releases C-terminally truncated nascent polypeptides from ribosomes stalled on polylysine stretches (Chiabudini et al., 2014). During this process, Sup35p binds to the ribosomal A-site although it does not contain a stop codon. The deletion of *ASC1* abolishes premature translation termination most likely due to its effect on overall translation rates (Chiabudini et al., 2014). Yet, the data presented here indicate a direct interplay between Asc1p and Sup35p that is further supported by the identification of two Asc1p-sensitive phospho-sites within Sup35p (T570 and S571).

Altogether, Asc1p/RACK1 seems to function in protein folding and degradation during translation and beyond. The involvement of Asc1p in protein degradation processes is further supported by the finding that three proteins with ubiquitin-binding activity namely Def1p, Cue5p, and Dsk2p associate with Asc1p-Strep and/or Asc1DEp-Strep. Both Def1p and Cue5p contain ubiquitin-binding CUE domains (Shih et al., 2003). The CUE domain of Def1p is required for its binding to the ubiquitin-like domain of Ela1p, a component of the Elongin-Cullin ubiquitin ligase complex. The simultaneous interaction of Def1p with this E3 ubiquitin ligase and the RNA polymerase II results in polyubiquitination of the largest subunit of the polymerase, Rpb1p, and its subsequent degradation (Wilson et al., 2013). The Def1p-mediated degradation of RNA polymerase II occurs in response to DNA-damage that causes transcriptional stress. Upon these conditions, Def1p is modified in a ubiquitin- and

proteasome-dependent process leading to removal of its C-terminal domain and its translocation from the cytoplasm to the nucleus where it mediates Rpb1p degradation (Wilson et al., 2013). Two phosphorylation sites T258 and S260 are reduced in their phosphorylation status in *asc1*$^{-}$ cells further implicating a functional link between Asc1p and Def1p.

The Cue5 protein was identified as a ubiquitin adaptor protein for the autophagy related protein 8 (Atg8) and thus seems to be involved in substrate recognition for selective macroautophagy (Lu et al., 2014). Dsk2p is involved in the delivery of polyubiquitinated proteins to the proteasome. The protein binds polyubiquitin-chains through its C-terminal ubiquitin-associated domain and interacts with the proteasome through its N-terminal ubiquitin-like domain (Funakoshi et al., 2002). Asc1p was described to be ubiquitinated at ten sites, and it remains to be determined whether the ubiquitin-binding proteins Def1, Cue5, and Dsk2 interact with the ubiquitinated forms of Asc1p-Strep and/or Asc1DEp-Strep (Swaney et al., 2013).

4.7 The β-propeller Asc1p represents a regulatory interface connecting mRNA translation with fundamental cellular processes according to signals

This work focused on the role of Asc1p in the cellular phosphorylation network of *S. cerevisiae*. The exposed localization of the β-propeller at the ribosome goes along with an important coordination function that connects a variety of cellular processes to local mRNA translation and signal transduction. It influences the activities of central signal transduction players, such as the kinases PKA, Cdc28p, Ste20p, Kss1p, Slt2p, and Hog1p as well as the phosphatase Glc7p, which coordinate cellular processes like cell cycle progression, maintenance of cell wall integrity, and adaptation to osmolarity and hypoxic growth conditions (Figure 32). Fundamental processes like cytoskeleton organization, protein folding and turnover, and even nuclear transcription processes are significantly affected by the absence of Asc1p. Translation of the transcription factor *YHR177W* mRNA seems highly Asc1p-dependent. This diversified impact of a single protein might be due to its high abundance and presence in almost every ribosome. Especially, different local activity of ribosomes, for example, at mitochondria, could be subject to Asc1p-dependent regulation. The interaction of Asc1p with mRNA-binding proteins or its effect on their phosphorylation status could provide a mechanism for translational regulation. Asc1p is itself phosphorylated at multiple sites. Here, four of these sites were identified to be involved in the regulation of Asc1p's abundance. Absence of Asc1p uncouples the translation machinery from certain signal transduction pathways and limits the ability of the cell to adapt to stress conditions.

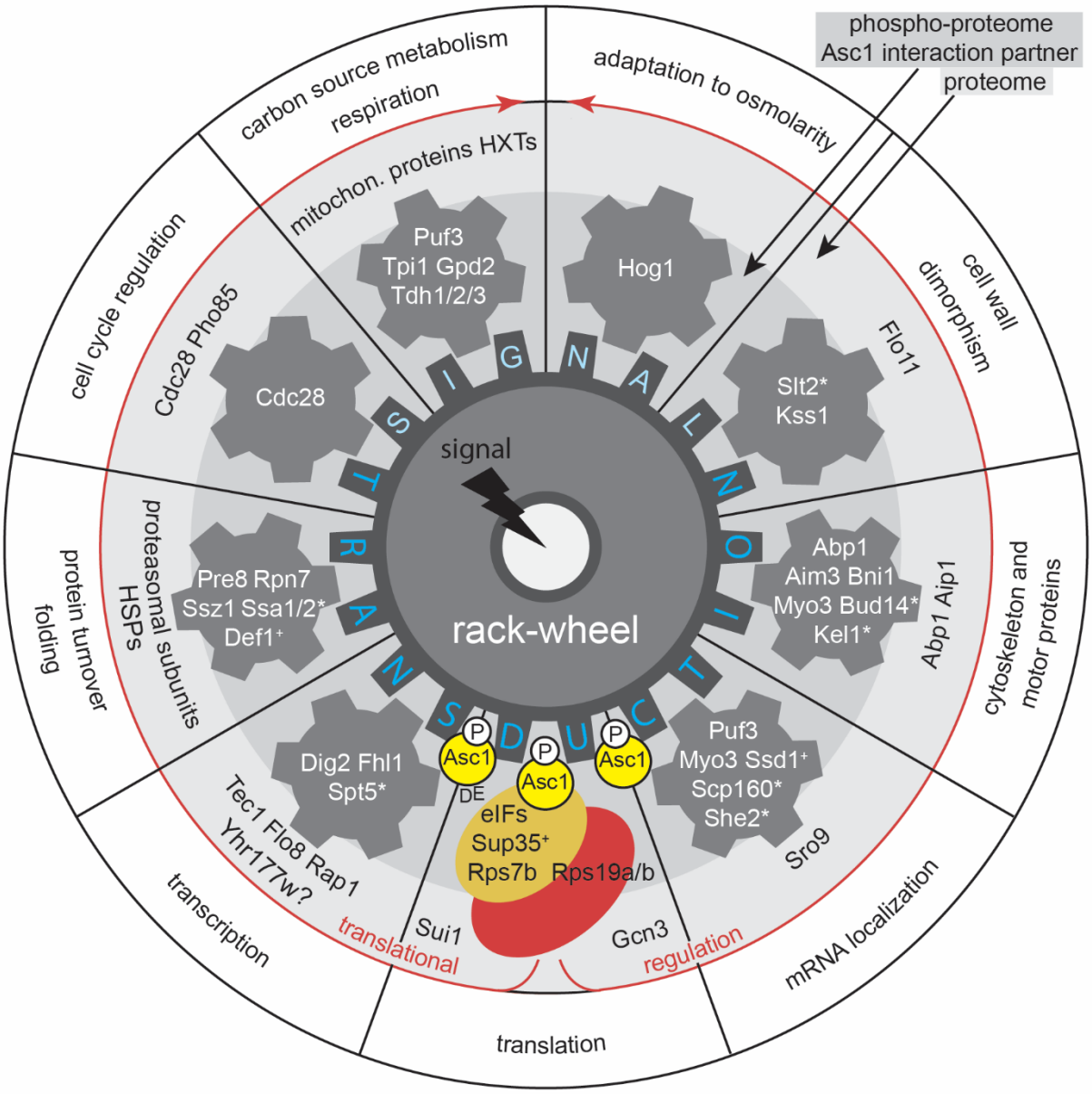

Figure 32. The rack-wheel of Asc1p-dependent signal transduction.
The proposed function of Asc1p in the adaptation of the cellular proteome and phospho-proteome in response to signal transduction is schematically depicted. Asc1p links cellular signal transduction to the ribosome leading to the adjustment of the cellular proteome as needed (indicated by red arrows). Simultaneously, Asc1p is important for the phosphorylation status of central components of various processes named in the outermost ring of the scheme. The inner ring around the central rack-wheel gives examples for proteins containing Asc1p-sensitive phosphorylation sites. Proteins labeled with a plus (+) were additionally identified as interaction partners of Asc1p. Proteins marked with an asterisk (*) were not identified with Asc1p-sensitive phospho-sites but as Asc1p-interacting proteins. In the outer gray ring, examples for proteins are given that are Asc1p-dependently regulated on the proteome level. For the transcription factor Yhr177wp, translation of its encoding mRNA seems to be directly Asc1p-dependent. Also, a ribosome-free form of Asc1p could be part of the signal transduction machinery. Ribosome-association of Asc1p can be impaired through the DE mutation. Phosphorylation (P) of Asc1p itself could modulate the protein's integrity as a link between translation and signal transduction. Additional references used apart from this study: Flo11p (Valerius et al., 2007), Kss1p (Zeller et al., 2007), Scp160p (Baum et al., 2004), and Slt2p (Chasse et al., 2006; Breitkreutz et al., 2010). (HSP = heat shock protein, Hxts = hexose transporters)

5. References

Adams, D.R., Ron, D., and Kiely, P.A. (2011). RACK1, A multifaceted scaffolding protein: Structure and function. Cell Commun Signal *9*, 22.

Alspaugh, J.A., Perfect, J.R., and Heitman, J. (1997). *Cryptococcus neoformans* mating and virulence are regulated by the G-protein α subunit GPA1 and cAMP. Genes Dev *11*, 3206-3217.

Amir, S., Wang, R., Simons, J.W., and Mabjeesh, N.J. (2009). SEPT9_v1 up-regulates hypoxia-inducible factor 1 by preventing its RACK1-mediated degradation. J Biol Chem *284*, 11142-11151.

Arimoto, K., Fukuda, H., Imajoh-Ohmi, S., Saito, H., and Takekawa, M. (2008). Formation of stress granules inhibits apoptosis by suppressing stress-responsive MAPK pathways. Nat Cell Biol *10*, 1324-1332.

Balakin, A.G., Smith, L., and Fournier, M.J. (1996). The RNA world of the nucleolus: two major families of small RNAs defined by different box elements with related functions. Cell *86*, 823-834.

Bardwell, L. (2005). A walk-through of the yeast mating pheromone response pathway. Peptides *26*, 339-350.

Baum, S., Bittins, M., Frey, S., and Seedorf, M. (2004). Asc1p, a WD40-domain containing adaptor protein, is required for the interaction of the RNA-binding protein Scp160p with polysomes. Biochem J *380*, 823-830.

Belozerov, V.E., Ratkovic, S., McNeill, H., Hilliker, A.J., and McDermott, J.C. (2014). *In vivo* interaction proteomics reveal a novel p38 mitogen-activated protein kinase/Rack1 pathway regulating proteostasis in *Drosophila* muscle. Mol Cell Biol *34*, 474-484.

Ben-Shem, A., Garreau de Loubresse, N., Melnikov, S., Jenner, L., Yusupova, G., and Yusupov, M. (2011). The structure of the eukaryotic ribosome at 3.0 A resolution. Science *334*, 1524-1529.

Berns, H., Humar, R., Hengerer, B., Kiefer, F.N., and Battegay, E.J. (2000). RACK1 is up-regulated in angiogenesis and human carcinomas. FASEB J *14*, 2549-2558.

Bird, R.J., Baillie, G.S., and Yarwood, S.J. (2010). Interaction with receptor for activated C-kinase 1 (RACK1) sensitizes the phosphodiesterase PDE4D5 towards hydrolysis of cAMP and activation by protein kinase C. Biochem J *432*, 207-216.

Böhl, F., Kruse, C., Frank, A., Ferring, D., and Jansen, R.P. (2000). She2p, a novel RNA-binding protein tethers *ASH1* mRNA to the Myo4p myosin motor via She3p. EMBO J *19*, 5514-5524.

Booher, R.N., Deshaies, R.J., and Kirschner, M.W. (1993). Properties of *Saccharomyces cerevisiae* wee1 and its differential regulation of $p34^{CDC28}$ in response to G_1 and G_2 cyclins. EMBO J *12*, 3417-3426.

Brandman, O., Stewart-Ornstein, J., Wong, D., Larson, A., Williams, C.C., Li, G.W., Zhou, S., King, D., Shen, P.S., Weibezahn, J., *et al.* (2012). A ribosome-bound quality

control complex triggers degradation of nascent peptides and signals translation stress. Cell *151*, 1042-1054.

Breitkreutz, A., Choi, H., Sharom, J.R., Boucher, L., Neduva, V., Larsen, B., Lin, Z.Y., Breitkreutz, B.J., Stark, C., Liu, G., *et al.* (2010). A global protein kinase and phosphatase interaction network in yeast. Science *328*, 1043-1046.

Brown, G.C. (2001). Regulation of mitochondrial respiration by nitric oxide inhibition of cytochrome c oxidase. Biochim Biophys Acta *1504*, 46-57.

Burnette, W.N. (1981). "Western blotting": electrophoretic transfer of proteins from sodium dodecyl sulfate--polyacrylamide gels to unmodified nitrocellulose and radiographic detection with antibody and radioiodinated protein A. Anal Biochem *112*, 195-203.

Cai, Z.D., Chai, Y.F., Zhang, C.Y., Qiao, W.R., Sang, H., and Lu, L. (2015). The Gβ-like protein CpcB is required for hyphal growth, conidiophore morphology and pathogenicity in *Aspergillus fumigatus*. Fungal Genet Biol *81*, 120-131.

Cain, C.W., Lohse, M.B., Homann, O.R., Sil, A., and Johnson, A.D. (2012). A conserved transcriptional regulator governs fungal morphology in widely diverged species. Genetics *190*, 511-521.

Cao, X.X., Xu, J.D., Liu, X.L., Xu, J.W., Wang, W.J., Li, Q.Q., Chen, Q., Xu, Z.D., and Liu, X.P. (2010). RACK1: A superior independent predictor for poor clinical outcome in breast cancer. Int J Cancer *127*, 1172-1179.

Casolari, J.M., Thompson, M.A., Salzman, J., Champion, L.M., Moerner, W.E., and Brown, P.O. (2012). Widespread mRNA association with cytoskeletal motor proteins and identification and dynamics of myosin-associated mRNAs in *S. cerevisiae*. PLoS One *7*, e31912.

Castello, P.R., David, P.S., McClure, T., Crook, Z., and Poyton, R.O. (2006). Mitochondrial cytochrome oxidase produces nitric oxide under hypoxic conditions: implications for oxygen sensing and hypoxic signaling in eukaryotes. Cell Metab *3*, 277-287.

Ceci, M., Gaviraghi, C., Gorrini, C., Sala, L.A., Offenhäuser, N., Marchisio, P.C., and Biffo, S. (2003). Release of eIF6 ($p27^{BBP}$) from the 60S subunit allows 80S ribosome assembly. Nature *426*, 579-584.

Ceci, M., Welshhans, K., Ciotti, M.T., Brandi, R., Parisi, C., Paoletti, F., Pistillo, L., Bassell, G.J., and Cattaneo, A. (2012). RACK1 is a ribosome scaffold protein for β-actin mRNA/ZBP1 complex. PLoS One *7*, e35034.

Chang, B.Y., Chiang, M., and Cartwright, C.A. (2001). The interaction of Src and RACK1 is enhanced by activation of protein kinase C and tyrosine phosphorylation of RACK1. J Biol Chem *276*, 20346-20356.

Chang, B.Y., Conroy, K.B., Machleder, E.M., and Cartwright, C.A. (1998). RACK1, a receptor for activated C kinase and a homolog of the β subunit of G proteins, inhibits activity of src tyrosine kinases and growth of NIH 3T3 cells. Mol Cell Biol *18*, 3245-3256.

Chang, B.Y., Harte, R.A., and Cartwright, C.A. (2002). RACK1: a novel substrate for the Src protein-tyrosine kinase. Oncogene *21*, 7619-7629.

Chantrel, Y., Gaisne, M., Lions, C., and Verdière, J. (1998). The transcriptional regulator Hap1p (Cyp1p) is essential for anaerobic or heme-deficient growth of *Saccharomyces cerevisiae:* Genetic and molecular characterization of an extragenic suppressor that encodes a WD repeat protein. Genetics *148*, 559-569.

Chasse, S.A., Flanary, P., Parnell, S.C., Hao, N., Cha, J.Y., Siderovski, D.P., and Dohlman, H.G. (2006). Genome-scale analysis reveals Sst2 as the principal regulator of mating pheromone signaling in the yeast *Saccharomyces cerevisiae*. Eukaryot Cell *5*, 330-346.

Chen, J.G., Ullah, H., Temple, B., Liang, J., Guo, J., Alonso, J.M., Ecker, J.R., and Jones, A.M. (2006). RACK1 mediates multiple hormone responsiveness and developmental processes in *Arabidopsis*. J Exp Bot *57*, 2697-2708.

Chen, S., Dell, E.J., Lin, F., Sai, J., and Hamm, H.E. (2004a). RACK1 regulates specific functions of Gβγ. J Biol Chem *279*, 17861-17868.

Chen, S., Lin, F., and Hamm, H.E. (2005). RACK1 binds to a signal transfer region of Gβγ and inhibits phospholipase C β2 activation. J Biol Chem *280*, 33445-33452.

Chen, S., Spiegelberg, B.D., Lin, F., Dell, E.J., and Hamm, H.E. (2004b). Interaction of Gβγ with RACK1 and other WD40 repeat proteins. J Mol Cell Cardiol *37*, 399-406.

Cheng, Z., Li, J.F., Niu, Y., Zhang, X.C., Woody, O.Z., Xiong, Y., Djonović, S., Millet, Y., Bush, J., McConkey, B.J., *et al.* (2015). Pathogen-secreted proteases activate a novel plant immune pathway. Nature *521*, 213-216.

Chi, A., Huttenhower, C., Geer, L.Y., Coon, J.J., Syka, J.E., Bai, D.L., Shabanowitz, J., Burke, D.J., Troyanskaya, O.G., and Hunt, D.F. (2007). Analysis of phosphorylation sites on proteins from *Saccharomyces cerevisiae* by electron transfer dissociation (ETD) mass spectrometry. Proc Natl Acad Sci U S A *104*, 2193-2198.

Chiabudini, M., Tais, A., Zhang, Y., Hayashi, S., Wölfle, T., Fitzke, E., and Rospert, S. (2014). Release factor eRF3 mediates premature translation termination on polylysine-stalled ribosomes in *Saccharomyces cerevisiae*. Mol Cell Biol *34*, 4062-4076.

Chou, M.F., and Schwartz, D. (2011). Biological sequence motif discovery using motif-x. Curr Protoc Bioinformatics *Chapter 13*, Unit 13 15-24.

Chou, Y.C., Chou, C.C., Chen, Y.K., Tsai, S., Hsieh, F.M., Liu, H.J., and Hseu, T.H. (1999). Structure and genomic organization of porcine RACK1 gene. Biochim Biophys Acta *1489*, 315-322.

Choudhury, K., Cardenas, D., Pullikuth, A.K., Catling, A.D., Aiyar, A., and Kelly, B.L. (2011). Trypanosomatid RACK1 orthologs show functional differences associated with translation despite similar roles in *Leishmania* pathogenesis. PLoS One *6*, e20710.

Chuang, S.M., Chen, L., Lambertson, D., Anand, M., Kinzy, T.G., and Madura, K. (2005). Proteasome-mediated degradation of cotranslationally damaged proteins involves translation elongation factor 1A. Mol Cell Biol *25*, 403-413.

Conti, M., Richter, W., Mehats, C., Livera, G., Park, J.Y., and Jin, C. (2003). Cyclic AMP-specific PDE4 phosphodiesterases as critical components of cyclic AMP signaling. J Biol Chem *278*, 5493-5496.

Cox, J., and Mann, M. (2008). MaxQuant enables high peptide identification rates, individualized p.p.b.-range mass accuracies and proteome-wide protein quantification. Nat Biotechnol *26*, 1367-1372.

Coyle, S.M., Gilbert, W.V., and Doudna, J.A. (2009). Direct link between RACK1 function and localization at the ribosome *in vivo*. Mol Cell Biol *29*, 1626-1634.

Cross, F.R., and Tinkelenberg, A.H. (1991). A potential positive feedback loop controlling *CLN1* and *CLN2* gene expression at the start of the yeast cell cycle. Cell *65*, 875-883.

de Oliveira, I.M., Zanotto-Filho, A., Moreira, J.C., Bonatto, D., and Henriques, J.A. (2010). The role of two putative nitroreductases, Frm2p and Hbn1p, in the oxidative stress response in *Saccharomyces cerevisiae*. Yeast *27*, 89-102.

Decker, C.J., and Parker, R. (2012). P-bodies and stress granules: possible roles in the control of translation and mRNA degradation. Cold Spring Harb Perspect Biol *4*, a012286.

Dell, E.J., Connor, J., Chen, S., Stebbins, E.G., Skiba, N.P., Mochly-Rosen, D., and Hamm, H.E. (2002). The βγ subunit of heterotrimeric G proteins interacts with RACK1 and two other WD repeat proteins. J Biol Chem *277*, 49888-49895.

Deng, Y., Singer, R.H., and Gu, W. (2008). Translation of *ASH1* mRNA is repressed by Puf6p-Fun12p/eIF5B interaction and released by CK2 phosphorylation. Genes Dev *22*, 1037-1050.

Dever, T.E., Feng, L., Wek, R.C., Cigan, A.M., Donahue, T.F., and Hinnebusch, A.G. (1992). Phosphorylation of initiation factor 2 α by protein kinase GCN2 mediates gene-specific translational control of *GCN4* in yeast. Cell *68*, 585-596.

Enserink, J.M., and Kolodner, R.D. (2010). An overview of Cdk1-controlled targets and processes. Cell Div *5*, 11.

Evangelista, M., Klebl, B.M., Tong, A.H., Webb, B.A., Leeuw, T., Leberer, E., Whiteway, M., Thomas, D.Y., and Boone, C. (2000). A role for myosin-I in actin assembly through interactions with Vrp1p, Bee1p, and the Arp2/3 complex. J Cell Biol *148*, 353-362.

Feng, C., Li, Y.F., Yau, Y.H., Lee, H.S., Tang, X.Y., Xue, Z.H., Zhou, Y.C., Lim, W.M., Cornvik, T.C., Ruedl, C., *et al.* (2012). Kindlin-3 mediates integrin αLβ2 outside-in signaling, and it interacts with scaffold protein receptor for activated-C kinase 1 (RACK1). J Biol Chem *287*, 10714-10726.

Fomenkov, A., Zangen, R., Huang, Y.P., Osada, M., Guo, Z., Fomenkov, T., Trink, B., Sidransky, D., and Ratovitski, E.A. (2004). RACK1 and stratifin target ΔNp63α for a

proteasome degradation in head and neck squamous cell carcinoma cells upon DNA damage. Cell Cycle *3*, 1285-1295.

Funakoshi, M., Sasaki, T., Nishimoto, T., and Kobayashi, H. (2002). Budding yeast Dsk2p is a polyubiquitin-binding protein that can interact with the proteasome. Proc Natl Acad Sci U S A *99*, 745-750.

Galibert, L., Tometsko, M.E., Anderson, D.M., Cosman, D., and Dougall, W.C. (1998). The involvement of multiple tumor necrosis factor receptor (TNFR)-associated factors in the signaling mechanisms of receptor activator of NF-κB, a member of the TNFR superfamily. J Biol Chem *273*, 34120-34127.

Gallina, A., Rossi, F., and Milanesi, G. (2001). Rack1 binds HIV-1 Nef and can act as a Nef-protein kinase C adaptor. Virology *283*, 7-18.

Gandin, V., Gutierrez, G.J., Brill, L.M., Varsano, T., Feng, Y., Aza-Blanc, P., Au, Q., McLaughlan, S., Ferreira, T.A., Alain, T., *et al.* (2013a). Degradation of newly synthesized polypeptides by ribosome-associated RACK1/c-Jun N-terminal kinase/eukaryotic elongation factor 1A2 complex. Mol Cell Biol *33*, 2510-2526.

Gandin, V., Senft, D., Topisirovic, I., and Ronai, Z.A. (2013b). RACK1 Function in Cell Motility and Protein Synthesis. Genes Cancer *4*, 369-377.

Ganot, P., Caizergues-Ferrer, M., and Kiss, T. (1997). The family of box ACA small nucleolar RNAs is defined by an evolutionarily conserved secondary structure and ubiquitous sequence elements essential for RNA accumulation. Genes Dev *11*, 941-956.

Gautschi, M., Mun, A., Ross, S., and Rospert, S. (2002). A functional chaperone triad on the yeast ribosome. Proc Natl Acad Sci U S A *99*, 4209-4214.

Gavin, A.C., Bösche, M., Krause, R., Grandi, P., Marzioch, M., Bauer, A., Schultz, J., Rick, J.M., Michon, A.M., Cruciat, C.M., *et al.* (2002). Functional organization of the yeast proteome by systematic analysis of protein complexes. Nature *415*, 141-147.

Gelin-Licht, R., Paliwal, S., Conlon, P., Levchenko, A., and Gerst, J.E. (2012). Scp160-dependent mRNA trafficking mediates pheromone gradient sensing and chemotropism in yeast. Cell Rep *1*, 483-494.

George, R., Walsh, P., Beddoe, T., and Lithgow, T. (2002). The nascent polypeptide-associated complex (NAC) promotes interaction of ribosomes with the mitochondrial surface *in vivo*. FEBS Lett *516*, 213-216.

Gerbasi, V.R., Weaver, C.M., Hill, S., Friedman, D.B., and Link, A.J. (2004). Yeast Asc1p and mammalian RACK1 are functionally orthologous core 40S ribosomal proteins that repress gene expression. Mol Cell Biol *24*, 8276-8287.

Gnad, F., de Godoy, L.M., Cox, J., Neuhauser, N., Ren, S., Olsen, J.V., and Mann, M. (2009). High-accuracy identification and bioinformatic analysis of *in vivo* protein phosphorylation sites in yeast. Proteomics *9*, 4642-4652.

Goode, B.L., Eskin, J.A., and Wendland, B. (2015). Actin and endocytosis in budding yeast. Genetics *199*, 315-358.

Goode, B.L., Rodal, A.A., Barnes, G., and Drubin, D.G. (2001). Activation of the Arp2/3 complex by the actin filament binding protein Abp1p. J Cell Biol *153*, 627-634.

Gould, C.J., Chesarone-Cataldo, M., Alioto, S.L., Salin, B., Sagot, I., and Goode, B.L. (2014). *Saccharomyces cerevisiae* Kelch proteins and Bud14 protein form a stable 520-kDa formin regulatory complex that controls actin cable assembly and cell morphogenesis. J Biol Chem *289*, 18290-18301.

Grosso, S., Volta, V., Sala, L.A., Vietri, M., Marchisio, P.C., Ron, D., and Biffo, S. (2008). PKCβII modulates translation independently from mTOR and through RACK1. Biochem J *415*, 77-85.

Gu, W., Deng, Y., Zenklusen, D., and Singer, R.H. (2004). A new yeast PUF family protein, Puf6p, represses *ASH1* mRNA translation and is required for its localization. Genes Dev *18*, 1452-1465.

Gueldener, U., Heinisch, J., Koehler, G.J., Voss, D., and Hegemann, J.H. (2002). A second set of *loxP* marker cassettes for Cre-mediated multiple gene knockouts in budding yeast. Nucleic Acids Res *30*, e23.

Guo, J., and Chen, J.G. (2008). RACK1 genes regulate plant development with unequal genetic redundancy in *Arabidopsis*. BMC Plant Biol *8*, 108.

Guo, J., Wang, J., Xi, L., Huang, W.D., Liang, J., and Chen, J.G. (2009). RACK1 is a negative regulator of ABA responses in *Arabidopsis*. J Exp Bot *60*, 3819-3833.

Guo, J., Wang, S., Valerius, O., Hall, H., Zeng, Q., Li, J.F., Weston, D.J., Ellis, B.E., and Chen, J.G. (2011). Involvement of *Arabidopsis* RACK1 in protein translation and its regulation by abscisic acid. Plant Physiol *155*, 370-383.

Guo, M., Aston, C., Burchett, S.A., Dyke, C., Fields, S., Rajarao, S.J., Uetz, P., Wang, Y., Young, K., and Dohlman, H.G. (2003). The yeast G protein α subunit Gpa1 transmits a signal through an RNA binding effector protein Scp160. Mol Cell *12*, 517-524.

Guo, Y., Wang, W., Wang, J., Feng, J., Wang, Q., Jin, J., Lv, M., Li, X., Li, Y., Ma, Y., *et al.* (2013). Receptor for activated C kinase 1 promotes hepatocellular carcinoma growth by enhancing mitogen-activated protein kinase kinase 7 activity. Hepatology *57*, 140-151.

Hardcastle, T.J., and Kelly, K.A. (2010). baySeq: empirical Bayesian methods for identifying differential expression in sequence count data. BMC Bioinformatics *11*, 422.

Hartzog, G.A., Wada, T., Handa, H., and Winston, F. (1998). Evidence that Spt4, Spt5, and Spt6 control transcription elongation by RNA polymerase II in *Saccharomyces cerevisiae*. Genes Dev *12*, 357-369.

He, D.Y., Neasta, J., and Ron, D. (2010). Epigenetic regulation of *BDNF* expression via the scaffolding protein RACK1. J Biol Chem *285*, 19043-19050.

Helser, T.L., Baan, R.A., and Dahlberg, A.E. (1981). Characterization of a 40S ribosomal subunit complex in polyribosomes of *Saccharomyces cerevisiae* treated with cycloheximide. Mol Cell Biol *1*, 51-57.

Henriksen, P., Wagner, S.A., Weinert, B.T., Sharma, S., Bacinskaja, G., Rehman, M., Juffer, A.H., Walther, T.C., Lisby, M., and Choudhary, C. (2012). Proteome-wide analysis of lysine acetylation suggests its broad regulatory scope in *Saccharomyces cerevisiae*. Mol Cell Proteomics *11*, 1510-1522.

Hermanto, U., Zong, C.S., Li, W., and Wang, L.H. (2002). RACK1, an insulin-like growth factor I (IGF-I) receptor-interacting protein, modulates IGF-I-dependent integrin signaling and promotes cell spreading and contact with extracellular matrix. Mol Cell Biol *22*, 2345-2365.

Heym, R.G., and Niessing, D. (2012). Principles of mRNA transport in yeast. Cell Mol Life Sci *69*, 1843-1853.

Hoffman, C.S., and Winston, F. (1987). A ten-minute DNA preparation from yeast efficiently releases autonomous plasmids for transformation of *Escherichia coli*. Gene *57*, 267-272.

Hoffmann, B., Wanke, C., Lapaglia, S.K., and Braus, G.H. (2000). c-Jun and RACK1 homologues regulate a control point for sexual development in *Aspergillus nidulans*. Mol Microbiol *37*, 28-41.

Holt, L.J., Tuch, B.B., Villen, J., Johnson, A.D., Gygi, S.P., and Morgan, D.O. (2009). Global analysis of Cdk1 substrate phosphorylation sites provides insights into evolution. Science *325*, 1682-1686.

Horton, L.E., James, P., Craig, E.A., and Hensold, J.O. (2001). The yeast hsp70 homologue Ssa is required for translation and interacts with Sis1 and Pab1 on translating ribosomes. J Biol Chem *276*, 14426-14433.

Hotokezaka, Y., Tobben, U., Hotokezaka, H., Van Leyen, K., Beatrix, B., Smith, D.H., Nakamura, T., and Wiedmann, M. (2002). Interaction of the eukaryotic elongation factor 1A with newly synthesized polypeptides. J Biol Chem *277*, 18545-18551.

Huang da, W., Sherman, B.T., and Lempicki, R.A. (2009a). Bioinformatics enrichment tools: paths toward the comprehensive functional analysis of large gene lists. Nucleic Acids Res *37*, 1-13.

Huang da, W., Sherman, B.T., and Lempicki, R.A. (2009b). Systematic and integrative analysis of large gene lists using DAVID bioinformatics resources. Nat Protoc *4*, 44-57.

Huang, G., Wang, H., Chou, S., Nie, X., Chen, J., and Liu, H. (2006). Bistable expression of *WOR1*, a master regulator of white-opaque switching in *Candida albicans*. Proc Natl Acad Sci U S A *103*, 12813-12818.

Hunter, T., and Plowman, G.D. (1997). The protein kinases of budding yeast: six score and more. Trends Biochem Sci *22*, 18-22.

Inada, T. (2013). Quality control systems for aberrant mRNAs induced by aberrant translation elongation and termination. Biochim Biophys Acta *1829*, 634-642.

Inada, T., Winstall, E., Tarun, S.Z., Jr., Yates, J.R., 3rd, Schieltz, D., and Sachs, A.B. (2002). One-step affinity purification of the yeast ribosome and its associated proteins and mRNAs. RNA *8*, 948-958.

Inoue, H., Nojima, H., and Okayama, H. (1990). High efficiency transformation of *Escherichia coli* with plasmids. Gene *96*, 23-28.

Irie, K., Tadauchi, T., Takizawa, P.A., Vale, R.D., Matsumoto, K., and Herskowitz, I. (2002). The Khd1 protein, which has three KH RNA-binding motifs, is required for proper localization of *ASH1* mRNA in yeast. EMBO J *21*, 1158-1167.

Ishida, S., Takahashi, Y., and Nagata, T. (1993). Isolation of cDNA of an auxin-regulated gene encoding a G protein β subunit-like protein from tobacco BY-2 cells. Proc Natl Acad Sci U S A *90*, 11152-11156.

Ito, H., Fukuda, Y., Murata, K., and Kimura, A. (1983). Transformation of intact yeast cells treated with alkali cations. J Bacteriol *153*, 163-168.

Ivan, M., Kondo, K., Yang, H., Kim, W., Valiando, J., Ohh, M., Salic, A., Asara, J.M., Lane, W.S., and Kaelin, W.G., Jr. (2001). HIFα targeted for VHL-mediated destruction by proline hydroxylation: implications for O_2 sensing. Science *292*, 464-468.

Iyer, N.V., Kotch, L.E., Agani, F., Leung, S.W., Laughner, E., Wenger, R.H., Gassmann, M., Gearhart, J.D., Lawler, A.M., Yu, A.Y., *et al.* (1998). Cellular and developmental control of O2 homeostasis by hypoxia-inducible factor 1 α. Genes Dev *12*, 149-162.

Jaakkola, P., Mole, D.R., Tian, Y.M., Wilson, M.I., Gielbert, J., Gaskell, S.J., von Kriegsheim, A., Hebestreit, H.F., Mukherji, M., Schofield, C.J., *et al.* (2001). Targeting of HIF-α to the von Hippel-Lindau ubiquitylation complex by O_2-regulated prolyl hydroxylation. Science *292*, 468-472.

Janke, C., Magiera, M.M., Rathfelder, N., Taxis, C., Reber, S., Maekawa, H., Moreno-Borchart, A., Doenges, G., Schwob, E., Schiebel, E., *et al.* (2004). A versatile toolbox for PCR-based tagging of yeast genes: new fluorescent proteins, more markers and promoter substitution cassettes. Yeast *21*, 947-962.

Jannot, G., Bajan, S., Giguère, N.J., Bouasker, S., Banville, I.H., Piquet, S., Hutvagner, G., and Simard, M.J. (2011). The ribosomal protein RACK1 is required for microRNA function in both *C. elegans* and humans. EMBO Rep *12*, 581-586.

Jansen, J.M., Wanless, A.G., Seidel, C.W., and Weiss, E.L. (2009). Cbk1 regulation of the RNA-binding protein Ssd1 integrates cell fate with translational control. Curr Biol *19*, 2114-2120.

Jansen, R.P., Dowzer, C., Michaelis, C., Galova, M., and Nasmyth, K. (1996). Mother cell-specific HO expression in budding yeast depends on the unconventional myosin myo4p and other cytoplasmic proteins. Cell *84*, 687-697.

Jeong, H.T., Oowatari, Y., Abe, M., Tanaka, K., Matsuda, H., and Kawamukai, M. (2004). Interaction between a negative regulator (Msa2/Nrd1) and a positive regulator (Cpc2) of sexual differentiation in *Schizosaccharomyces pombe*. Biosci Biotechnol Biochem *68*, 1621-1626.

Kadrmas, J.L., Smith, M.A., Pronovost, S.M., and Beckerle, M.C. (2007). Characterization of RACK1 function in *Drosophila* development. Dev Dyn *236*, 2207-2215.

Kang, D., Gho, S., Suh, M., and Kang, C. (2002). Highly Sensitive and Fast Protein Detection with Coomassie Brilliant Blue in Sodium Dodecyl Sulfate-Polyacrylamide Gel Electrophoresis. Bull Korean Chem Soc *11*, 1511–1512.

Kanshin, E., Michnick, S.W., and Thibault, P. (2013). Displacement of N/Q-rich peptides on TiO_2 beads enhances the depth and coverage of yeast phosphoproteome analyses. J Proteome Res *12*, 2905-2913.

Kiely, P.A., Baillie, G.S., Barrett, R., Buckley, D.A., Adams, D.R., Houslay, M.D., and O'Connor, R. (2009). Phosphorylation of RACK1 on tyrosine 52 by c-Abl is required for insulin-like growth factor I-mediated regulation of focal adhesion kinase. J Biol Chem *284*, 20263-20274.

Kiely, P.A., Leahy, M., O'Gorman, D., and O'Connor, R. (2005). RACK1-mediated integration of adhesion and insulin-like growth factor I (IGF-I) signaling and cell migration are defective in cells expressing an IGF-I receptor mutated at tyrosines 1250 and 1251. J Biol Chem *280*, 7624-7633.

Kiely, P.A., O'Gorman, D., Luong, K., Ron, D., and O'Connor, R. (2006). Insulin-like growth factor I controls a mutually exclusive association of RACK1 with protein phosphatase 2A and β1 integrin to promote cell migration. Mol Cell Biol *26*, 4041-4051.

Kim, S.W., Joo, Y.J., and Kim, J. (2010). Asc1p, a ribosomal protein, plays a pivotal role in cellular adhesion and virulence in *Candida albicans*. J Microbiol *48*, 842-848.

Kiss-László, Z., Henry, Y., Bachellerie, J.P., Caizergues-Ferrer, M., and Kiss, T. (1996). Site-specific ribose methylation of preribosomal RNA: a novel function for small nucleolar RNAs. Cell *85*, 1077-1088.

Kleinschmidt, M., Schulz, R., and Braus, G.H. (2006). The yeast *CPC2/ASC1* gene is regulated by the transcription factors Fhl1p and Ifh1p. Curr Genet *49*, 218-228.

Knaus, M., Cameroni, E., Pedruzzi, I., Tatchell, K., De Virgilio, C., and Peter, M. (2005). The Bud14p-Glc7p complex functions as a cortical regulator of dynein in budding yeast. EMBO J *24*, 3000-3011.

Kong, Q., Wang, L., Liu, Z., Kwon, N.J., Kim, S.C., and Yu, J.H. (2013). Gβ-like CpcB plays a crucial role for growth and development of *Aspergillus nidulans* and *Aspergillus fumigatus*. PLoS One *8*, e70355.

Kouba, T., Rutkai, E., Karásková, M., and Valášek, L. (2012). The eIF3c/NIP1 PCI domain interacts with RNA and RACK1/ASC1 and promotes assembly of translation preinitiation complexes. Nucleic Acids Res *40*, 2683-2699.

Kuroha, K., Akamatsu, M., Dimitrova, L., Ito, T., Kato, Y., Shirahige, K., and Inada, T. (2010). Receptor for activated C kinase 1 stimulates nascent polypeptide-dependent translation arrest. EMBO Rep *11*, 956-961.

Laemmli, U.K. (1970). Cleavage of structural proteins during the assembly of the head of bacteriophage T4. Nature *227*, 680-685.

Langmead, B., and Salzberg, S.L. (2012). Fast gapped-read alignment with Bowtie 2. Nat Methods *9*, 357-359.

Lee, C.D., and Tu, B.P. (2015). Glucose-Regulated Phosphorylation of the PUF Protein Puf3 Regulates the Translational Fate of Its Bound mRNAs and Association with RNA Granules. Cell Rep *11*, 1638-1650.

Lenssen, E., James, N., Pedruzzi, I., Dubouloz, F., Cameroni, E., Bisig, R., Maillet, L., Werner, M., Roosen, J., Petrovic, K., *et al.* (2005). The Ccr4-Not complex independently controls both Msn2-dependent transcriptional activation--via a newly identified Glc7/Bud14 type I protein phosphatase module--and TFIID promoter distribution. Mol Cell Biol *25*, 488-498.

Letzring, D.P., Dean, K.M., and Grayhack, E.J. (2010). Control of translation efficiency in yeast by codon-anticodon interactions. RNA *16*, 2516-2528.

Letzring, D.P., Wolf, A.S., Brule, C.E., and Grayhack, E.J. (2013). Translation of CGA codon repeats in yeast involves quality control components and ribosomal protein L1. RNA *19*, 1208-1217.

Li, D., and Roberts, R. (2001). WD-repeat proteins: structure characteristics, biological function, and their involvement in human diseases. Cell Mol Life Sci *58*, 2085-2097.

Li, J.J., and Xie, D. (2015). RACK1, a versatile hub in cancer. Oncogene *34*, 1890-1898.

Li, S., Esterberg, R., Lachance, V., Ren, D., Radde-Gallwitz, K., Chi, F., Parent, J.L., Fritz, A., and Chen, P. (2011). Rack1 is required for Vangl2 membrane localization and planar cell polarity signaling while attenuating canonical Wnt activity. Proc Natl Acad Sci U S A *108*, 2264-2269.

Liebman, S.W., and Chernoff, Y.O. (2012). Prions in yeast. Genetics *191*, 1041-1072.

Liedtke, C.M., Yun, C.H., Kyle, N., and Wang, D. (2002). Protein kinase C ε-dependent regulation of cystic fibrosis transmembrane regulator involves binding to a receptor for activated C kinase (RACK1) and RACK1 binding to Na^+/H^+ exchange regulatory factor. J Biol Chem *277*, 22925-22933.

Lin, J., Lee, D., Choi, Y., and Lee, S.Y. (2015). The scaffold protein RACK1 mediates the RANKL-dependent activation of p38 MAPK in osteoclast precursors. Sci Signal *8*, ra54.

Lindstrom, D.L., Squazzo, S.L., Muster, N., Burckin, T.A., Wachter, K.C., Emigh, C.A., McCleery, J.A., Yates, J.R., 3rd, and Hartzog, G.A. (2003). Dual roles for Spt5 in pre-mRNA processing and transcription elongation revealed by identification of Spt5-associated proteins. Mol Cell Biol *23*, 1368-1378.

Link, A.J., Eng, J., Schieltz, D.M., Carmack, E., Mize, G.J., Morris, D.R., Garvik, B.M., and Yates, J.R., 3rd (1999). Direct analysis of protein complexes using mass spectrometry. Nat Biotechnol *17*, 676-682.

Liu, L., Zeng, M., Hausladen, A., Heitman, J., and Stamler, J.S. (2000). Protection from nitrosative stress by yeast flavohemoglobin. Proc Natl Acad Sci U S A *97*, 4672-4676.

Liu, X., Nie, X., Ding, Y., and Chen, J. (2010). Asc1, a WD-repeat protein, is required for hyphal development and virulence in *Candida albicans*. Acta Biochim Biophys Sin (Shanghai) *42*, 793-800.

Liu, Y., Warfield, L., Zhang, C., Luo, J., Allen, J., Lang, W.H., Ranish, J., Shokat, K.M., and Hahn, S. (2009). Phosphorylation of the transcription elongation factor Spt5 by yeast Bur1 kinase stimulates recruitment of the PAF complex. Mol Cell Biol *29*, 4852-4863.

Liu, Y.V., Baek, J.H., Zhang, H., Diez, R., Cole, R.N., and Semenza, G.L. (2007a). RACK1 competes with HSP90 for binding to HIF-1α and is required for O_2-independent and HSP90 inhibitor-induced degradation of HIF-1α. Mol Cell *25*, 207-217.

Liu, Y.V., Hubbi, M.E., Pan, F., McDonald, K.R., Mansharamani, M., Cole, R.N., Liu, J.O., and Semenza, G.L. (2007b). Calcineurin promotes hypoxia-inducible factor 1α expression by dephosphorylating RACK1 and blocking RACK1 dimerization. J Biol Chem *282*, 37064-37073.

Loewith, R., Jacinto, E., Wullschleger, S., Lorberg, A., Crespo, J.L., Bonenfant, D., Oppliger, W., Jenoe, P., and Hall, M.N. (2002). Two TOR complexes, only one of which is rapamycin sensitive, have distinct roles in cell growth control. Mol Cell *10*, 457-468.

Lohse, M.B., Zordan, R.E., Cain, C.W., and Johnson, A.D. (2010). Distinct class of DNA-binding domains is exemplified by a master regulator of phenotypic switching in *Candida albicans*. Proc Natl Acad Sci U S A *107*, 14105-14110.

López-Bergami, P., Habelhah, H., Bhoumik, A., Zhang, W., Wang, L.H., and Ronai, Z. (2005). RACK1 mediates activation of JNK by protein kinase C [corrected]. Mol Cell *19*, 309-320.

Loreni, F., Iadevaia, V., Tino, E., Caldarola, S., and Amaldi, F. (2005). RACK1 mRNA translation is regulated via a rapamycin-sensitive pathway and coordinated with ribosomal protein synthesis. FEBS Lett *579*, 5517-5520.

Lu, J., and Deutsch, C. (2008). Electrostatics in the ribosomal tunnel modulate chain elongation rates. J Mol Biol *384*, 73-86.

Lu, K., Psakhye, I., and Jentsch, S. (2014). Autophagic clearance of polyQ proteins mediated by ubiquitin-Atg8 adaptors of the conserved CUET protein family. Cell *158*, 549-563.

Majzoub, K., Hafirassou, M.L., Meignin, C., Goto, A., Marzi, S., Fedorova, A., Verdier, Y., Vinh, J., Hoffmann, J.A., Martin, F., *et al.* (2014). RACK1 controls IRES-mediated translation of viruses. Cell *159*, 1086-1095.

Mamidipudi, V., Zhang, J., Lee, K.C., and Cartwright, C.A. (2004). RACK1 regulates G_1/S progression by suppressing Src kinase activity. Mol Cell Biol *24*, 6788-6798.

Manogaran, A.L., Hong, J.Y., Hufana, J., Tyedmers, J., Lindquist, S., and Liebman, S.W. (2011). Prion formation and polyglutamine aggregation are controlled by two classes of genes. PLoS Genet *7*, e1001386.

Mašek, T., Valášek, L., and Pospišek, M. (2011). Polysome analysis and RNA purification from sucrose gradients. Methods Mol Biol *703*, 293-309.

Matsuda, R., Ikeuchi, K., Nomura, S., and Inada, T. (2014). Protein quality control systems associated with no-go and nonstop mRNA surveillance in yeast. Genes Cells *19*, 1-12.

Mazanek, M., Mituloviae, G., Herzog, F., Stingl, C., Hutchins, J.R., Peters, J.M., and Mechtler, K. (2007). Titanium dioxide as a chemo-affinity solid phase in offline phosphopeptide chromatography prior to HPLC-MS/MS analysis. Nat Protoc *2*, 1059-1069.

McLeod, M., Shor, B., Caporaso, A., Wang, W., Chen, H., and Hu, L. (2000). Cpc2, a fission yeast homologue of mammalian RACK1 protein, interacts with Ran1 (Pat1) kinase To regulate cell cycle progression and meiotic development. Mol Cell Biol *20*, 4016-4027.

Melamed, D., Bar-Ziv, L., Truzman, Y., and Arava, Y. (2010). Asc1 supports cell-wall integrity near bud sites by a Pkc1 independent mechanism. PLoS One *5*, e11389.

Michelot, A., Grassart, A., Okreglak, V., Costanzo, M., Boone, C., and Drubin, D.G. (2013). Actin filament elongation in Arp2/3-derived networks is controlled by three distinct mechanisms. Dev Cell *24*, 182-195.

Mizukami, J., Takaesu, G., Akatsuka, H., Sakurai, H., Ninomiya-Tsuji, J., Matsumoto, K., and Sakurai, N. (2002). Receptor activator of NF-κB ligand (RANKL) activates TAK1 mitogen-activated protein kinase kinase kinase through a signaling complex containing RANK, TAB2, and TRAF6. Mol Cell Biol *22*, 992-1000.

Mok, J., Kim, P.M., Lam, H.Y., Piccirillo, S., Zhou, X., Jeschke, G.R., Sheridan, D.L., Parker, S.A., Desai, V., Jwa, M., *et al.* (2011). Deciphering protein kinase specificity through large-scale analysis of yeast phosphorylation site motifs. Sci Signal *3*, ra12.

Müller, M., Kötter, P., Behrendt, C., Walter, E., Scheckhuber, C.Q., Entian, K.D., and Reichert, A.S. (2015). Synthetic quantitative array technology identifies the Ubp3-Bre5 deubiquitinase complex as a negative regulator of mitophagy. Cell Rep *10*, 1215-1225.

Mumberg, D., Müller, R., and Funk, M. (1994). Regulatable promoters of *Saccharomyces cerevisiae*: comparison of transcriptional activity and their use for heterologous expression. Nucleic Acids Res *22*, 5767-5768.

Murzin, A.G. (1992). Structural principles for the propeller assembly of β-sheets: the preference for seven-fold symmetry. Proteins *14*, 191-201.

Musti, A.M., Treier, M., and Bohmann, D. (1997). Reduced ubiquitin-dependent degradation of c-Jun after phosphorylation by MAP kinases. Science *275*, 400-402.

Nakashima, A., Chen, L., Thao, N.P., Fujiwara, M., Wong, H.L., Kuwano, M., Umemura, K., Shirasu, K., Kawasaki, T., and Shimamoto, K. (2008). RACK1 functions in rice innate immunity by interacting with the Rac1 immune complex. Plant Cell *20*, 2265-2279.

Neasta, J., Kiely, P.A., He, D.Y., Adams, D.R., O'Connor, R., and Ron, D. (2012). Direct interaction between scaffolding proteins RACK1 and 14-3-3ζ regulates brain-derived neurotrophic factor (BDNF) transcription. J Biol Chem *287*, 322-336.

Ni, J., Tien, A.L., and Fournier, M.J. (1997). Small nucleolar RNAs direct site-specific synthesis of pseudouridine in ribosomal RNA. Cell *89*, 565-573.

Nilsson, J., Sengupta, J., Frank, J., and Nissen, P. (2004). Regulation of eukaryotic translation by the RACK1 protein: a platform for signalling molecules on the ribosome. EMBO Rep *5*, 1137-1141.

Nuñez, A., Franco, A., Madrid, M., Soto, T., Vicente, J., Gacto, M., and Cansado, J. (2009). Role for RACK1 orthologue Cpc2 in the modulation of stress response in fission yeast. Mol Biol Cell *20*, 3996-4009.

Nuñez, A., Franco, A., Soto, T., Vicente, J., Gacto, M., and Cansado, J. (2010). Fission yeast receptor of activated C kinase (RACK1) ortholog Cpc2 regulates mitotic commitment through Wee1 kinase. J Biol Chem *285*, 41366-41373.

Ogur, M., St. John, R., and Nagai, S. (1957). Tetrazolium overlay technique for population studies of respiration deficiency in yeast. Science *125*, 928-929.

Olivas, W., and Parker, R. (2000). The Puf3 protein is a transcript-specific regulator of mRNA degradation in yeast. EMBO J *19*, 6602-6611.

Olsen, J.V., Blagoev, B., Gnad, F., Macek, B., Kumar, C., Mortensen, P., and Mann, M. (2006). Global, *in vivo*, and site-specific phosphorylation dynamics in signaling networks. Cell *127*, 635-648.

Olsen, J.V., and Mann, M. (2004). Improved peptide identification in proteomics by two consecutive stages of mass spectrometric fragmentation. Proc Natl Acad Sci U S A *101*, 13417-13422.

Otsuka, M., Takata, A., Yoshikawa, T., Kojima, K., Kishikawa, T., Shibata, C., Takekawa, M., Yoshida, H., Omata, M., and Koike, K. (2011). Receptor for activated protein kinase C: requirement for efficient microRNA function and reduced expression in hepatocellular carcinoma. PLoS One *6*, e24359.

Palmer, D.A., Thompson, J.K., Li, L., Prat, A., and Wang, P. (2006). Gib2, a novel Gβ-like/RACK1 homolog, functions as a Gβ subunit in cAMP signaling and is essential in *Cryptococcus neoformans*. J Biol Chem *281*, 32596-32605.

Papavassiliou, A.G., Treier, M., and Bohmann, D. (1995). Intramolecular signal transduction in c-Jun. EMBO J *14*, 2014-2019.

Paquin, N., Ménade, M., Poirier, G., Donato, D., Drouet, E., and Chartrand, P. (2007). Local activation of yeast *ASH1* mRNA translation through phosphorylation of Khd1p by the casein kinase Yck1p. Mol Cell *26*, 795-809.

Parsons, A.B., Brost, R.L., Ding, H., Li, Z., Zhang, C., Sheikh, B., Brown, G.W., Kane, P.M., Hughes, T.R., and Boone, C. (2004). Integration of chemical-genetic and genetic interaction data links bioactive compounds to cellular target pathways. Nat Biotechnol *22*, 62-69.

Qu, L.H., Henry, Y., Nicoloso, M., Michot, B., Azum, M.C., Renalier, M.H., Caizergues-Ferrer, M., and Bachellerie, J.P. (1995). U24, a novel intron-encoded small nucleolar RNA with two 12 nt long, phylogenetically conserved complementarities to 28S rRNA. Nucleic Acids Res *23*, 2669-2676.

Rabl, J., Leibundgut, M., Ataide, S.F., Haag, A., and Ban, N. (2011). Crystal structure of the eukaryotic 40S ribosomal subunit in complex with initiation factor 1. Science *331*, 730-736.

Rachfall, N., Schmitt, K., Bandau, S., Smolinski, N., Ehrenreich, A., Valerius, O., and Braus, G.H. (2013). RACK1/Asc1p, a ribosomal node in cellular signaling. Mol Cell Proteomics *12*, 87-105.

Radi, R. (2004). Nitric oxide, oxidants, and protein tyrosine nitration. Proc Natl Acad Sci U S A *101*, 4003-4008.

Rappsilber, J., Ishihama, Y., and Mann, M. (2003). Stop and go extraction tips for matrix-assisted laser desorption/ionization, nanoelectrospray, and LC/MS sample pretreatment in proteomics. Anal Chem *75*, 663-670.

Rappsilber, J., Mann, M., and Ishihama, Y. (2007). Protocol for micro-purification, enrichment, pre-fractionation and storage of peptides for proteomics using StageTips. Nat Protoc *2*, 1896-1906.

Regmi, S., Rothberg, K.G., Hubbard, J.G., and Ruben, L. (2008). The RACK1 signal anchor protein from *Trypanosoma brucei* associates with eukaryotic elongation factor 1A: a role for translational control in cytokinesis. Mol Microbiol *70*, 724-745.

Rivero-Gutiérrez, B., Anzola, A., Martínez-Augustin, O., and de Medina, F.S. (2014). Stain-free detection as loading control alternative to Ponceau and housekeeping protein immunodetection in Western blotting. Anal Biochem *467*, 1-3.

Robles, M.S., Boyault, C., Knutti, D., Padmanabhan, K., and Weitz, C.J. (2010). Identification of RACK1 and protein kinase Cα as integral components of the mammalian circadian clock. Science *327*, 463-466.

Ron, D., Chen, C.H., Caldwell, J., Jamieson, L., Orr, E., and Mochly-Rosen, D. (1994). Cloning of an intracellular receptor for protein kinase C: a homolog of the β subunit of G proteins. Proc Natl Acad Sci U S A *91*, 839-843.

Ron, D., Jiang, Z., Yao, L., Vagts, A., Diamond, I., and Gordon, A. (1999). Coordinated movement of RACK1 with activated βIIPKC. J Biol Chem *274*, 27039-27046.

Ron, D., Luo, J., and Mochly-Rosen, D. (1995). C2 region-derived peptides inhibit translocation and function of β protein kinase C *in vivo*. J Biol Chem *270*, 24180-24187.

Ron, D., and Mochly-Rosen, D. (1994). Agonists and antagonists of protein kinase C function, derived from its binding proteins. J Biol Chem *269*, 21395-21398.

Rotenberg, M.O., Moritz, M., and Woolford, J.L., Jr. (1988). Depletion of *Saccharomyces cerevisiae* ribosomal protein L16 causes a decrease in 60S ribosomal subunits and formation of half-mer polyribosomes. Genes Dev *2*, 160-172.

Ruan, Y., Sun, L., Hao, Y., Wang, L., Xu, J., Zhang, W., Xie, J., Guo, L., Zhou, L., Yun, X., *et al.* (2012). Ribosomal RACK1 promotes chemoresistance and growth in human hepatocellular carcinoma. J Clin Invest *122*, 2554-2566.

Rubinfeld, H., and Seger, R. (2005). The ERK cascade: a prototype of MAPK signaling. Mol Biotechnol *31*, 151-174.

Ruiz Carrillo, D., Chandrasekaran, R., Nilsson, M., Cornvik, T., Liew, C.W., Tan, S.M., and Lescar, J. (2012). Structure of human Rack1 protein at a resolution of 2.45 A. Acta Crystallogr Sect F Struct Biol Cryst Commun *68*, 867-872.

Saiki, R.K., Scharf, S., Faloona, F., Mullis, K.B., Horn, G.T., Erlich, H.A., and Arnheim, N. (1985). Enzymatic amplification of β-globin genomic sequences and restriction site analysis for diagnosis of sickle cell anemia. Science *230*, 1350-1354.

Saint-Georges, Y., Garcia, M., Delaveau, T., Jourdren, L., Le Crom, S., Lemoine, S., Tanty, V., Devaux, F., and Jacq, C. (2008). Yeast mitochondrial biogenesis: a role for the PUF RNA-binding protein Puf3p in mRNA localization. PLoS One *3*, e2293.

Satoh, R., Morita, T., Takada, H., Kita, A., Ishiwata, S., Doi, A., Hagihara, K., Taga, A., Matsumura, Y., Tohda, H., *et al.* (2009). Role of the RNA-binding protein Nrd1 and Pmk1 mitogen-activated protein kinase in the regulation of myosin mRNA stability in fission yeast. Mol Biol Cell *20*, 2473-2485.

Schneider, D.A., French, S.L., Osheim, Y.N., Bailey, A.O., Vu, L., Dodd, J., Yates, J.R., Beyer, A.L., and Nomura, M. (2006). RNA polymerase II elongation factors Spt4p and Spt5p play roles in transcription elongation by RNA polymerase I and rRNA processing. Proc Natl Acad Sci U S A *103*, 12707-12712.

Schwartz, D., and Gygi, S.P. (2005). An iterative statistical approach to the identification of protein phosphorylation motifs from large-scale data sets. Nat Biotechnol *23*, 1391-1398.

Semenza, G.L. (2013). HIF-1 mediates metabolic responses to intratumoral hypoxia and oncogenic mutations. J Clin Invest *123*, 3664-3671.

Semenza, G.L., Roth, P.H., Fang, H.M., and Wang, G.L. (1994). Transcriptional regulation of genes encoding glycolytic enzymes by hypoxia-inducible factor 1. J Biol Chem *269*, 23757-23763.

Sengupta, J., Nilsson, J., Gursky, R., Spahn, C.M., Nissen, P., and Frank, J. (2004). Identification of the versatile scaffold protein RACK1 on the eukaryotic ribosome by cryo-EM. Nat Struct Mol Biol *11*, 957-962.

Sezen, B., Seedorf, M., and Schiebel, E. (2009). The SESA network links duplication of the yeast centrosome with the protein translation machinery. Genes Dev *23*, 1559-1570.

Sha, Z., Brill, L.M., Cabrera, R., Kleifeld, O., Scheliga, J.S., Glickman, M.H., Chang, E.C., and Wolf, D.A. (2009). The eIF3 interactome reveals the translasome, a supercomplex linking protein synthesis and degradation machineries. Mol Cell *36*, 141-152.

Shen, Z., St-Denis, A., and Chartrand, P. (2010). Cotranscriptional recruitment of She2p by RNA pol II elongation factor Spt4-Spt5/DSIF promotes mRNA localization to the yeast bud. Genes Dev *24*, 1914-1926.

Shevchenko, A., Wilm, M., Vorm, O., and Mann, M. (1996). Mass spectrometric sequencing of proteins silver-stained polyacrylamide gels. Anal Chem *68*, 850-858.

Shih, S.C., Prag, G., Francis, S.A., Sutanto, M.A., Hurley, J.H., and Hicke, L. (2003). A ubiquitin-binding motif required for intramolecular monoubiquitylation, the CUE domain. EMBO J *22*, 1273-1281.

Sil, A., and Herskowitz, I. (1996). Identification of asymmetrically localized determinant, Ash1p, required for lineage-specific transcription of the yeast *HO* gene. Cell *84*, 711-722.

Smolka, M.B., Albuquerque, C.P., Chen, S.H., and Zhou, H. (2007). Proteome-wide identification of *in vivo* targets of DNA damage checkpoint kinases. Proc Natl Acad Sci U S A *104*, 10364-10369.

Southern, E.M. (1975). Detection of specific sequences among DNA fragments separated by gel electrophoresis. J Mol Biol *98*, 503-517.

Speth, C., Willing, E.M., Rausch, S., Schneeberger, K., and Laubinger, S. (2013). RACK1 scaffold proteins influence miRNA abundance in *Arabidopsis*. Plant J *76*, 433-445.

Stark, C., Breitkreutz, B.J., Reguly, T., Boucher, L., Breitkreutz, A., and Tyers, M. (2006). BioGRID: a general repository for interaction datasets. Nucleic Acids Res *34*, D535-539.

Stirnimann, C.U., Petsalaki, E., Russell, R.B., and Müller, C.W. (2010). WD40 proteins propel cellular networks. Trends Biochem Sci *35*, 565-574.

Subauste, M.C., Ventura-Holman, T., Du, L., Subauste, J.S., Chan, S.L., Yu, V.C., and Maher, J.F. (2009). RACK1 downregulates levels of the pro-apoptotic protein Fem1b in apoptosis-resistant colon cancer cells. Cancer Biol Ther *8*, 2297-2305.

Swaney, D.L., Beltrao, P., Starita, L., Guo, A., Rush, J., Fields, S., Krogan, N.J., and Villén, J. (2013). Global analysis of phosphorylation and ubiquitylation cross-talk in protein degradation. Nat Methods *10*, 676-682.

Tarnowski, K., Fituch, K., Szczepanowski, R.H., Dadlez, M., and Kaus-Drobek, M. (2014). Patterns of structural dynamics in RACK1 protein retained throughout evolution: a hydrogen-deuterium exchange study of three orthologs. Protein Sci *23*, 639-651.

Tarumoto, Y., Kanoh, J., and Ishikawa, F. (2013). Receptor for activated C-kinase (RACK1) homolog Cpc2 facilitates the general amino acid control response through Gcn2 kinase in fission yeast. J Biol Chem *288*, 19260-19268.

Tedford, K., Kim, S., Sa, D., Stevens, K., and Tyers, M. (1997). Regulation of the mating pheromone and invasive growth responses in yeast by two MAP kinase substrates. Curr Biol *7*, 228-238.

Thornton, C., Tang, K.C., Phamluong, K., Luong, K., Vagts, A., Nikanjam, D., Yaka, R., and Ron, D. (2004). Spatial and temporal regulation of RACK1 function and N-methyl-D-aspartate receptor activity through WD40 motif-mediated dimerization. J Biol Chem *279*, 31357-31364.

Tkach, J.M., Yimit, A., Lee, A.Y., Riffle, M., Costanzo, M., Jaschob, D., Hendry, J.A., Ou, J., Moffat, J., Boone, C., *et al.* (2012). Dissecting DNA damage response pathways by analysing protein localization and abundance changes during DNA replication stress. Nat Cell Biol *14*, 966-976.

Tsukahara, K., Yamamoto, H., and Okayama, H. (1998). An RNA binding protein negatively controlling differentiation in fission yeast. Mol Cell Biol *18*, 4488-4498.

Ullah, H., Scappini, E.L., Moon, A.F., Williams, L.V., Armstrong, D.L., and Pedersen, L.C. (2008). Structure of a signal transduction regulator, RACK1, from *Arabidopsis* thaliana. Protein Sci *17*, 1771-1780.

Urano, D., Czarnecki, O., Wang, X., Jones, A.M., and Chen, J.G. (2015). *Arabidopsis* receptor of activated C kinase1 phosphorylation by WITH NO LYSINE8 KINASE. Plant Physiol *167*, 507-516.

Urban, J., Soulard, A., Huber, A., Lippman, S., Mukhopadhyay, D., Deloche, O., Wanke, V., Anrather, D., Ammerer, G., Riezman, H., *et al.* (2007). Sch9 is a major target of TORC1 in *Saccharomyces cerevisiae*. Mol Cell *26*, 663-674.

Valerius, O., Kleinschmidt, M., Rachfall, N., Schulze, F., López Marín, S., Hoppert, M., Streckfuss-Bömeke, K., Fischer, C., and Braus, G.H. (2007). The *Saccharomyces* homolog of mammalian RACK1, Cpc2/Asc1p, is required for *FLO11*-dependent adhesive growth and dimorphism. Mol Cell Proteomics *6*, 1968-1979.

Vani, K., Yang, G., and Mohler, J. (1997). Isolation and cloning of a *Drosophila* homolog to the mammalian RACK1 gene, implicated in PKC-mediated signalling. Biochim Biophys Acta *1358*, 67-71.

Volta, V., Beugnet, A., Gallo, S., Magri, L., Brina, D., Pesce, E., Calamita, P., Sanvito, F., and Biffo, S. (2012). RACK1 depletion in a mouse model causes lethality, pigmentation deficits and reduction in protein synthesis efficiency. Cell Mol Life Sci *70*, 1439-1450.

Vomastek, T., Iwanicki, M.P., Schaeffer, H.J., Tarcsafalvi, A., Parsons, J.T., and Weber, M.J. (2007). RACK1 targets the extracellular signal-regulated kinase/mitogen-activated protein kinase pathway to link integrin engagement with focal adhesion disassembly and cell motility. Mol Cell Biol *27*, 8296-8305.

Voytas, D. (2001). Agarose gel electrophoresis. Curr Protoc Mol Biol *Chapter 2*, Unit2 5A.

Wang, G.L., and Semenza, G.L. (1995). Purification and characterization of hypoxia-inducible factor 1. J Biol Chem *270*, 1230-1237.

Wang, L., Berndt, P., Xia, X., Kahnt, J., and Kahmann, R. (2011). A seven-WD40 protein related to human RACK1 regulates mating and virulence in *Ustilago maydis*. Mol Microbiol *81*, 1484-1498.

Wang, M., Herrmann, C.J., Simonovic, M., Szklarczyk, D., and von Mering, C. (2015a). Version 4.0 of PaxDb: Protein abundance data, integrated across model organisms, tissues, and cell-lines. Proteomics *15*, 3163-3168.

Wang, M., Weiss, M., Simonovic, M., Haertinger, G., Schrimpf, S.P., Hengartner, M.O., and von Mering, C. (2012). PaxDb, a database of protein abundance averages across all three domains of life. Mol Cell Proteomics *11*, 492-500.

Wang, Q., Zhou, S., Wang, J.Y., Cao, J., Zhang, X., Wang, J., Han, K., Cheng, Q., Qiu, G., Zhao, Y., *et al.* (2015b). RACK1 antagonizes TNF-α-induced cell death by promoting p38 activation. Sci Rep *5*, 14298.

Wang, S., Sakai, H., and Wiedmann, M. (1995). NAC covers ribosome-associated nascent chains thereby forming a protective environment for regions of nascent chains just emerging from the peptidyl transferase center. J Cell Biol *130*, 519-528.

Wang, X., and Huang, L. (2008). Identifying dynamic interactors of protein complexes by quantitative mass spectrometry. Mol Cell Proteomics *7*, 46-57.

Wang, Y., Shen, G., Gong, J., Shen, D., Whittington, A., Qing, J., Treloar, J., Boisvert, S., Zhang, Z., Yang, C., *et al.* (2014). Noncanonical Gβ Gib2 is a scaffolding protein promoting cAMP signaling through functions of Ras1 and Cac1 proteins in *Cryptococcus neoformans*. J Biol Chem *289*, 12202-12216.

Wang, Z., Zhang, B., Jiang, L., Zeng, X., Chen, Y., Feng, X., Guo, Y., and Chen, Q. (2009). RACK1, an excellent predictor for poor clinical outcome in oral squamous carcinoma, similar to Ki67. Eur J Cancer *45*, 490-496.

Warner, J.R., and McIntosh, K.B. (2009). How common are extraribosomal functions of ribosomal proteins? Mol Cell *34*, 3-11.

Watkins, N.J., and Bohnsack, M.T. (2012). The box C/D and H/ACA snoRNPs: key players in the modification, processing and the dynamic folding of ribosomal RNA. Wiley Interdiscip Rev RNA *3*, 397-414.

Wehner, P., Shnitsar, I., Urlaub, H., and Borchers, A. (2011). RACK1 is a novel interaction partner of PTK7 that is required for neural tube closure. Development *138*, 1321-1327.

Weinert, B.T., Schölz, C., Wagner, S.A., Iesmantavicius, V., Su, D., Daniel, J.A., and Choudhary, C. (2013). Lysine succinylation is a frequently occurring modification in prokaryotes and eukaryotes and extensively overlaps with acetylation. Cell Rep *4*, 842-851.

Weiss, C., Schneider, S., Wagner, E.F., Zhang, X., Seto, E., and Bohmann, D. (2003). JNK phosphorylation relieves HDAC3-dependent suppression of the transcriptional activity of c-Jun. EMBO J *22*, 3686-3695.

Wek, S.A., Zhu, S., and Wek, R.C. (1995). The histidyl-tRNA synthetase-related sequence in the eIF-2α protein kinase GCN2 interacts with tRNA and is required for activation in response to starvation for different amino acids. Mol Cell Biol *15*, 4497-4506.

Wen, Y., and Shatkin, A.J. (1999). Transcription elongation factor hSPT5 stimulates mRNA capping. Genes Dev *13*, 1774-1779.

Wessel, D., and Flügge, U.I. (1984). A method for the quantitative recovery of protein in dilute solution in the presence of detergents and lipids. Anal Biochem *138*, 141-143.

Wilson-Grady, J.T., Villén, J., and Gygi, S.P. (2008). Phosphoproteome analysis of fission yeast. J Proteome Res *7*, 1088-1097.

Wilson, M.D., Harreman, M., Taschner, M., Reid, J., Walker, J., Erdjument-Bromage, H., Tempst, P., and Svejstrup, J.Q. (2013). Proteasome-mediated processing of Def1, a critical step in the cellular response to transcription stress. Cell *154*, 983-995.

Wiśniewski, J.R., Zougman, A., Nagaraj, N., and Mann, M. (2009). Universal sample preparation method for proteome analysis. Nat Methods *6*, 359-362.

Wolf, A.S., and Grayhack, E.J. (2015). Asc1, homolog of human RACK1, prevents frameshifting in yeast by ribosomes stalled at CGA codon repeats. RNA *21*, 935-945.

Woodcock, D.M., Crowther, P.J., Doherty, J., Jefferson, S., DeCruz, E., Noyer-Weidner, M., Smith, S.S., Michael, M.Z., and Graham, M.W. (1989). Quantitative evaluation of *Escherichia coli* host strains for tolerance to cytosine methylation in plasmid and phage recombinants. Nucleic Acids Res *17*, 3469-3478.

Wu, C., Lytvyn, V., Thomas, D.Y., and Leberer, E. (1997). The phosphorylation site for Ste20p-like protein kinases is essential for the function of myosin-I in yeast. J Biol Chem *272*, 30623-30626.

Yaka, R., He, D.Y., Phamluong, K., and Ron, D. (2003). Pituitary adenylate cyclase-activating polypeptide (PACAP(1-38)) enhances N-methyl-D-aspartate receptor function and brain-derived neurotrophic factor expression via RACK1. J Biol Chem *278*, 9630-9638.

Yaka, R., Thornton, C., Vagts, A.J., Phamluong, K., Bonci, A., and Ron, D. (2002). NMDA receptor function is regulated by the inhibitory scaffolding protein, RACK1. Proc Natl Acad Sci U S A *99*, 5710-5715.

Yao, S., Neiman, A., and Prelich, G. (2000). *BUR1* and *BUR2* encode a divergent cyclin-dependent kinase-cyclin complex important for transcription *in vivo*. Mol Cell Biol *20*, 7080-7087.

Yarwood, S.J., Steele, M.R., Scotland, G., Houslay, M.D., and Bolger, G.B. (1999). The RACK1 signaling scaffold protein selectively interacts with the cAMP-specific phosphodiesterase PDE4D5 isoform. J Biol Chem *274*, 14909-14917.

Yatime, L., Hein, K.L., Nilsson, J., and Nissen, P. (2011). Structure of the RACK1 dimer from *Saccharomyces cerevisiae*. J Mol Biol *411*, 486-498.

Zeller, C.E., Parnell, S.C., and Dohlman, H.G. (2007). The RACK1 ortholog Asc1 functions as a G-protein β subunit coupled to glucose responsiveness in yeast. J Biol Chem *282*, 25168-25176.

Zhang, D., Chen, L., Li, D., Lv, B., Chen, Y., Chen, J., XuejiaoYan, and Liang, J. (2014). *OsRACK1* is involved in abscisic acid- and H_2O_2-mediated signaling to regulate seed germination in rice (*Oryza sativa*, L.). PLoS One *9*, e97120.

Zhang, J., Zhu, F., Li, X., Dong, Z., Xu, Y., Peng, C., Li, S., Cho, Y.Y., Yao, K., Zykova, T.A., *et al.* (2012a). Rack1 protects N-terminal phosphorylated c-Jun from Fbw7-mediated degradation. Oncogene *31*, 1835-1844.

Zhang, W., Cheng, G.Z., Gong, J., Hermanto, U., Zong, C.S., Chan, J., Cheng, J.Q., and Wang, L.H. (2008). RACK1 and CIS mediate the degradation of BimEL in cancer cells. J Biol Chem *283*, 16416-16426.

Zhang, W., Zong, C.S., Hermanto, U., Lopez-Bergami, P., Ronai, Z., and Wang, L.H. (2006). RACK1 recruits STAT3 specifically to insulin and insulin-like growth factor 1 receptors for activation, which is important for regulating anchorage-independent growth. Mol Cell Biol *26*, 413-424.

Zhang, Y., Berndt, U., Gölz, H., Tais, A., Oellerer, S., Wölfle, T., Fitzke, E., and Rospert, S. (2012b). NAC functions as a modulator of SRP during the early steps of protein targeting to the endoplasmic reticulum. Mol Biol Cell *23*, 3027-3040.

Zhao, Y., Wang, Q., Qiu, G., Zhou, S., Jing, Z., Wang, J., Wang, W., Cao, J., Han, K., Cheng, Q., *et al.* (2015). RACK1 Promotes Autophagy by Enhancing the Atg14L-Beclin 1-Vps34-Vps15 Complex Formation upon Phosphorylation by AMPK. Cell Rep *13*, 1407-1417.

Zhou, K., Kuo, W.H., Fillingham, J., and Greenblatt, J.F. (2009). Control of transcriptional elongation and cotranscriptional histone modification by the yeast BUR kinase substrate Spt5. Proc Natl Acad Sci U S A *106*, 6956-6961.

Online tools and databases

http://motif-x.med.harvard.edu

http://smart.embl-heidelberg.de

http://www.ch.embnet.org/software/BOX_form.html

http://www.genome.jp/kegg

http://www.pax-db.org

http://www.phosphogrid.org

http://www.rcsb.org

http://www.uniprot.org

http://www.yeastgenome.org

6. Supplementary Material

```
            1          11         21         31         41
ASC1 SNR24  ATGGCATCTA ACGAAGTTTT AGTTTTGAGA GGTACCTTGG AAGGTCACAA
Asc1p       M  A  S  N   E  V  L   V  L  R   G  T  L  E   G  H  N
asc1-       ATGGCATCTA ACGAAGTTTT AGTTTTGAGA GGTACCTTGG AAGGTCACAA
Asc1p-      M  A  S  N   E  V  L   V  L  R   G  T  L  E   G  H  N

            51         61         71         81         91
ASC1 SNR24  CGGTTGGGTC ACATCTTTGG CTACTTCTGC TGGTCAACCA AACCTATTGT
Asc1p        G  W  V   T  S  L  A   T  S  A   G  Q  P   N  L  L  L
asc1-       CGGTTGGGTC ACATCTTTGG CTACTTCTGC TGGTCAACCA AACCTATTGT
Asc1p-       G  W  V   T  S  L  A   T  S  A   G  Q  P   N  L  L  L

            101        111        121        131        141
ASC1 SNR24  TGTCCGCTTC CCGTGATAAG ACTTTGATCT CCTGGAAGTT GACTGGTGAC
Asc1p         S  A  S   R  D  K   T  L  I  S   W  K  L   T  G  D
asc1-       TGTCCGCTTC CCGTGATAAG ACTTTGATCT CCTGGAAGTT GACTGGTGAC
Asc1p-        S  A  S   R  D  K   T  L  I  S   W  K  L   T  G  D

            151        161        171        181        191
ASC1 SNR24  GACCAAAAGT TTGG------ ---------- ---------- ----------
Asc1p       D  Q  K  F   G  -  -   -  -  -   -  -  -  -   -  -  -
asc1-       GACCAAAAGT TTGGAGCAGC TGAAGCTTCG TACGCTGCAG GTCGACAACC
Asc1p-      D  Q  K  F   G  A  A   E  A  S   Y  A  A  G   R  Q  P

            201        211        221        231        241
ASC1 SNR24  ---------- ---------- ---------- ---------- ----------
Asc1p        -  -  -   -  -  -  -   -  -  -   -  -  -   -  -  -  -
asc1-       CTTAATATAA CTTCGTATAA TGTATGCTAT ACGAAGTTAT TAGGTGATAT
Asc1p-       L  I  *   -  -  -  -   -  -  -   -  -  -   -  -  -  -

            251        261        271        281        291
ASC1 SNR24  ---------- ---------- --TGTCCCAG TTAGATCTTT CAAGGGTCAC
Asc1p         -  -  -   -  -  -   -  V  P  V   R  S  F   K  G  H
asc1-       CAGATCCACT AGTGGCCTAT GCTGTCCCAG TTAGATCTTT CAAGGGTCAC
Asc1p-        -  -  -   -  -  -   -  -  -  -   -  -  -   -  -  -
```

Supplementary Figure 1. DNA and amino acid sequence alignments of the *ASC1 SNR24* wild-type strain and the *asc1*$^{-}$ strain.
The figure illustrates the differences in the DNA and amino acid sequence between the *ASC1 SNR24* wild-type and the *asc1*$^{-}$ strain. Due to the presence of a stop codon (TAA labeled with an asterisks) within the *loxP* site in the *asc1*$^{-}$ strain, translation of the corresponding mRNA is abrogated leading to the formation of truncated Asc1p^{-}.

Supplementary Table 1. LC-MS-based identification of Asc1p-derived phospho-peptides.
Phospho-sites with the highest post-translational modification (PTM) score are printed in black, and all other putative phospho-sites within the peptides in gray.

Amino acid	Position	Highest PTM score	Peptide sequence	Spectral counts	Highest Xcorr (*SequestHT*)	Highest IonScore (*Mascot*)
T	12	100.00	G**T**LEGHNGWVTSLATSAGQPN LLLSASR	19	5.42	70
T	21	45.5				
S	22	33.3				
T	25	60.1				
S	26	39				
S	35	9.9				
S	37	79.6				
S	120	100	KA**S**MIISGSR	2	-	47
S	124	0				
S	126	0				
T	143	100	GQCLA**T**LLGHNDWVSQVR	29	4.54	59
S	152	0				
S	166	100	ADDD**S**V**T**IISAGNDK VVPNEKADDD**S**V**T**IISAGNDK	121 25	4.87 4.37	108 60
T	168	100				
S	171	90				
Y	250	100	**Y**WLAAATATGIK	21	3.51	56
T	256	0.3				
T	258	0				
S	291	77.4	AAEPHAVSLAWSADGQ**T**LFAG YTDNVIR	17	5.19	91
S	295	93.2				
T	300	99.9				
Y	305	0.6				
T	306	0.2				

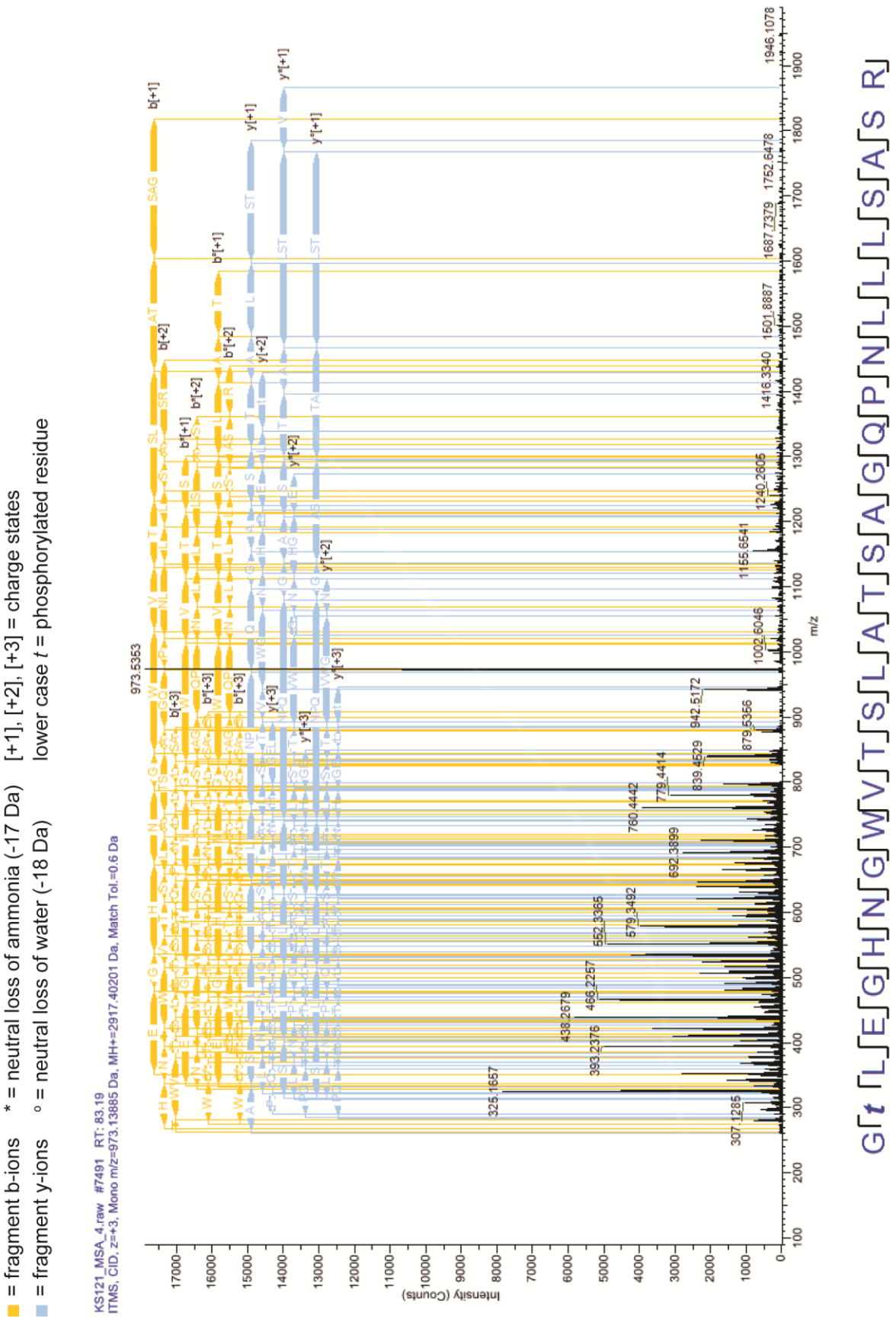

Supplementary Figure 2. Annotated fragmentation spectra of Asc1p phospho-peptides.
(A) Annotated fragmentation spectrum of the peptide GTLEGHNGWVTSLATSAGQPNLLLSASR phosphorylated at T12.

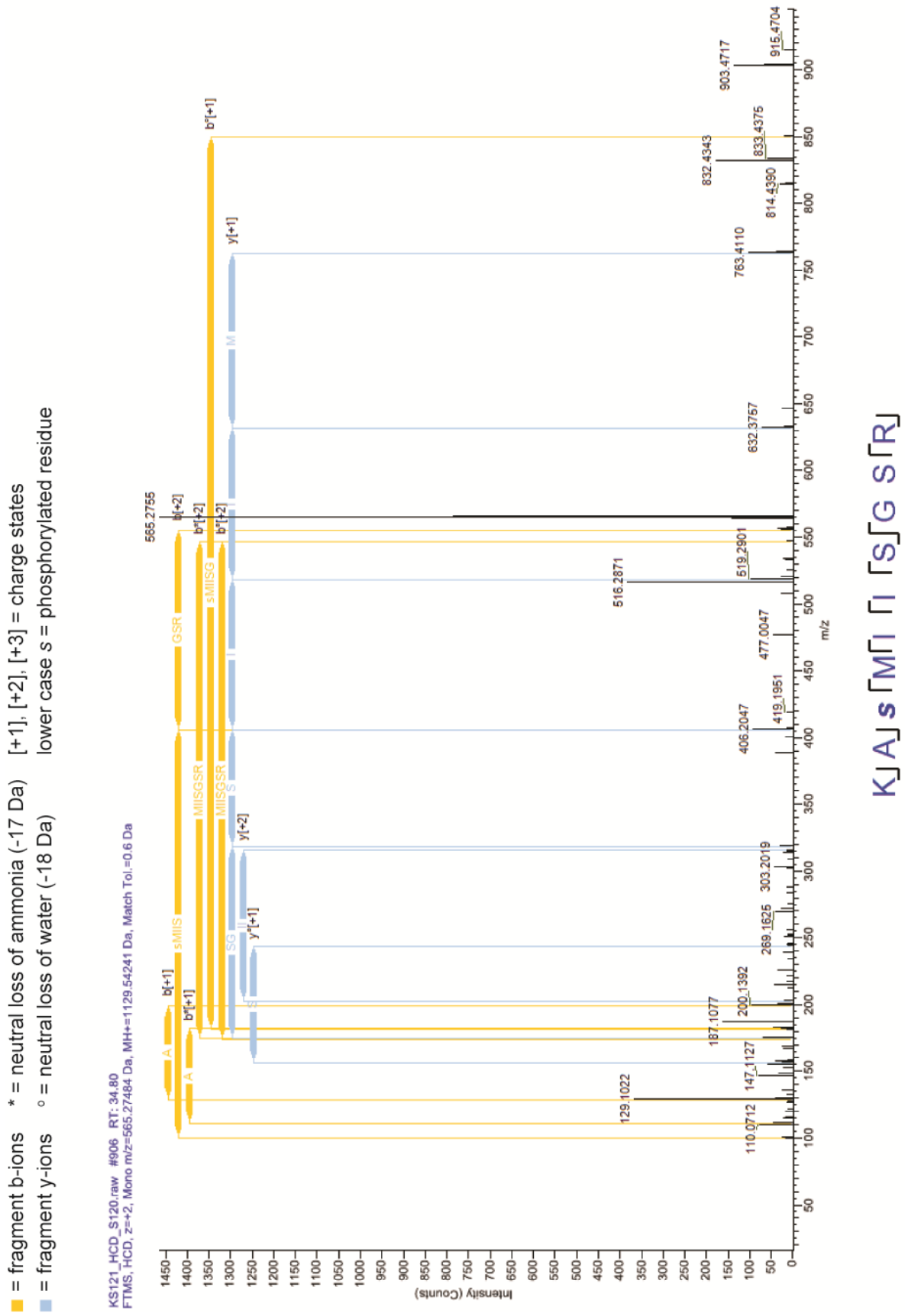

(B) Annotated fragmentation spectrum of the peptide KASMIISGSR phosphorylated at S120.

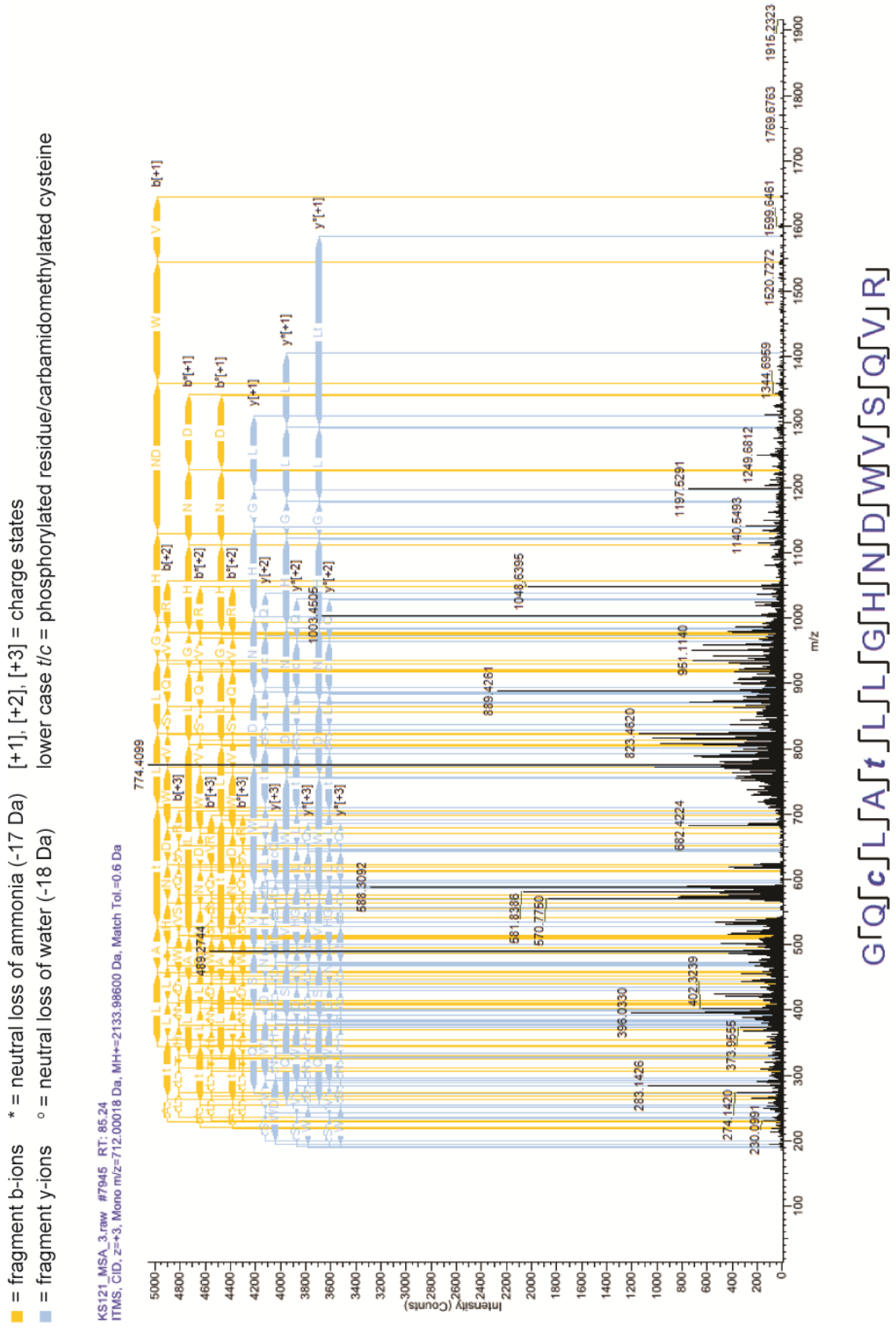

(C) Annotated fragmentation spectrum of the peptide GQCLATLLGHNDWVSQVR phosphorylated at T143.

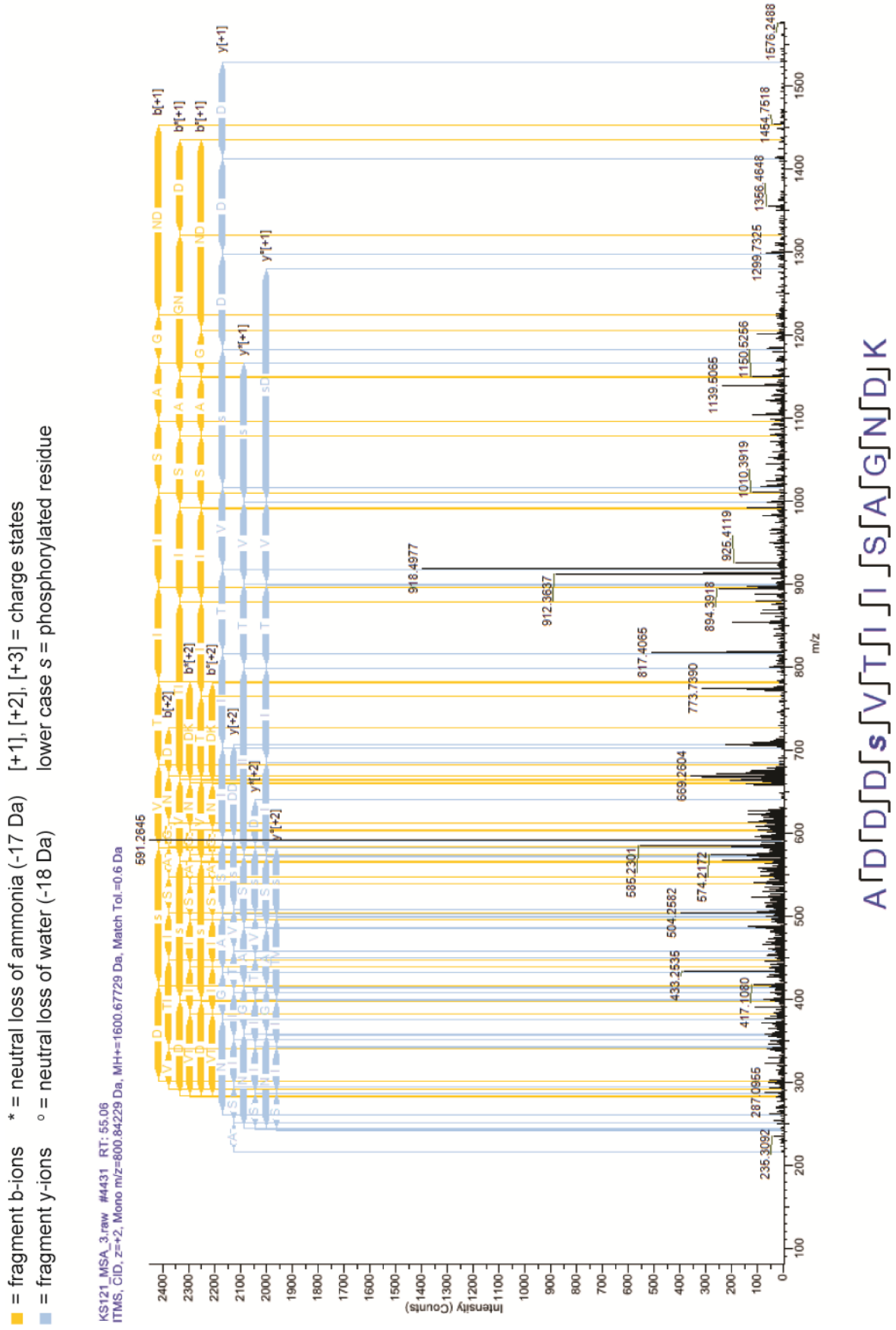

(D) Annotated fragmentation spectrum of the peptide ADDDSVTIISAGNDK phosphorylated at S166.

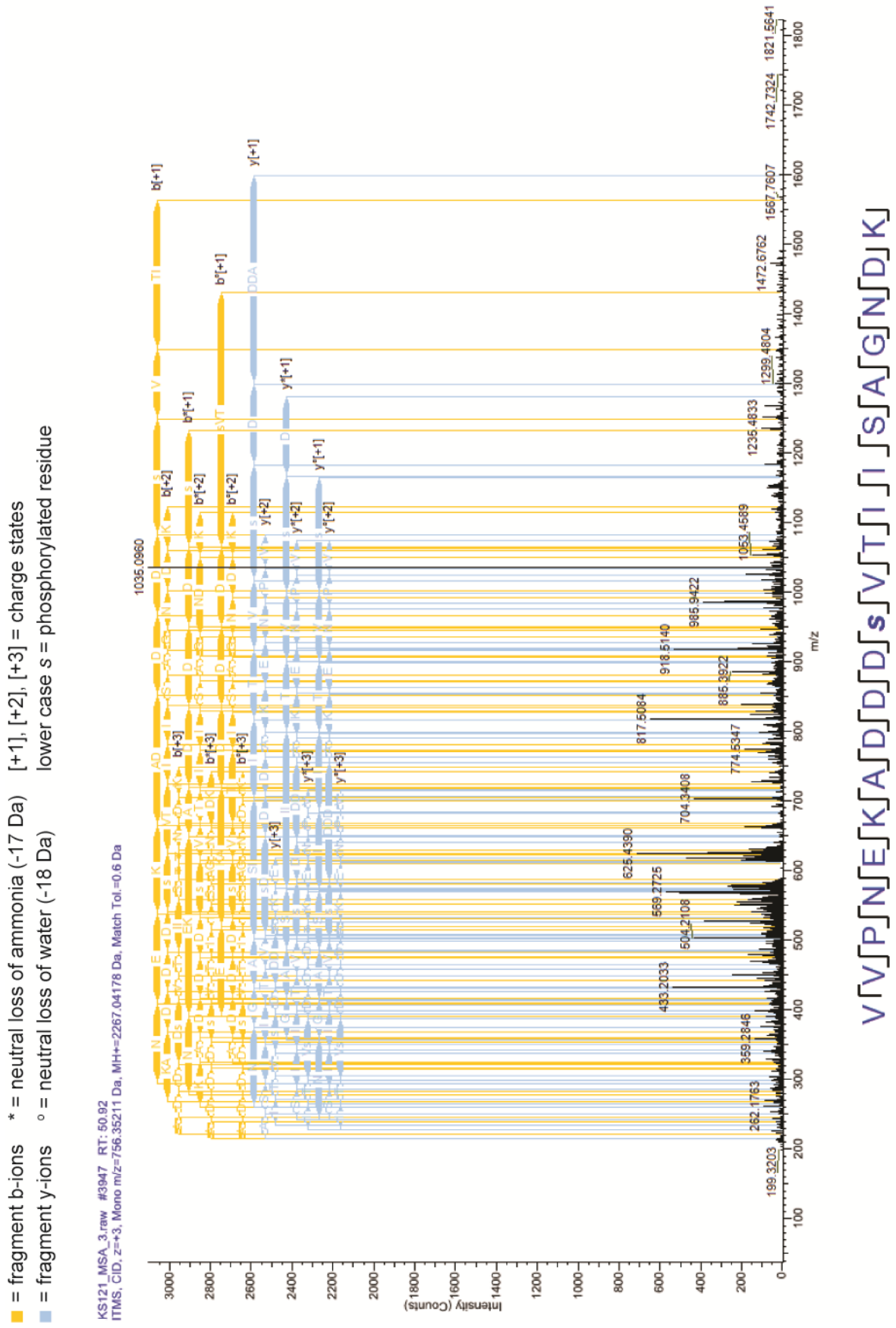

(E) Annotated fragmentation spectrum of the peptide VVPNEKADDDSVTIISAGNDK phosphorylated at S166.

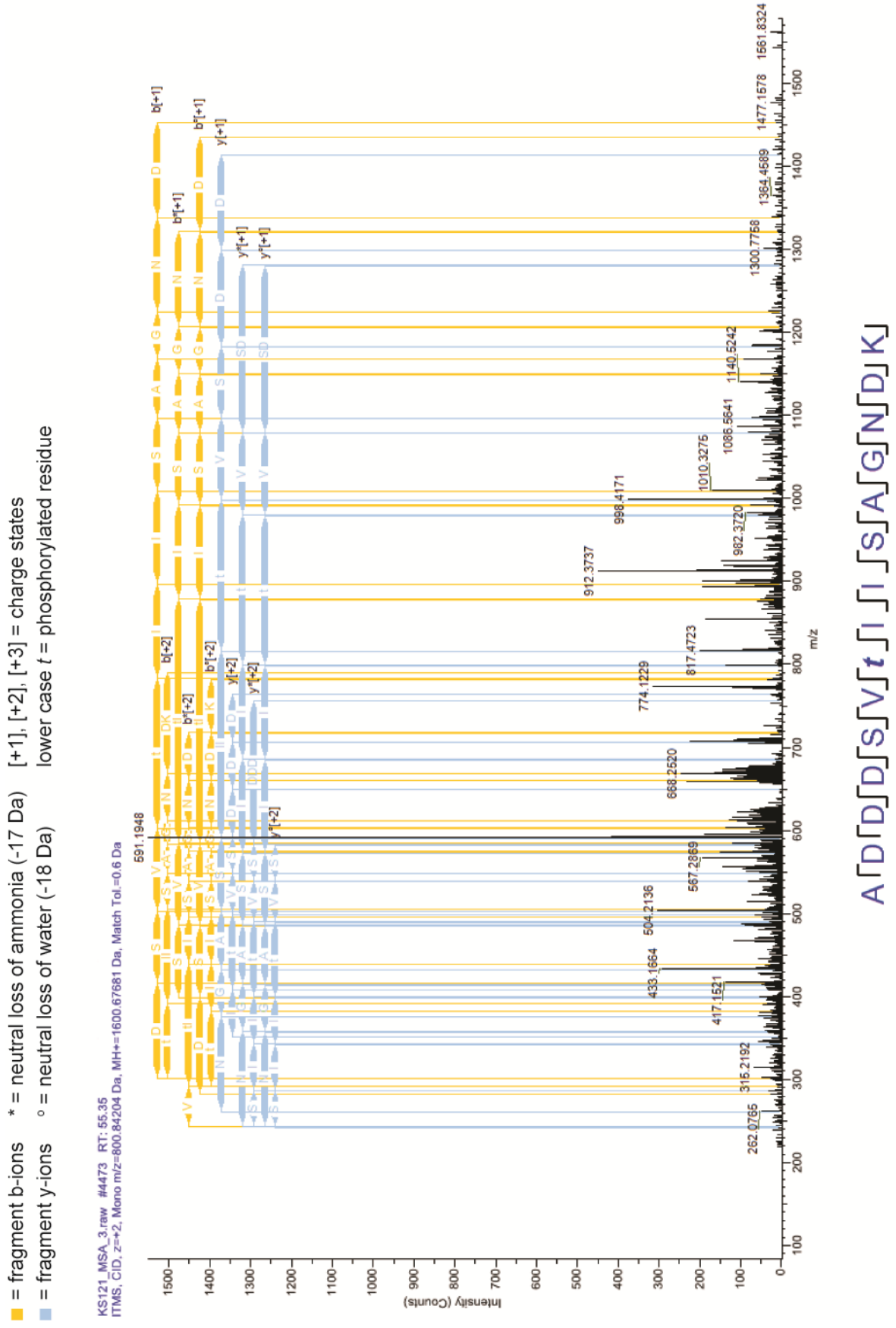

(F) Annotated fragmentation spectrum of the peptide ADDDSVTIISAGNDK phosphorylated at T168.

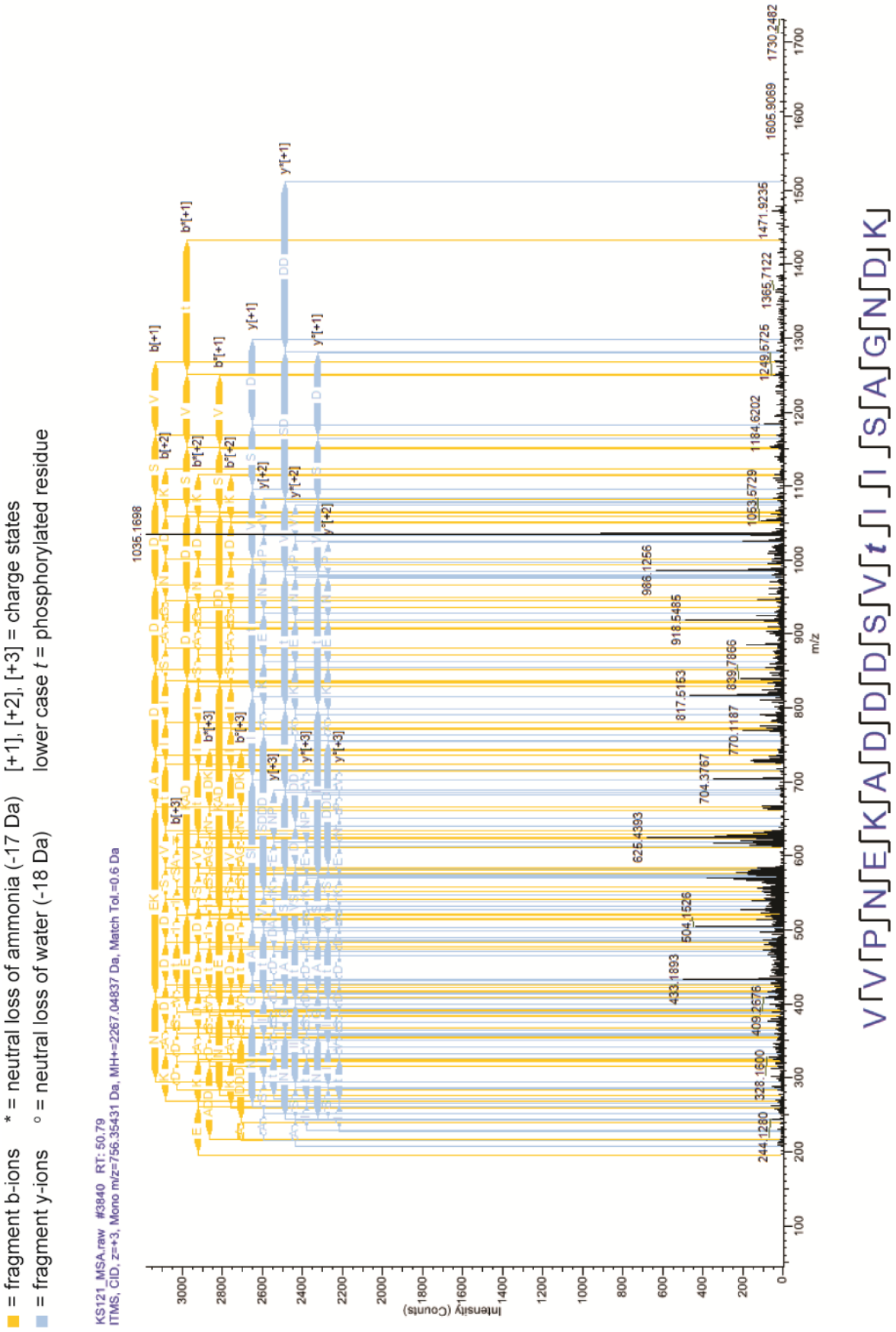

(G) Annotated fragmentation spectrum of the peptide VVPNEKADDDSVTIISAGNDK phosphorylated at T168.

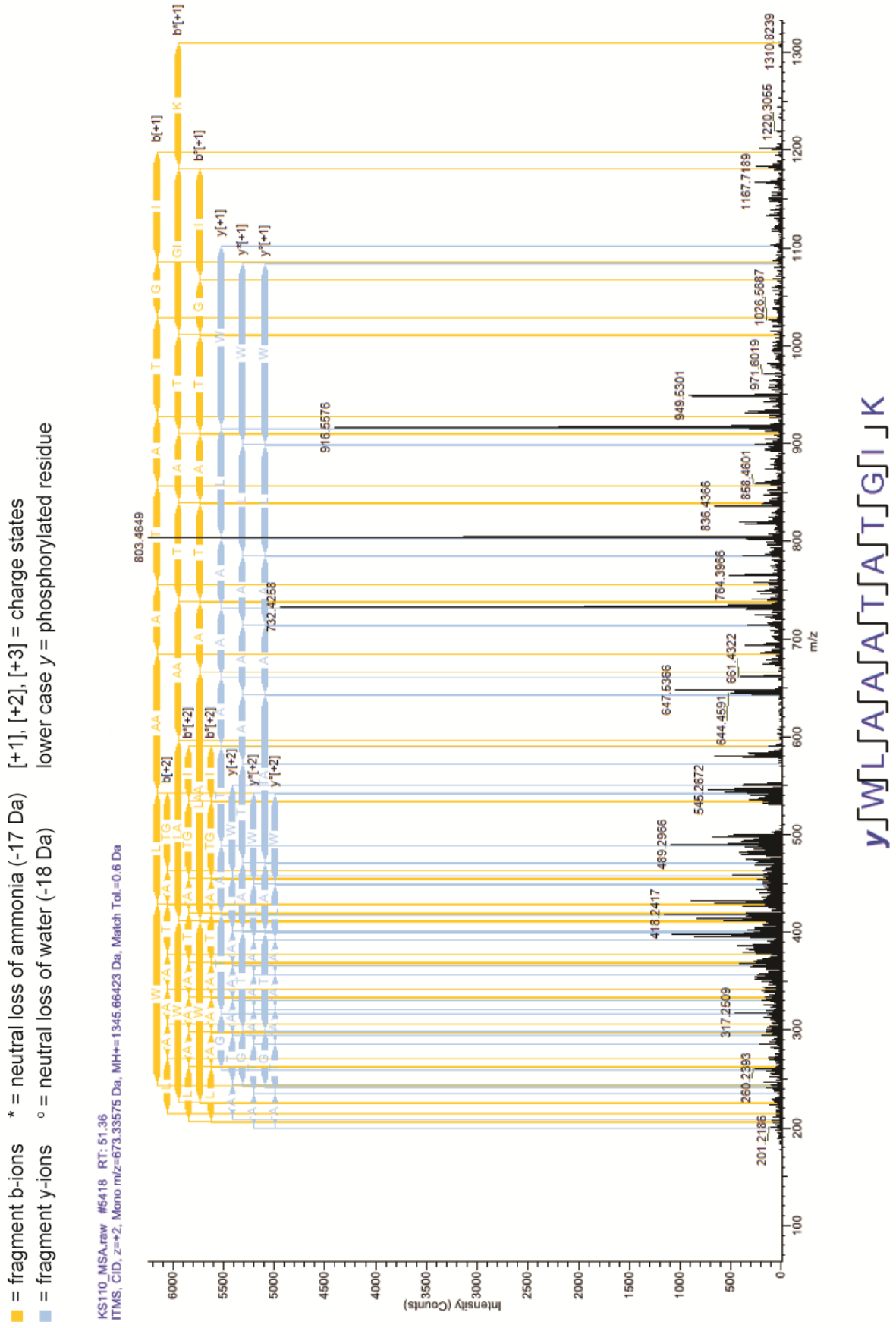

(H) Annotated fragmentation spectrum of the peptide YWLAAATATGIK phosphorylated at Y250.

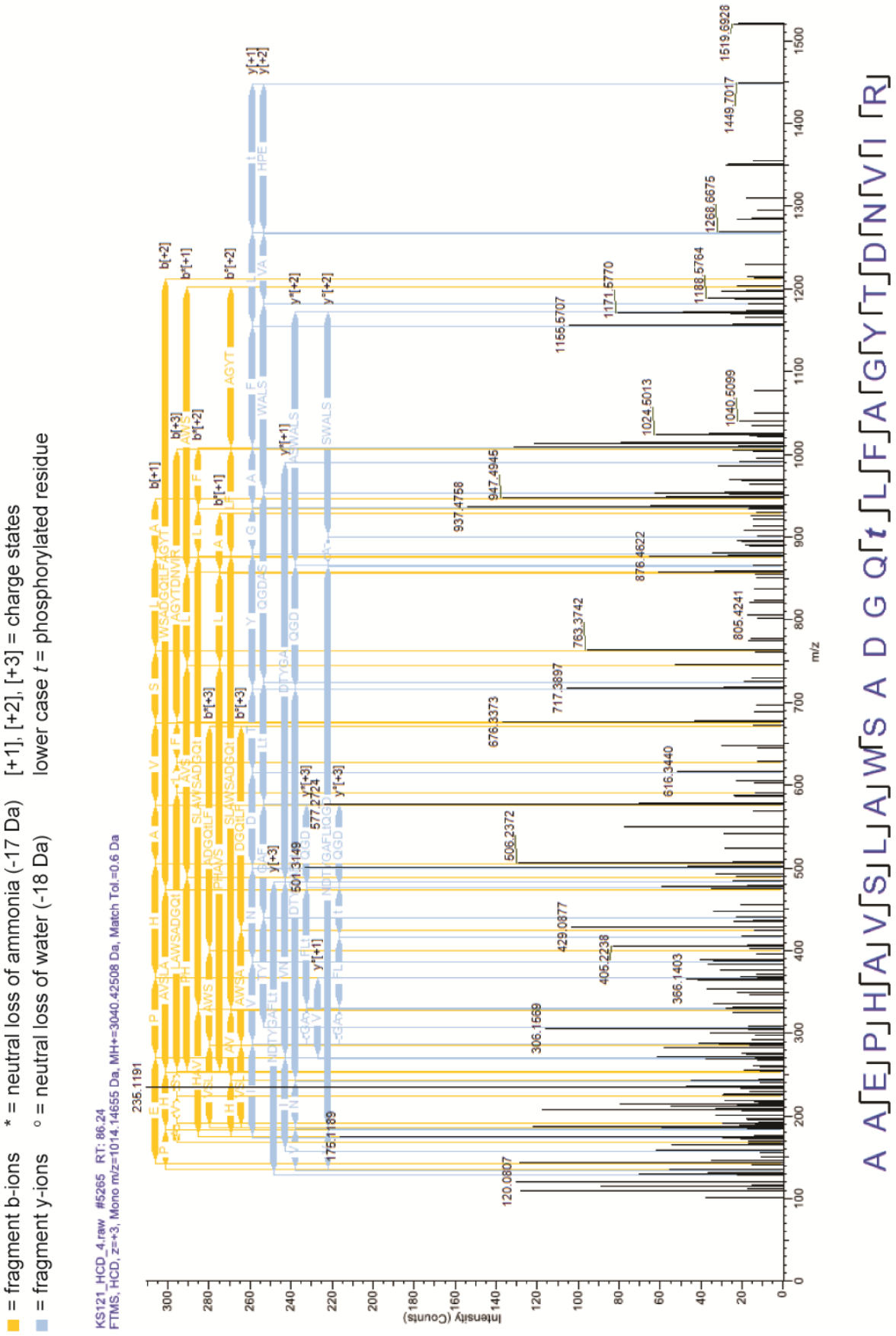

(I) Annotated fragmentation spectrum of the peptide AAEPHAVSLAWSADGQTLFAGYTDNVIR phosphorylated at T300.

Supplementary Table 2. Overview of proteome data evaluation with *Perseus.*
Abbreviations: Prot = protein, vs. = versus

No.	Command	Description	
		asc1^{-} and *asc1*DE	T143 phospho-site mutant strains, for example, a*sc1*^{T143A}
1	Generic matrix upload	proteinGroups.txt normalized ratios etc.	
2.1 2.2 2.3	Filter rows based on categorical column	Remove rows with + in reverse column Remove rows with + in potential contaminant column Remove rows with + in only identified by site column	
3	Transform	Inverse ratios (1/x) when *ASC1* is not in the denominator	
4	Transform	$\log_2(x)$	
5	Normalization	Subtract column median of ratios	
6	Categorical annotation rows	Group biological replicates	
7	Reorder/ remove columns	Select Prot ratios of interest for the following steps	
8.1	Average groups	Calculate median of each group → *protein ratio*	Calculate mean of each group
8.2	Combine expression columns	-	Calculation of difference between mean of *asc1*^{T143A}/*ASC1* ratios and *ASC1*^{Aux}/*ASC1* ratios → *protein ratio*
9	Change column type	Change numerical column with *protein ratio* (steps 8.1 and 8.2) to expression column	
10	Categorical annotation rows	Define column with protein ratio as own group	
11	One/Two sample(s) tests	One-sample *t*-test, p-value 0.01	Two-sample *t*-test, p-value 0.01 Prot ratios *asc1*^{T143A}/*ASC1* vs. Prot ratios *ASC1*^{Aux}/*ASC1*
12	Filter rows based on categorical column	Keep rows with + (significant) from step 11	
13	Filter rows based on valid values	Filter *protein ratio* (steps 8.1 and 8.2) for values outside -0.26 to 0.26	

Supplementary Table 3. Overview of phospho-proteome data evaluation with *Perseus*.
Abbreviations: PP = phospho-peptide, Prot = protein, vs. = versus

No.	Command	Description	
		asc1^{-}	T143 phospho-site mutant strains, for example, *asc1*^{T143A}
1	Generic matrix upload	Phospho (STY)Sites.txt normalized ratios, localization probability etc.	
2.1 2.2	Filter rows based on categorical column	Remove rows with + in reverse column Remove rows with + in potential contaminant column	
3	Expand site table	In order to have only one column per sample	
4	Transform	Inverse ratios (1/x) when *ASC1* is not already in the denominator	
5	Transform	$\log_2(x)$	
6	Reorder/ remove columns	Select PP ratios of interest for the following steps	
7	Matching rows by name	Matching PP ratios with respective Prot ratios from step 7 of Supplementary Table 2 (in the case that a phospho-peptide cannot be assigned to a single protein the median of the protein ratios is calculated)	
8	Categorical annotation rows	Group PP ratios and Prot ratios for biological replicates	
9	Average groups	Calculate median of each group	Calculate mean of each group
10.1	Combine expression columns	Correction of PP ratios with Prot ratios: median PP ratios - median Prot ratios → *phospho regulation*	
10.2		-	Calculation of difference between proteome-corrected PP ratios of *asc1*^{T143A}/*ASC1* and *ASC1*^{Aux}/*ASC1* → *phospho regulation*
11	Change column type	Change numerical column with *phospho regulation* (steps 10.1 and 10.2) to expression column	
12	Categorical annotation rows	Define column with *phospho regulation* as an own group for later filtering of values	
13	Categorical annotation rows	Group PP ratios for biological replicates for the next step	
14	Filter rows based on valid values	Filter for two valid PP ratios	Filter for one valid PP ratio
15.1	Two samples tests	*t*-test, p-value 0.01 PP ratios vs. Prot ratios	*t*-test, p-value 0.05 PP ratios vs. Prot ratios for *asc1*^{T143A}/*ASC1*
15.2		-	*t*-test, p-value 0.05 PP ratios *asc1*^{T143A}/*ASC1* vs. PP ratios *ASC1*^{Aux}/*ASC1*
16.1	Filter rows based on categorical column	Keep rows with + (significant) from step 15.1	
16.2		-	Keep rows with + (significant) from step 15.2
17	Filter rows based on valid values	Filter *phospho regulation* (steps 10-12) for values outside -0.26 to 0.26	

Supplementary Table 3. Continued.

No.	Command	Description	
The following steps were only performed for the *asc1*$^-$ phospho-proteome analysis and for phosphorylated peptides with zero to two corresponding Prot ratios. Start from step 15.1			
18	One sample tests	*t*-test, p-value 0.01 only phospho-peptide ratios	
19	Filter rows based on categorical column	Discard rows with + (significant) from step 15.1 (these candidates showed regulation of PP ratios with respect to Prot values)	
20	Filter rows based on categorical column	Keep rows with + (significant) from step 18	
21	Categorical annotation rows	Group Prot ratios → *proteome*	
22	Filter rows based on valid values	Filter rows based on three valid values in the *proteome* group, add categorical column (assumption: less than three valid values might be insufficient for two-samples *t*-test)	
23	Filter rows based on categorical column	Keep rows that were specified as *discarded* in the previous step (remaining candidates have less than three valid values in the *proteome* group)	
24	Filter rows based on valid values	Filter rows based on one valid value in *proteome* group, add categorical column	
		phosphorylated peptides with no corresponding Prot ratio	phosphorylated peptides with one or two corresponding Prot ratio(s)
25	Filter rows based on categorical column	Keep rows that were specified as *discarded* in the previous step, they have no *proteome* values	Keep rows that were specified as *keep* in the previous step, they have one or two *proteome* value(s)
26	Change column type	Change numerical column with PP median ratio (step 9) to expression column	-
27	Categorical annotation rows	Define column with PP median ratio from the previous step as an own group for filtering of values in the next step → *phospho regulation with no Prot value*	-
28	Filter rows based on valid values	Filter *phospho regulation with no Prot value* (step 27) for values outside -0.26 to 0.26	Filter *phospho regulation* (step 10.1) for values outside -0.26 to 0.26

Color scale for Supplementary Tables 4-11, 15, and 16

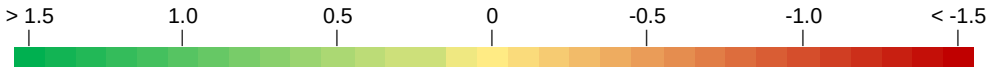

Supplementary Table 4. SILAC-based proteome data for the comparison of the *asc1*⁻ strain and the *ASC1* wild-type strain.

The table lists proteins with a median *asc1*⁻/*ASC1* $\log_2$ SILAC-ratio ≤ -0.58 or ≥ 0.58 and a p-value < 0.01. Proteins with SILAC-ratios > 0.26 or < -0.26 are not shown. Replicates are numbered 1-8 and 13 (see Figure 21, Ø = median of SILAC-ratios, SD = standard deviation, gray/NaN = not a number).

proteins	protein IDs	*asc1*⁻/*ASC1*										
		1	2	3	4	5	6	7	8	13	Ø	SD
Aro9	P38840	1.70	2.00	2.15	NaN	NaN	NaN	NaN	NaN	1.75	1.88	0.21
Hbn1	Q96VH4	1.27	1.15	1.27	1.58	1.50	1.85	2.01	1.65	1.26	1.50	0.30
Yhb1	P39676	1.32	1.26	1.28	1.43	1.63	1.52	1.62	1.68	1.29	1.43	0.17
Bna2	P47125	NaN	NaN	0.96	0.99	1.40	1.39	1.43	1.56	1.21	1.39	0.23
Sam3	Q08986	NaN	NaN	1.57	1.10	1.01	NaN	1.50	1.39	1.38	1.38	0.22
Ty1a[1]	P0CX58[1]	NaN	NaN	0.64	NaN	NaN	1.33	0.91	1.34	1.33	1.33	0.32
Ty2b[2]	P25384[2]	0.63	1.18	0.93	0.82	1.68	NaN	1.63	1.21	NaN	1.18	0.40
Ty1b[3]	Q03612[3]	1.07	1.11	1.10	1.12	1.39	1.31	1.29	1.32	1.03	1.12	0.13
Hsp82	P02829	1.02	1.13	1.04	0.90	0.93	1.36	1.17	1.11	1.13	1.11	0.14
Ty1a[4]	P0CX73[4]	1.13	1.01	1.10	NaN	NaN	NaN	1.44	1.58	1.06	1.11	0.24
Ych1	P42937	1.14	1.16	1.09	0.81	1.06	0.71	1.43	1.05	1.05	1.06	0.21
Mtd1	Q02046	1.03	0.81	0.86	1.12	1.20	0.85	1.13	1.11	0.85	1.03	0.15
Sui1	P32911	0.89	1.01	1.02	1.02	1.03	0.91	1.02	1.06	0.78	1.02	0.09
Ty2b[5]	Q12337[5]	0.84	0.94	0.87	0.93	1.89	1.51	1.86	1.68	0.67	0.94	0.48
Dak1	P54838	0.89	0.99	0.88	0.72	0.81	1.22	0.99	0.94	0.94	0.94	0.14
Hsp104	P31539	0.89	0.93	0.80	0.73	0.82	1.30	1.09	1.01	1.02	0.93	0.17
Sro9	P25567	0.92	0.80	0.80	0.85	1.00	1.15	1.01	0.99	0.70	0.92	0.14
Rcn2	Q12044	NaN	0.85	0.81	NaN	0.94	NaN	NaN	0.92	1.01	0.92	0.08
Dcs1	Q06151	1.07	0.69	0.86	0.73	0.83	1.07	0.79	1.07	0.92	0.86	0.15
Aap1	P37898	0.85	0.35	1.01	0.96	0.58	0.75	0.87	0.93	0.78	0.85	0.21
Gly1	P37303	0.85	0.75	0.88	0.95	0.99	0.78	0.88	0.79	0.74	0.85	0.09
Nmd5	P46970	0.86	0.68	0.69	0.79	1.07	0.88	0.98	0.84	0.76	0.84	0.13
Fpr4	Q06205	0.05	0.92	0.66	0.87	1.05	1.11	0.60	0.74	0.84	0.84	0.32
Lst8	P41318	0.31	0.93	NaN	0.81	NaN	NaN	0.88	0.91	0.34	0.84	0.29
Ssa1	P10591	0.87	0.91	0.84	0.67	0.63	1.08	0.81	0.76	0.91	0.84	0.14
Lap3	Q01532	0.77	0.83	0.80	0.71	0.88	1.10	1.14	0.98	0.73	0.83	0.16
Cue5	Q08412	NaN	0.53	0.88	0.79	NaN	1.11	0.71	0.88	NaN	0.83	0.19
Fmp41	P53889	0.55	0.69	0.89	0.76	0.92	1.02	1.16	NaN	0.59	0.82	0.21
Bna1	P47096	0.82	0.79	0.77	0.83	1.02	0.74	1.03	0.99	0.71	0.82	0.13
Cex1	Q12453	0.89	0.90	0.64	0.81	0.89	1.07	0.76	0.78	0.69	0.81	0.13
Aro7	P32178	0.34	0.69	0.80	0.99	0.96	0.87	0.67	0.99	0.48	0.80	0.23
Hem15	P16622	0.69	0.81	0.73	0.80	0.82	0.99	0.79	0.65	0.57	0.79	0.12
Ddi1	P40087	0.75	0.78	0.80	0.95	0.71	1.02	0.77	0.81	0.67	0.78	0.11
Nbp2	Q12163	NaN	NaN	0.83	0.78	NaN	0.69	NaN	NaN	NaN	0.78	0.07
Gpm2	Q12008	0.92	0.66	0.58	0.43	0.96	0.99	0.78	1.13	0.70	0.78	0.22
Abp1	P15891	0.85	0.78	0.77	0.83	0.55	0.98	0.52	0.56	0.87	0.78	0.16
Sti1	P15705	0.68	0.80	0.76	0.67	0.70	0.83	0.82	0.73	0.78	0.76	0.06
Plb1	P39105	0.72	0.59	0.52	0.72	0.88	0.77	0.90	0.79	0.75	0.75	0.12
Atg18	P43601	NaN	NaN	0.76	NaN	NaN	NaN	0.74	NaN	NaN	0.75	0.01
His7	P33734	0.71	0.74	0.72	0.70	0.77	0.72	0.75	0.79	0.61	0.72	0.05
Fdc1	Q03034	0.93	0.22	0.58	0.68	NaN	0.86	1.07	0.75	0.43	0.72	0.28

Supplementary Table 4. Continued 1.

proteins	protein IDs	*asc1⁻/ASC1*										
		1	2	3	4	5	6	7	8	13	Ø	SD
Cki1	P20485	0.66	0.62	0.77	0.63	0.61	0.88	0.78	0.82	0.72	0.72	0.10
Grx3	Q03835	0.56	0.71	0.66	0.72	0.84	0.96	0.64	0.83	0.77	0.72	0.12
Lap4	P14904	0.78	0.69	0.71	0.62	0.69	1.06	0.89	0.85	0.70	0.71	0.14
Twf1	P53250	0.67	0.71	0.77	0.62	0.71	0.90	0.67	0.67	0.74	0.71	0.08
Aip1	P46680	0.83	0.78	0.69	0.69	0.60	0.76	0.71	0.67	0.82	0.71	0.07
Ubc1	P21734	0.75	0.69	0.72	0.70	0.57	0.68	0.70	0.56	0.77	0.70	0.07
Cdc28	P00546	0.54	0.60	0.70	0.52	0.89	0.74	0.78	0.89	0.61	0.70	0.14
Bbc1	P47068	0.64	0.52	0.79	0.57	0.69	0.89	0.77	0.35	0.86	0.69	0.17
Hsp42	Q12329	0.63	1.04	0.51	0.69	0.56	1.49	0.55	0.77	1.23	0.69	0.35
Ato3	Q12359	NaN	NaN	0.59	NaN	NaN	NaN	0.76	0.69	NaN	0.69	0.08
Nfu1	P32860	0.48	0.71	0.68	0.89	0.56	0.70	0.53	0.67	0.77	0.68	0.13
Ald2	P47771	0.27	0.78	0.33	NaN	0.62	1.03	0.74	NaN	NaN	0.68	0.29
Rbg2	P53295	0.62	0.45	0.41	0.37	0.90	0.68	0.76	0.69	1.00	0.68	0.22
Ycr016w	P25617	0.88	0.70	0.49	0.66	NaN	NaN	0.75	NaN	0.24	0.68	0.22
Eno1	P00924	0.68	0.58	0.36	0.36	0.80	0.63	0.95	0.89	0.67	0.67	0.21
Trp3	P00937	0.57	0.59	0.66	0.61	0.84	0.72	0.82	0.74	0.67	0.67	0.10
Aro8	P53090	0.68	0.68	0.60	0.64	0.64	0.67	0.72	0.64	0.68	0.67	0.04
Acs2	P52910	0.67	0.60	0.66	0.67	0.75	0.70	0.80	0.75	0.60	0.67	0.07
Krs1	P15180	0.60	0.67	0.61	0.58	0.71	0.69	0.75	0.70	0.63	0.67	0.06
Ypt52	P36018	0.66	0.55	0.63	0.45	0.70	0.59	0.75	0.66	0.68	0.66	0.09
Ent5	Q03769	0.17	0.47	0.25	0.82	0.78	0.79	0.66	0.76	0.56	0.66	0.24
Pan6	P40459	1.12	0.35	0.66	0.81	0.57	0.48	0.68	0.75	0.58	0.66	0.22
Sis1	P25294	0.62	0.53	0.58	0.49	0.75	0.67	0.65	0.72	0.67	0.65	0.08
Npa3	P47122	0.60	0.75	0.64	0.70	0.65	0.40	0.67	0.75	0.59	0.65	0.11
Trm5	P38793	0.59	0.65	0.15	NaN	1.03	0.43	0.69	0.62	0.66	0.63	0.25
Rio2	P40160	0.44	NaN	0.59	NaN	0.40	0.70	0.72	0.67	NaN	0.63	0.14
Car1	P00812	0.57	0.28	0.63	0.63	0.65	0.63	0.59	0.70	0.51	0.63	0.12
Ade1	P27616	0.63	0.63	0.58	0.58	0.87	0.62	0.84	0.91	0.61	0.63	0.14
His5	P07172	0.59	0.62	0.59	0.60	0.67	0.64	0.69	0.71	0.58	0.62	0.05
Aro3	P14843	0.64	0.59	0.53	0.50	0.67	0.62	0.79	0.66	0.59	0.62	0.08
Aim17	P23180	0.71	0.56	0.54	0.48	0.10	1.05	0.62	0.74	0.93	0.62	0.27
Bna5	Q05979	0.01	0.83	0.59	0.62	0.94	0.61	0.92	1.19	0.50	0.62	0.34
Trm82	Q03774	0.37	0.32	0.61	NaN	0.66	0.77	NaN	0.65	0.36	0.61	0.18
Glr1	P41921	0.55	0.63	0.57	0.62	0.43	0.61	0.81	0.67	0.58	0.61	0.10
Cys3	P31373	0.61	0.55	0.54	0.61	0.62	0.68	0.67	0.69	0.55	0.61	0.06
Trp5	P00931	0.58	0.60	0.63	0.59	0.59	0.60	0.78	0.64	0.61	0.60	0.06
Erg26	P53199	0.54	0.57	0.60	0.74	0.77	0.61	0.57	0.63	0.43	0.60	0.10
Faa4	P47912	0.60	0.86	0.35	0.49	0.72	0.44	0.72	0.80	0.32	0.60	0.20
Cpa2	P03965	0.58	0.75	0.73	0.62	0.43	0.51	0.59	0.54	0.64	0.59	0.10
Tps1	Q00764	0.63	0.66	0.58	0.31	0.25	0.73	0.45	0.41	0.69	0.58	0.18
Frd1	P32614	0.58	0.51	0.55	0.60	0.72	0.54	0.79	0.65	0.42	0.58	0.11
Gcn3	P14741	0.66	0.58	0.58	0.51	0.36	0.58	0.58	0.53	0.50	0.58	0.08
Rrp1	P35178	0.34	0.68	0.57	0.58	0.67	0.57	0.63	0.63	0.54	0.58	0.10
Ahp1	P38013	-0.41	-0.41	-0.45	-0.58	-0.94	-0.60	-0.81	-0.81	-0.42	-0.58	0.20

Supplementary Table 4. Continued 2.

proteins	protein IDs	*asc1⁻/ASC1*										
		1	2	3	4	5	6	7	8	13	Ø	SD
Lys4	P49367	-0.65	-0.69	-0.71	-0.47	-0.50	-0.75	-0.43	-0.58	-0.51	-0.58	0.12
Tom70	P07213	-0.59	-0.51	-0.57	-0.58	-0.68	-0.47	-0.62	-0.62	-0.57	-0.58	0.06
Hhf1	P02309	-0.50	-0.51	-0.61	-0.60	-0.59	-0.70	-0.59	-0.62	-0.56	-0.59	0.06
Pim1	P36775	-0.68	-0.48	-0.59	-0.64	-0.54	-0.59	-0.58	-0.65	-0.53	-0.59	0.06
Sec53	P07283	-0.57	-0.59	-0.60	-0.66	-0.61	-0.59	-0.63	-0.54	-0.55	-0.59	0.04
Dcp2	P53550	-0.76	-0.94	-0.65	-0.79	-0.31	-0.21	NaN	-0.56	-0.53	-0.60	0.25
Hem13	P11353	NaN	-0.72	-0.75	-0.40	-0.31	-0.66	-0.66	-0.29	-0.57	-0.61	0.19
Mam33	P40513	-0.84	-0.50	-0.39	-0.73	-1.04	-0.13	NaN	-0.46	-0.83	-0.61	0.30
Pmt2	P31382	-0.61	-0.66	-0.59	-0.76	-0.53	-0.61	-0.74	-0.70	-0.61	-0.61	0.08
Hta1; Hta2	P04911; P04912	-0.64	-0.61	-0.59	-0.73	-0.62	-0.66	-0.61	-0.64	-0.58	-0.62	0.04
Gcv3	P39726	NaN	-0.48	-0.62	-0.54	-0.80	-0.93	-0.73	-0.62	-0.42	-0.62	0.17
Mia40	P36046	-0.52	-0.56	-0.52	-0.61	-0.76	-0.63	-0.66	-0.81	-0.62	-0.62	0.10
Tuf1	P02992	-0.70	-0.54	-0.62	-0.71	-0.88	-0.52	-0.65	-0.62	-0.51	-0.62	0.12
Htb1; Htb2	P02293; P02294	-0.58	-0.53	-0.60	-0.62	-0.57	-0.70	-0.77	-0.71	-0.63	-0.62	0.08
Isc1	P40015	NaN	NaN	NaN	NaN	NaN	-0.63	-0.62	NaN	NaN	-0.63	0.01
Mrp13	P12686	-0.24	-0.46	-0.63	NaN	-0.75	NaN	-0.71	-0.83	-0.43	-0.63	0.21
Rpp2a	P05319	-0.61	-0.58	-0.55	-0.53	-0.64	-0.74	-0.63	-0.65	-0.69	-0.63	0.07
Tsa1	P34760	-0.56	-0.64	-0.64	-0.64	-0.69	-0.59	-0.62	-0.68	-0.62	-0.64	0.04
Gas3	Q03655	-0.67	-0.64	-0.48	-0.34	-0.28	-0.96	-0.60	-0.90	-0.99	-0.64	0.26
Hht1	P61830	-0.81	-0.66	-0.64	-0.72	-0.61	-0.69	-0.59	-0.71	-0.57	-0.66	0.08
Tim9	O74700	-0.66	-0.67	-0.67	-0.65	-0.53	-0.57	-0.72	-0.22	-0.74	-0.66	0.16
Ggc1	P38988	-0.78	-0.72	-0.70	-0.67	-0.67	-0.64	-0.54	-0.55	-0.68	-0.67	0.08
Pmc1	P38929	-0.36	NaN	-0.67	-0.28	-0.10	NaN	-1.10	-1.21	-0.68	-0.67	0.42
Mcd4	P36051	-0.76	-0.61	-0.80	-0.66	-0.49	-0.18	-0.69	-0.85	-0.67	-0.67	0.20
Tim10	P87108	-0.76	-0.66	-0.62	-0.41	-0.68	-0.69	-0.64	-0.68	-0.80	-0.68	0.11
Hho1	P53551	-0.69	-0.61	-0.89	-0.91	NaN	-0.62	NaN	NaN	NaN	-0.69	0.15
Pdi1	P17967	-0.67	-0.69	-0.73	-0.64	-0.70	-0.62	-0.67	-0.70	-0.70	-0.69	0.03
Adk1	P07170	-0.70	-0.60	-0.67	-0.70	-0.71	-0.70	-0.71	-0.66	-0.68	-0.70	0.03
Hem1	P09950	-0.76	-0.89	-0.64	-0.43	-0.70	-0.67	-0.83	-0.71	-0.55	-0.70	0.14
Mrp1	P10662	-0.74	-0.52	-0.29	-0.29	-0.82	-0.67	-0.89	-0.90	NaN	-0.71	0.25
Lys20	P48570	-0.94	-0.97	-0.87	-0.66	-0.42	-0.71	-0.30	-0.82	-0.66	-0.71	0.23
Sap190	P36123	-0.73	-0.71	-0.42	NaN	0.08	NaN	-0.82	-0.93	-0.59	-0.71	0.34
Ynl208w	P40159	-0.71	-0.83	-0.71	-0.66	-0.81	-0.94	-0.69	-0.79	-0.44	-0.71	0.14
Nce102	Q12207	-0.55	-0.75	-0.62	-0.72	-1.36	-0.55	-0.88	-0.97	-0.46	-0.72	0.28
Glt1	Q12680	-0.72	-0.73	-0.78	-0.64	-0.71	-0.83	-0.79	-0.79	-0.72	-0.73	0.06
Scw4	P53334	-0.49	-0.64	-0.75	-0.81	-0.57	-0.83	-1.17	-0.94	-0.37	-0.75	0.24
Ydl124w	Q07551	-0.48	-0.52	-0.79	-0.75	-0.96	-0.45	-0.85	-0.90	-0.57	-0.75	0.19
Gcv2	P49095	-0.78	-0.75	-0.86	-1.05	-0.58	-0.26	-0.73	-0.77	-0.47	-0.75	0.23
Axl2	P38928	NaN	NaN	-0.66	NaN	NaN	NaN	-0.77	-0.79	-0.74	-0.75	0.06
Ynl134c	P53912	-0.60	-0.76	-0.66	-0.57	-0.86	-0.78	-0.92	-0.78	-0.53	-0.76	0.14
Uth1	P36135	-0.65	-0.66	-1.42	-0.87	NaN	-1.03	-0.55	-0.95	-0.32	-0.76	0.34
Ycf1	P39109	-0.55	-0.38	-0.64	-0.77	-0.82	-1.27	-0.81	-0.83	-0.61	-0.77	0.25
Yjr098c	P47139	-0.61	-0.73	-0.67	-0.92	-0.80	NaN	NaN	-0.86	-0.78	-0.78	0.11

Supplementary Table 4. Continued 3.

proteins	protein IDs	*asc1⁻/ASC1*										
		1	2	3	4	5	6	7	8	13	Ø	SD
Ybr085c-A	O43137	-0.63	-0.79	-0.83	-1.15	-1.24	-0.71	-0.92	-0.68	-0.47	-0.79	0.25
Kar2	P16474	-0.72	-0.81	-0.80	-0.79	-0.75	-0.63	-0.76	-0.79	-0.80	-0.79	0.06
Nhp6a	P11632	NaN	-0.79	-0.64	-0.79	NaN	NaN	-0.94	NaN	NaN	-0.79	0.12
Taf5	P38129	NaN	NaN	-1.00	-0.40	-0.64	-0.69	-1.62	-0.90	NaN	-0.79	0.42
Yhm2	Q04013	-0.84	-0.73	-0.84	-0.75	-0.72	-0.85	-0.80	-0.88	-0.72	-0.80	0.06
Dic1	Q06143	NaN	-1.04	-0.80	-1.16	-0.84	NaN	-0.46	-0.33	-0.63	-0.80	0.30
Hxt1	P32465	-0.74	-0.58	-0.68	-0.81	-0.95	-1.02	-1.04	-1.26	-0.57	-0.81	0.23
Agp1	P25376	NaN	-0.84	-1.07	-0.83	-0.81	NaN	-0.48	-0.48	-0.81	-0.81	0.21
Hor2	P40106	-0.83	-0.72	-0.86	-1.10	-0.69	NaN	NaN	NaN	NaN	-0.83	0.16
Psa1	P41940	-0.75	-0.77	-0.86	-0.83	-0.88	-0.86	-0.86	-0.96	-0.84	-0.86	0.06
Var1	P02381	-1.00	NaN	NaN	-0.71	NaN	NaN	-0.87	NaN	NaN	-0.87	0.14
Gph1	P06738	-0.82	-0.87	-1.11	-1.51	-1.19	0.01	-1.07	-0.75	-0.21	-0.87	0.48
Ura4	P20051	-0.74	-0.90	-1.07	-0.87	-0.64	-1.00	-1.06	-0.80	-1.04	-0.90	0.15
Pbi2	P0CT04	-0.86	-0.64	-1.11	-1.22	-1.35	-0.52	-0.90	-1.12	-0.68	-0.90	0.28
Rhr2	P41277	-0.90	-0.99	-0.88	-0.91	-0.93	-1.22	-0.99	-0.91	-0.89	-0.91	0.11
Hxt6[6]	P39003[6]	-0.84	-0.94	-1.21	-1.09	-1.41	0.21	-1.07	-0.91	-0.28	-0.94	0.50
Tos1	P38288	-1.03	-0.81	-0.99	-1.03	NaN	-0.38	-1.06	-0.95	-0.69	-0.97	0.23
Ctp1	P38152	-1.32	-0.97	-0.97	-0.71	-0.81	-1.15	-0.70	-1.04	-0.57	-0.97	0.24
Exg1	P23776	-0.73	-0.90	-0.84	-1.12	-1.04	-1.00	-1.25	-1.16	-0.75	-1.00	0.18
Gsc2	P40989	-1.48	-1.09	-1.12	-0.92	-0.90	-0.13	-1.05	-1.00	-0.55	-1.00	0.38
Tma17	Q12513	NaN	-1.22	-0.98	NaN	NaN	NaN	NaN	NaN	-1.01	-1.01	0.13
Ftr1	P40088	-0.54	0.01	-0.97	-1.18	NaN	NaN	-1.19	NaN	-1.11	-1.04	0.48
Cpr1	P14832	-1.00	-0.94	-0.99	-1.07	-1.19	-1.08	-1.16	-1.12	-0.96	-1.07	0.09
Gre2	Q12068	NaN	NaN	-1.37	-1.19	-0.95	-0.57	-0.87	-1.65	NaN	-1.07	0.39
Sim1	P40472	-0.56	NaN	-1.41	-1.48	NaN	NaN	-1.13	-1.19	-0.85	-1.16	0.35
Mnn1	P39106	-0.97	-0.98	-1.18	-1.34	-1.17	-1.20	-1.05	-1.20	-0.85	-1.17	0.15
Pdr12	Q02785	-1.35	-0.49	-2.21	-1.32	-1.38	NaN	-1.84	-1.26	-0.82	-1.34	0.54
Ura1	P28272	-1.18	-1.37	-1.50	-1.35	-1.16	-1.42	-1.48	-1.22	-1.47	-1.37	0.13
Msc1	Q03104	-1.44	-0.89	-1.67	-0.93	NaN	-0.74	-2.13	-1.96	NaN	-1.44	0.55
Fet3	P38993	-1.26	-1.06	-0.82	-1.17	-1.45	-2.12	-1.59	-1.90	-1.65	-1.45	0.41
Cpa1	P07258	-1.87	NaN	-1.79	-1.50	NaN	NaN	NaN	NaN	-1.78	-1.78	0.16
Rib4	P50861	-1.64	-1.94	-1.84	-1.72	-1.58	-1.81	-1.98	-1.64	-2.03	-1.81	0.16
Ynr034w-A	Q3E841	NaN	-1.97	-2.69	NaN	-1.74	NaN	-1.58	NaN	NaN	-1.86	0.49
Mdh2	P22133	-2.03	-2.53	-3.29	-1.89	-1.34	-1.52	NaN	-1.95	-2.14	-1.99	0.61
Ctt1	P06115	-1.93	-1.57	-2.35	-2.00	-2.53	-1.08	-2.03	-2.55	-0.90	-2.00	0.59
Ygp1	P38616	-2.01	-1.14	-3.27	-3.16	NaN	NaN	-1.16	-2.17	NaN	-2.09	0.93
Hsp12	P22943	-3.06	-2.08	-2.41	-3.07	-3.79	-1.68	-3.96	NaN	NaN	-3.06	0.85
Asc1	P38011	-9.32	-10.8	-8.51	-8.96	-3.51	-3.63	-3.60	-4.19	-4.62	-4.62	2.97

[1]Ty1a-Pr1;Ty1a-A;Ty1a-Dr4;Ty1a-Jr2;Ty1a-Nl2;P0CX58;P0CX57;O74302;P47099;Q12470
[2]Ty2b-C;Ty2b-Gr2;Ty2b-F;Ty2b-Dr2;P25384;P0CX64;P0CX63;Q03494
[3]Ty1b-Er1;Ty1b-Ml2;Ty1b-Ol;Ty1b-Jr1;Ty1b-A;Q03612;Q03434;Q12273;P47098;O13527
[4]Ty1a-Pl;Ty1a-Lr2;Ty1a-Er1;Ty1a-Dr6;Ty1a-Pr3;Ty1a-Gr1;Ty1a-Ml2;Ty1a-Lr3;Ty1a-Jr1;Ty1a-Lr4;
Ty1a-Gr2;Ty1a-Ol;P0CX73;P0CX72;P0CX71;P0CX70;Q6Q5H1;Q12085;P0CX76;P0CX75;P0CX74;
P0C2I8;Q12485;Q92392;Q12391
[5]Ty2b-Gr1;Ty2b-Lr1;Ty2b-Dr1;Ty2b-Or2;Q12337;P0C2J3;Q12472;Q12501;P0C2J2
[6] Hxt7,P39004;Hxt10,P43581;Hxt12,P40441;Hxt13,P39924;Hxt17,P53631;Gal2,P13181

Supplementary Table 5. SILAC-based proteome data for the comparison of the *asc1*DE strain and the *ASC1* wild-type strain.
The table lists the two proteins with a median *asc1*DE/*ASC1* $\log_2$ SILAC-ratio ≥ 0.58 and a p-value < 0.01 (no protein with a median *asc1*DE/*ASC1* $\log_2$ SILAC-ratio ≤ -0.58 was identified). Proteins with this SILAC-ratio > 0.26 or < -0.26 are not shown). The replicates are numbered 9-13 according to Figure 21. (Ø = median of protein SILAC-ratios; SD = standard deviation; gray/NaN = not a number)

proteins	protein IDs	*asc1*DE/*ASC1*						
		9	10	11	12	13	Ø	SD
Ty1a[1]	P0CX73[1]	0.72	0.63	NaN	NaN	0.73	0.72	0.05
Nup57	P48837	0.35	NaN	0.60	0.58	0.58	0.58	0.12

*Ty1a-Pl;Ty1a-Lr2;Ty1a-Er1;Ty1a-Dr6;Ty1a-Pr3;Ty1a-Gr1;Ty1a-Ml2;Ty1a-Lr3;Ty1a-Jr1;
Ty1a-Lr4;Ty1a-Gr2;Ty1a-Ol
P0CX73;P0CX72;P0CX71;P0CX70;Q6Q5H1;Q12085;P0CX76;P0CX75;P0CX74;P0C2I8;Q12485;
Q92392;Q12391

Supplementary Table 6. SILAC-based proteome data for the comparison of the *asc1*^{T143A} strain and the *ASC1* wild-type strain.
The table lists the protein that fulfilled the criteria of the two-sample *t*-test (see Supplementary Table 2) and had a A-Aux $\log_2$ SILAC-ratio > 0.26. The replicates are numbered 1-3 and 4, 8, and 12 according to Figure 21. (Ø = mean of protein SILAC-ratios for A and Aux; A = *asc1*^{T143A}/*ASC1*; Aux = *ASC1*^{Aux}/*ASC1*; A-Aux = Ø of A minus Ø of Aux; SD = standard deviation; gray/NaN = not a number)

protein	protein ID	*asc1*^{T143A}/*ASC1*			*ASC1*^{Aux}/*ASC1*			A		Aux		A - Aux
		1	2	3	4	8	12	Ø	SD	Ø	SD	
Cox20	Q04935	NaN	0.19	0.22	NaN	-0.15	-0.15	0.20	0.02	-0.15	0.00	0.35

Supplementary Table 7. SILAC-based proteome data for the comparison of the *asc1*^{T143E} strain and the *ASC1* wild-type strain.
The table lists the proteins that fulfilled the criteria of the two-sample *t*-test (see Supplementary Table 2) and had a E-Aux $\log_2$ SILAC-ratio < -0.26 or > 0.26. The replicates are numbered 5-6 and 4, 8, and 12 according to Figure 21. (Ø = mean of protein SILAC-ratios for E and Aux; E = *asc1*^{T143E}/*ASC1*; Aux = *ASC1*^{Aux}/*ASC1*; E-Aux = Ø of E minus Ø of Aux; SD = standard deviation; gray/NaN = not a number)

proteins	protein IDs	*asc1*^{T143E}/*ASC1*			*ASC1*^{Aux}/*ASC1*			E		Aux		E - Aux
		5	6	7	4	8	12	Ø	SD	Ø	SD	
Rcl1	Q08096	NaN	0.07	0.04	-0.26	NaN	-0.29	0.06	0.02	-0.28	0.02	0.34
Aha1	Q12449	0.11	0.09	0.10	-0.18	-0.20	-0.11	0.10	0.01	-0.17	0.05	0.26
Efg1	Q3E705	-0.02	-0.02	NaN	0.24	0.32	0.24	-0.02	0.00	0.27	0.05	-0.29
Rvb2	Q12464	-0.17	-0.12	-0.14	0.18	0.10	0.18	-0.15	0.02	0.15	0.05	-0.30

Supplementary Table 8. SILAC-based proteome data *asc1*^{T143E}DE versus *ASC1* wild-type.
The table lists the proteins that fulfilled the criteria of the two-sample *t*-test (see Supplementary Table 2) and had a mean ^{E}DE-Aux $\log_2$ SILAC-ratio ≤ -0.58 or ≥ 0.58. Proteins with this SILAC-ratio < -0.26 or > 0.26 are not shown. The replicates are numbered 9-11 and 4, 8, and 12 according to Figure 21. (Ø = mean of protein SILAC-ratios for ^{E}DE and Aux; ^{E}DE = *asc1*^{T143E}DE/*ASC1*; Aux = *ASC1*^{Aux}/*ASC1*; ^{E}DE-Aux = Ø of ^{E}DE minus Ø of Aux; SD = standard deviation; gray/NaN = not a number)

proteins	protein IDs	*asc1*^{T143E}DE/*ASC1*			*ASC1*^{Aux}/*ASC1*			^{E}DE		Aux		^{E}DE -Aux
		9	10	11	4	8	12	Ø	SD	Ø	SD	
Nce103	P53615	0.57	0.85	0.81	-0.46	-0.43	-0.13	0.74	0.15	-0.34	0.18	1.08
Ty1b[1]	Q03612[1]	0.82	1.14	1.12	-0.11	0.13	-0.15	1.03	0.18	-0.05	0.15	1.07
Yhb1	P39676	0.88	0.73	0.68	-0.05	-0.29	-0.35	0.76	0.10	-0.23	0.16	0.99
Hbn1	Q96VH4	0.65	0.64	0.35	-0.16	-0.39	-0.55	0.55	0.17	-0.37	0.19	0.91
Hsp82	P02829	0.84	0.98	0.85	0.10	-0.13	0.12	0.89	0.08	0.03	0.14	0.86
Aap1	P37898	0.62	0.68	0.62	-0.02	-0.07	-0.13	0.64	0.03	-0.07	0.06	0.71
Ygl039w	P53183	0.50	0.18	0.58	-0.30	-0.16	-0.28	0.42	0.21	-0.25	0.07	0.67
Car1	P00812	0.53	0.73	0.68	0.07	0.06	-0.14	0.65	0.10	0.00	0.12	0.65
Ych1	P42937	0.44	0.35	0.43	-0.43	-0.19	-0.01	0.41	0.05	-0.21	0.21	0.62
Gly1	P37303	0.49	0.62	0.74	0.02	0.16	-0.12	0.62	0.12	0.02	0.14	0.60
Cpa2	P03965	0.49	0.57	0.58	-0.10	0.06	-0.10	0.55	0.05	-0.05	0.09	0.59
Sui1	P32911	0.62	0.66	0.67	0.03	0.18	-0.04	0.65	0.03	0.06	0.11	0.59
Arg1	P22768	0.92	0.83	0.97	0.26	0.47	0.23	0.91	0.07	0.32	0.13	0.59
Scw10	Q04951	-1.00	-0.77	-0.95	-0.34	-0.30	0.05	-0.91	0.12	-0.20	0.21	-0.71
Gsc2	P40989	-0.74	-0.83	-0.91	-0.07	-0.26	0.10	-0.83	0.08	-0.08	0.18	-0.75
Mnn1	P39106	-0.80	-0.62	-0.73	0.14	-0.01	0.12	-0.72	0.09	0.08	0.08	-0.80
Ura4	P20051	-0.80	-0.87	-0.86	0.02	-0.02	-0.04	-0.84	0.04	-0.01	0.03	-0.83
Ura1	P28272	-0.80	-0.90	-0.94	0.18	-0.04	0.16	-0.88	0.07	0.10	0.12	-0.98
Rib4	P50861	-1.04	-1.12	-1.03	0.10	0.04	-0.04	-1.07	0.04	0.03	0.07	-1.10
Arp7	Q12406	-1.65	-1.45	NaN	0.17	0.15	-0.06	-1.55	0.14	0.09	0.13	-1.64

[1]Ty1b-Er1;Ty1b-Ml2;Ty1b-Ol;Ty1b-Jr1;Ty1b-A
Q03612;Q03434;Q12273;P47098;O13527

Supplementary Table 9. SILAC-based phospho-proteome data for the comparison of the *asc1*$^-$ strain and the *ASC1* wild-type strain.
The table lists the proteins with a proteome-corrected phospho-peptide $\log_2$ *asc1*$^-$/*ASC1* SILAC-ratio (diff. phos-prot) > 0.26 or < -0.26 and a p-value < 0.01 in the two-sample *t*-test (Supplementary Table 2). The replicates are numbered 1-8, and 13 according to Figure 21. (Ø = median; SD = standard deviation; difference (diff.) phos-prot = Ø phospho-peptide (phos) minus Ø protein ratio (prot); positon = phosphorylated amino acid residue, printed in italic = site was previously unknown; loc. prob. = localization probability; gray/NaN = not a number; multiplicity = number of phospho-sites per peptide)

proteins	protein IDs	*asc1*$^-$/*ASC1* phospho-peptides 1 2 3 4 5 6 7 8 13	*asc1*$^-$/*ASC1* proteins 1 2 3 4 5 6 7 8 13	phos-peptides Ø	phos-peptides SD	proteins Ø	proteins SD	diff. phos-prot	position	multiplicity	loc. prob.
Tpi1	P00942			1.19	0.20	-0.28	0.04	1.47	S 215	1	1.00
Csr1	Q06705			1.31	0.22	-0.14	0.17	1.45	S 2	1	1.00
Pre8	P23639			1.44	0.17	0.28	0.04	1.16	*S 15*	1	1.00
Rpn7	Q06103			1.27	0.20	0.15	0.05	1.11	*S 196*	1	1.00
Isc1	P40015			0.33	0.01	-0.63	0.01	0.95	*T 361*	1	1.00
Rpl12a; Rpl12b	P0CX53; P0CX54			0.74	0.34	-0.19	0.05	0.93	S 38	1	1.00
Ste20	Q03497			0.56	0.47	-0.34	0.33	0.90	T 572	1	0.61
Pin4	P34217			0.69	0.25	-0.17	0.15	0.87	S 194	1	1.00
Ste20	Q03497			0.48	0.17	-0.34	0.33	0.82	S 169	1	1.00
Imh1	Q06704			0.41	0.18	-0.40	0.18	0.81	*T 304*	1	0.65
Acm1	Q08981			0.60	0.17	-0.20	0.08	0.80	S 48	1	1.00
Imh1	Q06704			0.32	0.08	-0.40	0.18	0.72	S 308	1	0.98
Smi1	P32566			0.49	0.53	-0.22	0.12	0.72	S 389	1	0.92
Iml2	P47031			0.39	0.26	-0.31	0.18	0.70	S 7	1	1.00
Kri1	P42846			0.68	0.01	0.00	0.21	0.68	Y 482	1	0.63
Rlp7	P40693			0.73	0.23	0.06	0.12	0.67	T 120	1	1.00
Rpn1	P38764			0.83	0.18	0.16	0.04	0.67	S 19	1	1.00
Tif1	P10081			0.68	0.24	0.01	0.03	0.67	S 2	1	1.00
Acc1	Q00955			0.11	0.22	-0.55	0.09	0.66	*S 9*	1	0.87
Fyv8	P46949			0.68	0.01	0.03	0.11	0.65	S 441	1	0.99
Rpo21	P04050			0.42	0.09	-0.22	0.08	0.64	T 1471	1	0.93
Imh1	Q06704			0.24	0.14	-0.40	0.18	0.64	S 827	1	0.52
Ste20	Q03497			0.30	0.20	-0.34	0.33	0.63	S 502	1	1.00
Myo3	P36006			0.86	0.12	0.24	0.46	0.62	S 357	1	1.00
Pda1	P16387			0.51	0.28	-0.11	0.05	0.62	S 313	1	1.00
Pdr16	P53860			0.50	0.14	-0.11	0.12	0.61	S 349	2	0.69
Pdr16	P53860			0.50	0.18	-0.11	0.12	0.61	S 346	2	0.97
Leu1	P07264			0.77	0.24	0.21	0.05	0.56	T 494	2	0.76
Sec3	P33332			0.35	0.20	-0.22	0.11	0.56	S 256	1	1.00
Yak1	P14680			0.29	0.40	-0.26	0.09	0.55	T 288	1	1.00
Pdr16	P53860			0.43	0.13	-0.11	0.12	0.55	S 346	1	0.97
Hrb1	P38922			0.37	0.07	-0.18	0.19	0.54	S 338	1	0.89
Crp1	P38845			0.76	0.24	0.23	0.13	0.53	S 440	1	0.96
Hrb1	P38922			0.33	0.26	-0.18	0.19	0.50	S 343	1	0.62
Yef3	P16521			0.52	0.28	0.02	0.04	0.50	S 642	1	0.91
Rcn2	Q12044			1.42	0.11	0.92	0.08	0.50	S 104	1	0.76
Kri1	P42846			0.49	0.09	0.00	0.21	0.49	S 486	1	1.00
Rcn2	Q12044			1.41	0.15	0.92	0.08	0.48	S 160	1	0.99
Cmd1	P06787			0.83	0.46	0.35	0.08	0.48	S 82	1	1.00

Supplementary Table 9. Continued 1.

proteins	protein IDs	*asc1*⁻/*ASC1* phospho-peptides 1 2 3 4 5 6 7 8 13	*asc1*⁻/*ASC1* proteins 1 2 3 4 5 6 7 8 13	phos-peptides Ø	phos-peptides SD	proteins Ø	proteins SD	diff. phos-prot	position	multiplicity	loc. prob.
Gea2	P39993			0.07	0.22	-0.41	0.14	0.48	S 284	1	1.00
Pho13	P19881			0.78	0.25	0.31	0.11	0.47	T 198	1	0.93
Rcn2	Q12044			1.39	0.30	0.92	0.08	0.47	T 105	1	0.89
Akr1	P39010			0.42	0.21	-0.04	0.16	0.46	S 51	1	1.00
Bcp1	Q06338			0.76	0.22	0.30	0.10	0.46	T 205	1	1.00
Sla2	P33338			0.76	0.33	0.30	0.05	0.46	T 294	2	0.87
Rcn2	Q12044			1.38	0.14	0.92	0.08	0.46	S 102	1	0.80
Erb1	Q04660			0.55	0.32	0.09	0.06	0.46	S 418	1	1.00
Pho13	P19881			0.76	0.23	0.31	0.11	0.45	S 197	1	0.94
Rps0a; Rps0b	P32905; P46654			0.32	0.23	-0.13	0.10	0.45	*T 6;6*	1	0.60
Rpg1	P38249			0.59	0.13	0.14	0.04	0.44	S 508	1	1.00
Nop12	Q08208			0.49	0.24	0.05	0.13	0.44	S 70	1	0.97
Gly1	P37303			1.27	0.30	0.85	0.09	0.42	S 367	1	0.79
Gly1	P37303			1.27	0.21	0.85	0.09	0.42	S 369	1	1.00
Spa2	P23201			0.42	0.24	0.01	0.12	0.42	S 1080	1	1.00
Sec3	P33332			0.19	0.12	-0.22	0.11	0.41	S 254	1	0.95
Ski2	P35207			0.87	0.09	0.46	0.13	0.41	*S 2*	1	1.00
Tif5	P38431			0.45	0.12	0.05	0.12	0.40	S 184	1	0.70
Leo1	P38439			0.33	0.15	-0.08	0.12	0.40	S 132	1	1.00
Shm2	P37291			0.93	0.17	0.54	0.10	0.39	S 26	1	1.00
Guk1	P15454			0.12	0.34	-0.28	0.05	0.39	S 149	1	1.00
Met6	P05694			0.25	0.25	-0.14	0.06	0.39	*S 675*	1	1.00
Crp1	P38845			0.62	0.07	0.23	0.13	0.38	S 153	1	0.66
Gcd6	P32501			0.38	0.12	0.00	0.16	0.38	S 538	1	1.00
Mkt1	P40850			0.37	0.18	-0.01	0.08	0.38	S 362	1	0.97
Tif35	Q04067			0.52	0.33	0.14	0.08	0.38	S 2	1	1.00
Rpl13a; Rpl13b	Q12690; P40212			0.26	0.32	-0.12	0.06	0.38	T 15	1	1.00
Ent2	Q05785			0.63	0.15	0.25	0.28	0.37	S 167	1	1.00
Leu1	P07264			0.58	0.15	0.21	0.05	0.37	S 488	2	1.00
Sup35	P05453			0.61	0.10	0.24	0.07	0.36	T 570	1	0.89
Not3	P06102			0.27	0.19	-0.09	0.14	0.36	S 322	1	0.79
Srp14	P38985			0.38	0.06	0.02	0.12	0.36	S 8	1	1.00
Vps13	Q07878			0.45	0.28	0.10	0.10	0.35	S 1731	1	0.99
Shp1	P34223			0.36	0.35	0.01	0.15	0.35	S 322	1	0.92
Kap123	P40069			0.25	0.04	-0.11	0.02	0.35	S 646	1	1.00
Sub2	Q07478			0.11	0.24	-0.24	0.06	0.35	*S 2*	2	1.00
Spa2	P23201			0.35	0.42	0.01	0.12	0.35	S 961	1	1.00
Apl5	Q08951			0.20	0.12	-0.15	0.16	0.35	S 888	1	1.00
Rfa2	P26754			0.43	0.17	0.08	0.15	0.35	S 122	1	1.00
Mak5	P38112			0.28	0.20	-0.07	0.14	0.35	S 678	1	1.00
Pdr5	P33302			0.31	0.13	-0.04	0.23	0.35	S 840	1	0.87
Ser1	P33330			0.86	0.26	0.52	0.09	0.35	T 20	1	1.00
Smc4	Q12267			0.24	0.19	-0.10	0.13	0.34	S 128	1	1.00
Kin28	P06242			0.27	0.19	-0.06	0.19	0.33	T 162	1	0.98
Acc1	Q00955			-0.22	0.14	-0.55	0.09	0.33	*S 10*	1	1.00

Supplementary Table 9. Continued 2.

proteins	protein IDs	*asc1*⁻/*ASC1* phospho-peptides 1 2 3 4 5 6 7 8 13	*asc1*⁻/*ASC1* proteins 1 2 3 4 5 6 7 8 13	phos-peptides Ø	phos-peptides SD	proteins Ø	proteins SD	diff. phos-prot	position	multiplicity	loc. prob.
Ssz1	P38788			0.50	0.21	0.17	0.04	0.32	S 480	1	1.00
Ils1	P09436			0.37	0.14	0.05	0.04	0.32	*S 4*	1	0.93
Prt1	P06103			0.42	0.19	0.10	0.03	0.32	S 61	1	1.00
Cdc37	P06101			0.50	0.21	0.18	0.12	0.32	S 17	2	1.00
Cdc37	P06101			0.50	0.21	0.18	0.12	0.32	S 14	2	1.00
Sec16	P48415			0.28	0.13	-0.03	0.11	0.31	T 808	1	0.77
Leu1	P07264			0.52	0.25	0.21	0.05	0.31	S 495	2	1.00
Pdc1	P06169			0.13	0.31	-0.17	0.02	0.30	S 196	1	0.90
Nop12	Q08208			0.35	0.09	0.05	0.13	0.30	S 184	1	1.00
Vps13	Q07878			0.40	0.14	0.10	0.10	0.30	S 1715	1	1.00
Rpn1	P38764			0.46	0.13	0.16	0.04	0.30	S 647	1	0.81
Tan1	P53072			0.52	0.19	0.22	0.21	0.30	S 72	1	1.00
Myo3; Myo5	P36006; Q04439			0.27	0.10	-0.03	0.26	0.30	S 777	1	1.00
Isw1	P38144			0.26	0.08	-0.04	0.14	0.29	S 175	1	0.99
Sec16	P48415			0.26	0.17	-0.03	0.11	0.29	S 607	1	1.00
Sup35	P05453			0.53	0.20	0.24	0.07	0.29	S 571	1	0.92
Spn1	Q06505			0.02	0.13	-0.27	0.13	0.28	S 89	1	1.00
Sec7	P11075			0.12	0.02	-0.16	0.09	0.28	Y 1221	1	0.78
Sub2	Q07478			0.04	0.24	-0.24	0.06	0.28	S 13	2	1.00
Nop12	Q08208			0.32	0.18	0.05	0.13	0.28	T 181	1	0.95
Vtc2	P43585			0.57	0.14	0.30	0.19	0.27	S 657	1	1.00
Rps0a; Rps0b	P32905; P46654			0.13	0.14	-0.13	0.10	0.27	S 2;2	1	0.99
Ser33	P40510			-0.37	0.29	-0.10	0.12	-0.27	S 29	2	0.96
Met5	P47169			-0.34	0.27	-0.06	0.04	-0.28	S 903	1	1.00
Gpd2	P41911			-0.40	0.20	-0.12	0.13	-0.28	S 75	1	1.00
Ser33	P40510			-0.39	0.12	-0.10	0.12	-0.29	T 31	2	0.97
Get2	P40056			0.01	0.16	0.31	0.14	-0.30	T 55	1	0.64
Ser33	P40510			-0.39	0.26	-0.10	0.12	-0.30	S 22	2	0.99
Rpn13	O13563			-0.02	0.13	0.28	0.11	-0.30	S 135	1	1.00
Gpm1	P00950			-0.63	0.29	-0.33	0.04	-0.31	S 127	1	0.76
Vps13	Q07878			-0.21	0.13	0.10	0.10	-0.31	S 1362	1	0.90
Qri1	P43123			0.04	0.17	0.36	0.11	-0.32	*S 218*	1	1.00
Tdh1; Tdh2; Tdh3	P00360; P00358; P00359			-0.26	0.09	0.06	0.29	-0.32	T 209	1	0.82
Chd1	P32657			-0.43	0.28	-0.10	0.18	-0.32	S 1336	1	0.85
Spa2	P23201			-0.32	0.17	0.01	0.12	-0.33	S 254	1	1.00
Fen1	P25358			-0.34	0.17	-0.01	0.08	-0.33	S 338	1	1.00
Gea2	P39993			-0.74	0.17	-0.41	0.14	-0.33	*S 315*	1	0.97
Hxt1; Hxt3; Hxt9; Hxt11	P32465; P32466; P40885; P54862			-0.81	0.17	-0.46	0.10	-0.35	S 3	1	0.99
Thr4	P16120			-0.14	0.27	0.21	0.02	-0.35	*S 411*	2	0.81
Thr4	P16120			-0.14	0.27	0.21	0.02	-0.35	S 410	2	0.81
Bcy1	P07278			-0.31	0.30	0.04	0.10	-0.35	S 145	1	0.92

Supplementary Table 9. Continued 3.

proteins	protein IDs	*asc1*⁻/*ASC1* phospho-peptides 1 2 3 4 5 6 7 8 13	*asc1*⁻/*ASC1* proteins 1 2 3 4 5 6 7 8 13	phos-peptides Ø	phos-peptides SD	proteins Ø	proteins SD	diff. phos-prot	position	multiplicity	loc. prob.
Fen1	P25358			-0.37	0.20	-0.01	0.08	-0.36	T 334	1	1.00
Sfk1	P35735			0.00	0.25	0.36	0.13	-0.36	*T 124*	1	0.94
Prt1	P06103			-0.26	0.07	0.10	0.03	-0.37	*S 187*	1	0.68
Eno1; Eno2	P00924; P00925			-0.09	0.16	0.28	0.11	-0.37	S 10	1	1.00
Vtc2	P43585			-0.08	0.06	0.30	0.19	-0.38	S 193	2	0.85
Met6	P05694			-0.52	0.16	-0.14	0.06	-0.38	*S 446*	1	0.99
Aro4	P32449			-0.24	0.23	0.15	0.11	-0.39	S 4	1	0.98
Ett1	Q08421			-0.38	0.26	0.02	0.18	-0.40	*S 41*	1	0.98
Ypr091c	Q06833			-0.89	0.14	-0.49	0.24	-0.40	S 669	1	1.00
Ser33	P40510			-0.50	0.24	-0.10	0.12	-0.40	S 2	1	1.00
Psk1	P31374			-0.48	0.23	-0.07	0.14	-0.41	S 1020	1	0.99
Vas1	P07806			-0.38	0.40	0.03	0.02	-0.41	S 294	1	1.00
Spc110	P32380			-0.36	0.14	0.05	0.20	-0.41	S 80	1	1.00
Gpd2	P41911			-0.55	0.01	-0.12	0.13	-0.43	S 72	2	1.00
Hom3	P10869			-0.27	0.34	0.16	0.07	-0.43	T 333	1	0.99
Aro8	P53090			0.24	0.54	0.67	0.04	-0.43	*S 14*	1	0.53
Sui3	P09064			-0.27	0.13	0.17	0.12	-0.44	T 116	2	1.00
Sec31	P38968			-0.40	0.27	0.04	0.07	-0.44	S 999	1	1.00
Reb1	P21538			-0.49	0.26	-0.04	0.26	-0.45	S 355	1	0.81
Ncl1	P38205			-0.69	0.70	-0.22	0.06	-0.47	S 424	1	0.98
Pkh3	Q03306			-0.41	0.09	0.06	0.05	-0.47	S 684	1	0.81
Vtc2	P43585			-0.19	0.07	0.30	0.19	-0.49	S 196	2	1.00
Pbp1	P53297			-0.49	0.23	0.00	0.13	-0.49	S 106	1	0.99
Rpl7a; Rpl7b	P05737; Q12213			-0.56	0.25	-0.07	0.03	-0.49	T 8;8	1	1.00
Cys3	P31373			0.11	0.32	0.61	0.06	-0.50	S 40	1	0.97
Ty1b[1]	P0C2I7[1]			0.61	0.24	1.11	0.21	-0.50	*T 583*[1]	1	0.56
Mlp1	Q02455			-0.69	0.22	-0.18	0.18	-0.51	T 337	1	1.00
Vip1	Q06685			-0.28	0.18	0.23	0.21	-0.51	S 31	1	0.98
Hom6	P31116			-0.35	0.21	0.17	0.02	-0.52	*S 240*	1	0.74
Sui3	P09064			-0.35	0.47	0.17	0.12	-0.52	S 112	2	0.96
Gpd2	P41911			-0.65	0.25	-0.12	0.13	-0.53	S 75	2	1.00
Esc1	Q03661			-0.66	0.33	-0.13	0.12	-0.53	S 532	1	1.00
Rps1a; Rps1b	P33442; P23248			-0.49	0.26	0.04	0.06	-0.53	S 236	1	1.00
Rpl7a; Rpl7b	P05737; Q12213			-0.61	0.05	-0.07	0.03	-0.54	T 8;8	2	1.00
Rpl7a; Rpl7b	P05737; Q12213			-0.61	0.05	-0.07	0.03	-0.54	S 11	2	1.00
Pdr1	P12383			-0.71	0.33	-0.17	0.08	-0.54	S 942	1	0.81
Cdc3	P32457			-0.31	0.40	0.24	0.08	-0.54	S 77	1	0.93
Ncl1	P38205			-0.77	0.21	-0.22	0.06	-0.55	S 423	1	0.90
Cho1	P08456			-0.41	0.14	0.14	0.18	-0.55	S 50	2	0.95
Cho1	P08456			-0.41	0.21	0.14	0.18	-0.55	S 47	2	1.00
Cho1	P08456			-0.41	0.22	0.14	0.18	-0.55	S 46	2	1.00
Pbp1	P53297			-0.56	0.12	0.00	0.13	-0.55	*S 104*	1	0.99

Supplementary Table 9. Continued 4.

proteins	protein IDs	*asc1⁻/ASC1* phospho-peptides 1 2 3 4 5 6 7 8 13	*asc1⁻/ASC1* proteins 1 2 3 4 5 6 7 8 13	phos-peptides Ø	phos-peptides SD	proteins Ø	proteins SD	diff. phos-prot	position	multiplicity	loc. prob.
Pfy1	P07274			-0.56	0.22	0.00	0.09	-0.56	S 2	1	1.00
Ent2	Q05785			-0.31	0.13	0.25	0.28	-0.56	S 173	1	0.88
Zeo1	Q08245			-0.73	0.36	-0.16	0.09	-0.56	T 49	1	1.00
Apa1	P16550			-0.53	0.19	0.03	0.07	-0.56	T 60	1	1.00
Gpm1	P00950			-0.90	0.34	-0.33	0.04	-0.57	S 128	1	0.80
Acc1	Q00955			-1.14	0.27	-0.55	0.09	-0.59	S 1157	1	1.00
Hom3	P10869			-0.44	0.21	0.16	0.07	-0.59	S 332	1	0.94
Tsa1	P34760			-1.23	0.03	-0.64	0.04	-0.60	T 174	1	1.00
Sod1	P00445			-0.81	0.15	-0.19	0.09	-0.62	S 39	1	1.00
Ura2	P07259			-1.20	0.28	-0.57	0.06	-0.62	T 1859	1	0.77
Pup2	P32379			-0.34	0.20	0.31	0.04	-0.65	S 56	1	0.89
Prr1	P28708			-0.51	0.22	0.14	0.18	-0.65	S 132	1	1.00
Rps19a; Rps19b	P07280; P07281			-0.71	0.36	-0.06	0.05	-0.65	S 117	1	1.00
Ssd1	P24276			-0.71	0.12	-0.06	0.14	-0.65	S 231	1	0.96
Trm2	P33753			-0.62	0.17	0.04	0.13	-0.66	*S 98*	1	0.95
Rad16	P31244			-0.67	0.22	-0.01	0.23	-0.66	S 25	1	1.00
Sec21	P32074			-0.82	0.27	-0.15	0.07	-0.67	T 638	1	1.00
Trm2	P33753			-0.63	0.11	0.04	0.13	-0.68	S 92	1	0.95
Rsc2	Q06488			-1.02	0.25	-0.34	0.22	-0.68	S 682	1	1.00
Abp1	P15891			0.08	0.52	0.78	0.16	-0.70	S 167	1	0.94
Ent3	P47160			-0.43	0.34	0.27	0.13	-0.70	*S 2*	1	1.00
Rad16	P31244			-0.74	0.47	-0.01	0.23	-0.73	*S 78*	1	0.99
Vps1	P21576			-0.48	0.20	0.26	0.07	-0.73	S 599	1	1.00
Rps7b	P48164			-0.47	0.41	0.27	0.05	-0.74	S 31	1	0.87
Trm2	P33753			-0.69	0.02	0.04	0.13	-0.74	T 96	1	0.87
Trm2	P33753			-0.70	0.29	0.04	0.13	-0.74	S 93	1	0.97
Gpd2	P41911			-0.89	0.19	-0.12	0.13	-0.77	S 70	2	0.97
Orm2	Q06144			-0.37	0.18	0.41	0.14	-0.77	S 9	1	1.00
Pup2	P32379			-0.47	0.19	0.31	0.04	-0.78	T 55	1	0.96
Cdc60	P26637			-0.45	0.34	0.33	0.05	-0.78	T 142	1	1.00
Rps7b	P48164			-0.52	0.20	0.27	0.05	-0.78	*S 30*	1	0.90
Rad9	P14737			-0.37	0.00	0.42	0.07	-0.79	S 494	1	0.81
Sui3	P09064			-0.63	0.30	0.17	0.12	-0.80	T 116	1	1.00
Sum1	P46676			-0.68	0.00	0.12	0.17	-0.80	S 736	1	0.71
Sui3	P09064			-0.63	0.10	0.17	0.12	-0.80	S 118	1	0.69
Yhr020w	P38708			-0.73	0.16	0.09	0.06	-0.82	*T 38*	1	0.50
Yhr020w	P38708			-0.73	0.16	0.09	0.06	-0.82	*S 36*	1	0.50
Zeo1	Q08245			-0.99	0.41	-0.16	0.09	-0.83	T 49	2	1.00
Zeo1	Q08245			-0.99	0.41	-0.16	0.09	-0.83	S 40	2	1.00
Gcs1	P35197			-0.55	0.32	0.29	0.09	-0.85	S 157	1	0.81
Ura2	P07259			-1.43	0.18	-0.57	0.06	-0.86	S 1857	1	0.98
Ty1b[2]	P0C2I7[2]			0.25	0.22	1.11	0.21	-0.86	*S 445*[2]	1	0.67
Def1	P35732			-0.96	0.49	0.00	0.19	-0.95	T 258	1	0.90
Tdh1; Tdh2; Tdh3	P00360; P00358; P00359			-0.94	0.21	0.06	0.29	-1.01	S 201	1	1.00
Gvp36	P40531			-1.06	0.48	-0.04	0.07	-1.03	*S 2*	1	1.00

Supplementary Table 9. Continued 5.

proteins	protein IDs	*asc1*⁻/*ASC1* phospho-peptides 1 2 3 4 5 6 7 8 13	*asc1*⁻/*ASC1* proteins 1 2 3 4 5 6 7 8 13	phos-peptides Ø	phos-peptides SD	proteins Ø	proteins SD	diff. phos-prot	position	multiplicity	loc. prob.
Abp1	P15891			-0.25	0.26	0.78	0.16	-1.03	S 169	1	1.00
Hsp42	Q12329			-0.37	0.19	0.69	0.35	-1.06	S 223	1	0.99
Def1	P35732			-1.08	0.10	0.00	0.19	-1.08	S 260	1	1.00
Tif4632	P39936			-0.97	0.27	0.21	0.12	-1.18	T 196	1	1.00
Bre5	P53741			-1.34	0.45	-0.14	0.24	-1.20	S 282	1	1.00
Grx2	P17695			-1.05	0.45	0.25	0.31	-1.30	S 94	1	0.94
Ctr9	P89105			-1.15	0.11	0.16	0.07	-1.31	S 1017	1	1.00
Puf3	Q07807			-1.03	0.20	0.31	0.11	-1.34	S 86	1	1.00
Ugp1	P32861			-1.26	0.63	0.16	0.15	-1.42	Y 13	1	0.55
Grx2	P17695			-1.17	0.43	0.25	0.31	-1.42	S 91	1	1.00
Cdc28	P00546			-0.76	0.59	0.70	0.14	-1.46	Y 19	1	0.98
Abp1	P15891			-0.76	0.54	0.78	0.16	-1.53	T 181	2	1.00
Abp1	P15891			-0.76	0.54	0.78	0.16	-1.53	S 183	2	1.00
Egd1	Q02642			-3.48	0.07	-0.12	0.12	-3.36	T 151	1	1.00
phospho-peptides with no proteome value											
Edc1	P53080			2.15	0.11	NaN	NaN	NaN	S 82	1	0.99
Rcn1	P36054			0.91	0.21	NaN	NaN	NaN	S 117	2	1.00
Rcn1	P36054			0.91	0.21	NaN	NaN	NaN	S 113	2	1.00
Nte1	Q04958			0.83	0.10	NaN	NaN	NaN	S 634	1	0.99
Ty2a[3]	Q99303[3]			0.81	0.48	NaN	NaN	NaN	*S 424*	1	0.99
Aim3	P38266			0.79	0.21	NaN	NaN	NaN	S 843	1	0.93
Nnk1	P36003			0.70	0.30	NaN	NaN	NaN	Y 739	1	1.00
Pgm3	Q03262			0.69	0.25	NaN	NaN	NaN	*T 156*	1	0.66
Dig2	Q03373			0.64	0.27	NaN	NaN	NaN	T 83	1	0.76
Pgm3	Q03262			0.64	0.27	NaN	NaN	NaN	S 158	1	0.97
Rrp36	Q12481			0.63	0.34	NaN	NaN	NaN	S 14	1	1.00
Dig2	Q03373			0.62	0.19	NaN	NaN	NaN	T 82	1	0.94
Stb1	P42845			0.60	0.36	NaN	NaN	NaN	T 99	1	1.00
Stb1	P42845			0.58	0.36	NaN	NaN	NaN	S 72	1	1.00
Ppq1	P32945			0.58	0.20	NaN	NaN	NaN	S 208	1	0.89
Ysc84	P32793			0.58	0.01	NaN	NaN	NaN	S 301	1	1.00
Gde1	Q02979			0.56	0.09	NaN	NaN	NaN	S 254	1	0.94
Air2	Q12476			0.52	0.17	NaN	NaN	NaN	S 49	1	1.00
Dcn1	Q12395			0.52	0.08	NaN	NaN	NaN	S 12	1	1.00
Rcn1	P36054			0.47	0.13	NaN	NaN	NaN	S 117	1	1.00
She3	P38272			0.46	0.19	NaN	NaN	NaN	S 361	1	1.00
Air2	Q12476			0.43	0.13	NaN	NaN	NaN	T 16	1	0.99
Bud21	Q08492			0.43	0.14	NaN	NaN	NaN	S 144	1	1.00
Pol1	P13382			0.42	0.23	NaN	NaN	NaN	S 170	1	0.95
Kha1	P40309			0.40	0.12	NaN	NaN	NaN	S 557	1	1.00
Pik1	P39104			0.38	0.15	NaN	NaN	NaN	S 236	1	0.96
Fip1	P45976			0.37	0.22	NaN	NaN	NaN	S 15	1	1.00
Ent1	Q12518			0.36	0.26	NaN	NaN	NaN	S 327	1	0.96
She3	P38272			0.35	0.10	NaN	NaN	NaN	S 394	1	0.73
Rho4	Q00246			0.30	0.29	NaN	NaN	NaN	S 58	1	1.00
Sng1	P46950			0.30	0.12	NaN	NaN	NaN	T 91	1	1.00
Vid27	P40157			0.29	0.16	NaN	NaN	NaN	S 222	1	1.00

Supplementary Table 9. Continued 6.

proteins	protein IDs	*asc1*⁻/*ASC1* phospho-peptides 1 2 3 4 5 6 7 8 13	*asc1*⁻/*ASC1* proteins 1 2 3 4 5 6 7 8 13	phos-peptides Ø	phos-peptides SD	proteins Ø	proteins SD	diff. phos-prot	position	multiplicity	loc. prob.
Ypi1	P43587			0.28	0.10	NaN	NaN	NaN	S 131	1	0.73
Bbp1	Q12365			-0.32	0.22	NaN	NaN	NaN	T 7	1	1.00
Taf3	Q12297			-0.32	0.15	NaN	NaN	NaN	S 346	1	0.76
Ecm21	P38167			-0.47	0.13	NaN	NaN	NaN	S 140	1	1.00
Ume6	P39001			-0.50	0.19	NaN	NaN	NaN	S 645	1	1.00
Mdv1	P47025			-0.50	0.23	NaN	NaN	NaN	S 376	1	1.00
Yel043w	P32618			-0.55	0.27	NaN	NaN	NaN	S 802	1	1.00
Yap1	P19880			-0.60	0.32	NaN	NaN	NaN	S 14	1	1.00
Bni1	P41832			-0.62	0.22	NaN	NaN	NaN	S 1889	1	0.99
Sch9	P11792			-0.64	0.12	NaN	NaN	NaN	S 726	1	1.00
Ycr023c	P25351			-0.72	0.16	NaN	NaN	NaN	S 313	1	1.00
Par32	Q12515			-0.75	0.49	NaN	NaN	NaN	S 39	1	1.00
Gat1	P43574			-0.82	0.27	NaN	NaN	NaN	S 262	1	0.98
Vid27	P40157			-0.94	0.30	NaN	NaN	NaN	T 220	2	1.00
Vid27	P40157			-0.94	0.30	NaN	NaN	NaN	S 222	2	1.00
Meh1	Q02205			-0.95	0.31	NaN	NaN	NaN	S 146	1	0.99
Vtc3	Q02725			-0.99	0.28	NaN	NaN	NaN	S 198	1	1.00
Rho5	P53879			-1.03	0.26	NaN	NaN	NaN	S 223	1	1.00
Mnr2	P35724			-1.05	0.17	NaN	NaN	NaN	T 177	1	0.99
Nrg2	P38082			-1.08	0.61	NaN	NaN	NaN	S 100	1	0.77
Kns1	P32350			-1.10	0.51	NaN	NaN	NaN	T 562	1	1.00
Mnr2	P35724			-1.14	0.21	NaN	NaN	NaN	S 152	1	1.00
Nrg2	P38082			-1.64	0.41	NaN	NaN	NaN	*T 99*	1	0.95
Mep2	P41948			-1.67	0.13	NaN	NaN	NaN	*S 460*	1	0.73
Mep2	P41948			-1.70	0.21	NaN	NaN	NaN	T 459	1	0.63
Tpo1	Q07824			-1.71	0.51	NaN	NaN	NaN	S 72	1	1.00
phospho-peptides with one or two proteome value(s)											
Dbf2	P22204			0.51	0.12	0.21		0.30	S 374	1	1.00
Kin82	P25341			0.37	0.10	0.09		0.28	T 499	1	0.76
Dbf20	P32328			-0.12	0.06	0.22		-0.34	S 366	1	1.00
Pct1	P13259			-0.23	0.22	0.15	0.62	-0.38	S 346	1	1.00
Fhl1	P39521			-0.52	0.19	-0.12		-0.40	S 264	1	1.00
Ssn2	P38931			-0.51	0.23	-0.01		-0.50	S 375	1	1.00
Fhl1	P39521			-0.65	0.15	-0.12		-0.53	S 44	1	0.97
Glc8	P41818			-0.21	0.10	0.35		-0.57	S 12	1	1.00
Cue4	Q04201			-0.65	0.41	-0.01		-0.64	S 48	1	1.00
Yjl070c	P40361			-0.48	0.05	0.17		-0.65	S 43	1	1.00
Yjl070c	P40361			-0.50	0.09	0.17		-0.67	S 41	1	0.99
Kin2	P13186			-0.49	0.14	0.38		-0.87	S 549	1	1.00

[1]Ty1b-Lr4;Ty1b-Pr1;Ty1b-Gr2;Ty1b-Pr2;Ty1b-Er1;Ty1b-Ml2;Ty1b-Ol;Ty1b-Jr1;Ty1b-A;Ty1b-Ml1;Ty1b-Pl;Ty1b-Lr2
P0C2I7;P0C2J0;Q03612;Q03434;Q12273;P47098;O13527; *583; 1142; 1143*
[2]Ty1b-Lr4;Ty1b-Pr1;Ty1b-Gr2;Ty1b-Pr2;Ty1b-Er1;Ty1b-Ml2;Ty1b-Ol;Ty1b-Jr1;Ty1b-A;Ty1b-Ml1;Ty1b-Pl;Ty1b-Lr2
P0C2I7;P0C2J0;Q03612;Q03434;Q12273;P47098;O13527; *445; 1004; 1005*
[3]Ty2a-Dr3;Ty2a-C;Ty2a-Or1;Ty2a-Lr2;Ty2a-Gr2;Ty2a-F
Q99303;P25383;Q12439;P0C2J6;P0CX62;P0CX61

Supplementary Table 10. SILAC-based phospho-proteome data for the comparison of the *asc1*^{T143A} strain and the *ASC1* wild-type strain.

The table lists the proteins that fulfilled the criteria described in Supplementary Table 3. The replicates are numbered 1-3 and 4, 8, and 12 according to Figure 21. (A = *asc1*^{T143A}/*ASC1*; Aux = *ASC1*^{Aux}/*ASC1*; Ø = mean of phospho-peptide (PP) and protein (Prot) log_2 SILAC-ratios for A and Aux; A Ø PP - Prot = mean of PP ratios minus mean of Prot ratios for A; Aux Ø PP - Prot = mean of PP ratios minus mean of Prot ratios for Aux; SD = standard deviation, gray = no value determined, position = phosphorylated amino acid residue, multiplicity = number of phosphorylations within the identified phospho-peptide; loc. prob. = localization probability

proteins	protein IDs	A PP 1 2 3	Aux PP 4 8 12	A Prot 1 2 3	Aux Prot 4 8 12	A PP Ø SD	Aux PP Ø SD	A Prot Ø SD	Aux Prot Ø SD	1: A Ø PP-Prot	2: Aux Ø PP-Prot	1-2	position	multiplicity	loc. prob.
Nth1	P32356					0.02 ±0.06	-0.15 ±0.09	-0.27 ±0.16	-0.10 ±0.12	0.29	-0.05	0.34	S 60	1	1.00
Ent3	P47160					-0.20 ±0.03	0.14 ±0.09	-0.07 ±0.06	-0.03 ±0.08	-0.12	0.17	-0.30	S 2	1	1.00
Met17	P06106					-0.24 ±0.02	0.02 ±0.01	0.03 ±0.05	-0.02 ±0.05	-0.27	0.03	-0.30	S 34	1	0.94
Rps1a; Rps1b	P33442; P23248					-0.22 ±0.06	0.20 ±0.10	-0.05 ±0.01	-0.01 ±0.06	-0.17	0.21	-0.38	S 236	1	1.00
Saf1	P38352					0.05 ±0.04	0.44 ±0.02	-0.09 ±0.01	-0.13 ±0.04	0.14	0.56	-0.42	S 16	1	1.00
Sec31	P38968					-0.26 ±0.10	0.25 ±0.27	0.06 ±0.02	-0.02 ±0.11	-0.32	0.27	-0.59	S 980	1	1.00

Supplementary Table 11. SILAC-based phospho-proteome data for the comparison of the *asc1*^{T143E} strain and the *ASC1* wild-type strain.

The table lists the proteins that fulfilled the criteria described in Supplementary Table 3. The replicates are numbered 5-7 and 4, 8, and 12 according to Figure 21. (E = *asc1*^{T143E}/*ASC1*; Aux = *ASC1*^{Aux}/*ASC1*; Ø = mean of phospho-peptide (PP) and protein (Prot) log_2 SILAC-ratios for E and Aux; E Ø PP - Prot = mean of PP ratios minus mean of Prot ratios for E; Aux Ø PP - Prot = mean of PP ratios minus mean of Prot ratios for Aux; SD = standard deviation, gray = no value determined, position = phosphorylated amino acid residue, multiplicity = number of phosphorylations within the identified phospho-peptide; loc. prob. = localization probability

proteins	protein IDs	E PP 5 6 7	Aux PP 4 8 12	E Prot 5 6 7	Aux Prot 4 8 12	E PP Ø SD	Aux PP Ø SD	E Prot Ø SD	Aux Prot Ø SD	1: E Ø PP-Prot	2: Aux Ø PP-Prot	1-2	position	multiplicity	loc. prob.
Sbp1	P10080					1.40 ±0.10	0.29 ±0.25	-0.02 ±0.04	-0.02 ±0.07	1.41	0.32	1.09	T 91	1	1.00
Tif1	P10081					-0.25 ±0.06	0.26 ±0.16	-0.01 ±0.02	0.03 ±0.02	-0.24	0.24	-0.48	S 2	1	1.00
Bmh1; Bmh2	P29311; P34730					-0.20 ±0.02	0.21 ±0.06	0.12 ±0.05	0.01 ±0.10	-0.32	0.20	-0.52	S 104	1	0.95

Supplementary Table 12. Cellular processes affected by Asc1p-dependent phosphorylation.
Proteins containing Asc1p-sensitive phospho-sites were assigned to different cellular processes. Protein names highlighted in green indicate that the proteins contain phospho-sites that are up-regulated in the Asc1p mutant strains, accordingly, red indicates a down-regulation.

mRNA translation	transcription & mRNA fate	protein turnover	traffic & transport	cytokinesis, cytoskeleton & budding	primary metabolism	cell signaling	others
Bud21	Air2	Cdc37	Akr1	Acm1	Csr1	Akr1	Crp1
Erb1	Dig2	Dcn1	Apl5	Aim3	Gde1	Cdc37	Fyv8
Gcd6	Edc1	Pre8	Bcp1	Cmd1	Gly1	Cmd1	Guk1
Ils1	Fip1	Rpn1	Ent1	Ent1	Leu1	Dbf2	Iml2
Kap123	Isw1	Rpn7	Hrb1	Myo3/5	Nth1**	Dig2	Pol1
Kri1	Kin28	Shp1	Imh1	Pin4	Pda1	Isc1	Rfa2
Mak5	Leo1	Vid27°	Kap123	Rho4	Pdc1	Kin28	Smc4
Mkt1	Not3	Bre5	Kha1	Sla2	Pdr16	Kin82	Sng1
Nop12	Rpo21	Cue4	Myo3/5	Smi1	Pgm3	Nnk1	Ty2a^{+}
Rlp7	Ski2	Def1	Pdr5	Ste20	Ser1	Nte1	Grx2
Rpg1	Spn1	Hsp42	Sec16	Ysc84	Shm2	Pho13	Mdv1
Rpl12a/b	Stb1	Pup2	Sec3	Ent2°	Tpi1	Pik1	Par32
Rpl13a/b	Sub2	Rpn13	Sec7	Gea2°	Acc1°	Ppq1	Qri1
Rps0a/b	Chd1	Saf1**	She3	Spa2°	Met6°	Rcn1	Rad16
Rrp36	Ctr9		Sla2	Abp1	Apa1	Rcn2	Sod1
Sbp1**	Fhl1		Ysc84	Bbp1	Aro4	Rho4	Ty1b^{++}
Srp14	Gat1		Ent2°	Bni1	Aro8	Sec3	Ycr023c
Ssz1	Nrg2		Gea2°	Cdc3	Cho1	Shp1	Yjl070c
Sup35	Pdr1		Vps13°	Cdc28	Cys3	Ste20	
Tan1	Puf3		Vtc2°	Ent3*	Eno1/2	Yak1	
Tif35	Reb1		Bmh1/2**	Gcs1	Elo2	Ypi1	
Tif5	Rsc2		Bre5	Gvp36	Gpd2	Spa2°	
Yef3	Ssn2		Ecm21	Hsp42	Gpm1	Bcy1	
Tif1 ↓	Sum1		Ent3*	Pfy1	Hom3	Bmh1/2**	
Prt1°	Taf3		Esc1	Spc110	Hom6	Bni1	
Cdc60	Ume6		Gcs1	Ssd1	Met17**	Cdc28	
Egd1	Yap1		Get2	Vip1	Met5	Dbf20	
Ett1			Gvp36	Vps1	Pct1	Glc8	
Ncl1			Hxt1/3		Ser33	Kin2	
Pbp1			Kin2		Tdh1/2/3	Kns1	
Puf3			Mep2		Thr4	Meh1	
Rpl7a/b			Mlp1		Ugp1	Orm2	
Rps19a/b			Mnr2		Ura2	Pkh3	
Rps1a/b*			Sec21			Prr1	
Rps7b			Sec31*			Psk1	
Ssd1			Tpo1			Rad9	
Sui3			Vps1			Rho5	
Tif4632			Vtc3			Sch9	
Trm2						Sfk1	
Tsa1						Vip1	
Vas1						Yel043w	
Yhr020w						Ypr091c	
						Zeo1	

° also contains an up-regulated Asc1p-sensitive phospho-site
* regulation also found in either the *asc1*^{T143A} or the *asc1*^{T143E} mutant strain
** regulation exclusively found in either the *asc1*^{T143A} or the *asc1*^{T143E} mutant strain
↓ regulated in the opposite direction in the *asc1*^{T143E} strain compared to the *asc1*$^{-}$ strain
$^{+}$ Ty2a-Dr3;Ty2a-C;Ty2a-Or1;Ty2a-Lr2;Ty2a-Gr2;Ty2a-F
$^{++}$ Ty1b-Lr4;Ty1b-Pr1;Ty1b-Gr2;Ty1b-Pr2;Ty1b-Er1;Ty1b-Ml2;Ty1b-Ol;Ty1b-Jr1;Ty1b-A;Ty1b-I1;Ty1b-Pl;Ty1b-Lr2

Supplementary Table 13. Overview of data evaluation of SILAC-based Asc1p-Strep and Asc1DEp-Strep enrichment experiments with *Perseus*.

No.	Command	Description	
1	Generic matrix upload	proteinGroups.txt normalized ratios etc.	
2.1 2.2 2.3	Filter rows based on categorical column	Remove rows with + in reverse column Remove rows with + in potential contaminant column Remove rows with + in only identified by site column	
3	Transform	Inverse ratios (1/x) when the control is not in the denominator	
4	Transform	$\log_2(x)$	
5	Normalization	Subtract column median of ratios	
6	Combine expression columns	Eluate ratios minus respective proteome ratios → proteome-corrected eluate ratios	
7 7.1/4 7.2/5 7.3/6 7.7 7.8	Categorical annotation rows	Group for Asc1p-Strep/control ratios and for Asc1DEp-Strep/control ratios: - proteome-corrected eluate ratios - eluate ratios - proteome ratios Group for two-sample *t*-test: - eluate and proteome Asc1p-Strep/control ratios - eluate and proteome Asc1DEp-Strep/control ratios	
8 8.1 8.2	Two-samples test	Two-sample *t*-test (p-value < 0.05 and p-value < 0.1) eluate versus proteome Asc1p-Strep/control ratios eluate versus proteome Asc1DEp-Strep/control ratios	
9 9.1 9.2	One-sample test	One-sample *t*-test (p-value < 0.05 and p-value < 0.1) eluate ratios Asc1p-Strep eluate ratios Asc1DEp-Strep	
		proteins with 0-1 valid proteome ratio	proteins with 2-3 valid proteome ratios
10	Filter rows based on valid values	2 proteome-corrected eluate ratios, add categorical column	2 proteome-corrected eluate ratios ≥ 0.26
11	Filter rows based on categorical column	Remove rows with *keep* from previous step	-
12	Filter rows based on valid values	1 proteome-corrected eluate ratios < 0.26, add categorical column	
13	Filter rows based on categorical column	Remove rows with *keep* from previous step	
14	Filter rows based on valid values	2 eluate ratios ≥ 0.26	
15	Filter rows based on valid values	1 eluate ratio < 0.26 add categorical column	
16	Filter rows based on categorical column	Remove rows with *keep* from previous step	
17	Select rows manually and remove selected rows	Check remaining candidates manually. Example for removed candidate: Two eluate ratios of a protein that could not be proteome-corrected were ≥ 0.26. For the third replicate, the protein was not detected in the eluate fraction but with a ratio ≥ 0.26 in the proteome indicating unspecific enrichment of the protein in the other samples.	

Supplementary Table 14. Expanded view for the Asc1p-dependent changes in the translatome.
For the transcripts of each of the six samples the normalized readcounts are provided. The mean of these readcounts was calculated as well as the $\log_2$ ratio of these values (*asc1*$^-$*/ASC1*). The logarithmized ratios are colored according to the scale below the table. (FDR = false discovery rate)

gene	*asc1*$^-$*/ ASC1*	normalized readcounts *asc1*$^-$			normalized readcounts *ASC1*			likelihood	FDR
		1	2	3	1	2	3		
COS8	2.68	48	40	47	9	8	4	0.9965	1.7E-03
ZPS1	2.35	494	801	783	174	111	124	0.9973	1.3E-03
PRM5	1.84	268	214	260	78	53	76	0.9981	7.7E-04
HBN1	1.69	290	294	302	74	101	99	0.9995	1.4E-04
GSY1	1.65	286	267	310	98	99	78	0.9994	2.2E-04
HSP42	1.61	226	360	329	89	110	100	0.9916	3.5E-03
HSP26	1.48	67	59	78	31	22	20	0.9160	3.2E-02
YCL021W-A	1.45	138	181	189	62	57	67	0.9909	4.0E-03
GAL3	1.38	110	140	167	54	60	46	0.9595	1.3E-02
YLL053C	1.36	494	411	543	212	201	153	0.9834	5.5E-03
ZRT1	1.35	4059	5193	5339	2244	1731	1744	0.9397	1.8E-02
YKL070W	1.34	78	110	124	40	41	42	0.9268	2.8E-02
FET4	1.32	388	355	388	186	130	137	0.9935	2.6E-03
VTI1	1.27	275	181	236	110	87	89	0.9608	1.2E-02
AHA1	1.26	1459	1381	1438	678	556	548	0.9973	1.1E-03
AQY2	1.22	509	425	431	237	211	136	0.9322	2.4E-02
FKS3	1.22	134	150	162	63	67	62	0.9886	4.5E-03
STI1	1.17	1427	1395	1514	646	608	670	0.9983	6.0E-04
AGA1	1.16	209	294	208	94	107	117	0.9495	1.5E-02
GAL80	1.15	444	382	586	211	215	209	0.9826	5.9E-03
GSY2	1.12	428	427	450	205	189	206	0.9986	4.2E-04
NDJ1	1.07	160	213	251	95	95	107	0.9298	2.5E-02
URA10	1.05	169	137	148	83	60	76	0.9182	3.1E-02
HXK1	1.05	391	346	394	229	164	155	0.9409	1.7E-02
GRX3	1.02	847	882	856	385	416	477	0.9943	2.2E-03
SMA2	1.01	228	297	285	126	122	153	0.9343	2.2E-02
DCS1	1.01	254	238	242	127	123	115	0.9921	3.3E-03
YGR161W-C	1.00	335	337	341	169	172	167	0.9970	1.5E-03
YHB1	0.95	9465	9433	8816	5197	4475	4671	0.9749	8.0E-03
UBC1	0.91	674	818	776	356	416	436	0.9280	2.6E-02
LST8	0.91	429	415	525	267	221	243	0.9278	2.7E-02
ALG13	0.90	281	280	285	149	162	142	0.9891	4.2E-03
HSP78	0.86	462	415	420	266	215	234	0.9564	1.4E-02
APE1	0.84	435	401	409	237	203	256	0.9644	1.2E-02
YMR315W	0.84	942	820	931	508	451	548	0.9340	2.3E-02
FMP41	0.82	507	471	478	286	309	227	0.9207	2.8E-02
GLO2	0.80	578	444	527	292	309	286	0.9352	2.2E-02
GLK1	0.78	2089	2031	2049	1308	1137	1145	0.9392	1.9E-02
TWF1	0.77	356	400	412	232	206	246	0.9140	3.2E-02

Supplementary Table 14. Continued.

gene	*asc1*⁻/*ASC1*	normalized readcounts *asc1*⁻			normalized readcounts *ASC1*			likelihood	FDR
		1	2	3	1	2	3		
MXR1	0.76	719	627	730	427	367	428	0.9046	3.4E-02
SFG1	0.76	446	449	448	290	214	287	0.9011	3.5E-02
ARC18	0.76	335	367	367	208	185	238	0.9075	3.3E-02
YKL151C	0.76	522	478	541	314	291	306	0.9710	8.6E-03
EXG2	0.71	386	371	378	232	252	208	0.9366	2.0E-02
YDR327W	0.70	1080	1115	1213	669	723	710	0.9187	3.0E-02
DFR1	-0.66	249	275	279	418	412	440	0.9357	2.1E-02
HTB1	-0.68	604	705	684	1062	1057	1071	0.9396	1.8E-02
FAA2	-0.75	116	136	136	214	224	215	0.9290	2.5E-02
HO	-0.75	443	449	487	763	745	813	0.9699	1.0E-02
TDA1	-0.91	112	122	109	199	214	230	0.9708	9.1E-03
YHR177W	-0.93	71	63	81	125	142	144	0.9188	2.9E-02
URA4	-1.02	625	609	658	1173	1321	1351	0.9922	3.1E-03
AAC3	-1.02	82	66	87	164	167	147	0.9702	9.7E-03
SNO1	-1.04	161	114	139	298	272	283	0.9755	7.5E-03
ARN1	-1.06	267	278	246	674	495	482	0.9594	1.4E-02
ALD6	-1.06	1507	1567	1758	3052	3510	3527	0.9682	1.1E-02
YJL213W	-1.16	137	132	139	368	272	271	0.9800	7.0E-03
BAP3	-1.23	51	43	53	121	119	105	0.9802	6.7E-03
YIL165C	-1.25	101	98	118	249	268	236	0.9970	1.4E-03
AQR1	-1.29	466	411	395	1232	968	904	0.9823	6.2E-03
ECM13	-1.36	126	121	125	367	308	277	0.9960	2.0E-03
SNZ1	-1.47	987	698	1224	2697	2602	2733	0.9933	2.8E-03
RIB4	-1.49	616	620	636	1362	1894	2011	0.9976	9.5E-04
TPO1	-1.64	307	403	370	971	1297	1091	0.9961	1.8E-03
YGR035C	-1.64	95	71	93	334	246	228	0.9909	3.7E-03
YMR141W-A	-1.67	18	18	10	49	48	49	0.9491	1.6E-02
FMP48	-1.71	20	19	19	63	60	67	0.9877	4.8E-03
TPO4	-1.74	715	1388	1142	3217	4068	3577	0.9650	1.1E-02
TIS11	-1.86	39	33	38	182	102	115	0.9857	5.1E-03
URA3	-1.87	440	341	391	1855	1003	1421	0.9936	2.4E-03
URA1	-2.14	833	1025	993	4083	4112	4328	1.0000	2.5E-05
EEB1	-2.56	245	264	238	1717	1361	1329	1.0000	8.6E-06
MDH2	-2.64	69	103	102	543	556	605	1.0000	2.0E-05

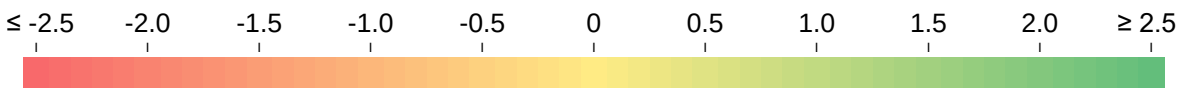

Supplementary Table 15. Mitochondrial proteins down-regulated in their abundance in the *asc1*$^{-}$ strain.

proteins	protein IDs	description	median log_2 *asc1*$^{-}$/*ASC1* ratio
mitochondrial translation			
Img1	P25626	54S ribosomal protein IMG1. mitochondrial	-0.50
Img2	P25642	54S ribosomal protein IMG2. mitochondrial	-0.53
Mam33	P40513	Mitochondrial acidic protein MAM33	-0.61
Mnp1	P53163	54S ribosomal protein L12. mitochondrial	-0.57
Mrp1	P10662	37S ribosomal protein MRP1. mitochondrial	-0.71
Mrp13	P12686	37S ribosomal protein MRP13. mitochondrial	-0.63
Mrpl15	P36523	54S ribosomal protein L15. mitochondrial	-0.48
Mrpl19	P53875	54S ribosomal protein L19. mitochondrial	-0.52
Mrpl3	P36516	54S ribosomal protein L3. mitochondrial	-0.54
Mrpl33	P20084	54S ribosomal protein L33. mitochondrial	-0.48
Mrpl38	P35996	54S ribosomal protein L38. mitochondrial	-0.30
Mrpl49	P40858	54S ribosomal protein L49. mitochondrial	-0.55
Mrpl51	Q06090	54S ribosomal protein L51. mitochondrial	-0.53
Mrps8	Q03799	37S ribosomal protein S8. mitochondrial	-0.38
Mss51	P32335	Protein MSS51. mitochondrial	-0.46
Rsm10	Q03201	37S ribosomal protein S10. mitochondrial	-0.49
Rsm7	P47150	37S ribosomal protein S7. mitochondrial	-0.52
Tuf1	P02992	Elongation factor Tu. mitochondrial	-0.62
Var1	P02381	Ribosomal protein VAR1. mitochondrial	-0.87
mitochondrial protein import			
Mia40	P36046	Mitochondrial intermembrane space import and assembly protein 40	-0.62
Tim10	P87108	Mitochondrial import inner membrane translocase subunit TIM10	-0.68
Tim12	P32830	Mitochondrial import inner membrane translocase subunit TIM12	-0.31
Tim44	Q01852	Mitochondrial import inner membrane translocase subunit TIM44	-0.28
Tim50	Q02776	Mitochondrial import inner membrane translocase subunit TIM50	-0.28
Tim8	P57744	Mitochondrial import inner membrane translocase subunit TIM8	-0.30
Tim9	O74700	Mitochondrial import inner membrane translocase subunit TIM9	-0.66
Tom20	P35180	Mitochondrial import receptor subunit TOM20	-0.26
Tom22	P49334	Mitochondrial import receptor subunit TOM22	-0.42
Tom40	P23644	Mitochondrial import receptor subunit TOM40	-0.47
Tom7	P53507	Mitochondrial import receptor subunit TOM7	-0.42
Tom70	P07213	Mitochondrial import receptor subunit TOM70	-0.58

Supplementary Table 15 continued 1.

proteins	protein IDs	description	median log_2 *asc1*$^-$/*ASC1* ratio
further mitochondrial transport processes			
Aac1	P04710	ADP, ATP carrier protein 1	-0.42
Ctp1	P38152	Tricarboxylate transport protein	-0.97
Dic1	Q06143	Mitochondrial dicarboxylate transporter	-0.80
Ggc1	P38988	Putative mitochondrial carrier protein YHM1/SHM1	-0.67
Mir1	P23641	Mitochondrial phosphate carrier protein	-0.57
Om14	P38325	Mitochondrial outer membrane protein OM14	-0.45
Pet9	P18239	ADP, ATP carrier protein 2	-0.40
Por1	P04840	Mitochondrial outer membrane protein porin 1	-0.47
respiration			
Atp1	P07251	ATP synthase subunit α, mitochondrial	-0.52
Atp2	P00830	ATP synthase subunit β, mitochondrial	-0.49
Atp3	P38077	ATP synthase subunit γ, mitochondrial	-0.38
Atp4	P05626	ATP synthase subunit 4, mitochondrial	-0.32
Atp5	P09457	ATP synthase subunit 5, mitochondrial	-0.43
Atp7	P30902	ATP synthase subunit d, mitochondrial	-0.33
Atp15	P21306	ATP synthase subunit ε, mitochondrial	-0.41
Atp16	Q12165	ATP synthase subunit δ, mitochondrial	-0.32
Atp17	Q06405	ATP synthase subunit f, mitochondrial	-0.28
Atp18	P81450	ATP synthase subunit J, mitochondrial	-0.34
Cox4	P04037	Cytochrome c oxidase subunit 4, mitochondrial	-0.39
Cox6	P00427	Cytochrome c oxidase subunit 6, mitochondrial	-0.26
Nde1	P40215;Q07500	External NADH-ubiquinone oxidoreductase 2, mitochondrial	-0.42
Sdh1	Q00711;P47052	Succinate dehydrogenase [ubiquinone] flavoprotein subunit 2, mitochondrial	-0.57
Sdh2	P21801	Succinate dehydrogenase [ubiquinone] iron-sulfur subunit, mitochondrial	-0.32
Tim11	P81449	ATP synthase subunit e, mitochondrial	-0.31
tricarboxylic acid cycle			
Aco2	P39533	Probable aconitate hydratase 2	-0.55
Kgd1	P20967	2-oxoglutarate dehydrogenase E1 component, mitochondrial	-0.47
Lsc2	P53312	Succinyl-CoA ligase [ADP-forming] subunit β, mitochondrial	-0.30
assembly of respiratory chain complexes			
Cbp3	P21560	Protein CBP3, mitochondrial	-0.28
Cbp4	P37267	Assembly factor CBP4	-0.30
Coa1	P40452	Cytochrome oxidase assembly protein 1	-0.29
Cox15	P40086	Cytochrome c oxidase assembly protein COX15	-0.32
Yta12	P40341	Mitochondrial respiratory chain complexes assembly protein RCA1	-0.39

Supplementary Table 15 continued 2.

proteins	protein IDs	description	median log_2 *asc1*$^-$/*ASC1* ratio
mitochondrial contact site and cristae organizing system (MICOS) complex			
Mic10	Q96VH5	UPF0327 protein YCL057C-A	-0.31
Mic12	P38341	Uncharacterized protein YBR262C	-0.40
Mic19	P43594	UPF0726 protein YFR011C	-0.41
Mic60	P36112	Uncharacterized protein YKR016W	-0.31
glycine decarboxylase complex			
Gcv1	P48015	Aminomethyltransferase, mitochondrial	-0.47
Gcv2	P49095	Glycine dehydrogenase [decarboxylating], mitochondrial	-0.75
Gcv3	P39726	Glycine cleavage system H protein, mitochondrial	-0.62
protein folding and degradation			
Hsp10	P38910	10 kDa heat shock protein, mitochondrial	-0.40
Phb1	P40961	Prohibitin-1	-0.27
Pim1	P36775	Lon protease homolog, mitochondrial	-0.59
proteins with described mitochondria-associated functions			
Adh3	P07246	Alcohol dehydrogenase 3, mitochondrial	-0.38
Adk1	P07170	Adenylate kinase 1	-0.70
Arg5,6	Q01217	Protein ARG5,6, mitochondrial	-0.34
Arg8	P18544	Acetylornithine aminotransferase, mitochondrial	-0.36
Arh1	P48360	Probable NADPH:adrenodoxin oxidoreductase, mitochondrial	-0.26
Dld1	P32891	D-lactate dehydrogenase [cytochrome] 1, mitochondrial	-0.49
Dld2	P46681	D-lactate dehydrogenase [cytochrome] 2, mitochondrial	-0.26
Erv1	P27882	Mitochondrial FAD-linked sulfhydryl oxidase ERV1	-0.54
Hem1	P09950	5-aminolevulinate synthase, mitochondrial	-0.70
Isc1	P40015	Inositol phosphosphingolipids phospholipase C	-0.63
Mae1	P36013	NAD-dependent malic enzyme, mitochondrial	-0.48
Mmf1	P40185	Protein MMF1, mitochondrial	-0.38
Mss116	P15424	ATP-dependent RNA helicase MSS116, mitochondrial	-0.47
Num1	Q00402	Nuclear migration protein NUM1	-0.30
Prx1	P34227	Mitochondrial peroxiredoxin PRX1	-0.45
Sod2	P00447	Superoxide dismutase [Mn], mitochondrial	-0.52
Uth1	P36135	Protein UTH1	-0.76
Yhm2	Q04013	Mitochondrial DNA replication protein YHM2	-0.80

Supplementary Table 15 continued 3.

proteins	protein IDs	description	median log_2 *asc1*$^-$/*ASC1* ratio
further proteins found to be associated with mitochondria			
Aim36	Q03798	Uncharacterized protein YMR157C	-0.54
Aim9	P40053	Uncharacterized protein YER080W	-0.39
Cpr1	P14832	Peptidyl-prolyl cis-trans isomerase	-1.07
Gpm1	P00950	Phosphoglycerate mutase 1	-0.33
Imo32	P53219	Uncharacterized abhydrolase domain-containing protein YGR031W	-0.33
Msc1	Q03104	Meiotic sister chromatid recombination protein 1	-1.44
Ncp1	P16603	NADP-cytochrome P450 reductase	-0.54
Pep4	P07267	Saccharopepsin	-0.49
Pth2	P34222	Peptidyl-tRNA hydrolase 2	-0.28
Tdh3	P00359	Glyceraldehyde-3-phosphate dehydrogenase 3	-0.48
Tma19	P35691	Translationally-controlled tumor protein homolog	-0.37
Tpi1	P00942	Triosephosphate isomerase	-0.28

Supplementary Table 16. Proteasomal proteins up-regulated in their abundance in the *asc1*$^-$ strain.

proteins	protein IDs	description	median log_2 *asc1*$^-$/*ASC1* ratio
20S core particle			
Pre2	P30656	Proteasome subunit β type-5	0.42
Pre3	P38624	Proteasome subunit β type-1	0.29
Pre4	P30657	Proteasome subunit β type-7	0.34
Pre5	P40302	Proteasome subunit α type-6	0.39
Pre6	P40303	Proteasome subunit α type-4	0.32
Pre7	P23724	Proteasome subunit β type-6	0.48
Pre8	P23639	Proteasome subunit α type-2	0.28
Pre9	P23638	Proteasome subunit α type-3	0.30
Pre10	P21242	Probable proteasome subunit α type-7	0.33
Pup1	P25043	Proteasome subunit β type-2	0.30
Pup2	P32379	Proteasome subunit α type-5	0.31
Pup3	P25451	Proteasome subunit β type-3	0.33
Scl1	P21243	Proteasome subunit α type-1	0.41
19S regulatory particle			
Rpn13	O13563	26S proteasome regulatory subunit RPN13	0.28
Rpn5	Q12250	26S proteasome regulatory subunit RPN5	0.27

Abbreviations

aa	= amino acid
AC	= adenylyl cyclase
AMP	= adenosine monophosphate
Aux	= auxotrophy
3-AT	= 3-amino-1,2,4-triazole
BCA	= bicinchoninic acid
bp	= base pair
BSA	= bovine serum albumin
cAMP	= cyclic adenosine monophosphate
cDNA	= complementary DNA
CID	= collision-induced dissociation
C-terminal/-terminus	= carboxyl-terminus
d	= days
DE	= R38D K40E
DETA-NONOate	= (*Z*)-1-[*N*-(2-Aminoethyl)-*N*-(2-ammonioethyl)amino]diazen-1-ium 1,2-diolate)
DNA	= deoxyribonucleic acid
dNTP	= deoxynucleoside triphosphate
DTT	= dithiotreitol
ECL	= enhanced chemoluminescence
EDTA	= ethylenediaminetetraacetic acid
EGTA	= ethylene glycol tetraacetic acid
et al.	= et alii
FASP	= filter-aided sample preparation
FDR	= false discovery rate
FT	= fourier transform
G_1/G_2	= gap phase 1/2
GDP	= guanosine diphosphate
glc	= glucose
GPCR	= G-protein-coupled receptor
GTP	= guanosine triphosphate
h	= hour(s)

HCC = hepatocellular carcinoma
HCD = higher energy collisional dissociation
HEK293 = human embryonic kidney 293
HeLa = Henrietta Lacks
Huh7 = human hepatocellular carcinoma
ID = identifier
IRES = internal ribosomal entry site
LB = lysogeny broth
LC = liquid chromatography
M = mitosis
MAPK = mitogen activated protein kinase
min = minute(s)
miRISC = miRNA-induced silencing complex
miRNA = micro RNA
mRNA = messenger RNA
mRNP = ribonucleoprotein containing mRNA
MS = mass spectrometry
MSA = multistage activation
MV = minimal with vitamins
N/A = not applicable
NaN = not a number
N-terminal/-terminus = amino-terminus
OD = optical density
ORF = open reading frame
PACAP = pituitary adenylyl cyclase-activating polypeptide
PAGE = polyacrylamide gel electrophoresis
P-bodies = processing bodies
PBS = phosphate buffered saline
PCR = polymerase chain reaction
PEG = polyethylene glycol
PKA = protein kinase A
PKC = protein kinase C
PMSF = phenylmethane sulfonyl fluoride
PTM = post-translational modification

RNA = ribonucleic acid
RNP = ribonucleoprotein
rpm = revolutions per minute
rRNA = ribosomal RNA
S = synthesis phase or Svedberg unit
SD = standard deviation
SDS = sodium dodecyl sulfate
sec = second(s)
SESA = Scp160p, Eap1p, Smy2p, Asc1p
SILAC = stable isotope labeling with amino acids in cell culture
snoRNA = small nucleolar RNA
snoRNP = ribonucleoprotein containing snoRNA
SOB = super optimal broth
SOD = superoxide dismutase
TAE = Tris base, acetic acid, EDTA
TB = transformation buffer
TBS = Tris-buffered saline
TE = Tris EDTA
TFA = trifluoracetic acid
Tris = Tris(hydroxymethyl)aminomethane
tRNA = transfer RNA
$tRNA_i$ = initiator tRNA
TTC = triphenyltetrazolium chloride
UA = first urea buffer of FASP protocol
UB = second urea buffer of FASP protocol
UTR = untranslated region
UV = ultraviolet
V = volume
vs. = versus
WD = tryptophan-aspartate
YEPD = yeast extract peptone dextrose
YNB = yeast nitrogen base